Investigation into the Mechanisms of Intraneuronal Amyloid-ß and Apolipoprotein E Driven Pathology in Alzheimer's Disease

Jade Diana Marsh

School of Biological Sciences

Royal Holloway, University of London

Research thesis submitted for the degree of Doctor of Philosophy

Declaration of Authorship

I, Jade Marsh, hereby declare that this thesis and the work presented in it is entirely my own. Where I have consulted the work of others, this is always clearly stated.

Signed: _____

Date: _____

Abstract

Whilst the causal mechanisms underpinning Alzheimer's disease (AD) are still elusive, there is increasing evidence to support a role for oligomeric amyloid-beta (Aß) peptides in the progression of this neurodegenerative disease. Studies have shown that Aß42 can contribute to synaptic dysfunction, an early event in AD, through altering synaptic vesicle (SV) dynamics. However, the molecular basis of this is poorly understood. Here, the regulation of SynapsinI, a key modulator of SV pools and availability, was examined using primary rat neurons acutely exposed to Aß42. The results showed that Aß42 induced sustained phosphorylation of SynapsinI at Ser9, which was hypothesised to disrupt physiological SV dynamics. Interestingly, treatment of Aß42-exposed neurons with Valproic acid (VPA), an approved anti-epileptic drug, restored the physiological phosphorylation cycle of SynapsinI at Ser9. Collectively, these findings suggest a novel mechanism for Aß42-mediated dysfunction in SV dynamics and support a therapeutic role for VPA in Aß-related pathology in AD. Another key player in AD pathophysiology is apolipoprotein E (apoE), a multifunctional glycoprotein that has roles in the cardiovascular and central nervous system. There are three variants of the *APOE* gene: *APOE4* (strongest genetic risk factor for AD), the 'neutral' *APOE3* and the 'neuroprotective' *APOE2*. Although neuron-specific proteolysis of apoE4 is suggested to lead to a toxic gain of function, it is not known whether the neuroprotective role of apoE2 is related to differential processing when expressed in neurons. To investigate this, apoE2, apoE3 and apoE4 were overexpressed in neuronal cell models and the fragmentation of each isoform was first characterised using commercially available antibodies. Although the proteolytic susceptibility of apoE was isoform- and cell-dependent, no unique fragments were observed. Moreover, the data indicated that all three apoE isoforms are cleaved within the N-terminus and hinge region, generating C-terminal fragments of similar composition. The effect of apoE isoform on cytoskeletal-associated proteins and cell viability/survival was also explored to test for a gain of toxic or protective function. While isoform-specific effects on tau phosphorylation and vimentin levels were observed, none of the isoforms were found to be toxic. Finally, the data showed that expression of apoE2 in SH-SY5Y cells is neuroprotective, suggesting

that apoE2 expression in human neurons after injury or stress may contribute to decreased risk for AD. Collectively, these findings indicate that the differential effects of each apoE isoform could be linked to structural differences in the full-length protein and/or fragments.

Acknowledgments

Firstly, I would like to thank my supervisors, Pavlos Alifragis and George Dickson, and my advisor, Philip Chen, for guiding me and my research during the four years of my PhD. You have all helped me to grow as a scientist through your expert knowledge, discussions and support throughout this process. Pavlos, I would also like to thank you for teaching me the ways of protein work, for your patience, and for Belgian chocolate!

I would also like to express my thanks to Simona Ursu for her vital support in assisting in the production of the lentiviral vectors used in this thesis, preparing primary neuronal cultures, and also for offering sage advice during the hard times. You are by far the most amazing and helpful technician – you are indeed, Mary Poppins of the lab. My thanks also go to Linda Popplewell for making me believe that I could be a researcher in the first place. You are a tremendously inspiring and supportive person and I am lucky to have met and worked with you.

To all members of lab 302A (Anila, Helena, Amninder, Ilda, Al and unofficially Marc), you have been the force that has kept me going during the long working hours. Thank you for all the laughs, for helping me during the teary moments and for generally being the amazing people that you are. In particular, thank you to Anila for the power walking sessions during incubation times and for keeping me mentally as well as physically fit during this PhD. I also want to say thank you to Amninder for the never-ending stash of sweets (making me need to go to the gym in the first place!), but also for your very kind support and encouragement. Thanks also go to Helena for teaching me the ways of experiments, posters and presentations during my beginner days – you are indeed, a true Ravenclaw.

To my very special friend Stella Victorelli, I am still so happy that I claimed you as my lab partner during our undergraduate days. You have been instrumental throughout my undergraduate degree but also during my PhD in countless ways and I will be eternally grateful for that. I will always treasure you as my forever “lab partner”.

Very special thanks go to ‘’The Ridgeon family’’ (Irene, Nigel and Evan), you are by far, one of the most loving and supportive families that I know and I am so very grateful to have been allowed to wiggle my way in. I don’t know how I would have managed to write this thesis without your advice, love, and of course, your attic room and garden. Importantly, thank you to my Evan. You have been a pillar of support throughout this PhD. Thank you for being there during the highs and lows, for being my biggest cheerleader and always believing in me, for coming with me to the lab at 2am, for helping me to make pretty figures and to navigate my way out of writing blocks – I am truly grateful to have had you with me on this journey. Thank you for making each day better.

Finally, thank you to my parents, Veronica O’brien and Dean Marsh, who have believed in me from the very beginning. I wholeheartedly thank you for your love and support throughout it all and for helping me to get to where I am today.

Publications

Marsh, J. et al., 2019. Differential fragmentation and effects of neuronally expressed apoE isoforms in neuronal cell models. Submitted.

Marsh, J. & Alifragis, P., 2018. Synaptic dysfunction in Alzheimer's disease: the effects of amyloid beta on synaptic vesicle dynamics as a novel target for therapeutic intervention. ***Neural regeneration research***, 13(4), pp.616–623.

Marsh, J. et al., 2017. Synapsin I phosphorylation is dysregulated by beta-amyloid oligomers and restored by valproic acid. ***Neurobiology of Disease***, 106, pp.63–75.

Table of Contents

Table of Figures

Table of Tables

List of Abbreviations

aa	Amino acid
ABC	ATP- binding cassette transporters
AD	Alzheimer's disease
AICD	APP intracellular domain
AMPAR	α-amino-3-hydroxy-5-methyl-4-isoxazolepropionic acid receptor
APH-1	Anterior defective pharynx 1 protein
apoE	Apolipoprotein E protein
APP	Amyloid Precursor Protein
AraC	Cytosine arabinoside
Aß	Amyloid-ß
ATP	Adenosine triphosphate
BBB	Blood brain barrier
BSA	Bovine serum albumin
cDNA	Complementary DNA
CMV	Cytomegalovirus
CNS	Central nervous system
CSF	Cerebrospinal fluid
CTFα or CTFß	Membrane-bound carboxyl APP fragment
DEPC	Diethyl pyrocarbonate
DIV	Days in vitro
DMEM	Dulbecco's Modified Eagle's Medium
DMSO	Dimethyl sulfoxide
DNA	Deoxyribonucleic acid
DPBS	Dulbecco's phosphate buffered saline solution
E	Embryonic day
ETC	Electron transport chain
FA	Formaldehyde
FACS	Fluorescence-activated cell sorting
fAD	Familial Alzheimer's disease

$FADH_2$	Flavin adenine dinucleotide
FBS	Foetal Bovine Serum
FRAP	Fluorescence recovery after photobleaching
FRET	Fluorescence resonance energy transfer
GFAP	Glial fibrillary acidic protein
GFP	Green fluorescent protein
GWAS	Genome wide association studies
HBSS	Hanks' Balanced Salt Solution
HDL	High density lipoprotein
HEK293T	Human embryonic kidney cells
HIV-1	Human immunodeficiency virus 1
HNE	4-hydroxynonenal
IDE	Insulin-degrading enzyme
IDLV	Integration-deficient lentiviral vector
iPSC	Induced pluripotent stem cells
KI	Knock in
KPI	Kunitz protease inhibitory motif
LB	Lysogeny Broth
LDLR	Low-density lipoprotein receptor
LPP	Lamba phosphatase
LRP1	Low-density lipoprotein receptor-related protein
LTD	Long term depression
LTP	Long term potentiation
LTR	Lentiviral late reverse transcript
MCI	Mild cognitive impairment
MOI	Multiplicity of infection
MRI	Magnetic resonance imaging
mRNA	Messenger RNA
N2a	Neuro-2a cells
nAChRs	α7-nicotinic acetylcholine receptors
NADH	Nicotinamide adenine dinucleotide

NEP	Neprilysin protein
NFTs	Neurofibrillary tangles
NMDAR	N-methly-D-aspartate receptors
NPC	Niemann Pick Type C cholesterol storage disorder
NSE	Neuron specific enolase
PAGE	Polyacrylamide Gel Electrophoresis
PBS	Phosphate-buffered saline
PDG	Fluorodeoxyglucose-18F
PEN-2	Presenilin enhancer 2 protein
PET	Positron emission tomography
PFA	Paraformaldehyde
PSEN1	Presenilin 1 protein
PSEN2	Presenilin 2 protein
p-Tau	Phosphorylated Tau protein
PTMs	Post translational modifications
qPCR	Quantitative polymerase chain reaction
RER	Rough endoplasmic reticulum
RNA	Ribonucleic acid
RRP	Readily releasable pool
sAD	Sporadic Alzheimer's disease
SAGE	Serial Analysis of Gene Expression
sAPPα or sAPPß	Soluble APP N-terminal fragment
SDS	Sodium dodecyl sulfate
SEM	Standard error of the mean
SnpI	Synapsin I protein
SNPs	Single nucleotide polymorphisms
SP	Signal peptide
SV	Synaptic vesicle
TAE	Tris-acetate-EDTA buffer
TBS	Tris-buffered saline
VLDLR	Very-low density lipoprotein receptor

VPA	Valproic acid
WT	Wild-type
ε2	epsilon-2 allele
ε3	epsilon-3 allele
ε4	epsilon-4 allele
α-2M	α-2-macroglobulin protein

Chapter 1 INTRODUCTION

1.1 Clinical overview of Alzheimer's disease

Alzheimer's disease (AD) is a debilitating, progressive neurodegenerative disorder that is placing increasing pressure on healthcare systems globally, costing an estimated total of 817.00 billion (USD) worldwide in 2015 (Wimo et al., 2017). So far, there is no available cure or disease-modifying agent for AD and the vast majority of recent clinical trials have not been successful (Cummings et al., 2014, Amanatkar et al., 2017, Cummings et al., 2018). Considering that the number of affected individuals worldwide, currently estimated at over 50 million, is predicted to triple by 2050 (ADI, 2018), there is an increasingly urgent need to better understand the basic mechanisms of the disease to find an effective clinical solution.

AD involves the selective atrophy of specific brain regions (see Figure 1-1, A), as observed using imaging techniques such as magnetic resonance imaging (MRI), and this is associated with a gradual regression of cognitive and behavioural function (Frisoni et al., 2010, McDonald et al., 2009). Atrophy typically begins within medial temporal lobe structures such as the hippocampus and entorhinal cortex during the mild cognitive impairment (MCI) stage of AD (Spulber et al., 2013, Clerx et al., 2013, McDonald et al., 2009), which leads to the hallmark symptomatic presentation of short-term memory deficits (Gaugler et al., 2016, Visser et al., 1999, Duara et al., 2008). Such deficits can include forgetting names, misplacing objects and struggling to recall recent events or conversations. As the disease spreads to the lateral temporal and parietal lobes during the mild AD stage (McDonald et al., 2009, Scahill et al., 2002), problems with declarative memory (memory of facts or events) worsen and problems with language, number and visuospatial processing become apparent (Bilello et al., 2015). This may affect a person's ability to find the right word or have a coherent conversation, to manage their finances, or to find their way home. The frontal lobe is next affected during the moderate stage of AD (McDonald et al., 2009). Atrophy in this region can lead to Impairment of procedural memory (task organisation and learning of new tasks) and executive functions, which can result in daily activities such as making a cup of tea become challenging. Additionally, problem solving and decision making may become increasingly difficult at this stage, and

changes in behaviour such as irritability, aggression or even apathy may occur. In some cases, as the disease advances, the occipital lobe can also degenerate (McDonald et al., 2009), leading to the presentation of visual problems. It is notable though, that the variety and severity of these symptoms vary in those affected by AD, but generally these worsen over time as atrophy of the brain becomes more severe and widespread (see Figure 1-1, B). This results in complete dependency and impacts the lives of not only those with the condition, but also their families. The final stages of the disease can be fatal. Whilst it is established that atrophy of the brain is due to loss of synapses and neurophil (axons and dendrites of neurons), neuronal death and brain shrinkage, the cause behind it is still poorly understood.

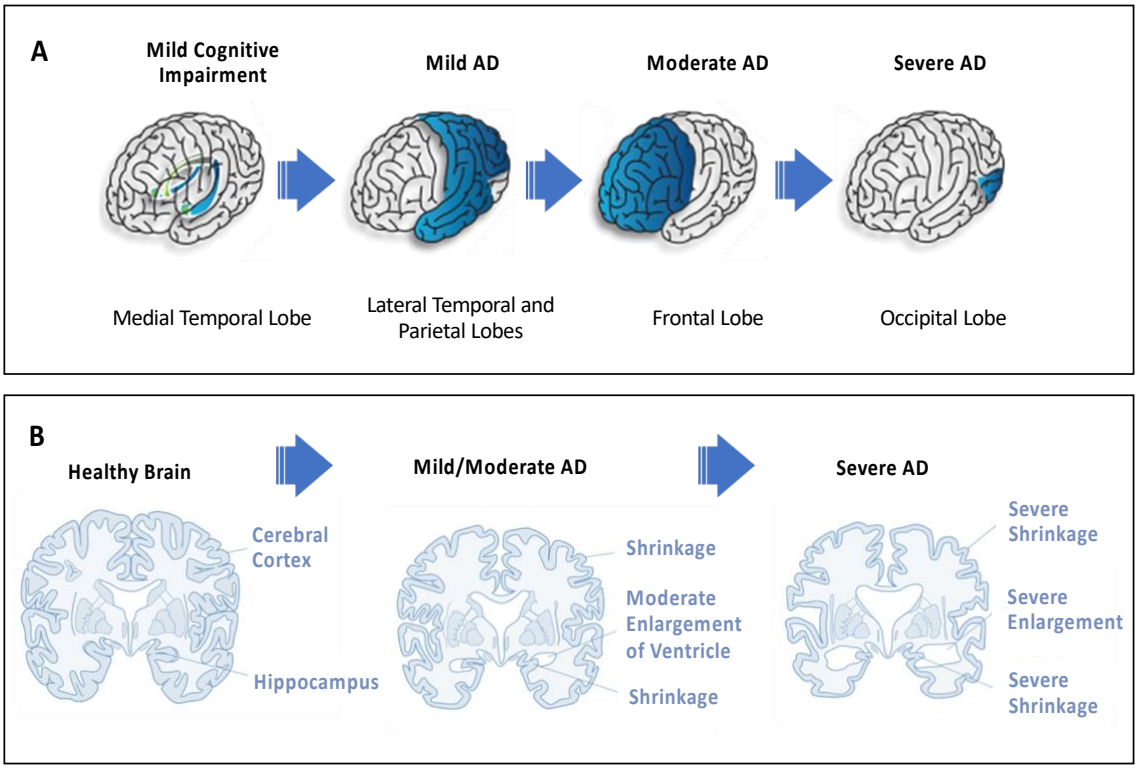

Figure 1-1 The progressive and selective atrophy of the brain in Alzheimer's disease
(A) Illustration showing the brain regions typically affected in each clinical stage of AD. At the mild cognitive impairment stage of AD, structures within the medial temporal lobe begin to atrophy. The brain atrophy spreads to the lateral temporal and parietal lobes in mild AD in a cumulative manner, the frontal lobe in moderate AD and in some cases, the occipital lobe in the severe stage of the disease. (B) Illustration showing how selective atrophy in AD leads to gradual shrinkage of specific brain regions. Images adapted from https://www.save-years.com/alzheimers (A) and https://plasmalogen.me/en/pathophysiology-of-alzheimers-disease (B).

1.2 Histopathological hallmarks of AD

AD is also characterised by the presence of extracellular plaques and intraneuronal neurofibrillary tangles, two distinct pathological lesions which were initially observed by Alois Alzheimer over a century ago. Isolation and purification of extracellular plaques from AD-afflicted brains led to the identification a small (~4kDa) peptide called amyloid-ß (Aß) as the major constituent of plaques (Glenner and Wong, 1984, Masters et al., 1985), whilst labelling of intraneuronal neurofibrillary tangles (NFTs) with tau specific antibodies revealed that they contained aggregates of hyperphosphorylated tau (Grundke-Iqbal et al., 1986). These findings strongly implicated the build-up of Aß and the dysregulation of tau in the pathogenesis of the disorder. As a result, the presence and spread of these two lesions in the brain are still used for diagnosis of AD and as a reference for the staging of the disease (Braak and Braak, 1991, Braak and Braak, 1995, Serrano-Pozo et al., 2011).

1.3 The preclinical phase of AD and biomarkers

By the time a person presents with clinical symptoms of AD, significant changes in the brain at the molecular, metabolic and structural levels have already occurred (Masters et al., 2015). In fact, changes in the brain that are associated with AD are thought to occur approximately two decades before the onset of clinical symptoms at the MCI stage, during what is recognised as the preclinical phase of the disease (Sperling et al., 2011). Analysis of the cerebrospinal fluid (CSF), which reflects the biochemistry of the brain, and positron emission tomography (PET) imaging, have been instrumental in monitoring these early changes at the molecular level and identifying promising biomarkers to diagnose AD. For instance, these approaches have revealed alterations in the metabolism of the Aß peptide up to 20 years prior to onset of clinical symptoms of AD (Skoog et al., 2003, Gustafson et al., 2007, van Harten et al., 2013, Villemagne et al., 2013). In an early study measuring Aß42 and Aß40 (species of the Aß peptide that vary by 2 amino acids (aa)) in the CSF of cognitively normal elderly patients, the levels of Aß42, but not Aß40, were found to decline in patients who developed AD (Skoog et al., 2003). Moreover, low CSF levels of Aß42 were determined to confer an 8-fold risk for the development of AD in the 3-year follow up period of the study (Skoog et al., 2003).

Later studies have also demonstrated that low levels of CSF Aß42, detected as early as 8 years before clinical presentation of AD, correlate with cognitive decline and the development of AD (Gustafson et al., 2007, Stomrud et al., 2007, van Harten et al., 2013, Palmqvist et al., 2015). Whilst these studies provide evidence for an early preclinical phase of AD, they also demonstrate that CSF levels of Aß42 can be used as a biomarker for the development of AD. Imaging of Aß in the brain by PET has provided further evidence for a link between early accumulation and deposition of Aß and the development of AD. In a 3-year follow up Aß PET imaging study, positive Aß PET scans (higher Aß burden compared to baseline) in cognitively normal individuals were found to be associated with a higher risk for developing AD, and a poorer prognosis in patients with MCI (Rowe et al., 2013). Moreover, longitudinal Aß PET imaging studies of the rates of Aß accumulation have provided data to support a prolonged preclinical stage of AD, with PET scans showing positivity for accumulation of the peptide up to 17 years before the full onset of AD dementia (Jack et al., 2013, Villemagne et al., 2013). In addition to changes in Aß42 levels, increases in the levels of total tau and phosphorylated tau (p-Tau) have been detected by CSF analysis and PET imaging in the preclinical and MCI stages of AD (Sutphen et al., 2015, Visser et al., 2009, Sjogren et al., 2001, Scholl et al., 2016, Betthauser et al., 2019). However, CSF total tau is considered to not be a specific biomarker for AD because increases in CSF total tau have also been observed in other neurodegenerative diseases such as Creutzfeldt–Jakob disease (Riemenschneider et al., 2003, Skillback et al., 2014). Hence CSF total tau is considered as an indicator of the intensity of degeneration of the brain (Blennow, 2017). On the other hand, there is evidence to suggest that CSF p-Tau levels may be an accurate biomarker to distinguish AD from other types of dementias (Hampel et al., 2004, Vanmechelen et al., 2000, Buerger et al., 2002). Moreover, Tau PET imaging studies have shown that the regional distribution of p-Tau can be an accurate predictor of cognitive decline and also a good correlate of neurofibrillary tau pathology (Schwarz et al., 2016, Scholl et al., 2016). Therefore p-Tau levels and distribution are considered useful biomarkers for the progression of AD-related pathology (Masters et al., 2015). Overall, the mounting evidence from biomarker studies suggests that the “AD profile” of CSF biomarkers is low Aβ42, high total tau and high p-Tau, and using them in combination for diagnosis of AD

increases the sensitivity and accuracy of an AD diagnosis (Maddalena et al., 2003, Palmqvist et al., 2015, Dubois et al., 2014). The discovery of the preclinical phase of AD and biomarkers to identify it is of great importance since this period is when disease-modifying treatments may be most effective. Furthermore, finding accurate and specific biomarkers for the early diagnosis of AD is crucial for correctly identifying preclinical and asymptomatic patients with AD to be included in clinical trials. However, since CSF sample collection involves an invasive procedure and the costs of PET are high, the detection of biomarkers in blood samples would be preferable for routine diagnosis of preclinical stage AD. Research into such biomarkers is underway and promising (Nakamura et al., 2018).

1.4 Genetic basis and risk factors of AD

It is becoming increasingly evident that the neurodegenerative process of AD involves an interplay of multiple risk genes and factors, some of which converge on the regulation and functions of Aß and tau. There are two types of AD: the rare (2-5% of AD cases) form called familial AD (fAD; or early-onset AD) and the more common form known as sporadic AD (sAD; or late-onset AD). The fAD form is inherited in an autosomal dominant manner and manifests symptomatically before the age of 65 years. Conversely, no causal mutations have been associated with sAD, which develops much later in life, typically after 65 years of age. However, this form also has a strong genetic component, with a heritability of up to 80% (Gatz et al., 2006).

SAD is genetically complex, with over 21 risk genes identified (see Figure 1-2) so far by genome wide association studies (GWAS) (Karch and Goate, 2015). The main genetic determinants of AD risk are the polymorphic alleles (ε2, ε3 and ε4) of the *APOE* gene encoding the apolipoprotein E protein (referred to hereafter as apoE), located on chromosome 19q13. Genetic analysis identified the ε4 allele of *APOE* as the strongest genetic risk factor for sAD and it is estimated to account for up to 30% of the disease heritability of sAD cases (Corder et al., 1993, Chartier-Hariln et al., 1994). In fact, the risk for AD is estimated to be three-fold for heterozygous carriers of the ε4 allele, whilst homozygosity for *APOE4* was estimated to increase the risk by 8- to 12-fold (Gaugler et

al., 2016). In addition, *APOE4* has a gene-dose effect on reducing the age of disease onset. Contrastingly, the ε2 variant was found to be associated with a decreased risk for AD and to delay the age of onset for the disorder (Chartier-Hariln et al., 1994, Corder et al., 1994), indicating that it confers a neuroprotective effect. Non-genetic risk factors have also been associated with sAD, which include aging, poor education attainment, lack of physical exercise, and vascular diseases, amongst others (Sando et al., 2008, Baumgart et al., 2015, Xu et al., 2015b).

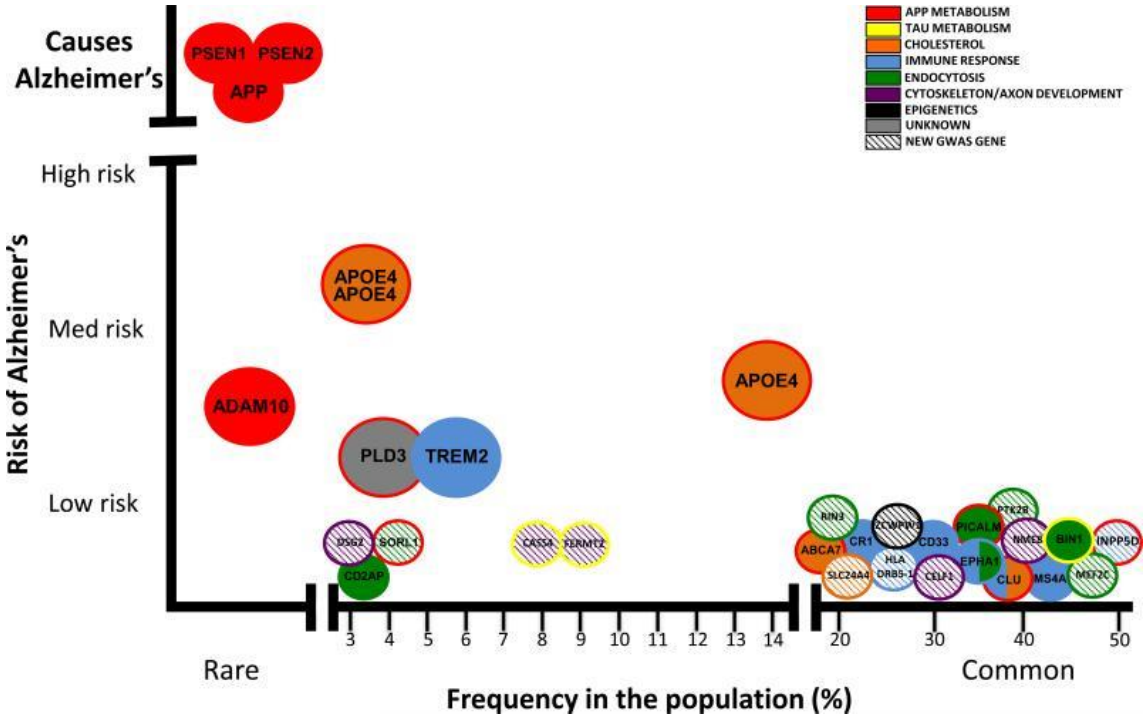

Figure 1-2 Graph showing the frequency and risk level of risk loci in Alzheimer's Disease
GWAS and meta analysis studies have identified polymorphisms in 21 genes to be associated with increased risk for AD. The frequency of these gene variants in the population vary from rare (<3%) such as those in *ADAM10* to being more common (>20%) such as those in *CLU.* In addition, they confer different levels of risk that can also be gene-dose dependent. For instance, two copies of the *APOE4* gene confers the greatest level of risk for AD, whilst one copy decreases the risk. Nonetheless, the *APOE4* gene remains the strongest genetic risk factor for AD so far. Image taken from (Karch and Goate, 2015).

Furthermore, causal and rare risk mutations in genes encoding Presenilin 1 (*PSEN1*; on chromosome 14), Presenilin 2 (*PSEN2*; on chromosome 1) and the Amyloid Precursor Protein (*APP*; on chromosome 21) have been identified in people with fAD and sAD respectively (Cruts et al., 2012, Cruchaga et al., 2012). To date, over 286 pathogenic

mutations have been found in these genes (see database: http://www.molgen.ua.ac.be/ADMutations), with mutations in the *PSEN1* gene being the most common and severe. Duplication of *APP* has also been found to cause fAD (Rovelet-Lecrux et al., 2006, Sleegers et al., 2006). Ultimately, mutations in these genes either alter the proteolytic processing of APP in favour of longer forms of the Aß peptide, or lead to increased levels of Aß produced such as in the case of APP duplication. These findings in conjunction with the observation of Aß deposits in post-mortem brains from individuals with by fAD or sAD established Aß as a key player in the pathogenesis of AD.

1.5 Aß in AD

1.5.1 Proteolysis of APP: Generation of the Aß peptide

APP was identified as the precursor protein to Aß in 1987 following cloning of the *APP* gene (Kang et al., 1987). Full length APP is a type 1 integral membrane protein which has a large extracellular domain, a transmembrane domain and a short cytoplasmic domain. This protein structure is conserved amongst the three major splice variants of APP that are generated by alternative splicing of exons 7 and 8: APP770, APP751 and APP695 (Nalivaeva and Turner, 2013). Whilst APP770 and APP751 are expressed in many cell types, APP695 is predominantly expressed by neurons in the central nervous system (CNS) (Kang and Muller-Hill, 1990, Rohan de Silva et al., 1997). Once synthesised in the endoplasmic reticulum (ER), APP undergoes sequential proteolytic processing by various secretases. Multiple processing pathways have recently been described for APP (Andrew et al., 2016), however the most established are the non-amyloidogenic and amyloidogenic pathways (Aß forming), which are summarised in Figure 1-3. Notably, a Kunitz protease inhibitory (KPI) motif found in the APP751 and APP770 but not APP695, is thought to promote amyloidogenic processing of APP (Ho et al., 1996). The amyloidogenic and non-amyloidogenic pathways are distinguished by the initial secretase action, which leads to the generation of different proteolytic cleavage products. APP is predominately processed by the non-amyloidogenic pathway, which is initiated by α-secretase mediated cleavage of APP within the Aß domain at the cell surface. This produces a soluble N-terminal fragment (sAPPα) that is released into the

extracellular space and a membrane-bound carboxyl fragment (CTFα). There is evidence to suggest that the major α-secretase is ADAM10, a zinc metalloprotease, since RNAi knockdown or mutation of this protein significantly reduced the generation of sAPPα, whilst overexpression of ADAM10 increased it (Kuhn et al., 2010, Lammich et al., 1999). The CTFα fragment then undergoes cleavage by the γ-secretase complex at the cell surface or in the endosomal/lysosomal pathway following its internalisation (Nordstedt et al., 1993), liberating a 3kDa fragment termed p3 (Haass et al., 1993) and the APP intracellular domain (AICD). In the amyloidogenic pathway, APP is initially cleaved by ß-secretase (BACE1) within the N-terminal domain at the cell surface, or more commonly, in the endosomal pathway (Nordstedt et al., 1993, Kinoshita et al., 2003). This generates a smaller N-terminal fragment (sAPPß) and a membrane-anchored C-terminal fragment (CTFß) containing an intact Aß domain. CTFß is also cleaved by the γ-secretase complex, generating the AICD fragment and the Aß peptide, which can vary in length due to variable sequential γ-secretase activity along the C-terminus of the peptide (Zhao et al., 2007). The predominant Aß variant produced under physiological conditions is 40 aa in length (Aß40), and is found in abundance in the CSF, whereas the levels of the longer variants are much lower (Tamaoka, 1998).

The γ-secretase complex contains four subunits: Presenilin (PS; comprising either PSEN1 or PSEN2), nicastrin, anterior defective pharynx 1 (APH-1) and presenilin enhancer 2 (PEN-2) (De Strooper, 2003, De Strooper et al., 2012). PSEN1 and PSEN2 are thought to form the catalytic component of the γ-secretase complex, as partly based on the discovery that fAD-causative mutations in the *PSEN1* and *PSEN2* lead to increased generation of Aß peptides that are 42aa in length (Aß42 variant) (Borchelt et al., 1996, Lemere et al., 1996, Xia et al., 1997). The notion that PSEN1 has γ-secretase activity was further supported by later studies showing that deficiency or mutagenesis of PSEN1 was associated with an accumulation of carboxyl-terminal fragments of APP and a decrease in Aß production (De Strooper et al., 1998, Wolfe et al., 1999). From this evidence, it was proposed that mutations in PSEN1 alter its ability to trim the Aß peptide due to reduced structural stability of the complex resulting in the release of longer (>40aa) Aß peptides, in particular Aß42 (De Strooper and Karran, 2016). Whilst a potential role for the other

APP metabolites in AD pathology cannot be discounted, the discovery that Aß peptides with longer C-termini such as Aß42 aggregate more readily to form plaques (Jarrett et al., 1993), further supported the notion that accumulation of Aß42 may play a pivotal role in AD. Collectively, these findings gave rise to the Aß cascade hypothesis, initially proposed by Selkoe, Hardy and fellow co-workers (Selkoe, 1991, Hardy and Allsop, 1991, Hardy and Higgins, 1992).

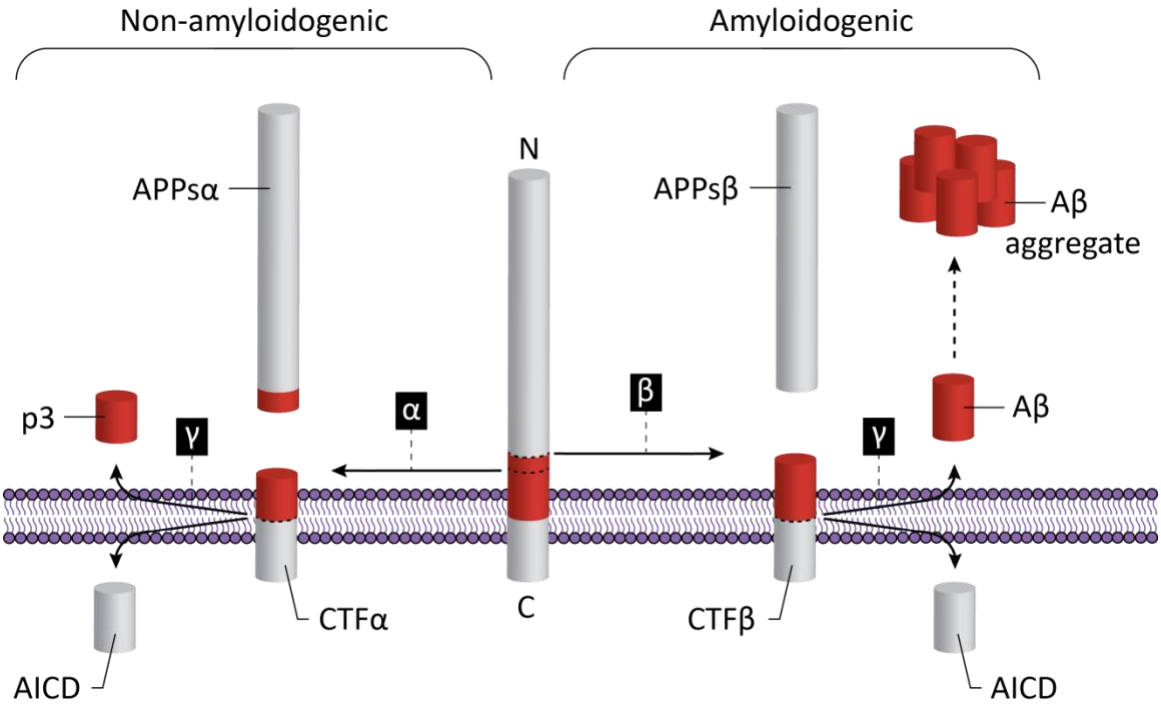

Figure 1-3 APP Processing and Aß generation

APP can be processed through two different pathways, the amyloidogenic and non-amyloidogenic pathway. The former leads to the generation of the neurotoxic peptide, Aß, implicated in the pathology of AD. The pathways are distinguished by the initial secretase action. The amyloidogenic pathway is initiated by the proteolytic action of ß-secretase, producing a 99 amino acid C-terminal fragment (CTFß) and a secreted fragment (sAPPß). The non-amyloidogenic pathway is instead initiated by α-secretase cleavage of APP within the Aß domain, thus precluding subsequent generation of Aß. A smaller C-terminal fragment (CTFα) is subsequently produced along with sAPPα which is also secreted. The C-terminal fragment is cleaved by γ-secretase in both types of processing, however cleavage of CTFß results in the generation of Aß, whilst cleavage of CTFα leads to the generation of small fragment termed p3. Longer variants of Aß peptides (Aß peptides 42aa in length or more) have a high propensity to aggregate and as Aß levels generated increase, Aß monomers aggregate to form Aß oligomers, protofibrils, fibrils and plaques.

1.5.2 The Aß cascade hypothesis: a central role for soluble Aß42 oligomers

The Aß cascade hypothesis which posits a central role for Aß42 in the pathogenesis of AD, is still one of the main working models for AD today. In the original hypothesis, the accumulation of Aß42 and its subsequent deposition as plaques was considered the initial trigger for a sequence of toxic events that results in neuronal death and ultimately AD. This was largely founded upon the histopathological observations of Aß plaques and the finding that fAD-causal mutations promote the production of Aß42. However, studies emerged showing that the soluble, oligomeric forms of Aß are a better correlate of cognitive decline than plaque densities (McLean et al., 1999, Naslund et al., 2000). In addition, soluble Aß oligomers were found to be more toxic to neurons than plaques (Pike et al., 1991, Pike et al., 1993), thus indicating a more causal role for this form of the peptide in AD. Subsequently, the Aß cascade hypothesis was reformed to incorporate the accumulation of soluble Aß42 oligomers as a primary driver of AD pathology (summarised in Figure 1-4). This updated hypothesis has been further supported by the recent identification of a protective missense mutation (A673T) within the Aß region of the *APP* gene (Jonsson et al., 2012), which has been found to decrease the amyloidogenic processing of APP (Aß forming pathway) and the ability of the Aß42 peptide to aggregate (Maloney et al., 2014, Zheng et al., 2015).

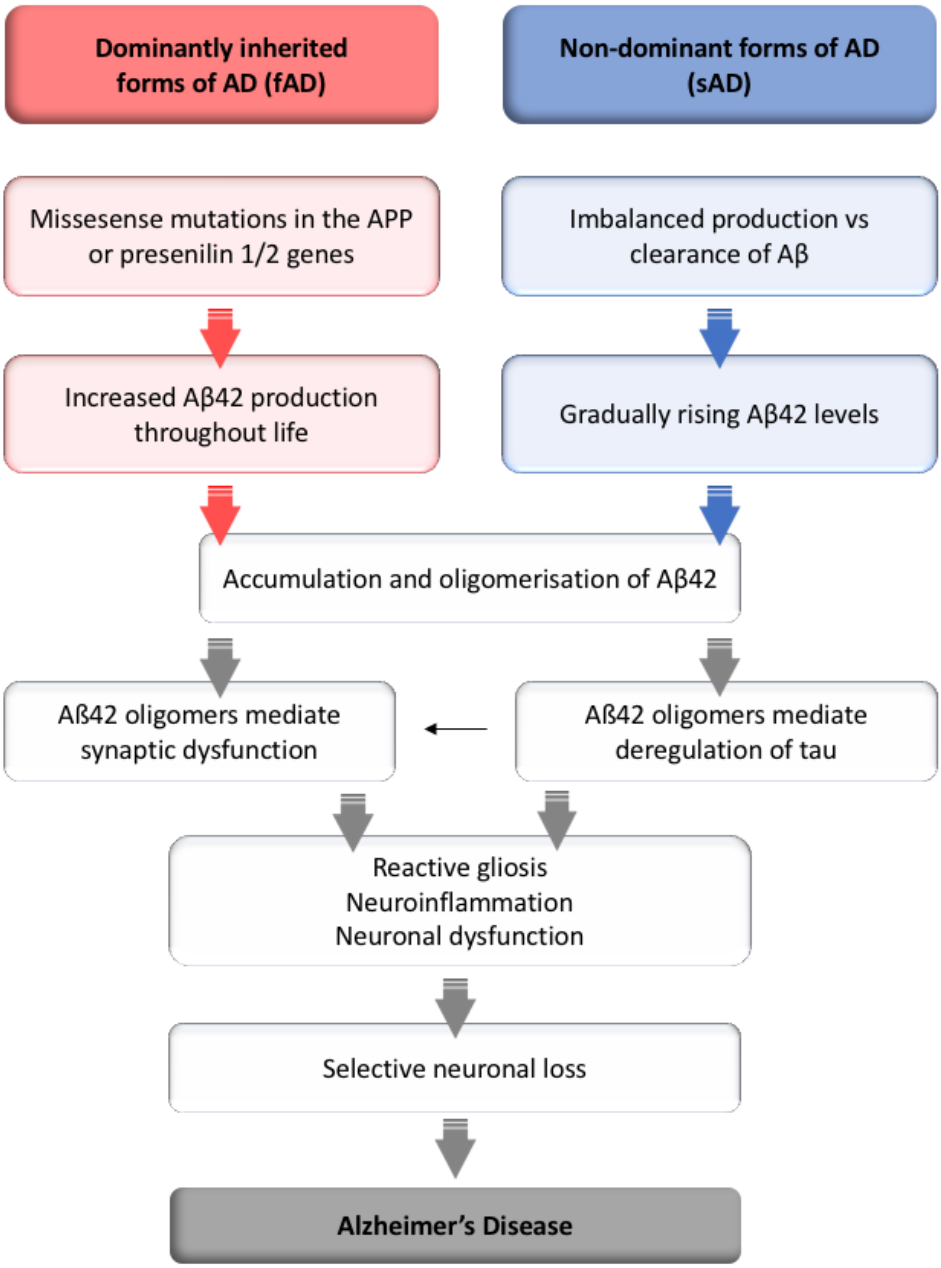

Figure 1-4 Modified Aß cascade hypothesis showing the sequence of neuropathological events in AD
The Aß cascade hypothesis proposes a central role for the progressive accumulation and aggregation of Aß in AD pathology. Dominantly inherited forms of AD typically involve altered proteolytic processing of APP, leading to an increased production of the toxic Aß42 peptide throughout life. Non-dominant forms of AD likely involve a combination of genetic, environmental and lifestyle risk factors that contribute to an imbalance between the production and clearance of Aß42. As a result, Aß42 levels gradually rise in in this form of AD, leading to a later age of onset compared to fAD. The accumulation and aggregation of Aß42 in the brain induces synaptic dysfunction, which may partly underlie the manifestation of cognitive deficits in the early stages of AD. In addition, Aß42 oligomers may mediate the deregulation of tau, leading to its hyperphosphorylation and oligomerisation, but also the formation of NFTs in later stages of AD. Pathological tau may also contribute to synaptic dysfunction. Aß42 oligomers and pathological tau synergistically trigger reactive gliosis, neuroinflammation and neuronal dysfunction, leading to selective neuronal loss and the onset of Alzheimer's disease.

1.5.2.1 Evidence for Aß42 accumulation in sAD

Whilst the causal mutations underlying fAD provide a clear mechanism for the accumulation of Aß42 in this type of dementia, the basis for this in sAD is not so clear. However, it is thought that the accumulation of Aß42 in sAD likely involves defective clearance and catabolism of the peptide (Selkoe and Hardy, 2016, Mawuenyega et al., 2010). Aß is normally cleared from the brain by crossing the blood brain barrier (BBB) via interactions with receptors on endothelial cells of the BBB, such as low-density lipoprotein receptor (LDLR) family members (Bell et al., 2007, Kang et al., 2000, Shibata et al., 2000, Deane et al., 2004). LDLR family members are widely recognised as cell surface endocytic receptors that, when expressed by endothelial cells of the BBB, mediate transcytosis (Dehouck et al., 1997, Spuch et al., 2012). Several factors which can interfere with the clearance of Aß at the BBB in AD have been identified. For instance, variation in the genotype of the low-density lipoprotein receptor-related protein (LRP1), which belongs to the LDLR family, has been implicated in AD by genetics studies (Kang et al., 1997, Baum et al., 1998, Hollenbach et al., 1998, Lambert et al., 1998a, Wavrant-DeVrieze et al., 1999). These studies showed that polymorphisms within exon 3 and exon 6 of the gene are associated with increased risk for AD. Although the functional implications of the different LRP1 genotypes in AD are yet to be fully addressed, a recent amyloid-based PET study of patients with AD revealed that the polymorphism in exon 3 was associated with increased Aß load and deposition (Grimmer et al., 2014), thus providing more direct evidence for an effect of LRP1 genotype on Aß clearance. Additionally, a decrease in LRP1 levels has been observed in brain microvessels of aged mice, AD transgenic mice and in post-mortem brains of AD patients (Shibata et al., 2000, Deane et al., 2004), indicating that Aß accumulation in AD could also involve reduced LRP1-mediated transcytosis of Aß at the BBB due to less cell surface LRP1.

Interestingly, a few LRP1 ligands such as α-2-macroglobulin (α-2M) and apoE which are genetically associated with AD (Blacker et al., 1998, Saunders et al., 2003, Corder et al., 1993, Chartier-Hariln et al., 1994), have also been identified as interacting partners of Aß (Hughes et al., 1998, Du et al., 1997, Strittmatter et al., 1993, LaDu et al., 1994). In addition, the risk variants of these genes have been found to be associated with

increased Aß load in human AD brains (Myllykangas et al., 1999, Walker et al., 2000, Grimmer et al., 2010, Drzezga et al., 2009), raising the prospect that these variants increase risk for AD by adversely affecting Aß clearance. Interestingly, it has been hypothesised that the risk-associated polymorphism in α-2M (deletion within the polypyrimidine tract of intron 17) may promote the production of truncated α-2M protein that can still bind to Aß, but cannot be endocytosed via LRP1 (Kovacs, 2000). Although this remains to be confirmed, this would prevent transcytosis of Aß at the BBB and thus reduce clearance of Aß. On the other hand, the effect of apoE isoform on Aß clearance has been more extensively investigated. Earlier studies revealed that apoE2 and apoE3 bind Aß more efficiently than apoE4 (LaDu et al., 1994, Yang et al., 1997, Aleshkov et al., 1997), indicating that apoE4 may confer risk for AD due to being an ineffective chaperone for Aß removal from the brain. Interestingly, it has also been proposed that apoE isoforms may differentially influence clearance of Aß at the BBB due to differing affinity of apoE isoforms for either LRP1 or very-low density lipoprotein receptor (VLDLR)(Deane et al., 2008). This is based upon evidence from an *in vivo* clearance study using receptor-specific antibodies to inhibit receptor function, which found that Aß-apoE4 complexes were cleared from the brain primarily via interaction with VLDLR at a slower rate, whereas Aß and apoE2 or apoE3 complexes underwent rapid clearance by both LRP1 and VLDLR (Deane et al., 2008). Other *in vivo* studies have also demonstrated that Aß clearance is isoform dependent (apoE2>apoE3>apoE4) (Castellano et al., 2011, Bales et al., 2009). These findings suggest that the isoform-specific effect of apoE on Aß clearance may contribute to the differential effect that these isoforms have on AD risk, and further support that reduced Aß clearance plays a role in sAD pathophysiology.

Aß catabolism has been shown to be partly mediated by neprilysin (NEP) and insulin-degrading enzyme (IDE) *in vivo* (Iwata et al., 2001, Newell et al., 2003, Marr et al., 2003, Farris et al., 2003). Interestingly, a reduction in the levels and activities of NEP and IDE has been observed in ageing and AD human brains (Caccamo et al., 2005, Maruyama et al., 2005, Carpentier et al., 2002, Morelli et al., 2004), indicating that Aß catabolism may be affected in AD. Hence reduced degradation of Aß may also play a part in the

accumulation of Aß in AD, alongside many of the aforementioned factors contributing to defective clearance of the peptide.

There is also evidence to suggest that accumulation of Aß in sAD may involve increased production of Aß due to a combination of risk factors affecting APP expression and metabolism (Menendez-Gonzalez et al., 2005). For instance, analysis of APP protein and mRNA levels in AD brains revealed that the there is an increase in the levels of KPI-containing APP variants (APP751 and APP770) relative to APP695 (Preece et al., 2004, Moir et al., 1998, Johnson et al., 1990), which has also been found to correlate with increased Aß deposition (Johnson et al., 1990). These results imply that dysregulation of APP splicing may contribute to the pathogenesis of AD. In addition, it has been suggested that Aß levels may increase in sAD as a result of apoE stimulating APP transcription in neurons through receptor mediated ERK1/2 MAPK signalling (Huang et al., 2017). This was demonstrated by using ES-cell-derived human neurons treated with apoE secreted from glia (Huang et al., 2017). Interestingly, this effect was shown to occur in an isoform-dependent manner too (apoE4>apoE3>apoE2), indicating that apoE isoforms may also influence AD risk through altering APP expression. Collectively, the many factors that can lead to an imbalance between Aß production and clearance clearly support a pivotal role for Aß accumulation in sAD too.

1.5.2.2 Neurotoxic properties of Aß42 oligomers

It is well established that soluble Aß42 oligomers have neurotoxic properties (Walsh and Selkoe, 2007). This is supported by several studies showing that soluble Aß42 oligomers reduce neuronal viability and induce neuronal death *in vitro* (Hoshi et al., 2003, Deshpande et al., 2006, Dahlgren et al., 2002, Zhang et al., 2002, Pike et al., 1991, Pike et al., 1993). Moreover, Aß42 oligomers have been reported to induce memory impairment, cognitive deficits and synaptic dysfunction in AD-transgenic mice producing high levels of Aß42 (Westerman et al., 2002, Lesne et al., 2006, Oddo et al., 2003, Jacobsen et al., 2006), as well as in young wild-type (WT) mice injected with Aß42 oligomers isolated from AD-transgenic mice (Lesne et al., 2006). However, it is increasingly evident that the neurotoxic properties of Aß42 are multifaceted, and can

range from reversible dysfunction of various cellular processes to neuronal death (Walsh and Selkoe, 2007). Numerous studies have since revealed that the toxic effects of Aß42 oligomers in AD may be mediated by a variety of mechanisms such as mitochondrial dysfunction, cytoskeletal defects, oxidative stress, inflammation, membrane alterations and synaptic dysfunction (Carrillo-mora et al., 2014). Notably, Aß42 oligomers have been linked to the deregulation of tau, a key microtubule-associated protein that when hyperphosphorylated, forms the characteristic NFTs in AD. For example, soluble Aß oligomers isolated from the cortices of AD subjects were found to induce hyperphosphorylation of tau at AD-relevant epitopes in rodent hippocampal neuronal cultures (Jin et al., 2011, De Felice et al., 2008), leading to microtubule network dysfunction and neuritic dystrophy (Jin et al., 2011). Similar effects on tau phosphorylation were also observed from application of synthetic Aß42 oligomers to rodent hippocampal neurons and B103 neuroblastoma cells (Zempel et al., 2010, De Felice et al., 2008). Accumulation of Aß oligomers has also been demonstrated to induce tau hyperphosphorylation and NFT formation in AD-transgenic mice (APPOSK/tau-Tg mice) harbouring transgenes for WT human tau and a mutant form of APP (Osaka mutation E693Δ) (Umeda et al., 2014). Importantly, because the Osaka mutation E693Δ prevents the formation of Aß plaques, the results in the study by Umeda and co-workers suggest that the effect was due to the oligomeric form of Aß (Umeda et al., 2014). Collectively, these findings provide compelling evidence for Aß oligomers as a mediator of tau pathology, and further support the concept that Aß42 oligomers are a key toxic agent that may act upstream of tau during the early stages of AD.

1.5.3 Aß and synaptic dysfunction

Although there is a growing body of literature revealing more mechanisms for Aß42-mediated toxicity in AD, the effect of Aß on synaptic dysfunction remains an attractive aspect to explore since it is one of the earliest defects in AD. Loss of synaptic contacts in the neocortex and hippocampus is another well-established neuropathological characteristic of AD and there are reports showing that it is a strong correlate of cognitive decline and memory deficits in AD (Davies et al., 1987, Terry et al., 1991, DeKosky and Scheff, 1990, Scheff et al., 2006, Scheff et al., 2007). Significant reductions

in the total number of synapses are apparent in post-mortem brain tissue from human subjects with early AD/MCI and greater losses in synapse number are observed at the mild AD stage (Scheff et al., 2006, Scheff et al., 2007). Taken together, these findings support the notion that synapse loss is a very early event in AD that worsens as the disease progresses, resulting in the characteristic gradual cognitive decline. Although the mechanisms underpinning synaptic dysfunction and loss in AD are still not fully understood, there is mounting evidence supporting the involvement of Aß42 oligomers (Mucke and Selkoe, 2012). For instance, accumulation of Aß oligomers in AD-transgenic mice has been shown by immunostaining for synaptic markers, to correlate with a reduction in synapse number and this was found to be independent of Aß plaque formation (Mucke et al., 2000, Umeda et al., 2014, Tomiyama et al., 2010, Hsia et al., 1999). In addition, behavioural tests for spatial memory showed that intraneuronal Aß accumulation and synapse loss are also associated with a concomitant decline in cognitive function and memory *in vivo* (Tomiyama et al., 2010, Umeda et al., 2014), thus revealing a relationship between the synaptic changes mediated by Aß and the symptomatic characteristics of AD.

1.5.4 Aß oligomers affect synaptic transmission and plasticity

Electrophysiology experiments have provided further information for the role of Aß at the synapse by showing that Aß oligomers can impair synaptic plasticity, an important process underlying learning and memory that involves a balance between long term potentiation (LTP) and long term depression (LTD). Indeed, accumulation of Aß oligomers has been linked to impairment of LTP in the CA1 region of the hippocampus in AD-transgenic mice (Oddo et al., 2003, Tomiyama et al., 2010). Similarly, synthetic and cell-derived Aß oligomers has been shown to inhibit LTP in the hippocampus of WT rodents following cerebral microinjection of the peptide (Walsh et al., 2002, Walsh et al., 2005, Klyubin et al., 2005) and in rat hippocampal slices exposed to the peptide (Lambert et al., 1998b, Wang et al., 2002, Wang et al., 2004, Townsend et al., 2006). Hence there is considerable evidence to suggest that Aß oligomers may contribute to cognitive and memory deficits through disrupting synaptic plasticity. Intriguingly, a series of studies later revealed that Aß can modulate synaptic transmission in a time-

and concentration- dependent manner (Puzzo et al., 2008, Abramov et al., 2009, Parodi et al., 2010, Puzzo et al., 2011). For example, it was shown that picomolar concentrations of Aß oligomers induced LTP in hippocampal slices and improved performance in tests for memory *in vivo*, whereas nanomolar concentrations inhibited LTP and impaired memory function (Puzzo et al., 2008). These findings led to the notion that Aß may have a physiological role in regulating synaptic transmission that is disrupted in AD due to an imbalance of Aß levels (Mucke and Selkoe, 2012).

1.5.5 Aß oligomers affect synaptic plasticity via pre- and post- synaptic mechanisms

There is mounting evidence to suggest that Aß oligomers can inhibit LTP and facilitate LTD by affecting postsynaptic N-methly-D-aspartate receptors (NMDAR) and α-amino-3-hydroxy-5-methyl-4-isoxazolepropionic acid receptors (AMPAR) (Mucke and Selkoe, 2012, Koffie et al., 2011), which play a pivotal role in the induction of LTP or LTD at the postsynapse. In particular, synaptic NMDAR activation has important involvement in synaptic plasticity because it can trigger either LTP or LTD in response to strong or weak activation respectively, since this affects the levels of postsynaptic calcium influx and NMDAR-dependent signalling cascades (Hunt and Castillo, 2012, Luscher and Malenka, 2012). A large increase in intracellular calcium from strong synaptic NMDAR activation induces NMDAR-dependent signalling that favours LTP, leading to recruitment of AMPARs and growth of dendritic spines (Lu et al., 2001, Toni et al., 1999). Conversely, a small increase in intracellular calcium from weak synaptic NMDAR activation induces NMDAR-dependent signalling that favours LTD (Harney et al., 2006, Cummings et al., 1996), triggering shrinkage of dendritic spines and synaptic loss (Zhou et al., 2004, Shinoda et al., 2010). In addition, activation of extrasynaptic NMDARs by excess glutamate can also induce LTD (Liu et al., 2013). One explanation for the inhibition of LTP and induction of LTD by Aß oligomers has been suggested to involve a partial block in the activity of synaptic NMDARs and the subsequent induction of NMDAR-dependent LTD-related signalling (Shankar et al., 2007). This hypothesis was based on the finding that sustained exposure of rat hippocampal slices to Aß oligomers reduced NMDAR-dependent postsynaptic calcium influx and induced loss of dendritic spines (Shankar et al., 2007). It has also been suggested that Aß oligomers may inhibit LTP and facilitate

LTD by promoting endocytosis of NMDARs and AMPARs at the postsynaptic membrane (Snyder et al., 2005, Hsieh et al., 2006), and by enhancing activation of extrasynaptic NMDARs through disrupting glutamate uptake from the synaptic cleft (Li et al., 2009, Li et al., 2011). Taken together, these findings indicate that Aß oligomers affect synaptic plasticity and promote synapse loss by inhibiting NMDAR-dependent LTP-related signalling and promoting NMDAR-dependent LTD-related signalling at the postsynapse.

There is also evidence to suggest that Aß may affect synaptic plasticity through modulating presynaptic mechanisms too. Several studies have demonstrated that brief application of Aß can positively modulate glutamatergic synaptic transmission at the presynaptic level by increasing the release probability of synaptic vesicles (SVs) (Puzzo et al., 2008, Abramov et al., 2009, Parodi et al., 2010, Puzzo et al., 2011, Brito-Moreira et al., 2011). A possible mechanism for this increase is believed to involve an Aß-induced elevation of intracellular calcium levels required for neurotransmitter release, either via altering the activity of α7-nicotinic acetylcholine receptors (nAChRs) (Puzzo et al., 2008) or by Aß oligomers forming calcium permeable pores in the synaptic membrane (Parodi et al., 2010, Sepulveda et al., 2010). On the other hand, it has also been shown that prolonged exposure of hippocampal slices to Aß oligomers impairs synaptic transmission by reducing the number of SVs near presynaptic active zones required for neurotransmitter release (Parodi et al., 2010). In consideration of this evidence, it is conceivable that enhancement of neurotransmitter release by low levels of Aß oligomers in the early stages of AD could inhibit LTP and promote LTD through desensitisation of NMDARs and activation of extrasynaptic NMDARs by increased glutamate at the synaptic cleft. In addition, it is also possible that chronic exposure and increasing levels of Aß oligomers in the later stages of AD disrupt the maintenance of SVs required for neurotransmitter release, which would ultimately lead to synaptic failure and loss.

1.5.6 Aß oligomers disrupt the regulation of synaptic vesicle dynamics

SVs are organised into three pools at the presynapse: (i) the readily releasable pool (RRP) which contains SVs docked at the active zone, some of which are primed for fusion with the presynaptic membrane for immediate neurotransmitter release upon a stimulus-

triggered calcium influx; (ii) the recycling pool which constitutes endocytosed SVs that replenish the RRP and contribute to neurotransmitter release upon moderate to strong stimulation; and (iii) the reserve pool which acts as a depot and supplies SVs for neurotransmitter release during intense stimulation (Rizzoli and Betz, 2005). As mentioned before, it has been reported that Aß can increase the release probability of the RRP and subsequently promote the release of glutamate into the synaptic cleft at low concentrations or when applied for short durations *in vitro* (Parodi et al., 2010, Russell et al., 2012, Park et al., 2013, Brito-Moreira et al., 2011). One possible mechanism for this effect has been suggested to involve increased priming of SVs in the RRP (Russell et al., 2012). In the study by Russell and co-workers, Aß42 was found to interact with synaptophysin, thereby disrupting the interaction between synaptophysin and VAMP2, two key SV-associated proteins involved in the regulation of SV priming (Russell et al., 2012). Since VAMP2 participates in the formation of the SNARE complex required to prime SVs for exocytosis (Edelmann et al., 1995), it was hypothesised that the interaction between intraneuronal Aß42 and synaptophysin would promote the availability of VAMP2 for SV priming and thus enhance neurotransmitter release. Consistent with this hypothesis, FM dye labelling experiments have shown that acute exposure of neurons to Aß oligomers increases exocytosis of the RRP (Russell et al., 2012, Parodi et al., 2010). These findings suggest that the early enhancement of presynaptic activity and induction of LTP by Aß oligomers may involve increasing SV release by modulating the function of key SV-associated proteins that regulate this process.

On the other hand, chronic exposure (2 hours or more) and/or high concentrations of Aß oligomers has been associated with reduced SV release and defective SV recycling in neurons (Parodi et al., 2010). Indeed, electron micrographs of synapses from neurons exposed to Aß for a prolonged duration revealed a significant reduction in the number of SVs at the presynapse, particularly near active zones, and also signs of incomplete SV endocytosis (Parodi et al., 2010, Kelly and Ferreira, 2007). This is consistent with FM dye labelling experiments showing a slower rate of endocytosis in neurons exposed to Aß oligomers (Parodi et al., 2010, Kelly and Ferreira, 2007, Park et al., 2013). In view of these data, it could be hypothesised that Aß may reduce SV release by causing deficits in

endocytosis since this step is required to replenish the recycling pool and thus the RRP. It is feasible that the subsequent reduction in the RRP and SV release could be a significant contributing factor to LTP inhibition and LTD induction associated with chronic exposure of neurons to high levels of Aß oligomers, since reduced glutamate release would weaken postsynaptic NMDAR activation. Although the molecular basis for this is still poorly understood, there is evidence to suggest that the impairment in endocytosis may be partly mediated through a reduction in the levels of dynamin 1, a GTPase protein that aids endocytosis by pinching off SVs at the plasma membrane for SV recycling (Damke et al., 1994). Indeed, a reduction in the levels of dynamin I has been observed in cultured hippocampal neurons exposed to Aß oligomers for a prolonged duration, but also in brain tissue of human AD subjects and AD-transgenic mice (Yao et al., 2003, Kelly et al., 2005, Kelly and Ferreira, 2006b). There is also evidence to suggest that Aß oligomers promote the proteolytic degradation of dynamin I by inducing the activation of a protease called calpain through sustained calcium influx (Kelly and Ferreira, 2006a). Collectively these findings suggest that Aß oligomers impair SV endocytosis and recycling through altering calcium-dependent signalling cascades that regulate key SV-associated proteins such as dynamin I.

Taken together, these studies reveal that accumulation of Aß oligomers may cause an imbalance between exocytosis and endocytosis, which could lead to the reported depletion of SVs and synaptic failure. These studies also highlight that the Aß disrupts many aspects of the SV cycle, raising the possibility that there may be other proteins involved in SV dynamics that are affected by Aß accumulation. Indeed, loss of other synaptic proteins in Aß-treated neuronal cultures and in brain tissue from human AD subjects has been documented (Parodi et al., 2010, Masliah et al., 2001, Sze et al., 2000). As such, targeting SV dynamics is starting to be considered an attractive therapeutic area (Li and Kavalali, 2017, Ovsepian et al., 2018, Marsh and Alifragis, 2018) and further research into elucidating other SV-associated proteins affected by Aß oligomers is a growing area of interest. In this thesis, evidence is presented indicating that Aß oligomers affect another key SV-associated protein called Synapsin I (SnpI).

1.6 Apolipoprotein E in AD

1.6.1 The apoE gene and protein

The *APOE* gene, located on chromosome 19, is composed of four exons that are separated by three introns (shown in Figure 1-5). Exon 1 and a portion of exon 2 contains 5' untranslated sequence, whilst the remainder of exon 2 and exons 3-4 contain the translated sequence. Two (C/T) single nucleotide polymorphisms (SNPs) within exon 4 of *APOE* give rise to the three main allelic variants: epsilon-2 (ε2), epsilon-3 (ε3), and epsilon-4 (ε4) (described in Figure 1-6). Although the frequency of *APOE* alleles varies considerably amongst populations, the ε3 allele is typically the most common, followed by ε4 and ε2 (Gaugler et al., 2016). The three major protein isoforms produced from these alleles differ at residues 112 and/or 158 as follows: apoE2 (Cys112, Cys158), apoE3 (Cys112, Arg158) and apoE4 (Arg112, Arg158).

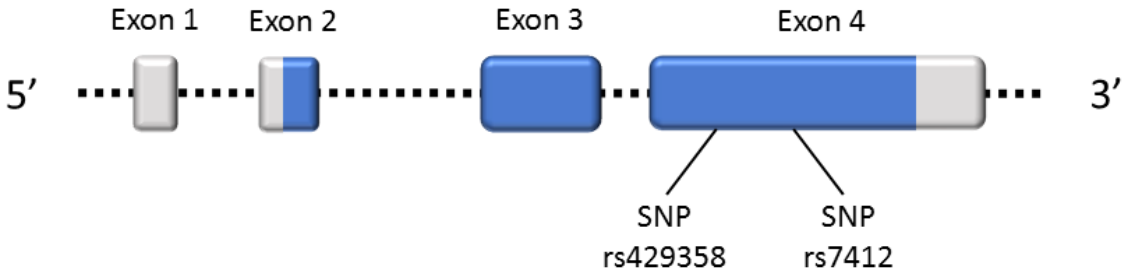

APOE	SNP rs429358	Amino acid residue 112	SNP rs7412	Amino acid residue 158
ε2	TGC	Cys	TGC	Cys
ε3	TGC	Cys	CGC	Arg
ε4	CGC	Arg	CGC	Arg

Figure 1-5 *APOE* gene and polymorphisms encoding apoE2, apoE3 and apoE4
The *APOE* gene contains four exons (boxes) that are separated by three introns. The 5' and 3' untranslated sequence regions are shown in grey, whereas the coding sequence regions are coloured blue. The SNPs which distinguish the three apoE isoforms are located within exon 4 and are listed in the table below the gene schematic.

ApoE is expressed as a 317aa protein containing an 18aa N-terminal signal peptide, which facilitates the transfer of nascent apoE to the rough endoplasmic reticulum (RER). At the RER, the signal peptide is cleaved and the protein undergoes post translational

modifications (PTMs) to form a 299aa glycoprotein of approximately 34kDa (Reardon et al., 1984, Zannis et al., 1984). ApoE protein has two structural domains which are separated by a hinge region (shown in Figure 1-6) (Wetterau et al., 1988). The N-terminal domain spans residues 1-191 and the C-terminal domain contains residues 225-299. The N-terminal domain is composed of four α-helices arranged in an anti-parallel bundle and contains the receptor-binding region (136-150aa) for LDLR and LRP within the fourth helix (Wilson et al., 1991, Innerarity et al., 1983, Lalazar et al., 1988). The C-terminal domain has an amphipathic α-helix structure and contains the lipid-binding region (244-272aa), which enables its interaction with lipoproteins (Rall et al., 1982, Westerlund and Weisgraber, 1993, Dong et al., 1994, Dong and Weisgraber, 1996). There are also two heparin binding sites, one located within the receptor-binding region and the other within the lipid binding region (Weisgraber et al., 1986, Mahley et al., 1979, Saito et al., 2003). Whilst these structural domains are present in all three isoforms, there is evidence to suggest that the tertiary structure differs between them due to isoform-specific domain-domain interactions (Hatters et al., 2006, Frieden and Garai, 2013). Early X-ray crystallography and site-directed mutagenesis experiments comparing apoE4 and apoE3 showed that presence of Arg112 in apoE4 altered the positioning of the Arg61 side chain in helix 2, subsequently enabling it to form a salt bridge with Glu255 in the C-terminus (Dong et al., 1994, Dong and Weisgraber, 1996). Thus, this salt bridge was hypothesised to facilitate an inter-domain interaction in apoE4 that affects the orientation and/or exposure of the lipid-binding region, which was suggested not to occur in apoE3 or apoE2 due to the presence of a cysteine at position 112 (Mahley, 2016b). Fluorescence resonance energy transfer (FRET) studies support this structural model, showing that the N- and C-terminal domains were within closer proximity in apoE4 than in apoE3 (Hatters et al., 2005, Xu et al., 2004). Moreover, mutagenesis of Arg61 to threonine or Glu255 to alanine in apoE4 was found to abolish FRET (Xu et al., 2004), providing further evidence for a salt bridge between these two residues being essential for domain interaction. However, more recent structural studies were unable to confirm the presence of the salt bridge between Arg61 and Glu255 in apoE4 (Williams et al., 2015) and have also demonstrated that domain-domain interactions exist in apoE3, predominately through hydrogen bonds and salt bridges

between helix 3 and 4 of the N-terminus with the C-terminus (Chen et al., 2011b). An alternative model of isoform-specific domain-domain interaction in apoE has also been recently proposed (Frieden and Garai, 2013). In this model, the positive charge of Arg112 in helix 3 of apoE4 was suggested to be propagated to His140 of helix 4 via altering the movement of Arg114, resulting in alterations of the charge distribution of helix 4 and thus modifying interactions between helix 4 of the N-terminus and the C-terminus (Frieden and Garai, 2012). Interestingly, a recent a molecular dynamics simulation study modelling apoE structure showed that mutating Cys112 to Arginine in apoE3 (i.e. converting to apoE4) produced a different distribution of charges in helix 4 (Williams et al., 2015), supporting the model proposed by Frieden and Garai. Although these conflicting data show that the isoform-specific structures of apoE are yet to be resolved, they still support the notion that the polymorphisms cause structural differences between the isoforms, which may be responsible for the differences in their function and by extension, their risk for AD. Indeed, many apoE isoform-dependent effects have been reported and include differences in metabolism of lipids and cholesterol, metabolism of Aß, neuronal/synaptic growth and maintenance, regulation of the inflammation process and neuronal viability and survival (Rebeck, 2017, Mahley, 2016b, Huynh et al., 2017, Kim et al., 2014, Mahley and Huang, 2012).

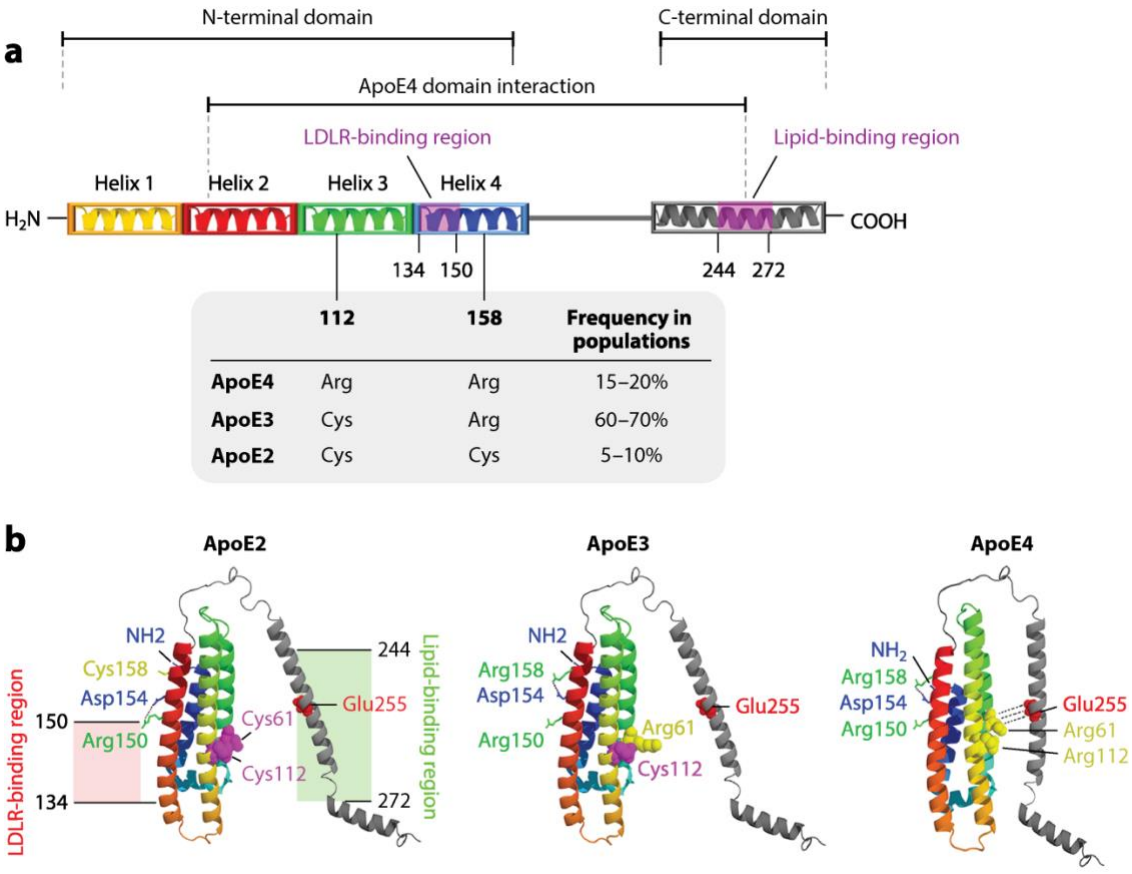

Figure 1-6 ApoE protein structure and isoform-specific protein domain-domain interactions

(A) A linear diagram of the three structural domains of human apolipoprotein E (apoE), which is composed of 299 amino acids. The two polymorphic residues that characterize the three isoforms are located at positions 112 and 158 within the N-terminal domain. (B) Structural models of the three apoE isoforms in the lipid-free state. ApoE3 and apoE4 form a salt bridge between Arg158 and Asp154. However, in apoE2, a salt bridge is formed between Arg150 located in the LDLR-binding region and Asp154. In addition, the N- and C-terminal domains interact in apoE4, whereas this occurs to a lesser extent in apoE2 and apoE3. This interaction is facilitated by the association of the Arg61 side chain, which is oriented into the aqeous environment due to Arg112, with Glu255. Cys112, found in both apoE2 and apoE3, results in a different conformation of Arg61, which has a reduced affinity for domain interaction. Image taken from (Yu et al., 2014).

1.6.2 The role of apoE in phospholipid and cholesterol metabolism in AD

ApoE plays a critical role in the transport and metabolism of lipids and cholesterol in the central nervous system (CNS) as well as in the peripheral circulation. However, the source of apoE and cholesterol is distinct in these two systems since the BBB prevents apoE in the circulatory system from crossing into the CNS (Liu et al., 2012, Dietschy, 2009). Hence apoE and cholesterol in the brain are synthesised locally, predominately by glial cells. In the CNS, apoE is the major apolipoprotein and is primarily expressed by astrocytes to form lipid poor high density lipoprotein (HDL)-like particles upon its secretion and lipidation by ATP- binding cassette transporters (ABC) such as ABCA1 (LaDu et al., 1998, Pitas et al., 1987, Boyles et al., 1985). The HDL-like lipoprotein particles have a discoidal shape and are predominately composed of phospholipid and unesterified cholesterol, although they can gain cholesteryl esters and become spherical on route to the CSF (LaDu et al., 1998). This indicates that HDL-like lipoprotein particles are involved in the trafficking of cholesterol and lipids to neurons and glial cells, but also in the clearance of excess cholesterol from the brain. Although neurons can synthesise cholesterol, they are mostly reliant on cholesterol produced by astrocytes (Nieweg et al., 2009, Pfrieger, 2003). Cholesterol uptake occurs upon endocytosis of the HDL-like lipoprotein particles, which is facilitated by apoE-mediated interaction with members of the LDLR family present on the surface of neuronal membranes (Pfrieger, 2003). This process ensures that neurons have sufficient levels of cholesterol and is essential for a variety of functions such as synaptogenesis, axonal growth, neuronal maintenance and neuronal repair following injury (Mauch et al., 2001, Posse De Chaves et al., 2000, Ignatius et al., 1986, White et al., 2001). In view of this, it is conceivable that defective distribution of cholesterol could contribute to AD pathology. Interestingly, there is evidence to suggest that this may be a possible mechanism for how apoE4 confers risk for AD. Studies have shown that secreted apoE3 associates with more phospholipid and cholesterol than apoE4 in primary cultured astrocytes from transgenic mice expressing human apoE3 or apoE4 (Gong et al., 2002), and also in apoE-transfected Neuro-2a (N2a) cells (Xu et al., 2004). Notably, the reduced phospholipid binding capacity of apoE4 was demonstrated to involve the domain-domain interaction mediated by the salt bridge between Arg61 and Glu255, since expression of mutant human apoE4 with a threonine

at Arg61 to abolish this salt bridge, increased the phospholipid content associated with this isoform (Xu et al., 2004). As such, it was proposed that apoE3 secreted by astrocytes may promote the supply of cholesterol and phospholipids to neurons more efficiently than apoE4 secreted by astrocytes (Gong et al., 2002), and thus apoE4 may increase the risk for AD through reduced delivery of phospholipids and cholesterol to neurons.

Removal of excess cholesterol in neurons is also an important process and this can occur through conversion of cholesterol into 24(S)-hydroxycholesterol, a more lipophilic metabolite that can cross the BBB and be excreted from the body (Lund et al., 2003, Russell et al., 2009), or through cholesterol efflux to lipid-poor apoE by ABCA1 (Minagawa et al., 2009). There is evidence to suggest that cholesterol and lipid metabolism may be dysfunctional in AD, as cholesterol levels have been observed to increase in the AD-vulnerable brain regions in AD subjects in a manner associated with the clinical progression of the disease (Xiong et al., 2008, Cutler et al., 2004). It is notable that many factors could contribute to this such as defective cholesterol efflux by ABCA1, which has been observed in patients with MCI (Yassine et al., 2016). Indeed, several genes encoding proteins involved in cholesterol and lipid metabolism have been associated with increased risk for AD, including *APOE* and *ABCA1* (Karch and Goate, 2015). It is possible that the apoE4 variant may play a role in this by hindering removal of excess cholesterol, since studies have shown that apoE4 is less efficient at promoting cholesterol efflux than apoE3 and apoE2 (Michikawa et al., 2000, Minagawa et al., 2009). This isoform-specific effect on cholesterol efflux has also been attributed to the domain-domain interaction of apoE4 as site-directed mutagenesis of Glu255 to alanine to abolish the Glu255-Arg61 salt bridge was shown to improve apoE4-associated cholesterol efflux (Minagawa et al., 2009). Whilst an imbalance in cholesterol levels may disrupt the aforementioned physiological neuronal functions, it has also been linked to Aß generation, thus providing an additional connection between apoE, cholesterol metabolism and Aß-driven AD pathology. It was shown that excess cholesterol in primary rodent neuronal cultures and N2a cell cultures increased the levels of Aß by promoting the amyloidogenic processing of APP (Marquer et al., 2011, Xiong et al., 2008). Therefore, apoE4 may confer risk for AD through indirectly promoting Aß

production due to cholesterol dyshomeostasis, in addition to disrupting neuronal functions dependent on regulated cholesterol levels.

1.6.3 ApoE Influences Aß-driven AD pathology through multiple pathways

There is increasing evidence showing that the apoE isoforms differentially affect Aß metabolism (Kanekiyo et al., 2014, Wildsmith et al., 2013, Potter and Wisniewski, 2012, Huynh et al., 2017), and thus affect the levels of Aß present in the brain, an established key factor in the pathogenesis of AD. As discussed previously, apoE isoforms have been shown to differentially affect the clearance of Aß (see section 1.5.2.1), such that apoE4 is the least efficient isoform at clearing Aß from the brain. ApoE4 has also been associated with increased Aß generation compared to apoE3 by stimulating amyloidogenic processing of APP either through affecting cholesterol levels (see section 1.6.2), LRP signalling (Ye et al., 2005), or increasing BACE1 levels (Dafnis et al., 2018). It has also been suggested that apoE isoforms can differentially affect the oligomerisation of Aß (Potter and Wisniewski, 2012, Huynh et al., 2017, Tai et al., 2014). Some *in vitro* studies have shown that apoE4 can promote the aggregation of Aß (Hashimoto et al., 2012, Dafnis et al., 2018, Kang et al., 2015), whilst others have shown that apoE isoforms can differentially enhance (apoE4>apoE3>apoE2) the stabilsation of soluble intermediate species of Aß, such as the toxic oligomeric assemblies (Garai et al., 2014, Cerf et al., 2011, Ly et al., 2013, Hashimoto et al., 2012). In support of the latter effect, expression of human apoE4 in transgenic mouse models of AD such as PDAPP, Tg2576 and 5xFAD mice has been reported to delay deposition of Aß as plaques (Holtzman et al., 1999, Fryer et al., 2005, Youmans et al., 2012, Tai et al., 2011) and increase the levels of soluble Aß42, including oligomeric forms (Youmans et al., 2012, Bales et al., 2009). In agreement with these *in vivo* studies, the *APOE4* genotype was found to be associated with increased levels of oligomeric Aß in post-mortem brain tissue of individuals with AD, when compared to those with an *APOE3* genotype (Koffie et al., 2012, Tai et al., 2013). Array tomography experiments have provided further information about the relationship between apoE isoform and Aß, by showing that an *APOE4* genotype is associated with increased synaptic localisation of oligomeric Aß and enhanced synaptic loss in human brains with AD, compared to brains from individuals with an *APOE3*

genotype (Koffie et al., 2012). Interestingly, it was also shown that apoE4 co-localised with Aß oligomers to a greater degree than apoE3 at synapses in post-mortem human brains with AD, but also in primary neuronal cultures exposed to cell-derived Aß oligomers and lipidated apoE3 or apoE4. (Koffie et al., 2012). Hence Koffie and colleagues proposed that apoE4 may enhance the localisation of Aß oligomers at synapses by directly delivering the peptide. Taken together, these findings indicate that apoE4 drives Aß-related AD pathology (discussed in section 1.5.2.2) by promoting the accumulation of the toxic, oligomeric forms of Aß, through affecting the production, clearance, and aggregation of the peptide. Furthermore, they also suggest that apoE4 may facilitate the early stages of AD pathology through trafficking of Aß oligomers to synapses and thus promoting Aß-induced synaptic dysfunction (see section 1.5.3). Hence the differential risk associated with each apoE isoform may be due to the different effects that they have on Aß metabolism.

1.6.4 Intraneuronal apoE as a possible key driver of AD

There is also increasing evidence to suggest that apoE4 (>apoE3) may induce toxicity independently of Aß when expressed in neurons (Huang, 2010, Huang, 2011, Mahley and Huang, 2012, Mahley, 2016a). Although apoE is normally synthesised by glial cells in the brain, studies have demonstrated that neurons can express apoE under conditions of stress. Indeed, kainic-acid induced excitotoxicity in rodents has been reported to stimulate the expression of apoE mRNA and protein in neurons, particularly those located in the hippocampus (Boschert et al., 1999, Xu et al., 2006b, Xu et al., 2008). Furthermore, increased levels of apoE protein and mRNA have been observed in hippocampal and cortical neurons in post-mortem brain tissue from individuals who suffered infarction (Aoki et al., 2003), or had AD (Han et al., 1994b, Bao et al., 1996, Xu et al., 1999). Considering that neurons express apoE in AD-vulnerable brain regions (Padurariu et al., 2012), it is plausible that intraneuronal apoE may play a role in AD and that this may also be isoform-dependent. In support of this, several studies have shown that transgenic mice expressing human apoE4 in neurons display age-dependent behavioural and memory impairments, synaptic defects and other pathologies characteristic of AD such as tau hyperphosphorylation and astrogliosis, whereas

transgenic mice mice expressing apoE3 in neurons do not (Raber et al., 1998, Tesseur et al., 2000b, Tesseur et al., 2000a, Harris et al., 2004, Brecht et al., 2004b). Whilst transgenic mice expressing human apoE isoforms in glial cells (Glial fibrillary acidic protein (GFAP)-apoE and apoE-knock in (KI) mice) have also been reported to show deficits in memory function and synaptic alterations in an isoform- (apoE4>apoE3) and age- dependent manner (Hartman et al., 2001, van Meer et al., 2007, Bour et al., 2008, Rodriguez et al., 2013), it is notable that they do not display other hallmarks of AD neuropathology as observed in transgenic mice expressing apoE4 in neurons (Hartman et al., 2001, Wang et al., 2005). This suggests that the cellular source of apoE, in addition to isoform, affects its role in AD. In agreement with this notion, expression of human apoE4 in astrocytes was shown to be protective against kainic-acid induced excitotoxicity *in vivo* (in GFAP-apoE4 mice), whereas human apoE4 expression in neurons (in Neuron specific enolase (NSE)-apoE4 mice) promoted neuronal death (Buttini et al., 2010). In contrast, expression of human apoE3 by either astrocytes in GFAP-apoE3 mice or neurons in NSE-apoE3 mice was shown to be excitoprotective (Buttini et al., 2010). Thus it was hypothesised that injured or stressed neurons may express apoE as part of a repair response mechanism, which in the case of apoE4 leads to a toxic gain of function instead (Huang, 2010, Huang, 2011, Mahley and Huang, 2012, Mahley, 2016a). Although the basis for this is still not fully understood, emerging evidence indicates that the isoform- and neuron- specific effects of apoE are linked to differential proteolytic processing of the protein (Mahley and Huang, 2012, Mahley, 2016a).

1.6.5 Role for differential proteolytic processing of apoE isoforms in AD pathology

Western blotting studies have shown that apoE is fragmented to a greater extent in AD brains compared to control brains (Harris et al., 2003, Jones et al., 2011, Tamboli et al., 2014, Koffie et al., 2012), raising the prospect of a role for apoE proteolysis in AD. Consistent with this notion, accumulation of Aß in AD-transgenic mouse models was found to be associated with elevated levels of murine apoE fragments (Saul and Wirths, 2016). Moreover, accumulation of Aß in SH-SY5Y cells overexpressing FAD-mutant APP also resulted in enhanced fragmentation of endogenous apoE, supporting a link

between apoE proteolysis and AD-related pathology (Saul and Wirths, 2016). Intriguingly, the level of apoE fragmentation was shown to be greater for apoE4 compared to apoE3 in post-mortem human AD brains (Harris et al., 2003, Jones et al., 2011, Tamboli et al., 2014), revealing differences in the proteolytic susceptibility between the apoE isoforms. Similarly, NSE-apoE4 mice have been reported to display greater levels of apoE fragments than NSE-apoE3 mice (Brecht et al., 2004b). These findings indicate that the loss of protective and gain of toxic function observed in transgenic mice expressing apoE4 in neurons may be related to the increased level of fragments generated due to differential processing. In further support of this, kainic-acid induced excitotoxicity in NSE-apoE4 and NSE-apoE3 mice was found to be associated with increased fragmentation of apoE4 but not of apoE3, indicating that the enhanced proteolysis of apoE4 in injured/stressed neurons may contribute to the increase in neuronal death observed in NSE-apoE4 mice (Brecht et al., 2004b). This isoform-specific processing has been shown to involve domain interaction since using structural molecule correctors to reduce the domain interaction in apoE4-expressing induced pluripotent stem cells (iPSC)-derived neurons and thus induce an apoE3-like structure, decreased the level of apoE4 fragments generated (Wang et al., 2018). Intriguingly, cellular source has also been shown to affect the proteolytic processing of apoE. For instance, apoE fragments were found to accumulate in an age-dependent manner in transgenic mice expressing human apoE in neurons, but not in astrocytes (Brecht et al., 2004b). Hence the neuron-specific effects of apoE in AD were also considered to be related to apoE proteolysis.

1.6.6 The apoE proteolysis hypothesis

Although the identity of apoE fragments is yet to be resolved, there is evidence to suggest that apoE may be cleaved at various sites across the protein to generate a mixture of N- and C-terminal fragments. For instance, microsequencing of ~10kDa apoE fragments purified from amyloid plaques in human brain tissue revealed them to be C-terminal fragments, containing residues 193-299 and 216-299 (Wisniewski et al., 1995). In addition, western blotting of human brain and NSE-apoE mice protein extracts using terminal specific antibodies revealed that high molecular weight apoE fragments

contained the N-terminus and at least the lipid binding region (241-272aa) of apoE, whereas the C-terminus was found to be the main constituent of the low molecular weight fragments (Cho et al., 2001, Huang et al., 2001, Harris et al., 2003, Brecht et al., 2004b, Jones et al., 2011). In view of this, numerous studies have explored the role of apoE fragments on neuronal function by using peptides of apoE, N-terminal-based apoE fragments and C-terminal-based apoE fragments (Crutcher et al., 1994, Marques et al., 1996, Tolar et al., 1997, Tolar et al., 1999, Huang et al., 2001, Harris et al., 2003, Chang et al., 2005, Nakamura et al., 2009). These studies demonstrated that apoE4 fragments but not apoE3 fragments, exert a disruptive effect on neuronal function and viability through a variety of mechanisms including the induction of cytoskeletal defects, tau hyperphosphorylation and mitochondrial dysfunction (discussed in further detail in the following sections). Whilst some of the neurotoxic roles were associated with cell surface receptor binding (Tolar et al., 1997, Tolar et al., 1999, Crutcher et al., 2010, Love et al., 2017), the cytoskeletal and mitochondrial defects were suggested to be mediated by apoE4 fragments in the cytosol (Huang et al., 2001, Chang et al., 2005, Nakamura et al., 2009). Intriguingly, immunofluorescence and MTT assay experiments demonstrated that the receptor binding region was necessary for translocation of apoE fragments to the cytosol, whilst exposure of the lipid binding region was required for mitochondrial localisation and dysfunction (Chang et al., 2005). Collectively these findings gave rise to the apoE proteolysis hypothesis illustrated and described in Figure 1-7.

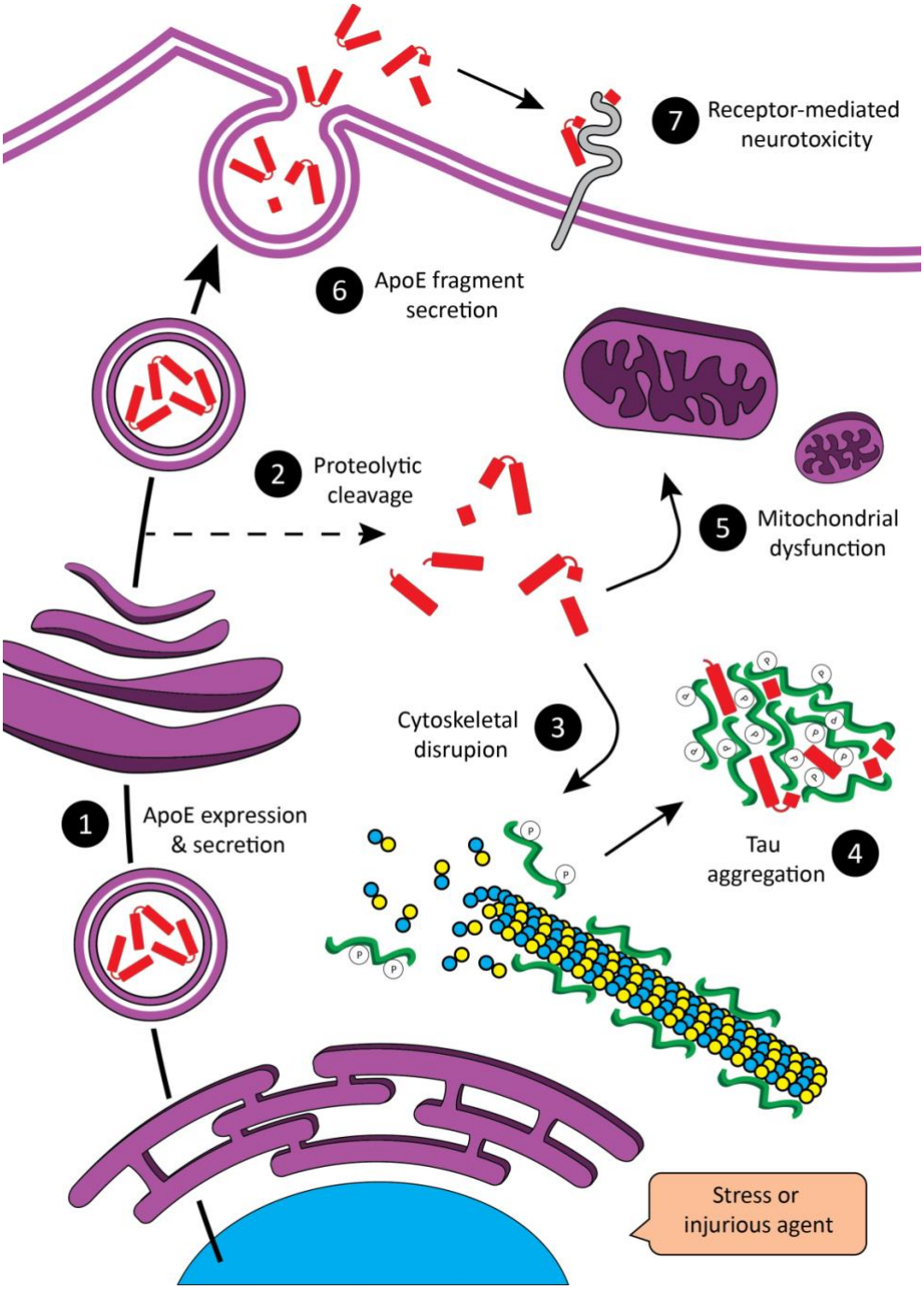

Figure 1-7 ApoE proteolysis hypothesis

ApoE expression and secretion in neurons (step 1) is triggered by stress or injury as a protection response mechanism, which may occur through increased levels of oligomeric Aß42 and/or cholesterol dyshomeostasis in the context of AD. However, apoE undergoes neuron-specific proteolysis in an isoform-dependent manner (apoE4>apoE3>apoE2) due to domain interaction (step 2), facilitating a toxic gain of function. Fragments escape the secretory pathway and induce tau hyperphosphorylation and subsequently destablisation of microtubules (step 3), aggregation of tau and formation of p-Tau tangles (step 4) and mitochondrial dysfunction (step 5). Fragments may also be secreted (step 6) and induce neurotoxicity via LDLR-family mediated signalling cascades (step 7). ApoE fragmentation may also lead to a loss of function since secretion of full length apoE facilitates lipid distribution, a key aspect of neuronal repair.

1.6.7 ApoE4 and fragments disrupt the cytoskeletal network

The neuronal cytoskeleton comprises three highly organised and interacting structural polymers: microtubules, neurofilaments and microfilaments. Together they provide architectural support and play key roles in neurite outgrowth, organelle organisation, signalling and intracellular transport (Kevenaar and Hoogenraad, 2015). As mentioned previously, there is evidence to suggest that apoE4 expression and fragmentation in neurons affects the cytoskeletal network. Indeed, neuronal expression of human apoE4 in transgenic mice has been associated with dysfunctional axonal transport, axonal degeneration and loss of dendritic spines (Tesseur et al., 2000b, Tesseur et al., 2000a, Jain et al., 2013), which are hallmarks of cytoskeletal disruption. Moreover, stable expression and exogenous application of apoE4 in N2a cells has been reported to inhibit neurite outgrowth and enhance depolymerisation of microtubules *in vitro* (Nathan et al., 1995, Nathan et al., 1994, Bellosta et al., 1995). It has been suggested that these effects may partly be due to apoE4-mediated deregulation of tau, since this protein plays an important role in microtubule polymerisation and stability (Mahley and Huang, 2012). Hyperphosphorylation of tau in AD is thought to reduce the affinity of tau for microtubules and thus promote microtubule disassembly (Mahley and Huang, 2012, Alonso et al., 1994). One line of evidence linking apoE to tau in AD is the co-localisation of apoE with tau tangles, as shown by immunohistochemistry of post-mortem AD brains and down syndrome-AD brains (Rohn et al., 2012, Day et al., 2016). Furthermore, the expression of apoE4 but not apoE3 in neurons of transgenic mice and in iPSC-derived neurons has been found to induce hyperphosphorylation of tau and formation of p-Tau tangles (Tesseur et al., 2000a, Tesseur et al., 2000b, Brecht et al., 2004b, Wang et al., 2018), thus demonstrating that apoE4 may be a key driver of tau deregulation and tau-related pathology in AD. Notably, tau hyperphosphorylation was not observed in GFAP-apoE4 mice (Brecht et al., 2004b), supporting the idea that this effect is associated with apoE4 fragments. In fact, expression of C-terminally truncated apoE4 (1-272aa) in neurons has also been reported to induce tau hyperphosphorylation and tau-tangles *in vitro* and *in vivo* (Huang et al., 2001, Harris et al., 2003), which provides more direct evidence that apoE4 fragments contribute to the deregulation of tau and thus cytoskeletal dysfunction.

It is also possible that apoE4 disrupts the cytoskeletal network through the deregulation of neurofilament proteins too. Neurofilament proteins have been identified as components of NFTs in the AD brain and have been shown to be abnormally phosphorylated in AD (Dahl et al., 1982, Cork et al., 1986, Haugh et al., 1986, Wang et al., 2001). In support of an association between apoE and neurofilament deregulation in AD, immunofluorescence experiments have demonstrated that apoE localises to a small portion of neurofilament-positive NFTs in the AD brain (Dickson et al., 1997). In addition, neuronal expression of apoE4 in Thy1-apoE transgenic mice has been shown to induce the accumulation of neurofilament-containing inclusion bodies in dilated axons (Tesseur et al., 2000a). There is also evidence to suggest that neuron-specific apoE proteolysis may contribute to the disruption of the neurofilament network in AD. Indeed, overexpression studies using C-terminally truncated apoE (1-272aa) have been shown to induce the formation of tangle-like structures that are immunoreactive for both apoE and neurofilament protein in neuroblastoma cells but not non-neuronal cells (Huang et al., 2001, Ljungberg et al., 2002). Hence there is considerable evidence to support a role for neuronal apoE4 expression and proteolysis in cytoskeletal disruption and thus neuronal dysfunction in AD.

1.6.8 ApoE4 and fragments disrupt bioenergetics pathways

The generation of energy in the form of adenosine triphosphate (ATP) by various bioenergetics pathways is a core requirement for cellular function. Mitochondrial oxidative phosphorylation, which involves redox reactions mediated by protein complexes within the electron transport chain (ETC), is the most efficient of these pathways. It is notable though that oxidative phosphorylation is dependent on the supply of electrons from Nicotinamide adenine dinucleotide (NADH) and flavin adenine dinucleotide ($FADH_2$), electron carriers that are produced alongside ATP either through the metabolism of glucose or pyruvate via glycolysis and the citric acid cycle respectively. Hence disruption to either of these processes can have downstream effects on mitochondrial function and thus the production of ATP to meet energy demands. Intriguingly, early PET studies using a glucose analogue called fluorodeoxyglucose-18F (FDG) identified that glucose metabolism was reduced in the AD brain (Friedland et al.,

1985, Minoshima et al., 1997, Ibanez et al., 1998, Hirono et al., 1998), raising the idea that impaired bioenergetics pathways may contribute to AD. Later FDG PET studies have since shown that glucose metabolism is modulated by *APOE* genotype in a gene dose-dependent manner, whereby *APOE4* is associated with glucose hypometabolism (Mosconi et al., 2004b, Mosconi et al., 2004a, Mosconi et al., 2005, Drzezga et al., 2005). This led to the notion that *APOE* genotype may alter the risk for AD through affecting cellular bioenergetics in the brain. In support of this, comparisons of gene expression in hippocampi from post-mortem *APOE4* and *APOE3* AD brains by microarray analysis and Serial Analysis of Gene Expression (SAGE) revealed that apoE4 expression is associated with the downregulation of transcripts involved in mitochondrial oxidative phosphorylation and energy metabolism (Xu et al., 2006a, Xu et al., 2007a). However, It is worth noting that multiple factors can affect the integrity and molecular preservation of post-mortem tissue, such as conditions prior to death and the duration between death and sample processing (Ferrer et al., 2008). Therefore, conclusions derived from studies involving post-mortem brain tissue need to be validated either *in vivo* or *in vitro*. Interestingly, a recent histochemistry study found that the activity of cytochrome oxidase (complex IV of the ETC) was lower in post-mortem brain tissue of *APOE4* carriers (Valla et al., 2010), a deficit that has also been observed in brain tissue from individuals with AD and AD transgenic mouse models (Valla et al., 2001, Valla et al., 2007). Similarly, cytochrome oxidase levels and other proteins involved in oxidative phosphorylation, glycolysis and the citric acid cycle were found to be lower in synaptosomal extracts from GFAP-apoE4 mice compared to GFAP-apoE3 mice (Shi et al., 2014), indicating that secreted apoE may also contribute to deficits in bioenergetics pathways and thus mitochondrial dysfunction. There is also evidence to support a role for neuronally expressed apoE4 and fragments in mitochondrial dysfunction. Indeed, a reduction in the protein levels of mitochondrial ETC complexes has been observed in cultured neurons from NSE-apoE4 mice, but not NSE-apoE3 mice (Chen et al., 2011a). Chen and colleagues also reported lower gene expression and protein levels of mitochondrial ETC complexes in apoE4-expressing N2a cells compared to apoE3-expressing N2a cells. Interestingly, the levels of mitochondrial ETC complexes did not differ in cultured astrocytes from GFAP-apoE3 or GFAP-apoE4 mice, indicating that

apoE-mediated mitochondrial dysfunction is neuron-specific (Chen et al., 2011a). Although the basis for this effect is still not fully understood, C-terminally truncated apoE4 (1-272aa) has been demonstrated to localise to the mitochondria and interact with ETC complexes (Chang et al., 2005, Nakamura et al., 2009), indicating that fragments of apoE4 may exert a direct effect on mitochondrial function. In addition to binding to components of complex III and complex IV (Nakamura et al., 2009), expression of full length apoE4 and the apoE4 1-272 fragment in N2a cells have been shown to reduce the activity of these complexes (Nakamura et al., 2009, Chen et al., 2011a), thus supporting a role for neuronal apoE4 expression and apoE4 fragments in reduced bioenergetics and mitochondrial dysfunction. Notably, Nakamura and colleagues found that the apoE4 1-272aa fragment impaired the enzymatic activities of complex III and IV to a greater extent compared to full length apoE4, which they proposed may be related to the stronger association between the apoE4 1-272aa fragment with the ETC complexes. Although the evidence discussed so far suggests that apoE4 disrupts mitochondrial function, studies assessing the effect of apoE4 expression on mitochondrial respiration and membrane potential have provided conflicting results. For instance, studies using Fluorescence-activated cell sorting (FACS) analysis of MitoTracker Deep Red 633 staining and oxygen consumption measurements in apoE4-expressing N2a cells have shown that full length apoE4 expression impairs mitochondrial membrane potential and respiration (Chang et al., 2005, Chen et al., 2011a). In contrast, FACS analysis of JC-1 staining and an ATP synthase activity assay did not reveal any significant differences in the mitochondrial membrane potential or synthesis of ATP in N2a cells expressing full length apoE4 or the apoE4 1-272aa fragment (Nakamura et al., 2009). Nonetheless, these findings implicate apoE4 expression and proteolysis in the downregulation of bioenergetics pathways and induction of mitochondrial dysfunction, but also highlight that the mechanisms underpinning this are yet to be determined.

1.7 Research project aims

1.7.1 Project 1

It is well established that the accumulation of soluble Aß42 oligomers in the brain is associated with synaptic dysfunction (Mucke and Selkoe, 2012, Shankar and Walsh, 2009), an early event in AD that is linked to the manifestation of cognitive deficits (Arendt, 2009). Recent evidence indicates that this may be partly mediated through alterations in SV dynamics at the presynapse (Li and Kavalali, 2017, Ovsepian et al., 2018), although the molecular mechanisms behind this are still poorly understood. Interestingly, a small branch-chained fatty acid called valproic acid (VPA), which is used in the treatment of bipolar disorder and epilepsy, has been shown to attenuate Aß42-induced disruption of SV recycling and to have therapeutic benefit in AD transgenic mouse models (Williams and Bate, 2016, Qing et al., 2008, Zhang et al., 2010). In view of this, the overall aim of project 1 was to investigate the molecular basis of oligomeric Aß42-mediated disruption to SV dynamics and to test whether VPA could be used as a treatment in this context. Following the identification of SnpI as a protein that may be deregulated by Aß42 oligomers, the work in project 1 specifically aimed to:

1. Determine whether Aß42 oligomers deregulate SnpI;
2. Determine whether VPA exerts a neuroprotective effect through SnpI regulation.

1.7.2 Project 2

Numerous studies have investigated the processing and function of apoE4 in neurons, many using apoE3 for comparison (as discussed in this chapter), to elucidate the mechanisms underpinning the increased risk for AD associated with the *APOE4* genotype. However, the neurobiology of the apoE2 isoform has been largely overlooked, even though genetics studies have revealed that this variant is associated with reduced risk for AD. Whilst mounting evidence has shown that the differential effects of apoE3 and apoE4 on neuronal function are linked to differences in proteolytic susceptibility (apoE4>apoE3) and thus different levels of bioactive fragments (Huang, 2010, Huang, 2011, Mahley and Huang, 2012, Mahley, 2016a), it is not known whether the 'protective' role of apoE2 is related to this. Furthermore, although the sequence identity of apoE fragments is still unresolved, several studies have explored the effect of 'apoE

fragments' *in vitro* and *in vivo* using apoE peptides, and N-/C-terminally truncated variants of apoE (Crutcher et al., 2010, Huang et al., 2001, Harris et al., 2003, Chang et al., 2005, Nakamura et al., 2009). Although these studies have shown that neuronal expression of some proposed apoE4 fragments induces toxicity through disruption of the cytoskeletal network and mitochondrial dysfunction, the existence of these fragments *in vitro* or *in vivo* is yet to be verified. In addition, the effect of full length apoE2 or apoE2 fragment expression on neuronal function and viability has not been investigated. Therefore the overall aim of project 2 was to explore the effect of apoE isoform, using the three major isoforms, on the proteolytic processing of apoE, neuronal function and viability. The specific aims addressed in this research are as follows:

1. Determine whether all three apoE isoforms are differentially processed when expressed in neurons by characterising the proteolytic susceptibility and fragment profiles of each isoform;
2. Characterise the composition of apoE fragments for all isoforms for insight into potential function and differences amongst apoE isoforms;
3. Determine whether the effect of apoE expression on neuronal function is isoform-dependent by using cytoskeletal-associated proteins as indicators of cytoskeletal function and also viability assays as a final indicator of toxic versus protective effects.

Chapter 2 Materials and Methodology

2.1 Chemicals

All chemicals used for the work in this thesis were purchased from Sigma-Aldrich Company Ltd (Poole, Dorset, UK) unless otherwise stated.

2.2 Bacterial Cultures and Plasmids

All bacterial work was carried out using aseptic technique.

2.2.1 Bacterial Culture Reagents and Solutions

Solution	Components and Procedure
Lysogeny Broth (LB) media	20g of LB (Lennox) powder was suspended in 1L of ddH_2O, autoclaved for 15 minutes at 121°C to sterilize and allowed to cool to room temperature before supplementing with antibiotic (if desired)
LB agar	35g of LB (Lennox) powder was suspended in 1L of ddH_2O, autoclaved for 15 minutes at 121°C to sterilize and allowed to cool to for approximately 1 hour before supplementing with antibiotic
50mg/ml ampicillin	Ampicillin powder was dissolved in water at 50mg/ml, filter sterilised through a 0.2µm membrane and stored at -20°C

Table 2-1 Recipes for solutions used in bacterial culture work

2.2.2 Culturing One Shot TOP10 Electrocomp E. Coli

Top 10 E. Coli competent cells (Invitrogen) were collected using a sterile loop and the bacteria streaked out on antibiotic-free LB agar plates, which were then incubated overnight at 37°C. A single colony was picked using a sterile pipette tip and used to create a starter culture by inoculating 5mL of antibiotic-free LB media (see Table 2-1 for formulation). Following incubation of the starter culture for approximately 16 hours at 37°C with horizontal shaking (200 rpm), 5mL of the overnight culture was added to 500mL of antibiotic-free LB media in a vented conical flask. This culture was incubated at 37°C with horizontal shaking (200 rpm) until the optical density measured between 0.2 and 0.5 (typically between the first and third hour of incubation), as determined by using a spectrophotometer at a wavelength of 600nm. The bacterial suspension was pelleted at 3000 rpm for 5 minutes at 4°C and the supernatant was removed. The cell pellet was resuspended in 50mL of sterile 100mM $CaCl_2$ by adding a small volume first, and then

adding the remainder. The bacteria were incubated on wet-ice for 20 minutes before pelleting again by centrifugation at 4000 rpm for 5 minutes at 4^{o}C. Following removal of the supernatant, the pelleted bacteria were resuspended in 5mL (1/10th of the original volume) sterile ice-cold 100mM $CaCl_2$/15% glycerol. The bacterial suspension was aliquoted (50 and 250µl) into pre-cooled 1.5mL micro centrifuge tubes on dry-ice immersed in methanol and stored at -80^{o}C.

2.2.3 Plasmids

Plasmid	Source
pCMV-ApoE2	Generated in Professor Dickon's lab (Centre of Biomedical Sciences, Royal Holloway University of London) and provided by PhD Candidate Lugi Zhang (National University of Singapore)
pCMV6-AC-ApoE3	Purchased from Cambridge Bioscience (#SC319433)
pCMV-ApoE4	Generated in Professor Dickon's lab and provided by PhD Candidate Lugi Zhang (National University of Singapore)
pCMV4-ApoE3	Provided by Professor Tadafumi Hashimoto (University of Tokyo)
pCMV4-ApoE3-NT Δ192-299	Provided by Professor Tadafumi Hashimoto (University of Tokyo)
pCMV4-ApoE3-CT Δ1-192	Provided by Professor Tadafumi Hashimoto (University of Tokyo)
pCMV4-ApoE3 Δ243-299	Provided by Professor Tadafumi Hashimoto (University of Tokyo)
pCMV4-ApoE3 Δ243-272	Provided by Professor Tadafumi Hashimoto (University of Tokyo)
pCMV4-ApoE3 Δ272-299	Provided by Professor Tadafumi Hashimoto (University of Tokyo)
pRRL-CMV-Wpre	Provided by Professor Rafael Yáñez-Muñoz (Centre of Biomedical Sciences, Royal Holloway University of London)
pRRL-CMV-ApoE2-Wpre	Generated by Jade Marsh via subcloning the apoE2 cDNA from pCMV-ApoE2 into the pRRL-CMV-Wpre backbone
pRRL-CMV-ApoE3-Wpre	Generated by Jade Marsh via subcloning a segment of the apoE3 cDNA (containing the SNPs) from pCMV6-AC-ApoE3 into the pRRL-CMV-ApoE4-Wpre backbone that had the complimentary segment (containing SNPs encoding for the apoE4 isoform) removed
pRRL-CMV-ApoE4-Wpre	Generated by Jade Marsh via subcloning the apoE4 cDNA from pCMV-ApoE4 into the pRRL-CMV-Wpre backbone
pRRL-CMV-GFP-Wpre	Provided by Professor Rafael Yáñez-Muñoz (Centre of Biomedical Sciences, Royal Holloway University of London)
pMDLgD64V (packing plasmid)	Provided by Professor Rafael Yáñez-Muñoz (Centre of Biomedical Sciences, Royal Holloway University of London)
pRSV-REV (Rev plasmid)	Provided by Professor Rafael Yáñez-Muñoz (Centre of Biomedical Sciences, Royal Holloway University of London)
pMD2-VSV-G (Env plasmid)	Provided by Professor Rafael Yáñez-Muñoz (Centre of Biomedical Sciences, Royal Holloway University of London)

Table 2-2 Plasmids used in this study

2.2.3.1 Plasmid DNA Elution from Filter Paper

The plasmids provided by PhD candidate Lugi Zhang and Professor Tadafumi Hashimoto (listed in Table 2-2) were received on filter paper. A section of filter paper containing the dried plasmid DNA (marked by a circle) was excised using clean scissors, transferred to a 1.5ml micro centrifuge tube, and the plasmid DNA eluted by adding 50µl of 1X TE buffer. Following incubation for 5mins at room temperature, 5µl of the eluted plasmid DNA was used to transform bacteria to prepare plasmid stocks.

2.2.3.2 Sanger Sequencing of Plasmid DNA

To validate apoE genotype and fidelity of apoE complementary DNA (cDNA) sequences of plasmids, sequencing was performed by using the Mix2Seq Kit (Eurofins Genomics) according to manufacturer's instructions. Plasmids were sequenced using four primers (shown in Table 2-3) to ensure sequence coverage. Sequence data was acquired from Eurofins MWG and analysed using alignment tools in CLC Main Workbench software (Qiagen).

Primer Name	Sequence (5'-3')
Human apoE 1_F	GAGGGCGCTGATGGACGA
Human apoE 1_R	CGCCACCTGCTCCTTCACCTC
Human apoE 2_F	AAATCGGAACTGGAGGAAC
Human apoE 2_R	CTTCTGCAGGTCATCGGC

Table 2-3 Primers used to sequence apoE cDNA

2.2.4 Transformation of Bacteria using Heat Shock

One Shot TOP10 Electrocomp E. Coli (250µl stock aliquots) were thawed on wet-ice, and 50µl working aliquots were prepared using pre-cooled micro centrifuge tubes. 5µl of plasmid DNA (10-100ng) was added to 50µl of bacteria, and gently mixed by flicking the tube. After incubation on wet-ice for 30 minutes, the bacteria were subjected to a heat-shock by incubation in a water bath at 42^{o}C for 30 seconds, followed by a brief incubation on wet-ice for 2 minutes. Next, 250µl of antibiotic-free LB was added to the bacterial suspension and incubated for 1 hour at 37^{o}C with horizontal shaking at 200rpm. During this incubation step, agar selection plates were warmed up to room temperature. Lastly, 50µl of bacterial suspension was streaked onto LB-agar plates

containing 50µg/mL ampicillin and incubated at 37°C overnight. The remaining 200µl of transformed bacteria were stored at 4°C for plating a larger culture volume, if a greater bacterial density was required.

2.2.5 Culturing of transformed Bacteria

For starter cultures, 5ml of ampicillin-supplemented (50µg/ml) LB media was inoculated with either a single colony picked from an LB-agar plate using a pipette, or bacteria from a glycerol stock that was collected using a plastic loop. The starter culture was incubated at 37°C for approximately 16 hours with shaking (200rpm) and used for either preparing glycerol stocks, inoculating maxi cultures, or plasmid DNA purification.

For maxi cultures, 500µl of a starter culture was used to inoculate 250ml of ampicillin-supplemented (50µg/ml) LB media in a 1L sterile vented conical flask, which was then incubated at 37°C for approximately 16 hours with shaking at 200rpm. The bacterial suspension was centrifuged at 3250 rpm for 30 minutes at 4°C, the supernatant removed and the bacterial pellet either used for plasmid purification same day or stored at -20°C.

2.2.6 Bacterial Glycerol stocks

Glycerol stocks were prepared by adding 500µl of bacterial culture from the previous step to 500µl of sterile 80% glycerol (40% final) in 1.5mL screw-top tubes. After brief mixing and snap-freezing on dry-ice, the tubes were transferred to -80°C for long-term storage.

2.2.7 Extraction and Purification of Plasmid DNA

Prior to plasmid DNA extraction and purification of starter cultures, bacterial suspensions were pelleted by centrifugation at 3250rpm for 10mins at 4°C and processed immediately, or stored at -20°C and processed at a later date. Plasmid DNA was extracted and purified from pelleted starter cultures using the QIAprep Spin Miniprep Kit (Qiagen, #27104) as per the manufacturer's instructions.

For plasmid DNA extraction and purification from maxi cultures, bacterial suspensions were initially pelleted by centrifugation at 3250rpm for 30mins at 4°C. Plasmid DNA was extracted and purified from pelleted maxi cultures using the GenElute HP Endotoxin-Free Plasmid Maxiprep Kit (#NA0410, Sigma Aldrich) as per the manufacturer's instructions with some exceptions. These exceptions include further drying of the binding column by centrifugation at 5000 x g for 10mins at 4°C and eluting the plasmid DNA using 1mL of E-Toxate free water. The plasmid DNA was concentrated using the ethanol precipitation method. 100µl of NaOAc (3M stock) and 2.5mL ethanol (100% stock) was added to the 1ml of eluted plasmid DNA, which was mixed and incubated overnight at -80°C. The plasmid DNA was pelleted by centrifugation for 2hrs at 5000 x g at 4°C. The supernatant was carefully removed and the remaining ethanol allowed to evaporate. The pellet was resuspended using 100-500µl of E-Toxate free water to give concentrations between 0.5µg-1µg/µl, and the plasmid DNA was stored at -20°C.

2.2.8 Nucleic Acid Quantification and Purity Assessment

The concentration and quality of plasmid DNA was assessed by using a Nanodrop Spectrophotometer. 260/280 and 260/230 ratios near 1.8 and 2.0-2.2 respectively indicated a relatively pure DNA sample.

2.3 Subcloning and Generation of Lentiviral Vectors

2.3.1 Reagents and Solutions

Agarose (Invitrogen)

10,000X SYBR Safe DNA Gel Stain (Invitrogen, #S33102)

DNA Loading Buffer Blue (Bioline, #BIO-37045)

Hyperladder I (Bioline, #BIO-33025)

T4 DNA ligase (Promega, #M1801)

DNAse I (Promega, #M6101)

Diethyl pyrocarbonate (DEPC)-treated water (Ambion, #AM9906)

Cell culture grade water (Sigma, #W-3500)

Endotoxin-free TE buffer (Qiagen)

Solution	Components
50X Tris-acetate-EDTA (TAE) buffer	242g Tris base, 57.1ml glacial acetic acid and 100ml of 500mM EDTA (pH 8.0) made up to 1L with ddH_2O
2X HEPES-buffered saline (HBS) solution	100mM HEPES, 281mM NaCl, 1.5mM Na2HPO4, pH to 7.12, filter sterilised through a 0.2µm membrane and stored at -20°C
2.5M CaCl2	14.3g of $CaCl_2$ dissolved in 50ml ddH_2O and stored as 1ml aliquots at -80°C
8mg/ml Polybrene	Hexadimethrine bromide (polybrene) was dissolved in ddH_2O at 8mg/ml, filter sterilised through a 0.2µm membrane and stored as aliquots at 4°C

Table 2-4 Recipes of solutions used for subcloning and lentiviral vector production

2.3.2 General Molecular Subcloning Protocols

2.3.2.1 Agarose Gel Electrophoresis

Agarose gel electrophoresis was routinely used to separate DNA for restriction mapping analysis and to facilitate isolation of plasmid DNA fragments for purposes such as subcloning. 1% agarose gels were prepared by adding 0.7g of agarose to 70ml of 1X TAE buffer, and the mixture dissolved by using a microwave and frequent agitation. Once fully dissolved, 7µl of SYBR Safe DNA Gel Stain (1X final) was added to the gel mixture, which was agitated once more and allowed to cool briefly, before being poured into a casting tray. After the gel had set at room temperature, it was placed into an electrophoresis tank and submerged in 1X TAE buffer. DNA samples were mixed with DNA Loading Buffer Blue (1X final) and added into wells alongside 5µl of Hyperladder I (Bioline, #BIO-33025). 1% agarose gels were run at 65V for approximately 1 hour and the DNA bands visualised by using ultraviolet light in a GELDOC system.

2.3.2.2 Endonuclease Restriction Digests

Endonuclease restriction digests were performed to validate plasmid DNA sequences, as based on digest product profiles, and for subcloning purposes. Suitable single and multiple cutting endonuclease restriction enzymes were identified by using SnapGene software, which also provided predicted digest product profiles. All restriction enzymes used were purchased from NEB. The compatible buffers and digest reaction conditions for each restriction enzyme were found on their respective product pages on the NEB website.

A digest reaction for restriction mapping analysis of plasmids was typically performed by combining 1µg of plasmid DNA, 10 units of enzyme and 1X compatible enzyme buffer in a total reaction volume of 20µl, which was made up with DEPC-treated water. Negative control reactions were also prepared by excluding the enzyme from the reaction. The digest reactions were incubated at 37^{o}C for 5 hours. To examine the digest profiles for each plasmid, digest products and uncut plasmid DNA samples were resolved by agarose gel electrophoresis, which involved loading 10µl of the digested plasmid DNA mixed with 3µl loading buffer (1X final) and 2µl DEPC-treated water.

2.3.2.3 Extraction and Purification of DNA

Desired DNA was isolated from agarose gels by using white light to visualise DNA bands and a sterile blade to excise individual DNA bands from the gel. Once the gel section containing the desired DNA was transferred to a 2.0ml sterile Eppendorf micro centrifuge tube, the DNA was extracted and purified using the QIAquick Gel Extraction Kit (Qiagen, #28704), according to the manufacturers protocol with some additional steps. These include: 2 repeats of Step 5, 2 repeats of Step 7, and elution of the cDNA (Step 9) using 50µl DEPC-treated water.

2.3.2.4 DNA Ligation Reaction

Ligation reactions were performed by using T4 DNA ligase (Promega, #M1801) to catalyse phosphodiester linkage between 100ng of linearised destination plasmid and increasing amounts of insert DNA, as based on destination plasmid to insert molar ratios of 1:1, 1:3, 1:5 and 1:10. The ligation reactions were prepared by mixing the plasmid DNA and insert DNA with 1µl of T4 DNA Ligase enzyme, 2µl of T4 DNA Ligase buffer (1X final) and DEPC-treated water to bring the total reaction volume to 20µl. Two negative control reactions were also prepared by excluding the insert DNA and T4 DNA ligase from the reaction, or by excluding the insert only. These negative control reactions were carried out to provide an indication of contamination from uncut plasmid DNA and background re-ligation of plasmid DNA. The ligation reactions were carried out in a PCR thermocycler, which incubated the mixture at 22^{o}C for 1 hour, followed by 15^{o}C for 16 hours, and then 4^{o}C until the ligated product was transformed into bacteria.

2.3.3 Subcloning of pRRL-CMV-ApoE2-Wpre and pRRL-CMV-ApoE4-Wpre

pCMV-ApoE2 and pCMV-ApoE4 were used as sources for apoE2 and apoE4 cDNA, whilst the pRRL-CMV-Wpre plasmid (lentiviral transfer plasmid) was used as the destination plasmid for apoE2 and apoE4 cDNA. Preparative restriction digests to liberate apoE2 and apoE4 cDNA were performed by mixing 10µg of the plasmid DNA with 5µl of XbaI (100 units) and 5µl of CutSmart Buffer (NEB, #B7204S) in a total reaction volume of 50µl, which was made up with DEPC-treated water. The digestion reaction to linearise pRRL-CMV-Wpre was run in parallel and performed by mixing 2µg of the plasmid DNA with 1µl of XbaI (20 units) and 4µl of CutSmart Buffer (NEB, #B7204S) in a total reaction volume of 40µl, which was made up with DEPC-treated water. The digest reactions were incubated at 37^{o}C for 10 hours, followed by an enzyme inactivation step of 65^{o}C for 20 minutes, and a storage step of 4^{o}C.

Linearised pRRL-CMV-Wpre was next treated with Antarctic Phosphatase (NEB, #M0289S) to de-phosphorylate the exposed 5' ends of the DNA backbone, preventing re-ligation of the plasmid. The de-phosphorylation reaction was prepared by mixing the linearised plasmid DNA with 5µl of Antarctic Phosphatase Reaction Buffer (1X final), 4µl of Antarctic Phosphatase (20 units; 10 units/1µg of approximately 6Kb plasmid DNA) and 1µl of DEPC-treated water to bring the reaction volume to 50µl. The sample was incubated at 37^{o}C for 15 minutes, and the Antarctic Phosphatase enzyme was heat inactivated by incubation at 70^{o}C for 5 minutes. The linearised pRRL-CMV-Wpre plasmid was stored at 4^{o}C until further processing.

The digest profiles of the samples were examined by resolving 400ng of plasmid DNA on 1% agarose gels to ensure that the plasmids were fully digested. Once complete digestion was verified, the remaining volume of digested pCMV-ApoE2 and pCMV-ApoE4 samples were resolved by agarose gel electrophoresis to enable isolation of apoE2 and apoE4 cDNA respectively. Following extraction and purification of the cDNA, ligation reactions were performed as described in sections 2.3.2.3 and 2.3.2.4 respectively. The ligated products were transformed into bacteria (see section 2.2.4), and single colonies

were picked and starter cultures prepared (see section 2.2.5). Plasmid DNA was extracted and purified from starter cultures and restriction mapping analysis was performed to verify the generation of pRRL-CMV-ApoE2-Wpre and pRRL-CMV-ApoE4-Wpre plasmids. Sanger sequencing (see section 2.2.3.2) was also used to validate the genotype of apoE cDNA and to confirm sequence fidelity. Once the plasmid sequences were fully validated, maxi cultures were prepared from an aliquot of starter culture, glycerol stocks were made, and the plasmid DNA was extracted and purified.

2.3.4 Subcloning of pRRL-CMV-ApoE3-Wpre

pCMV6-AC-ApoE3 was used the source for the desired apoE3 cDNA segment, whilst the pRRL-CMV-ApoE4-Wpre plasmid was used as the destination plasmid for the apoE3 cDNA segment. A preparative restriction digest to liberate the apoE3 cDNA segment was performed by mixing 10µg of pCMV6-AC-ApoE3 with 2µl of BlpI (40 units), 2µl of SbfI-HF (40 units), 2µl of XhoI (40 units) and 7µl of CutSmart Buffer (NEB, #B7204S) in a total reaction volume of 70µl, which was made up with DEPC-treated water. The digestion reaction to remove the corresponding apoE4 cDNA segment from pRRL-CMV-ApoE4-Wpre was run in parallel and performed by mixing 10µg of pRRL-CMV-ApoE4-Wpre with 2.5µl of BlpI (50 units), 2.5µl of SbfI-HF (50 units) and 6µl of CutSmart Buffer (NEB, #B7204S) in a total reaction volume of 60µl, which was made up with DEPC-treated water. The digest reactions were incubated at 37^{o}C for 4 hours, followed by an enzyme inactivation step of 65^{o}C for 20 minutes, and a storage step of 4^{o}C. 400ng of plasmid DNA from the digest reactions was resolved on 1% agarose gels to ensure completion of the reaction. Once the digest profiles were verified, the remaining volume of the digest reactions were also resolved by agarose gel electrophoresis to enable isolation of the desired apoE3 cDNA segment and the linearised pRRL-CMV-ApoE-Wpre backbone. These were extracted and purified from the agarose gel and ligation reactions were set up, as described in sections 2.3.2.3 and 2.3.2.4 respectively. The ligated products were transformed into bacteria (see section 2.2.4), and single colonies were picked and starter cultures prepared (see section 2.2.5). Plasmid DNA was extracted and purified from starter cultures and restriction mapping analysis was performed to verify the generation of the pRRL-CMV-ApoE3-Wpre plasmid. Sanger sequencing (see section

2.2.3.2) was also used to confirm sequence fidelity and to verify that the apoE cDNA was of APOE3 genotype. Once the plasmid sequence was fully validated, a maxi culture was prepared from an aliquot of starter culture, a glycerol stock was made, and the plasmid DNA was extracted and purified.

2.3.5 Production, Purification and Concentration of apoE-expressing Lentiviral Vectors

Lentiviral vectors were produced by calcium phosphate transfection of a four-plasmid system into HEK293T cells. HEK293T cells were seeded at 10^6 cells/plate on 15cm^2 plates (Corning, #430599) containing 25ml growth media and incubated for 4 days to allow cells to become 80-90% confluent. The media was then replaced with 20ml of fresh growth media 2 hours before transfection. The plasmids were mixed in a molar ratio of 1:1:1:2 (packaging:rev:envelope:transfer) by using 12.5µg of pMDLg-D64V, 6.25µg of pRSV-REV, 7µg of pMD2.VSV-G and 25µg of either pRRL-CMV-ApoE2-Wpre, or pRRL-CMV-ApoE3-Wpre, or pRRL-CMV-ApoE4-Wpre or pRRL-CMV-GFP-Wpre. TE buffer was added to bring the total volume up to 112.5µl, followed by the addition of 1012.5µl of cell culture grade water to dilute the TE buffer to 0.1X. Once 125µl of 2.5M $CaCl_2$ was added, the solution was vortexed and incubated at room temperature for 5 minutes. Whilst the DNA/$CaCl_2$ mix was vortexed again, 1250µl of 2X HBS was added in a dropwise manner. The mix was then immediately added to the HEK293T growth media, and the plates gently agitated in a circular motion before incubation at 37^{o}C with 5% CO_2. After a 16-hour incubation period, the media was replaced with 18ml of fresh growth media. At 2 days post-transfection, the media was harvested to collect the lentiviral vectors and replaced with 18ml of fresh growth media to allow for a final harvest at 3 days post-transfection. Harvested media was centrifuged at 2500rpm for 10 minutes at room temperature and then filtered through a 0.22µm filter (Nalgene, #190-2520) to remove cellular debris. To concentrate the lentiviral vectors, filtered media was transferred to high speed polyallomer centrifuge tubes (Beckman Coulter, #326823) and centrifuged in a SW32.1Ti rotor at 50,000 x g for 2 hours at 4^{o}C. The supernatant was completely removed and the concentrated virus was resuspended in either 50µl of serum-free Dulbecco's Modified Eagle's Medium (DMEM) if media was concentrated from one plate, or 100µl of serum-free DMEM if media was combined and concentrated

from 2 plates. The vector prep was then transferred to a sterile 1.5ml micro centrifuge tube and spun at 4000rpm for 10 minutes at room temperature to pellet any remaining cellular debris. The supernatant was transferred to sterile micro centrifuge tubes and the vector prep was adjusted to 10mM $MgCl_2$ before the addition of either 1 or 2µl of DNase I (5 units/ml). The vector prep was then incubated at 37°C for 30 minutes to allow the enzyme to degrade any plasmid DNA contamination. Lentiviral vector stocks were aliquoted and stored at - 80 °C until use.

2.3.6 Titration of Lentiviral Vectors by qPCR

HeLa cells were seeded at 10^5 cells per well on 6-well plates containing 2ml of growth media per well and incubated at 37°C and 5% CO_2. The next day, the media was replaced with 1ml of pre-warmed DMEM containing 16µg/ml polybrene (to enhance transduction efficiency), followed by the addition of either 1ml of DMEM containing lentiviral vector diluted to 1:2000 and 1:20000, or 1ml of DMEM only (negative control). The plate was gently agitated in a circular motion before being returned to the incubator. At 1 day post-transduction, cells were harvested. This was carried out by first washing cells with 1ml pre-warmed 1X DPBS, and then adding 150µl of trypsin-EDTA to each well. The plate was returned to the incubator for 5 minutes to allow for cells to detach from wells and then the trypsin was inactivated by the addition of 850µl pre-warmed growth media. The cell suspension was transferred to sterile micro centrifuge tubes and pelleted by centrifugation at 1000rpm for 5 minutes. Once the supernatant was removed, DNA was extracted and purified from the cell pellets by using a DNeasy Blood and Tissue kit (QIAGEN, #69504), as per manufacturer's instructions.

Quantitative polymerase chain reaction (qPCR) was used to measure the lentiviral DNA copy number and total cell number so that the viral titre could be calculated. To measure the lentiviral DNA copy number, qPCRs were set up using forward/reverse primers against the lentiviral late reverse transcripts (LTRs) and LTR standards of known copy numbers (10^2, 10^3, 10^4, 10^5, 10^6, 10^7). Total cell numbers were determined by using forward/reverse primers against the ß-actin and HeLa standards of known total cell numbers (10^1, 10^2, 10^3, 10^4, 10^5, 10^6). The primers used are listed in Table 2-5.

Primer Name	Sequence (5'-3')
LTR Forward Primer	TGTGTGCCCGTCTGTTGTGT
LRT Reverse Primer	GAGTCCTGCGTCGAGAGAGC
ß-actin Forward Primer	TCACCCACACTGTGCCCATCTACGA
ß-actin Reverse Primer	CAGCGGAACCGCTCATTGCCAATGG

Table 2-5 Primers used in qPCRs to determine lentiviral titre

The standard reactions were performed in triplicate, whilst all other reactions were performed in duplicate. The reactions for LTR-based qPCRs were prepared by mixing forward and reverse primers for LRTs (final concentration of 100nM), 1X SYBR Green qPCR master mix, either 5µl of DNA sample or LTR standard and DEPC-treated water to make the total volume up to 20µl. The reactions for ß-actin-based qPCRs were prepared by mixing forward and reverse primers for ß-actin (final concentration of 100nM), 1X SYBR Green qPCR master mix, either 5µl of DNA sample or HeLa standard and DEPC-treated water to make the total volume up to 20µl. Negative control reactions were also prepared by either excluding the DNA sample or by using DNA extracts from mock cells (not transduced). The qPCR reaction tubes were placed into a Rotor-Gene Q (QIAgen, UK) thermocycler and incubated using the following conditions: 50^{o}C for 2 minutes, 95^{o}C for 10 minutes and then 50 cycles of 95^{o}C for 15 second followed by 60^{o}C for 1 minute. Final lentiviral vector titres were based on the average of the vector titres derived from DNA extracts of HeLa cells transduced using 2x vector dilutions (1:2000 and 1:20000). The vector titres were calculated using the following formula:

$$Vector\ titre = \frac{lentiviral\ DNA\ copy\ number}{number\ of\ total\ cells} \times 10^5 cells \times vector\ dilution\ factor$$

2.4 Tissue Culture

All cell culture work was carried out using aseptic technique and sterile plasticware inside a class II laminar flow hood.

2.4.1 General Cell Culture Reagents and Solutions

1X Dulbecco's phosphate buffered saline solution (DPBS) (Gibco, #14190-094)

1X TrypLE Express Enzyme (Thermofisher, #12604-021)

1X ice-cold Hanks' Balanced Salt Solution (HBSS) (Gibco, #14175-053)

2.4.2 Cell Culture Media Reagents

2.4.2.1 Media for Neuro-2a and SH-SY5Y Cell Culture

General growth media for Neuro-2a and SH-SY5Y cells:

DMEM (Sigma, #D5796)

Foetal Bovine Serum (FBS), 10% final (Gibco, #10500-064)

Glutamax, 1X final (Gibco, #35050-061)

Penicillin-streptomycin, 100 units/ml final concentration (Gibco, #15140122)

2.4.2.2 Media for HEK293T Cell Culture

General HEK293T growth media:

DMEM (Sigma, #D5796)

FBS, 10% final (Gibco, #10500-064)

Glutamax, 1X final (Gibco, #35050-061)

Penicillin-streptomycin, 100 units/ml final concentration (Gibco, #15140122)

Growth media used to culture HEK293T cells for lentiviral generation:

DMEM with Glutamax (Gibco, #31966-021)

FBS, 10% final (Gibco, #10500-064)

Penicillin-streptomycin, 100 units/ml final concentration (Gibco, #15140122)

2.4.2.3 Media for HeLa Cell Culture

Growth media used to culture HeLa cells for lentiviral titration:

DMEM (Gibco, #31966-021)

FBS, 10% final (Gibco, #10500-064)

Penicillin-streptomycin, 100 units/ml final concentration (Gibco, #15140122)

2.4.2.4 Media for Primary Neuronal Culture

Dissociation media:

DMEM (Gibco, #21969-035)

TrypLE Express Enzyme, 0.1X final (Thermofisher, #12604-021)

DNase I, 100µg/ml final

Plating media:

DMEM (Gibco, #21969-035)

FBS, 5% final (Gibco, #10500-064)

Glutamax, 1X final (Gibco, #35050-061)

Penicillin-streptomycin, 100 units/ml final concentration (Gibco, #15140122)

Media was filtered through a 0.45µm filter.

Growth media:

Neurobasal Medium (Gibco, #21103-049)

B-27 Supplement, 1X final (Gibco, #17504-044)

Glutamax, 1X final (Gibco, #35050-061)

Penicillin-streptomycin, 100 units/ml final concentration (Gibco, #15140122)

Media was filtered through a 0.45µm filter.

2.4.2.5 Freezing Media for Cell Lines

DMEM (Sigma, #D5796)

FBS, 20% final (Gibco, #10500-064)

Dimethyl sulfoxide (DMSO), 10% final (Sigma, #D8418)

Freezing media was filtered through a 0.2µm filter and stored at 4^{o}C protected from light.

2.4.3 Cell Lines

The N2a cell line (murine neuroblasts) was kindly provided by Professor Robin Williams (Centre of Biomedical Sciences, Royal Holloway University of London).

The SH-SY5Y cell line (human neuroblasts) was kindly provided by Professor George Dickson (Centre of Biomedical Sciences, Royal Holloway University of London).

The HEK293T (human embryonic kidney cells) and HeLa cell lines were kindly provided by Professor Rafael Yáñez-Muñoz (Centre of Biomedical Sciences, Royal Holloway University of London).

2.4.4 Thawing Cells

Frozen cells were retrieved from storage in liquid nitrogen and thawed immediately by submersion of cryovial in a 37^{o}C water bath for approximately 2 minutes. Once thawed, cells were transferred into a 15ml falcon containing 9ml of pre-warmed growth media and pelleted by centrifugation at 3000 rpm for 5 minutes. Once the media was carefully aspirated, the cell pellet was resuspended in 1ml of pre-warmed growth media. After the addition of another 14ml of growth media, the cell suspension was seeded in a T75cm^3 flask (Corning, #430372). Cells were incubated at 37^{o}C and 5% CO_2 and subcultured when they reached approximately 70-80% confluency.

2.4.5 Sub-culturing Cell Lines

Cell confluency was monitored daily and when cells were approximately 70-80% confluent, they were sub-cultured. The growth media was aspirated and cells were washed with pre-warmed 1X DPBS. The cells were then detached from the flask by addition of 1ml TrypLE and incubation at 37^{o}C and 5% CO_2 for 1-2 minutes. Following neutralisation of TrypLE by the addition of 9ml pre-warmed growth media, the cell suspension was pelleted by centrifugation at 3000 rpm for 5 minutes. The media was carefully aspirated and cells were initially resuspended in 1ml of pre-warmed growth media, followed by an additional 9ml of pre-warmed growth media. A fraction of the suspended cells (1:10 for N2a, HEK293T and HeLa cells; 1:5 for SH-SY5Y cells) was then seeded in a new T75cm^3 flask (Corning, #430372) and a further 14ml of pre-warmed

growth media was added. Cells were incubated at 37°C and 5% CO_2 and subcultured when they reached approximately 70-80% confluency.

2.4.6 Cryogenic Storage of Cell Lines

Once cells reached 70-80% confluency, the media was aspirated and the cells washed with 1X DPBS. Cells were then detached from the flask by the addition of 1ml TrypLE and incubation at 37°C and 5% CO_2 for 1-2 minutes. After inactivation of TrypLE by the addition of 9ml pre-warmed growth media, cells were counted using a haemocytometer. Cells were pelleted by centrifugation at 3000 rpm for 5 minutes and resuspended at $1x10^5$ cells per ml in cold freezing media. Cells were quickly aliquoted at 1ml per vial into screw-top cryovials and gradually cooled overnight at -80°C, prior to long-term storage in a liquid nitrogen tank.

2.4.7 Primary Rat Hippocampal Neuronal Culture

All animal experiments were performed according to Home Office regulations and in compliance with the Animals Scientific Act 1986. Poly-D-lysine coated 6-well cell culture plates were prepared in advance by the addition of 1ml cold poly-D-lysine (100µg/ml final in 0.1M Borate buffer) to wells and incubation of plates at 4°C overnight. The wells were washed three times with sterile H_2O, air-dried and exposed to ultraviolet light for 20 minutes in the class II laminar flow hood, prior to dissection and plating of hippocampal neurons. Brains were obtained from embryonic day 18 (E18) Sprague Dawley rats and suspended in ice-cold 1X HBSS. The hippocampi were isolated and the meninges removed by dissection. The hippocampi were gently triturated in 5ml of pre-warmed dissociation media and incubated at 37°C for 10 minutes. After further trituration by pipetting, TrypLE was inactivated by the addition of 1.5ml FBS. Cells were pelleted by centrifugation at 1500 rpm for 3 minutes and the media carefully aspirated. Cells were resuspended in 1ml of pre-warmed plating media and counted using a haemocytometer. A further volume of pre-warmed plating media was added to yield a concentration of 2.5×10^5 cells/ml and cells were seeded at a density of 5×10^5 cells/well on coated 6-well plates or 2.5×10^5/well on coated 12-well plates. The plating media was replaced at 1 day in vitro (DIV) with pre-warmed growth media (2ml/well in 6

well plates and 1ml/well for 12 well plates) and the cultures were maintained at 37°C and 5% CO2. Additional growth media (500µl/well in 6 well plates and 250µl/well in 12 well plates) was added to cultures on a weekly basis from 7 DIV and cultures were routinely used for experiments at 18-21DIV.

2.5 Cell Treatments and Assays

2.5.1 Reagents and Solutions

Lipofectamine 2000 Transfection Reagent (Invitrogen, #11668-019)

FuGENE HD Transfection Reagent (Promega, #E2311)

The NUCLEAR-ID® Blue/Red cell viability reagent (GFP-CERTIFIED®) (Enzo, #ENZ-53005)

Solution	Components
HEPES-buffered saline wash solution	44mM NaCl2, 2mM CaCl2, 1mM MgCl2, 20mM HEPES (pH 7.4), and 30mM glucose
5ml/ml MTT solution	250mg MTT powder (Sigma, #M2128) dissolved in 250ml 1XPBS, filter sterilised through a 0.2µm membrane, aliquoted and stored at -20°C protected from light
1M VPA	1.66g of Valproic acid sodium salt dissolved in 10ml of ddH_2O, filter sterilised through a 0.2µm membrane and stored at 4°C

Table 2-6 Recipes of solutions used in cell treatments

2.5.2 Preparation of Aß42 peptide

Synthetic Aß42 peptide (American peptides) was reconstituted using 100% dimethyl sulfoxide (DMSO) to a stock concentration of 1mM, which was immediately stored as aliquots at -80 °C. Working stocks were also prepared by diluting the peptide with sterile 1X DPBS to a final concentration of 300µM and stored as aliquots at -80 °C. For use in cell treatments, working aliquots were thawed on wet-ice and diluted to a final concentration of 300nM in pre-warmed neuronal growth media and used immediately.

2.5.3 Acute treatment of neurons with Aß42 peptide and VPA

Primary hippocampal neurons were allowed to mature (18-21 DIV) in 6-well plates prior to treatment. Two 6-well plates were used on the same day for each experimental replicate. To ensure consistency for each replicate, both cultures were treated with the reagents made on that day. All cell culture reagents were warmed to 37°C prior to use.

Initially, the growth media of neuronal cultures was replaced with either 2ml of pre-warmed neuronal growth media alone or containing 300nM Aß42. Neurons were incubated for 30 minutes at 37 ^{o}C with 5% CO_2 to allow for internalisation of the peptide, as has been demonstrated to occur within this time-frame (Russell et al., 2012, Marsh et al., 2017). The growth media was replaced again with either 2ml of fresh pre-warmed growth media alone, or containing 1 or 10mM VPA. After a 2-hour incubation period at 37 ^{o}C with 5% CO_2, the media was aspirated and the cells washed with a HEPES-buffered saline wash solution. Next, neurons were depolarised by adding 2ml of a pre-warmed HEPES-buffered saline wash solution containing 70mM KCl and incubation for 5 minutes at 37 ^{o}C with 5% CO_2. Protein was then either extracted immediately or after a recovery period following depolarisation. Recovery of neurons from depolarisation involved a wash step using pre-warmed HEPES-buffered saline wash solution to remove residual KCl and a final incubation period of 15 minutes at 37 ^{o}C with 5% CO_2 in fresh growth media. Recovered neurons were washed with ice-cold HEPES-buffered saline wash solution prior to protein extraction.

2.5.4 Transient Transfection of HEK293T Cells using Lipofectamine 2000

HEK293T cells were seeded at a density of 5 x 10^5 cells/well in 6-well plates containing 2ml of growth media per well and incubated at 37 ^{o}C with 5% CO_2. Cells were transfected when 80-90% confluent, typically 1 day after seeding. For transfection of HEK293T cells in 6-well plates, a ratio of 5µl Lipofectamine 2000 Transfection reagent: 2.5µg of plasmid DNA per well was used. Initially, the Lipofectamine 2000 Transfection reagent and plasmid DNA were both diluted using 100µl of serum-free DMEM and incubated for 5 minutes at room temperature. The reagent and plasmid DNA were then combined and incubated for 20 minutes at room temperature so that plasmid DNA-lipid complexes could form. This mixture was then added to wells in a dropwise manner and the plate agitated and incubated again at 37 ^{o}C with 5% CO_2. At 24 hours post-transfection, the media was replaced with fresh pre-warmed growth media to reduce transfection-related toxicity and incubated for a further 24 hours. Cells were processed 48-hours post transfection. The volumes were scaled up according to the number of

wells to be transfected and included a 20% excess of the total volume needed to allow for pipetting error.

2.5.5 Transient Transfection of N2a Cells using Lipofectamine 2000

For protein analysis experiments, N2a cells were seeded at a density of 5 x 10^5 cells/well in 6-well plates containing 2ml of growth media per well. For immunocytochemistry experiments, 12-well plates were first prepared by allowing 18mm coverslips (washed in 100% ethanol overnight) to air dry in wells (1 coverslip/well), followed by exposure of plates containing coverslips to ultraviolet light for 20 minutes. Next, N2a cells were seeded at a density of 2 x 10^5 cells/well in 12-well plates containing 1ml of growth media per well. Cells were incubated at 37 ^oC with 5% CO_2 and transfected when 70-80% confluent, typically 1 day after seeding. For transfection of N2a cells in 6-well plates, a ratio of 10µl of Lipofectamine 2000 Transfection reagent: 2.5µg of plasmid DNA per well was used, whereas in 12-well plates, a ratio of 4µl of Lipofectamine 2000 Transfection reagent: 1µg of plasmid DNA per well was used. Initially, the Lipofectamine 2000 Transfection reagent and plasmid DNA were both diluted using 100µl of serum-free DMEM for 6-well plates and 50µl of serum-free DMEM for 12-well plates. After a 5-minute incubation at room temperature, the reagent and plasmid DNA were then combined and incubated for 20 minutes at room temperature so that plasmid DNA-lipid complexes could form. This mixture was then added to wells in a dropwise manner and the plate agitated and incubated again at 37 ^oC with 5% CO_2. At 24 hours post-transfection, the media was replaced with fresh pre-warmed growth media to reduce transfection-related toxicity and incubated for a further 24 hours. Cells were processed 48-hours post transfection. The volumes were scaled up according to the number of wells to be transfected and included a 20% excess of the total volume needed to allow for pipetting error.

2.5.6 Transient Transfection of SH-SY5Y Cells using FuGENE

SH-SY5Y cells were seeded at a density of 5 x 10^5 cells/well in 6-well plates containing 2ml of growth media per well and incubated at 37 ^oC with 5% CO_2. Cells were transfected when 80-90% confluent, typically 48 hours after seeding. For transfection of

SH-SY5Y cells in 6-well plates, a ratio of 10µl FuGENE HD Transfection reagent: 2.5µg of plasmid DNA per well was used. Initially, the plasmid DNA was diluted using 200µl of serum-free DMEM and incubated for 5 minutes at room temperature. The FuGENE HD Transfection reagent was then added to the diluted plasmid DNA and the mixture was incubated for 15 minutes at room temperature so that plasmid DNA-FuGENE complexes could form. This mixture was then added to wells in a dropwise manner and the plate agitated and incubated again at 37 ^{o}C with 5% CO_2. At 24 hours post-transfection, the media was replaced with fresh pre-warmed growth media to reduce transfection-related toxicity and incubated for a further 24 hours. Cells were processed 48-hours post transfection. The volumes were scaled up according to the number of wells to be transfected and included a 20% excess of the total volume needed to allow for pipetting error.

2.5.7 Transduction of Primary Neuronal Cultures with Lentiviral Vectors

18-21DIV neuronal cultures on 6-well plates and 12-well plates were transduced with apoE and GFP-expressing lentiviral vectors respectively. Lentiviral vectors were diluted to the desired multiplicity of infection (MOI) in 100µl of pre-warmed serum-free DMEM per well. This was scaled up according to the number of wells to be transduced and included a 20% excess of the total volume needed to allow for pipetting error. The diluted lentiviral vector was added dropwise to the neuronal culture media and the plates were gently agitated prior to incubation again at 37^{o}C with 5% CO_2. Neuronal cultures were processed at either 3 or 5 days post-transduction.

2.5.8 MTT Assay

The MTT (3-(4,5-dimethylthiazol-2-yl)-2,5-diphenyltetrazolium bromide) tetrazolium reduction assay is a colorimetric assay that provides an indication of cell viability, as based on the ability of metabolically active cells to reduce MTT to form formazan crystals that have an absorbance maximum near 570nm.

An aliquot of MTT solution was thawed at room temperature when the assay was to be carried out. 100µl of the MTT solution was added to the culture media of either N2a or SH-SY5Y cells seeded at a density of 2 x 10^5 cells/well onto 12-well plates containing 1ml

of growth media per well so that the final concentration of MTT was 0.5mg/ml. The plates were gently agitated to ensure mixing of the MTT solution within the media and then covered with foil to protect the MTT solution from light. The plates were incubated at 37^{o}C with 5% CO_2 for either 2 hours for N2a cells or 4 hours for SH-SY5Y cells and primary neurons to allow for conversion of MTT to formazan, a purple precipitate. The media was carefully aspirated and the plates were air dried at room temperature, protected from light. To solubilise the formazan crystals, 500µl of DMSO was added to each well and the plate was agitated on a horizontal shaker at 200rpm, protected from light. Once the formazan crystals had dissolved, 75µl of the formazan solution from each well was added to wells on a 96-well plate, followed by 75µl of DMSO for use as a blank. The absorbance values were read at 570nm using a GloMax-Microplate Multimode Reader (Promega, USA).

2.5.9 Live/Dead Assay

The NUCLEAR-ID Blue/Red cell viability reagent facilitates the determination of live and dead cell populations due to the differing permeability and fluorescence of the two nucleic acid dyes. The blue fluorescent nucleic acid dye is cell permeable and so labels all nuclei, whereas the red fluorescent nucleic acid dye is cell impermeable, labelling only nuclei of apoptotic and compromised cells.

NUCLEAR-ID Blue/Red cell viability reagent was first diluted 1:1000 in pre-warmed 1X DPBS. The growth media was aspirated from cells seeded onto 12-well plates and 300µl of the diluted reagent was added to each well to cover the cell monolayer. The plates were covered in foil to protect the dyes from light and then incubated for 15 minutes at 37^{o}C with 5% CO_2. The staining solution was aspirated from the wells and cells were processed for either FACS analysis or for fluorescence microscopy analysis as in the sections below.

2.5.9.1 Live/Dead Assay Procedure for FACS Analysis

350µl of 1X TrypLE was added to each well and cells were incubated at 37^{o}C with 5% CO_2 for approximately 1 minute. Once cells were detached from wells, 1ml of pre-warmed

growth media was added to each well to neutralise the trypsin and the cell suspension was transferred to micro centrifuge tubes. Cells were pelleted by centrifugation at 1000 x g for 1 minute at room temperature and the supernatant was removed. Cells were resuspended in 100µl of cold 1X DPBS and transferred to FACS tubes on wet-ice for analysis by FACS.

The BD FACSCanto II (BD Biosciences, UK) flow cytometer was first calibrated using Cell Sorting Set-up Beads (Invitrogen, #C16509) suspended in FACSFlow Solution as standards. The samples were processed by the flow cytometer using a medium flow rate and a 10,000 event count. The voltages for AmCyan-A and PerCP-Cy5 were used to detect blue and red fluorescence respectively. Control cells were used to set-up the gates to determine particular cell populations. The forward scatter (FSC) versus side scatter (SSC) of events was plotted and gated (P1 gate) to exclude cellular debris as shown in Figure 2-1, A. The area (FSC-A) versus height (FSC-H) of events from within the P1 gate was also plotted to facilitate selection of only single cells (P2 gate; Figure 2-1, B). These events were then plotted on an AmCyan-A versus PerCP-Cy5 histogram (Figure 2-1, C) to define live and dead cell populations as based on whether cells exhibited blue fluorescence only (Q4) or blue and red fluorescence (Q2) respectively. The data were analysed using BD FACSDiva software (BD Biosciences, UK) and the percentage of dead cells was based on the number of cells within Q2 over the number of cells in Q2+Q4.

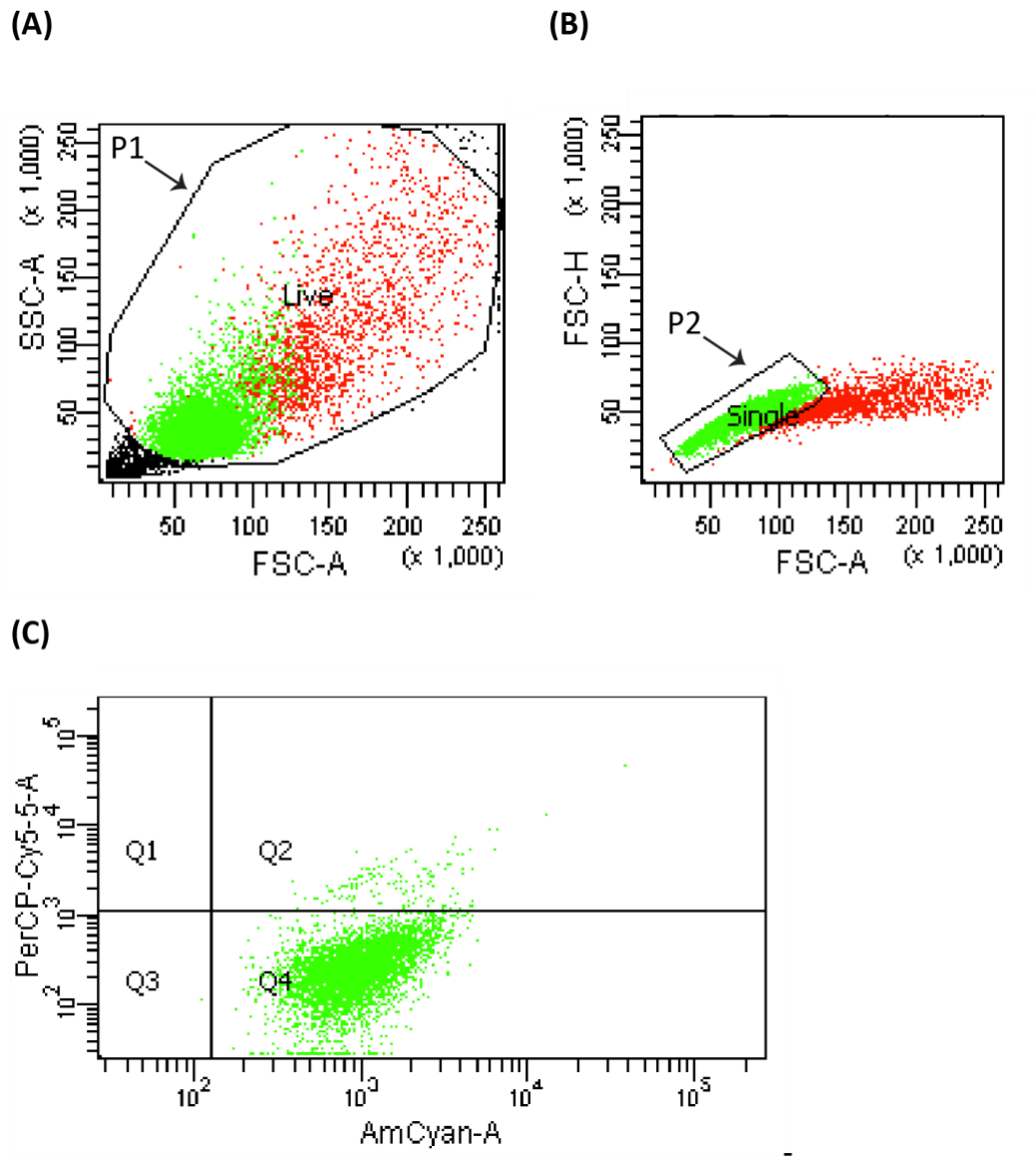

Figure 2-1 Representative FACs plots showing gating methods used to distinguish cell populations

(A) A forward scatter (FSC) versus side scatter (SSC) event plot was first used to select for the total cell population and to exclude cellular debris, as determined by the P1 gate. (B) An area versus height event plot was next used to select single cells only (P2 gate) from the events in the P1 gate. (C) An AmCyan-A versus PerCP-Cy5 event plot using events from P2 was used to determine the percentage of dead cells (Q2) from the total population of cells (P2).

2.5.9.2 Live/Dead Assay Procedure for Fluorescence Microscopy Analysis

Cells were washed 2x with pre-warmed 1X DPBS to remove excess staining solution. 500µl of 4% paraformaldehyde (PFA) was then each well and the plate was incubated for 7 minutes at room temperature to allow for fixation of cells. Cells were then washed 2x with cold 1X DPBS and imaged using an inverted fluorescence Axio Observer D1 microscope combined with AxioVision software (Carl Zeiss, UK) at a magnification of 20x. The exposure settings were optimised for both the DAPI and red fluorescence channels, and images then taken at constant exposure settings for all conditions. Images were analysed using ImageJ to determine the percentage of cells that were dead out of the total population of cells for each condition. To count the number of total cells in each image, images were first converted to 8-bit images and the LUT was inverted. Next, manual thresholding was performed to select the cells and exclude cellular debris which appeared as very small irregular shapes. The images were processed using watershed to define individual cells and then the number of cells were counted using the analyse particles option.

2.6 Protein Conformation, Expression and localisation Analysis

2.6.1 Reagents and Solutions

Bradford reagent (Bio-Rad, #500-0006)

30% Protogel (Bis-acrylamide solution; National Diagnostics, #EC-890)

Absolute Methanol (VWR)

Marvel Dried Milk Powder

16% PFA (Agar Scientific, #R1026)

20X NuPAGE MES sodium dodecyl sulfate (SDS) Running Buffer (Invitrogen, #NP0002)

NuPAGE Antioxidant (Invitrogen, #NP0005)

Solution	Components
NP40-based lysis buffer	20mM HEPES, 1mM EDTA, 150mM NaCl, 1% Nonidet P-40, 1mM dithiothreitol, 1 protease inhibitor tablet (#11873580001, Roche) per 50ml and 1 phosphatase inhibitor tablet (#88667SPCL, Pierce) per 10ml
Native loading dye	62.5mM Tris-HCl (pH 6.8), 40% glycerol, 0.01% Bromophenol Blue
1X Tris-glycine native running buffer	25mM Tris, 192mM glycine; pH 8.3
1X Tris-glycine transfer buffer	25mM Tris, 192mM glycine, 10% methanol
1X Tris-glycine running buffer	25mM Tris, 192mM glycine, 0.1% SDS; pH 8.3
4X Resolving buffer	1.5M Tris-base, 8mM EDTA, 0.4% SDS; pH 8.8
4X Stacking buffer	0.5M Tris-base, 8mM EDTA, 0.4% SDS; pH 6.8
1X Tris-buffered saline (TBS)	50mM Tris Base, 150mM NaCl
1X Phosphate-buffered saline (PBS)	1 PBS tablet (Gibco, #003002) dissolved in 500ml of ddH_2O
3% Bovine Serum Albumin (BSA)-PBST	3g of BSA (Melford) dissolved in 100ml of 1X PBS containing 0.02% Triton-X
1% BSA-PBS	1g of BSA (Melford) dissolved in 100ml of 1X PBS

Table 2-7 Western blotting solution recipes

2.6.2 Antibodies

Antibody	Host	WB dilution	ICC dilution	Company Cat No.
anti- ß-actin (AC-15)	Mouse	1:5000	-	Sigma, A1978
anti- ß amyloid 1-17aa	Mouse	1:1000	-	Abcam
anti- pSer9-SynapsinI	Rabbit	1:1000	-	Novus, NB300-180
anti- SynapsinI a/b (223)	Mouse	1:1000	-	Santa Cruz, sc-37662
anti- pTyr307-PP2A-Calpha/beta	Rabbit	1:1000	-	Santa Cruz, sc-112615-R
anti- vGlut 1	Mouse	-	1:1000	Synaptic systems
anti- GAD65	Mouse	-	1:1000	Chemicon, MAB351R
anti- apolipoprotein E	Goat	1:2500	1:2500	Calbiochem, 178479
anti- apolipoprotein E (E8)	Mouse	1:1000	1:500	Santa Cruz, sc-393302
anti- apolipoprotein E	Rabbit	1:1000	1:500	Aviva System, ARP54283_P050
anti- apolipoprotein E (16H22L18)	Rabbit	1:1000	1:500	Thermofisher, 701241
anti- apolipoprotein E (WU E-4)	Mouse	1:1000	1:500	Santa Cruz, sc-53570
anti- apolipoprotein E (3H1)	Mouse	1:100	-	Ottawa Heart Institute, 3H1
anti- vimentin (V9)	Mouse	1:5000	-	Sigma, V6389
anti- α-Tubulin (DM1A)	Mouse	1:5000	-	Sigma, T6199
anti- pSer9-GSK-3β (D85E12)	Rabbit	1:1000	-	Cell Signalling, 5558S
anti- pThr181-Tau (AT270)	Mouse	1:1000	-	Thermofisher, MN1050
anti- Tau-1 (PC1C6)	Mouse	1:1000	-	Chemicon, MAB3420
anti- Tau (D-8)	Mouse	1:1000	-	Santa Cruz, sc-166060

Table 2-8 Primary antibodies used for western blotting and immunocytochemistry

Antibody	Host	nm	WB dilution	ICC dilution	Company Cat No.
anti- mouse	Goat	680	1:5000	-	Cell Signalling, 5470S
anti- mouse (IgM)	Goat	680	1:5000	-	Biotium, 20384
anti- rabbit	Goat	800	1:5000	-	Cell Signalling, 5151S
anti- goat	Rabbit	680	1:5000	-	Biotium, 20068
anti- mouse	Donkey	568	-	1:1000	Alexafluor, A10037
anti- mouse	Donkey	488	-	1:1000	Alexafluor, A21202
anti- rabbit	Donkey	488	-	1:1000	Alexafluor, A21206
anti- goat	Donkey	488	-	1:1000	Alexafluor, A11055

Table 2-9 Secondary antibodies used for western blotting and immunocytochemistry

2.6.3 Protein Extraction

Following cell treatment, cells were washed twice with ice-cold 1X PBS and the culture plates were immediately placed on wet-ice. Cells were then immediately lysed using ice-cold NP40 lysis buffer at volumes of 100µl/well for primary neurons and 200µl/well for cell lines. Whilst the plate was tilted on wet-ice, wells were scrapped to collect protein lysate at the bottom of the well. Cell lysate was transferred to micro centrifuge tubes on wet-ice and cellular debris was pelleted by a brief centrifugation for 2 minutes at 13250rpm. The supernatant was transferred to new micro centrifuge tubes and stored at -20^{o}C.

2.6.4 Protein quantification

A Bradford assay was used to determine the concentration of protein for all samples. Whilst the protein samples were thawing on wet-ice, concentrated Bradford reagent (Bio-Rad, #500-0006) was diluted five-fold in ddH_2O and 1ml of this was added to 1mL cuvettes. Next, a series of BSA standards were prepared by diluting BSA stock (Bio-Rad, #500-0007) in diluted Bradford reagent in 1mL cuvettes. 2µl of each protein sample was also added to diluted Bradford reagent, mixed and the colour allowed to develop between for 5 minutes. For the blank, 2µl of NP40 lysis buffer was added instead. The standard curve was generated by reading the absorbance values of the BSA standards at 595nm using the SmartSpec^{TM}3000 spectrophotometer (Bio-Rad). The absorbance values of the protein samples were also measured at 595nm, which the

spectrophotometer used to determine the protein concentration based on the standard curve.

2.6.5 Preparation of Aß42 Samples for Native and SDS Polyacrylamide Gel Electrophoresis (PAGE)

Initially, an aliquot of 300µM Aß42 was thawed on wet-ice and then diluted to molarities of 5µM, 10µM, 15µM and 20µM in a total volume of 20µl that was adjusted with molecular grade water. For native PAGE, Aß42 samples were mixed with 5µl of native loading dye (1X final) and kept on wet-ice until used for native PAGE shortly after. For SDS PAGE, Aß42 samples were mixed with 5µl of LDS Sample Buffer (Invitrogen, #NP0008; 1X final) and 2µl of dithiothreitol (100mM final). After heating the Aß42 samples to 70^{o}C for 10 minutes with shaking, the Aß42 samples were kept on wet-ice until used for SDS PAGE.

2.6.6 Preparation of Protein Extracts for SDS PAGE

Protein lysate was diluted to final concentrations of either 1µg/µl or 2µg/µl, depending on the amount of protein available. Protein samples were prepared in a total volume of 100µl by diluting the lysate with 25µl of LDS Sample Buffer (Invitrogen, #NP0008; 1X final), 10µl of NuPAGE Reducing Agent (Invitrogen, #NP0009) and molecular grade water to adjust the sample volume to 100µl. Protein samples were denatured by heating to 70^{o}C for 10 minutes with shaking and then kept on wet-ice until used for SDS PAGE.

2.6.7 Native PAGE and Protein Staining

Non-denaturing 15% Tris-glycine gels were first prepared by pouring the resolving gel solution (see Table 2-10 for recipe) between glass-plate cassettes (1.0mm thickness) from the Mini-PROTEAN® Tetra handcast system (Bio-Rad). 100% isopropanol was added dropwise across the resolving gel to prevent gel dehydration and the resolving gel solution was incubated at room temperature until the resolving gel had polymerised. After removing the isopropanol overlay by washing with dH2O, the 4% stacking gel solution was cast (see

Table 2-10 for recipe) and the comb was inserted into the glass-plate cassette. Once the stacking gel had polymerised, the gel/glass-plate cassette was transferred to a Mini-PROTEAN® Tetra Electrode Assembly, which was then placed into the buffer tank. The chambers were filled with cold 1X Tris-Glycine Native running buffer and the comb was removed from the stacking gel. Protein samples were loaded into the wells along with 1µl of BLUeye Prestained Protein Ladder (Geneflow, #S6-0024), which was used as a reference for protein size (kDa). The gel tank was partially submerged in wet-ice and the gel was electrophoresed at 90V until the bromophenol blue dye ran off the gel, which occurred by approximately 4.5 hours. The gel was removed from the gel glass-plate cassette and then stained using GelCode Blue Stain Reagent (#24590, Pierce) as per the manufacturer's instructions. The protein bands were visualised by scanning the gel using the Odyssey® Infrared Imaging System (Li-Cor® Biosciences).

	Stacking Gel	**Resolving Gel**
	4%	**15%**
30% Bis-acrylamide	1.33ml	6ml
1.5M Tris pH8.8	-	3ml
1M Tris pH6.8	1.15ml	-
ddH_2O	7.46ml	2.93ml
TEMED	10µl	12µl
10% APS	50µl	60µl
Total Volume	10ml	12ml

Table 2-10 Recipes for native stacking and resolving gel solutions for native PAGE

2.6.8 Western Blotting

2.6.8.1 Hand-cast Tris-glycine based SDS PAGE

Resolving gels of varying bis-acrylamide percentages were first prepared according to the size of the proteins to be analysed (see Table 2-11 for resolving gel solution). The resolving gel solution was cast between glass-plate cassettes (1.0mm thickness) from the Mini-PROTEAN® Tetra handcast system (Bio-Rad) and overlayed with 100% isopropanol. The resolving gel was then incubated at room temperature until the resolving gel had polymerised. Once the isopropanol layer was removed by washing with dH_2O, a 4% stacking gel solution was cast (see Table 2-11 for recipe) and the comb was

inserted into the glass-plate cassette. Following polymerisation of the stacking gel, the gel/glass-plate cassette was transferred to a Mini-PROTEAN® Tetra Electrode Assembly, which was then placed into the buffer tank. The chambers were filled with 1X Tris-glycine running buffer and the comb was removed from the stacking gel. Equal amounts of protein ranging between 20-30µg were loaded into wells alongside 1µl of BLUeye Prestained Protein Ladder (Geneflow, #S6-0024), which was used as a reference for protein size (kDa). The gel was then electrophoresed at 125V until the bromophenol dye ran off the gel, which typically occurred after 1.5 hours.

	Stacking Gel	**Resolving Gel**		
	4%	**10%**	**12%**	**15%**
30% Bis-acrylamide	1.33ml	4ml	4.8ml	6ml
4X Resolving gel buffer pH8.8	-	3ml	3ml	3ml
4X Stacking gel buffer pH6.8	2.5ml	-	-	-
ddH_2O	8.81ml	4.93ml	4.13ml	2.93ml
TEMED	10µl	12µl	12µl	12µl
10% APS	50µl	60µl	60µl	60µl
Total Volume	10ml	12ml	12ml	12ml

Table 2-11 Recipes for 4X stacking and resolving gel solutions for SDS PAGE

2.6.8.2 Pre-cast Bis-Tris based SDS PAGE

10% Bis-Tris gels (Invitrogen, NP0303) were used to examine apoE fragmentation patterns from protein extracts of apoE-transfected N2a and SH-SY5Y cells, as well as primary neurons transduced with apoE-expressing lentiviral vectors. To set-up the Bis-Tris gel system, the comb and the gel wells were rinsed using dH_2O. The white tape at the bottom of the gel cassette was also removed and the gel cassette was then placed in the XCell SureLock Mini-Cell gel running tank. The upper chamber of the tank was filled with 200ml of 1X NuPAGE MES SDS Running Buffer containing 500µl of NuPAGE Antioxidant and the lower chamber was filled with 600ml of 1X NuPAGE MES SDS Running Buffer. 20µg of protein sample was loaded into each well alongside 1µl of BLUeye Prestained Protein Ladder (Geneflow, #S6-0024), which was used as a reference for protein size (kDa). The gel was then electrophoresed at 200V until the bromophenol dye reached the foot of the gel, which typically occurred after 45 minutes.

2.6.8.3 Protein transfer onto nitrocellulose membranes

Once resolving of proteins was complete, the transfer cassette was next assembled. The gel was released from the gel cassette and the placed onto nitrocellulose membrane of either 0.22µm (Amersham, #15249794) or 0.45µm pore size (Amersham, #15220033), which was sandwiched between 2x filter papers followed by 2x blotting sponges on either side, soaked in 1X Tris-glycine transfer buffer. Pressure was applied across the top of the sandwich using a plastic roller to ensure remove trapped air bubbles and excess liquid between the gel and nitrocellulose membrane. Next, the transfer cassette was firmly closed and placed into a transfer tank submerged in wet-ice. Once the transfer tank was filled with cold 1X Tris-glycine transfer buffer, the proteins were transferred onto the nitrocellulose membrane at 100V for 1 hour.

2.6.8.4 Immunoblotting

The nitrocellulose membranes were blocked with nonfat dried milk (typically 2.5%; 5% was used for goat anti- apoE) in TBS containing 0.05% Tween-20 for 1.5 hours at room temperature with agitation. Next, the membranes were incubated with primary antibodies (see Table 2-8) diluted in 2.5% or 5% nonfat dried milk in TBS for either 2 hours at room temperature or overnight at 4^{o}C. Following two washes in 1X TBS for 10 minutes each, the blots were incubated with secondary antibodies (see Table 2-9) diluted in 2.5% or 5% nonfat dried milk in TBS for 1 hour at room temperature whilst protected from light. The two wash steps were repeated and the damp membrane placed into an Odyssey CLx Imaging System (LI-COR Biosciences) to visualise the protein bands. The proteins were detected by scanning the blots at near-infrared fluorescence detection at either 800nm or 700nm. After scanning, the blots were stored at -20 ^{o}C in 1X TBS in sealed bags for further immunoblotting. For re-probing with additional antibodies, the blots were thawed at room temperature and washed briefly with 1X TBS. Blots were then incubated with antibodies as previously described.

2.6.9 Analysis of blots

Protein bands were quantified by using Image Studio 4.0 software (LI-COR) as per the Odyssey CLx Tutorial Guide. The ‘western analysis’ function was first applied after gel image acquisition, followed by the ‘boundary’ function to define the blot area. The ‘set

the lanes' function was next applied to define the protein lanes, and the lane lines were adjusted to transect the protein bands if necessary. The protein ladder marker was next set up by inputting the approximate size (kDa) for each band of the protein ladder so that the size (kDa) of sample protein bands could be determined. Protein bands of interest were selected in discrete boxes by using either 'find the bands automatically' function or by using the 'add rectangle' function. Once all protein bands of interest were selected, the background subtraction method was applied by using the background settings of: median value, a border width of 3 and either right/left or top/bottom according to the proximity of neighbouring bands. The signal values were then calculated by the software and displayed within the western bands table. These signal values were then processed by using Excel software.

2.6.10 Immunocytochemistry

Following cell treatment, cells in 12-well plates were briefly washed twice with 1X PBS and fixed using 500µl of 4% PFA per well. After a 7-minute incubation at room temperature, cells were briefly washed twice again. Cells were then blocked and permeabilised for 45 minutes at room temperature using 500µl of 3% BSA-PBST per well. Coverslips containing the cell monolayer on top were then carefully transferred onto a 12-well plate lid covered in parafilm. 100µl of primary antibody (see Table 2-8) diluted in 1% BSA-PBS was added to each coverslip and coverslips were incubated in a moist chamber for 2 hours at room temperature. Coverslips were transferred to wells in a clean 12-well plate and washed three times with 1X PBS for 5 minutes each time. After transferring coverslips back to the parafilm-covered lid, coverslips were incubated with 100µl of secondary antibody (see Table 2-9) diluted in 1% BSA-PBS and incubated for 1 hour at room temperature in a moist chamber protected from light. Coverslips were washed two times with 1X PBS as before and then incubated for 1 minute with 500µl of 1X Hoescht solution to stain cell nuclei. After two washes with 1X PBS for 5 minutes each to remove excess Hoescht staining, coverslips were mounted onto microscope slides cell side down using 5µl of ProLong Gold Anti-Fade Mountant (Invitrogen, #P36930). The microscope slides were incubated at room temperature overnight in a dry and dark chamber to allow for the mounting media to set and then stored at 4^{o}C for short-term

storage or -20^{o}C for long-term storage. Cells were visualised and imaged as Z-stacks using a spin disc confocal system (CARV from Digital Imaging Solutions) with an EM-CCD camera (Rolera/QI Cam 3500) combined with Image Pro 6.0 software.

2.7 Data Analysis and Statistics

Microsoft Excel was used to calculate percentage and ratio-fold changes from raw data. Statistical analysis of data was carried using GraphPad Prism 7 software. Initially, a Shapiro-Wilk normality test was performed to determine whether the data followed a normal distribution. Once confirming that the data were parametric, statistical significance was tested using either a Student's t-test or a one-way ANOVA followed by a Tukey's multiple comparison test on GraphPad Prism 7 software, as appropriate. GraphPad Prism 7 software was also used for graphical presentation of data, where all error bars shown are based on standard error of the mean (SEM). The measurement of data variability reported in text with the mean is SEM. N numbers represent independent experiments. Independent experiments involving primary neuronal cultures were performed using cultures from different neuronal preparations.

Chapter 3 Aß42 AND VPA AFFECT SYNAPSIN I REGULATION

3.1 INTRODUCTION

Synaptic dysfunction and loss is considered an early event that correlates strongly with cognitive decline in AD (Davies et al., 1987, Terry et al., 1991, DeKosky and Scheff, 1990, Scheff et al., 2006, Scheff et al., 2007). Whilst the molecular basis for this is still unclear, there is mounting evidence supporting the involvement of soluble Aß oligomers. Indeed, accumulation of soluble Aß oligomers has been linked to deficits in cognitive function and memory (Tomiyama et al., 2010, Umeda et al., 2014) and this is thought to be partly caused by an impairment of synaptic plasticity (reviewed in sections 1.5.4 and 1.5.5). Interestingly, there is evidence to suggest that the effects of Aß on synaptic plasticity may occur through Aß affecting multiple aspects of SV dynamics at the presynapse in a concentration and time dependent manner. It has been demonstrated that low concentrations or short exposure of hippocampal neurons to Aß oligomers increase the release probability of the RRP at the presynapse and induce LTP (Puzzo et al., 2008, Parodi et al., 2010, Russell et al., 2012), whereas high concentrations or longer exposure times disrupt endocytosis and SV recycling, reducing the size of the RRP and inhibiting LTP (Puzzo et al., 2008, Parodi et al., 2010, Kelly and Ferreira, 2007). Although the mechanisms underlying this are still not fully understood, it is increasingly evident that this involves interference with the function of proteins that regulate SV dynamics. Indeed, studies have shown that Aß oligomers can disrupt the function of proteins that modulate priming of SVs for neurotransmitter release and SV endocytosis (Kelly et al., 2005, Kelly and Ferreira, 2006b, Kelly and Ferreira, 2007, Yang et al., 2015, Russell et al., 2012). However, considering that there are many proteins that regulate SV dynamics (Rizzoli, 2014), it is possible that there are other proteins that may also be affected by Aß oligomers either directly, or indirectly through Aß-mediated alterations in calcium signalling. Since deregulation of SnpI, a key SV-associated protein, has been linked to AD (Parks et al., 1991), the present study explored the hypothesis that Aß42 oligomers deregulate SnpI.

SnpI belongs to a family of neuronal phosphoproteins that play an important role in synapse formation and plasticity. A key function of synapsins is to organise the pools of

SVs under resting conditions and during neuronal activity through transient interactions with SVs and cytoskeletal components (Cesca et al., 2010, Fornasiero et al., 2012, Baldelli et al., 2007). This function is tightly regulated by activity-dependent cycles of phosphorylation and dephosphorylation at multiple residues across the protein, which alter the binding affinity of synapsins for SVs, other synaptic proteins and the actin cytoskeleton (Cesca et al., 2010, Shupliakov et al., 2011). One such residue is Ser9 (site 1), which is located within a small lipid binding domain of the N-terminus and is conserved amongst all synapsin isoforms (Cesca et al., 2010). Cycles of phosphorylation and dephosphorylation at Ser9 of synapsins modulates the proteins phospholipid-binding activity, enabling the protein to act as a transient linker between SVs and actin, clustering them in the reserve pool (Huttner et al., 1983, Hosaka et al., 1999, Benfenati et al., 1989). It has been proposed that the activity-dependent phosphorylation of Ser9 by PKA and CAMKI/IV results in dissociation of SnpI from SVs, enabling them to participate in neurotransmitter release (Huttner et al., 1983, Hosaka et al., 1999, Fiumara et al., 2004). Conversely, dephosphorylation at Ser9 by PP2A increases the affinity of SnpI for SVs, tethering them to the actin cytoskeleton and replenishing the reserve pool (Jovanovic et al., 2001, Ceccaldi et al., 1995, Bloom et al., 2003). There is evidence to suggest that this function of SnpI may be affected in AD, as an early study showed that the levels of SnpI phosphorylated at Ser9 (pSer9-SnpI) were higher in post-mortem brain tissue from AD patients (Parks et al., 1991). Moreover, previous immunocytochemistry experiments in our lab indicated that this may be related to Aß42 oligomers. In this earlier work, Aß42 oligomers were found to induce an increase in the localisation of pSer9-SnpI at synaptic boutons of cultured hippocampal neurons recovering from neuronal activity, suggesting that Aß42 oligomers either affect the distribution of pSer9-SnpI or the phosphorylation cycle of SnpI at Ser9. Hence whether Aß42 oligomers deregulate the phosphorylation or dephosphorylation of SnpI at Ser9 was explored in the present study by examining the levels of SnpI, pSer9-SnpI and the active form of PP2A by western blotting. Here, the data revealed that Aß42 oligomers induce sustained phosphorylation of SnpI at Ser9 in neurons recovering from neuronal activity, suggesting that Aß oligomers deregulate SnpI.

There are few studies that have examined whether currently available drugs can block or reverse the effects of Aß42 on SV-associated proteins and SV dynamics. Interestingly though, a recent study showed that VPA, a short branch-chained fatty acid, can prevent Aß-induced reduction in SV recycling (Williams and Bate, 2016). In addition, this compound was previously shown to promote clustering of SnpI in cultured neurons (Hall et al., 2002). In view of these reports and the Aß42-mediated deregulation of SnpI shown here, VPA was considered a candidate therapeutic drug to attenuate the effect of Aß42 on SnpI. Therefore, the work in this this chapter also explored the hypothesis that the therapeutic action of VPA in SV recycling could be mediated through protection of SnpI regulation.

To investigate the above hypotheses, Aß42 and/or VPA was applied to primary hippocampal neurons that that had been cultured for 18-21DIV, because at this time point, neurons exhibit established synaptic junctions and increased levels of synaptic proteins (Grabrucker et al., 2009, Kim and Lee, 2012, Sapoznik et al., 2006). Since it has previously been shown in our lab that intraneuronal accumulation of Aß42 has been linked to SV-associated protein disruption (Russell et al., 2012), it was of interest to explore whether intraneuronal Aß42 oligomers deregulate SnpI. To do so, neurons were exposed to Aβ42 peptides for 30 minutes followed by a 2-hour period in the absence of peptide because immunocytochemistry experiments showed that Aß42 can be internalised and localised to the presynapse during this time-frame (Russell et al., 2012). Moreover, to assess whether Aß42 oligomers affect the activity-dependent phosphorylation cycle of SnpI at Ser9, neurons were depolarised with KCl for 5 minutes to induce neuronal activity and SnpI phosphorylation, and allowed to recover for 15 minutes after KCl-induced neuronal activity to allow time for SnpI dephosphorylation at Ser9.

The work presented here shows for the first time that Aß42 oligomers affect the regulation of SnpI phosphorylation at Ser9, thus indicating a possible mechanism for how Aß contributes to defects in SV dynamics and neurotransmitter release. The data here also show that VPA attenuates the effect of Aß42 on SnpI regulation, which could

play a part in its therapeutic role in restoring physiological SV dynamics. Hence, the work here provides support for its use in the treatment of AD, in addition to its clinically approved use in the treatment of epilepsy and bipolar disorder.

3.2 RESULTS

3.2.1 Characterisation of synthetic Aß42 peptide preparations

Since reconstituted synthetic Aß42 peptides readily aggregate to form oligomers, protofibriils and fibrils, it was important to routinely examine the aggregation state of the Aß42 peptide mixture for consistency between different preparations. Commercially available synthetic Aß42 was reconstituted in DMSO and diluted to working aliquots in 1X PBS. A sample of stock Aß42 was separated on both native and SDS polyacrylamide gels to examine the assembly state of each Aß42 preparation. The native gels were stained with GelCode blue stain reagent to reveal protein bands, and protein on SDS gels was transferred to nitrocellulose membrane and probed with a monoclonal anti-Aß (6E10) antibody that recognises 1-17aa of Aß.

On native gels, a single band with a molecular weight of ~20 kDa (Figure 3-1, A) was routinely observed indicating that the peptide preparations consist of small pentameric oligomers. Hence, the method of Aß42 preparation was efficient for the production of low molecular weight oligomeric Aß42, which are believed to be the more toxic assembly states of Aß42 to neurons (Ahmed et al., 2010b). These oligomers could be broken down into monomers (~4.5 kDa) and dimers/trimers (~13.5 kDa) on an SDS PAGE gel (Figure 3-1, B). This indicated that the pentameric oligomers were not SDS-stable and that they had not adopted a ß-sheet conformation (Ahmed et al., 2010b), a secondary structure that is characteristic of the less toxic, fibrillar form of the peptide (Kirschner et al., 1986). Indeed, this is in accordance with work showing that Aß42 does not exhibit a ß-sheet structure when dissolved in DMSO (Shen and Murphy, 1995). Considering this preparation method consistently produced low molecular weight oligomers, all Aß42 stocks used in this chapter were made according to this method.

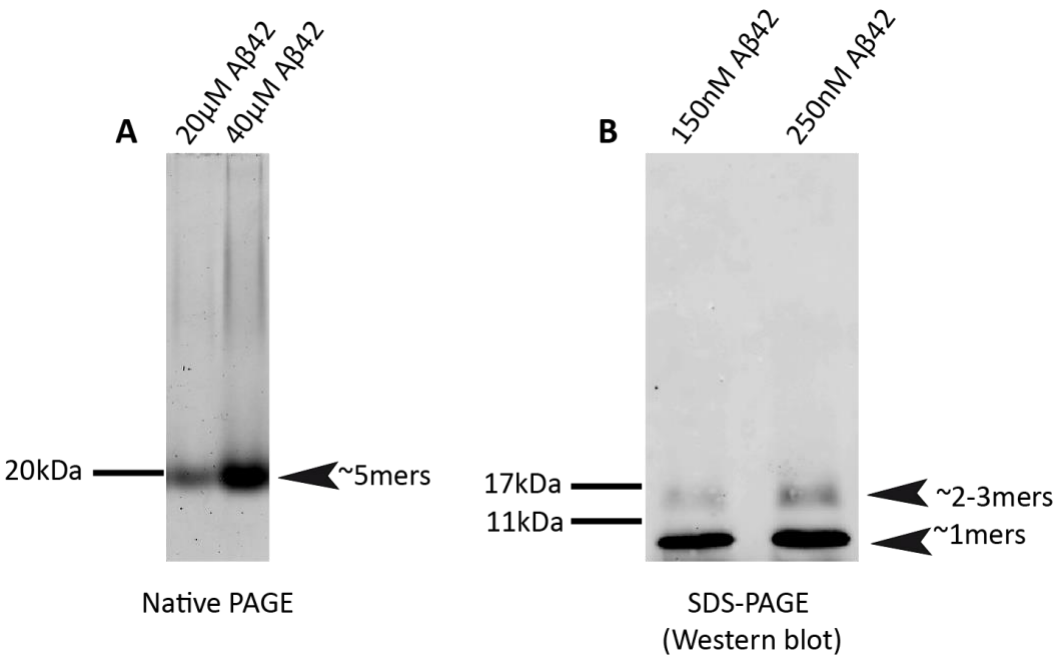

Figure 3-1 Aß42 preparation contains aggregated assembly states

(A) Native gel electrophoresis of increasing concentrations of synthetic Aβ42 reveals a single band at ~20 kDa, indicating a pentameric assembly state. (B) SDS-PAGE of increasing concentrations of synthetic Aβ42 shows that the oligomers can be broken down into monomers (4.5 kDa) and trimers (13.5 kDa) in the presence of SDS. Aß42 peptide was detected by monoclonal 6E10 anti-Aβ antibody.

3.2.2 Characterisation of primary hippocampal cultures

Since primary hippocampal neuronal cultures are typically not uniform and contain a combination of GABAergic interneurons and glutamatergic pyramidal neurons, the heterogeneity of the cultures were first assessed. Cultures were immunolabelled for the glutamate transporter, vGlut, and the GABA producing enzyme, GAD65, to visualise the proportion of glutamatergic and GABAergic synapses respectively (Figure 3-2). Immunostaining revealed a stronger and more wide-spread staining for vGlut compared to GAD65. This suggests that the neuronal cultures used were enriched in glutamatergic synapses. Hence any effects of Aß42 on the cultured hippocampal neurons are likely associated with an effect on glutamatergic neurons.

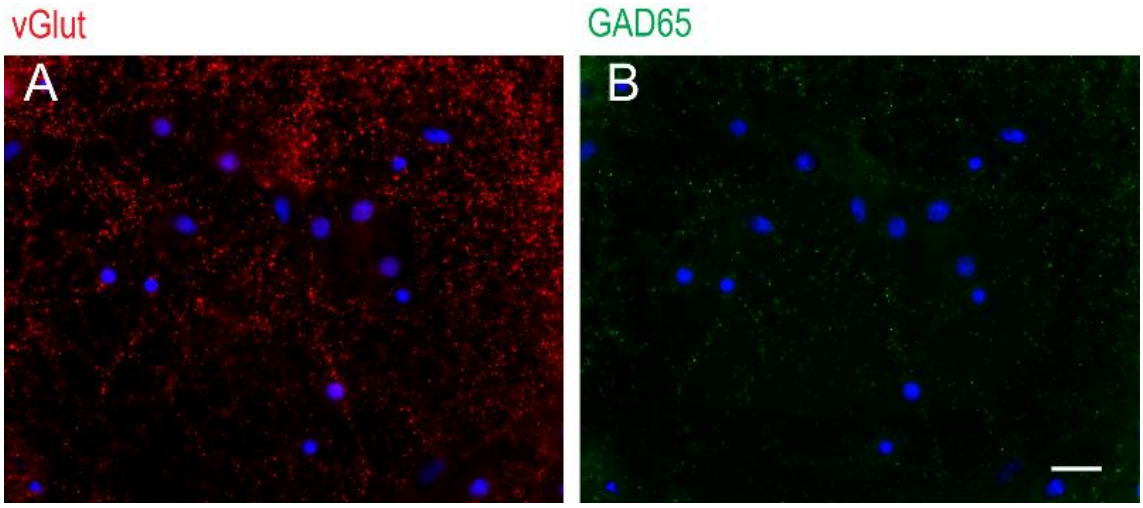

Figure 3-2 Primary hippocampal cultures are enriched in glutamatergic synapses.
Immunolabelling of primary hippocampal neurons for vGlut (A) and GAD65 (B) reveals that the primary cultures are enriched in glutamatergic synapses. Scale bar 50 µM.

3.2.3 Aß42 disrupts the phosphorylation cycle of SnpI

Previous immunocytochemistry experiments in our lab showed that the localisation of pSer9-SnpI at synaptic boutons remained elevated in cultured hippocampal neurons exposed to Aß42 oligomers and that this effect could be attenuated when neurons were treated with VPA after exposure to the peptide. This was hypothesised to be due to either an Aß42-induced restriction of pSer9-SnpI dispersal and/or disruption of the phosphorylation cycle of SnpI at Ser9. Hence in the present study, western blotting was performed to determine whether the phosphorylation cycle of SnpI at Ser9 was affected by Aß42 or VPA alone as well as a combination of both. To do so, the relative levels of

total SnpI and pSer9-SnpI in protein extracts from Aß-treated, VPA-treated and Aß/VPA-treated synchronised and recovering neurons were compared. First the effect of Aß42 and VPA on the relative levels of total SnpI was examined by densitometric analysis of SnpI and actin protein bands on immunoblots (Figure 3-3, A). The ratio of SnpI to actin was calculated for each condition, and then normalised to the SnpI/actin ratio of synchronised control neurons (considered as 100%). The relative levels of SnpI for each condition are shown in the bar chart in Figure 3-3, B. Statistical analysis of total SnpI levels did not reveal any significant differences between conditions in synchronised neurons (Figure 3-3, B; black bars; 147.6%±8.6 VPA 1mM, 124.8%±34.7 VPA 10mM, 222.2%±33.4 Aß42, 269.9%±70.6 Aß42/VPA 1mM, 166.2%±51.2 Aß42/VPA 10mM; $p>0.05$). or recovering neurons (Figure 3-3, B; grey bars; 87.1%±14.1 VPA 1mM, 123.9%±35 VPA 10mM, 195.5%±41.7 Aß42, 193.7%±63.1 Aß42/VPA 1mM, 125.2%±27.4 Aß42/VPA 10mM; $p>0.05$). Although there was an increase in the levels of SnpI in Aß42- and Aß42/VPA- treated neurons, this was not statistically significant because of high variation between experiments. Therefore, these data indicate that acute treatment of cultured hippocampal neurons with Aß42 or VPA does not affect the total levels of SnpI.

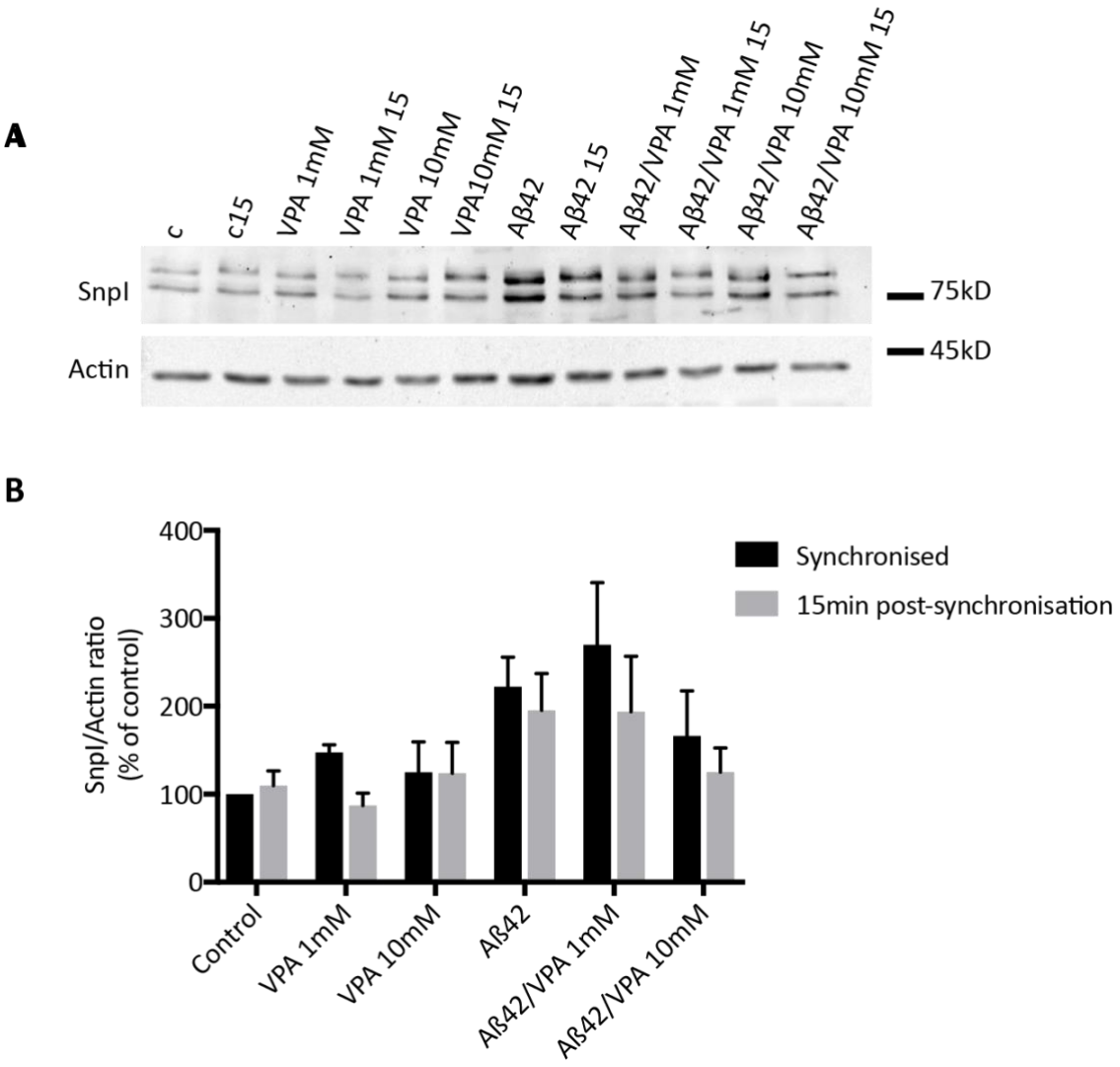

Figure 3-3 SnpI levels are unaffected by acute Aß42 or VPA treatment in rat hippocampal neuronal cultures

(A) Representative western blots showing SnpI and actin protein from synchronised or 15 minute post-synchronised rat hippocampal neuronal cultures treated with 300nM Aß42 for 30 minutes and/or VPA (1 or 10mM) for 2 hours after exposure to the peptide. Neurons were synchronised by a 5 minute KCl application to induce depolarisation. (B) Bar chart showing the levels of SnpI based on the intensity ratios of SnpI to actin. The ratio values were normalized to control as 100% for all conditions. The black bars show SnpI levels in synchronised neurons and the white bars show SnpI levels in neurons 15 minutes after synchronisation. Statistical anlaysis of SnpI levels by a one-way ANOVA followed by a Tukey's multiple comparison test did not reveal any significant differences for SnpI levels between conditions (p values >0.05). Data are mean ±SEM; n=4.

The effect of Aß42 and VPA on the relative levels of pSer9-SnpI was next examined by densitometric analysis of immunoblots probed for pSer9-SnpI and total SnpI protein (Figure 3-4, A). The ratio of pSer9-SnpI to SnpI was calculated for each condition and then normalised to the pSer9-SnpI/SnpI ratio of synchronised control neurons

(considered as 100%). The relative levels of pSer9-SnpI for each condition are shown in the bar chart in Figure 3-4, B. Statistical analysis of pSer9-SnpI levels did not reveal significant differences between conditions from synchronised neurons to control synchronised neurons (Figure 3-4, B; black bars; 100.3%±17.5 VPA 1mM, 92.2%±6.7 VPA 10mM, 88.9%±5.8 Aß42, 101.4%±15.1 Aß42/VPA 1mM, 99.54%±17.1 Aß42/VPA 10mM; $p>0.05$). This suggests that the activity-dependent phosphorylation of SnpI at Ser9 is not affected by Aß42, VPA or their combination in neuronal cultures. However, significant differences in pSer9-SnpI levels were found in neurons recovering from neuronal activity relative to synchronised neurons (Figure 3-4, B; grey bars). The level of pSer9-SnpI was significantly reduced in recovering control neurons compared to synchronised control neurons (48.7%±6 recovering control neurons, $p=0.003$), which is consistent with studies showing that the Ser9 residue of SnpI is dephosphorylated after neuronal activity (Hosaka et al., 1999). Likewise, a significant reduction in the level of pSer9-SnpI was observed in recovering VPA-treated neurons when compared to synchronised neurons (42.5%±5.7 recovering 1mM VPA-treated neurons and 47.8%±7.2 recovering 10mM VPA-treated neurons, $p<0.05$), suggesting that VPA does not affect the phosphorylation cycle of SnpI at Ser9. In contrast, the level of pSer9-SnpI in recovering Aß42-exposed neurons was not significantly different to synchronised Aß42-exposed neurons (74.1%±2.1 versus 88.9%±5.8, $p>0.05$). Moreover, recovering Aß42-treated neurons showed higher levels of pSer9-SnpI compared to recovering control neurons (74.1%±2.1 versus 48.7%±6, $p=0.015$). These data suggest that exposure of neurons to Aß42 either prevents dephosphorylation of SnpI at Ser9 or induces sustained phosphorylation of SnpI at Ser9 after neuronal activity. Interestingly, a significant reduction in the levels of pSer9-SnpI was observed in recovering Aß42/VPA-treated neurons compared to recovering Aß42-treated neurons (60.8%±9.2 recovering Aß42/1mM VPA-treated neurons, $p=0.045$ and 40.1%±7.1 recovering Aß42/10mM VPA-treated neurons, $p=0.005$). Moreover, recovering Aß/VPA-treated neurons showed similar pSer9-SnpI levels to recovering control neurons ($p>0.05$). Therefore, these data indicate that VPA may attenuate the Aß42-mediated deregulation of SnpI phosphorylation/dephosphorylation at Ser9.

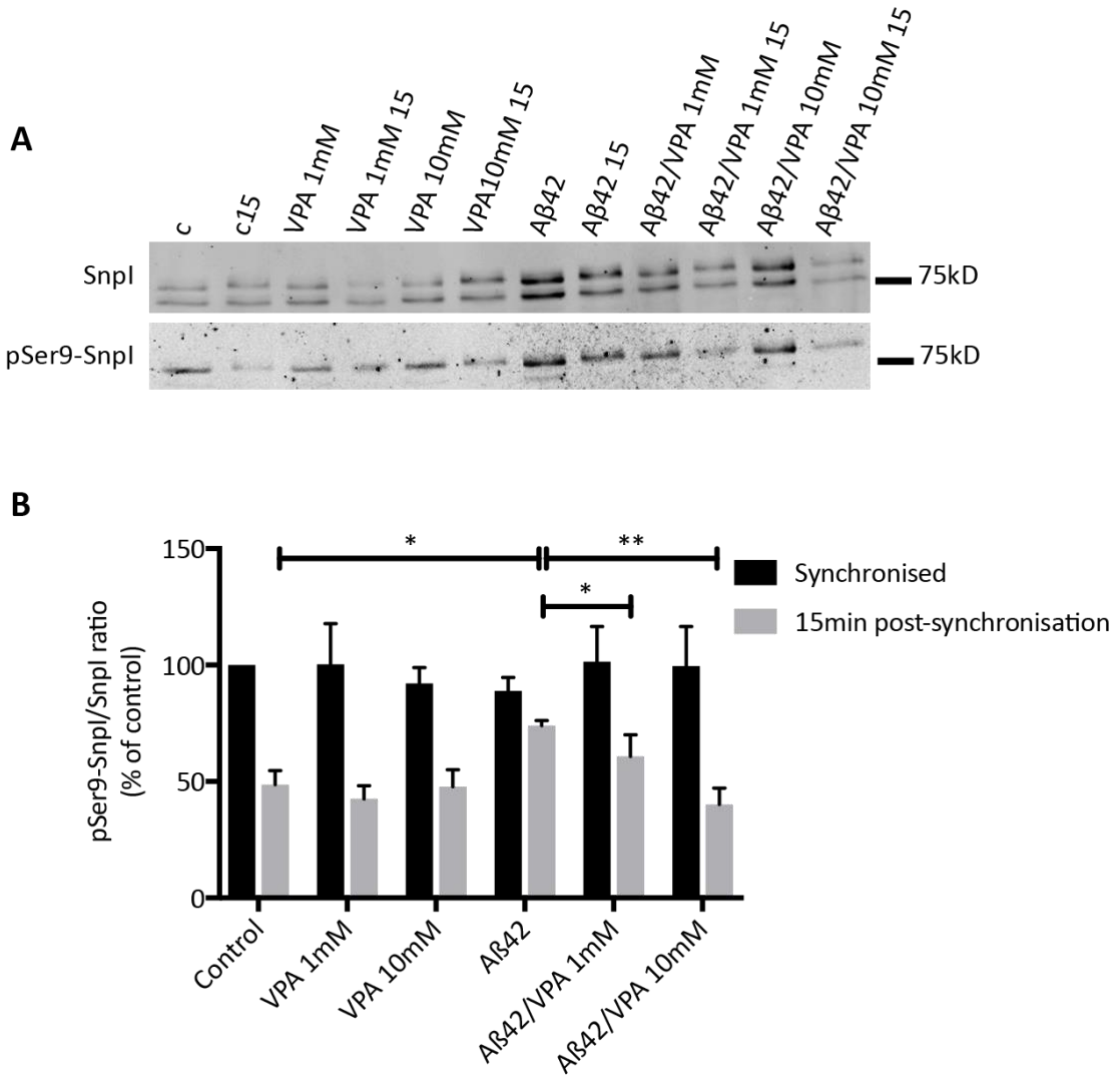

Figure 3-4 Aß42 and VPA affect pSer9-SnpI levels in rat hippocampal neuronal cultures

(A) Representative western blot showing pSer9-SnpI and SnpI protein from synchronised or 15 minute post-synchronised (recovering) rat hippocampal neuronal cultures treated with 300nM Aß42 for 30 minutes and/or VPA (1 or 10mM) for 2 hours after exposure to the peptide. Neurons were synchronised by a 5 minute KCl application to induce depolarisation. (B) Bar chart showing the levels of pSer9-SnpI based on the intensity ratios of pSer9-SnpI to SnpI. The ratio values were normalized to synchronised control neurons as 100% for all conditions. The black bars show pSer9-SnpI levels in synchronised neurons and the grey bars show pSer9-SnpI levels in neurons 15 minutes after synchronisation (recovering neurons). No significant differences for the levels of pSer9-SnpI were found between conditions in synchronised neurons. However, significant differences for pSer9-SnpI levels were found in recovering control and Aß42-treated neurons. Significant differences were also observed between recovering Aß42-treated neurons, Aß42/1mM VPA-treated neurons and Aß42/10mM VPA-treated neurons. Data are mean ±SEM, and differences were assessed using one-way ANOVA followed by a Tukey's multiple comparisons test. *p<0.05, **p<0.01; n=4.

3.2.4 Aß42 induces sustained phosphorylation of SnpI at Ser9

It was hypothesised that the elevated levels of pSer9-SnpI induced by Aß42 in recovering neurons could be due to sustained phosphorylation at Ser9 by PKA and/or CAMKI/IV (Czernik et al., 1987), or due to reduced dephosphorylation by PP2A (Jovanovic et al., 2001). The phosphatase function of PP2A is regulated by phosphorylation at Tyrosine 307, which is located within the conserved C-terminus of the catalytic regulatory subunit. Phosphorylation at this site inactivates PP2A, decreasing its phosphatase activity (Chen et al., 1992). Hence to investigate whether the elevated levels of pSer9-SnpI in recovering neurons exposed to Aß42 were due to reduced dephosphorylation activity, the relative levels of pTyr307-PP2A were examined for protein extracts from neurons treated as previously described. Western blotting was performed using anti- pTyr307-PP2A and anti- actin antibodies (Figure 3-5, A) and the relative levels of pTyr307-PP2A were calculated by densitometric analysis of pTyr307-PP2A and actin protein bands. The ratio of pTyr307-PP2A to actin was calculated for each condition and normalised to the pTyr307-PP2A:actin ratio of synchronised control neurons (100%). Statistical analysis was performed by a one-way ANOVA followed by a Tukey's multiple comparison post-hoc test to examine for significant differences in pTyr307-PP2A between conditions. The relative levels of pTyr307-PP2A for each condition are shown in the bar chart in Figure 3-5, B. No significant differences in the levels of phosphorylated Tyr307-PP2A were found in synchronised neurons (Figure 3-5, B; black bars; 136.1%±16.1 VPA 1mM, 109.8%±6.7 VPA 10mM, 126.5%±22.3 Aß42, 139.5%±27 Aß42/VPA 1mM, 115.3%±15.4 Aß42/VPA 10mM; $p>0.05$) or in recovering neurons (Figure 3-5, B; grey bars; 104.3%±7.7 control, 136.7%±30.8 VPA 1mM, 101.1%±9.6 VPA 10mM, 107.5%±17.5 Aß42, 128.5%29.2 Aß42/VPA 1mM, 105.7%±15.5 Aß42/VPA 10mM; $p>0.05$). This result suggests that acute exposure of neurons to Aß42 does not alter the catalytic activity of PP2A. Therefore, the elevated levels of pSer9-SnpI in Aß42-exposed recovering neurons are likely not due to defective dephosphorylation of Ser9 by PP2A, but may instead involve sustained phosphorylation of Ser9 by prolonged CAMKI/IV or PKA activity.

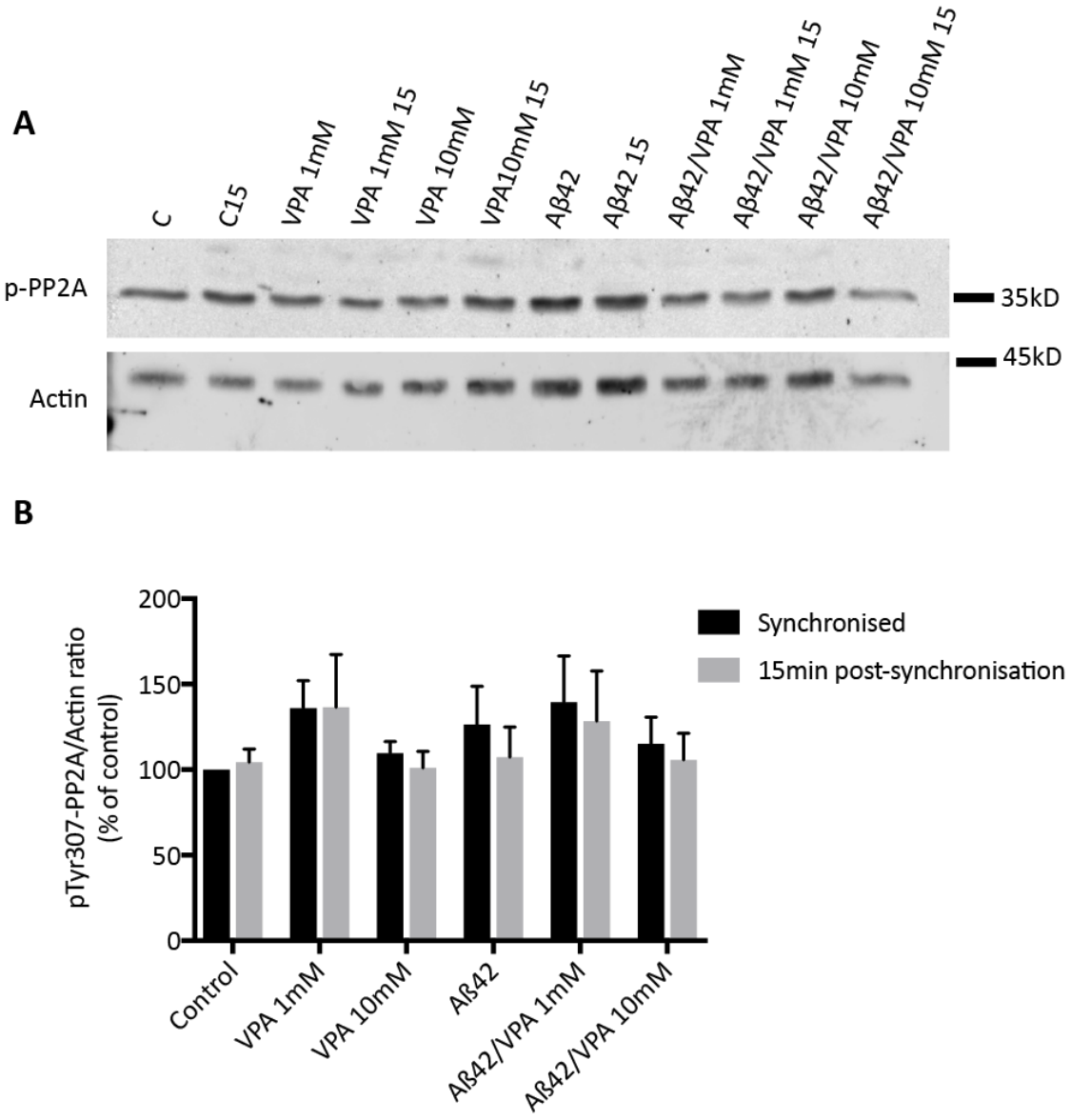

Figure 3-5 Aß42/VPA treatment does not affect the phosphorylation of PP2A at Tyrosine 307 in rat hippocampal neuronal cultures

(A) Representative western blots showing pTyr307-PP2A and actin protein from synchronised or 15 minute post-synchronised (recovering) rat hippocampal neuronal cultures treated with 300nM Aß42 for 30 minutes and/or VPA (1 or 10mM) for 2 hours after exposure to the peptide. Neurons were synchronised by a 5 minute KCl application to induce depolarisation. (B) Bar chart showing the levels of pTyr307-PP2A based on the intensity ratios of pTyr307-PP2A to SnpI, expressed as percentages of synchronised control neurons. The black bars show pTyr307-PP2A levels in synchronised neurons and the white bars show pTyr307-PP2A levels in neurons 15 minutes after synchronisation. Statistical analysis by a one-way ANOVA followed by a Tukey's multiple comparison test did not reveal any significant differences for pTyr307-PP2A levels between conditions in both synchronised and recovering neurons ($p>0.05$). Data are mean ±SEM; n=4.

3.3 Discussion

The work presented in this chapter was carried out to investigate the molecular basis of Aß-mediated SV disruption and the protective effect of VPA on SV dynamics through exploring the hypothesis that Aß oligomers deregulate SnpI and that VPA may attenuate this effect. The data confirmed that Aß42 does indeed deregulate SnpI and that VPA can attenuate this, highlighting a novel molecular mechanism underpinning Aß42-mediated disruption and the therapeutic effect of VPA in AD.

3.3.1 Aß42 oligomers deregulate the phosphorylation cycle of SnpI at Ser9

To investigate the effect of Aß42 oligomers on SnpI regulation, the assembly state of synthetic Aß42 used in this work was first characterised to confirm that the preparation method used could generate low molecular weight oligomeric Aß42. This was of importance since these assemblies of Aß42 are thought to be more toxic compared to higher molecular weight aggregates of the peptide (Ahmed et al., 2010a). Moreover, low molecular weight oligomers have been shown to disrupt the function of other SV-associated proteins such as synaptophysin (Russell et al., 2012). Having confirmed this, the effect of Aß42 oligomers on the levels of SnpI protein was assessed. The results presented here showed that the overall levels of SnpI were unaffected in neurons exposed to Aß42 for a short time-period, indicating that Aß42 oligomers do not affect the expression or degradation of SnpI under the conditions used here. It is notable though that several studies have reported a reduction of synaptic proteins in neurons exposed to Aß oligomers, including SnpI (Parodi et al., 2010, Kelly et al., 2005, Ripoli et al., 2013). There are several factors that could contribute to this difference, such as the length of time neurons are incubated with the peptide and concentration used. Indeed, a time- and concentration- dependent effect on the reduction of the levels of synaptic proteins by Aß oligomers has been demonstrated (Kelly et al., 2005, Parodi et al., 2010). For instance, a significant reduction in SnpI levels was only evident in neuronal cultures after a continuous exposure to 500nM oligomeric Aß for 12 hours in the study by Parodi and colleagues. Taken together, this finding supports the notion that the reduction of SV proteins associated with Aß42 is likely a chronic effect, occurring in the later stages of Aß-mediated synaptic dysfunction. The relative levels of SnpI phosphorylated at Ser9

were next examined to determine if Aß42 oligomers affect the regulation of SnpI. Neurons that were exposed to Aß42 and recovering from neuronal activity exhibited elevated levels of SnpI phosphorylated at Ser9. Consistent with this observation, a later independent study also showed that Aß42 increased SnpI phosphorylation at Ser9 in primary neuronal cultures, but also in cultured neurons from 5XFAD rodents (Park et al., 2017). Overall, these data demonstrate that Aß42 oligomers disrupt the physiological regulation of SnpI phosphorylation at Ser9.

3.3.2 Aß42 oligomers induce sustained phosphorylation of SnpI at Ser9

The mechanism underpinning the deregulation of SnpI by Aß42 oligomers was also explored in this work. The sustained phosphorylation of SnpI at Ser9 could be due to sustained kinase activity by CAMKI/IV and/or PKA, or reduced phosphatase activity by PP2A. To determine whether sustained pSer9-SnpI levels was a result of reduced phosphatase activity, the activity of PP2A was examined. Since PP2A is inactivated by phosphorylation at Tyrosine-307 (Chen et al., 1992), the relative levels of pTyr307-PP2A were calculated to provide an indicator of its activity. The results presented here showed similar levels of pTyr307-PP2A in all conditions suggesting that the activity of PP2A was unaffected by acute exposure of neurons to Aß42. This result indicates that the sustained phosphorylation of SnpI in Aß42-exposed neurons is likely due to maintained activity-dependent kinase activity. Indeed, this has since been confirmed by Park and colleagues who showed that levels of activated CAMKIV (pThr196-CAMKIV) were higher in neurons following acute application (2-hours) of Aß42 at a similar concentration (200nM) (Park et al., 2017). In addition, inhibition of CAMKK, the kinase responsible for increasing CAMKIV activity by phosphorylating CAMKIV at Threonine 196 (Selbert et al., 1995), reduced the levels of pSer9-SnpI in Aß42-exposed neurons (Park et al., 2017). In further support of a relationship between Aß42 and enhanced CAMK signalling, AD rodent models such as 3xTG-AD mice have been reported to display high levels of pThr196-CAMKIV (Muller et al., 2011). Importantly, initial activation of CAMKIV is dependent on intracellular calcium levels and calmodulin, since calcium/calmodulin binding is required for exposure and thus phosphorylation of the Thr196 site by CAMKK (Selbert et al., 1995, Tokumitsu and Soderling, 1996). Thereafter, pThr196-CAMKIV

activity is autonomous and persists for a period after the calcium stimulus. In view of this and studies showing that Aß42 induces increased calcium influx in primary neurons (Parodi et al., 2010, Park et al., 2017), it is feasible that the sustained phosphorylation of SnpI at Ser9 is mediated by autonomous CAMKIV activity triggered by Aß42-induced calcium influx. It is also tempting to hypothesise that the autonomous CAMKIV activity triggered by Aß42 oligomers may lead to prolonged SnpI deregulation, thereby also implicating SnpI deregulation in chronic effects of Aß42 too. In summary, these findings suggest that Aß42-induced deregulation of SnpI phosphorylation dynamics may be consequent to Aß-mediated calcium influx, which in turn promotes CAMK signalling, thus altering the regulation of CAMK substrates such as SnpI. Further work could involve confirming that the levels of activated CAMKIV are increased under the experimental conditions used here. It would also be of interest to investigate whether the regulation of other CAMK substrates at the pre-synapse are affected in further work.

3.3.3 Aß42-mediated deregulation of SnpI may contribute to SV cycle defects

Aß42-induced deregulation of SnpI is notable since SnpI plays a key role in the availability of SVs for neurotransmission and organisation of the SV reserve pool. As mentioned previously, these functions are tightly regulated by activity-dependent cycles of phosphorylation and dephosphorylation at various residues across the protein. The Ser9 residue is responsible for modulating the phospholipid-binding activity that facilitates SnpI to act as a transient linker between SVs and actin (Huttner et al., 1983). Whilst the activity-dependent phosphorylation of Ser9 has been suggested to promote dissociation of SnpI from SVs and subsequently enable SVs to participate in neurotransmission, dephosphorylation of Ser9 is thought to promote SnpI-SV association, leading to SV re-clustering and replenishment of the reserve pool (Hosaka et al., 1999, Fiumara et al., 2004, Ceccaldi et al., 1995, Bloom et al., 2003). On this basis, it is possible that sustained phosphorylation of SnpI at Ser9 by Aß42 could result in increased availability of SVs for neurotransmitter release. Indeed, this hypothesis is in accordance with studies which have shown that acute exposure of neurons Aß oligomers promotes neurotransmitter release (Puzzo et al., 2008, Abramov et al., 2009, Russell et al., 2012). Furthermore, sustained phosphorylation at Ser9 by autonomous

CAMKIV activity could disrupt SnpI-SV association during recovery from neuronal activity, which in turn, could impair SV recycling and the maintenance of the reserve pool. Hence it is conceivable that Aß42-mediated deregulation of SnpI may contribute to the reported deficits in SV recycling, but also the depletion of SV pools observed in primary neurons following chronic exposure to Aß oligomers (Kelly and Ferreira, 2007, Parodi et al., 2010, Williams and Bate, 2016). Overall, these findings support the notion that the deregulation of SnpI by Aß42 oligomers may contribute to both the early and chronic deficits in SV dynamics and synaptic transmission triggered by Aß oligomers. Indeed, SnpI phosphorylation at Ser9 may initially enhance glutamate release during the early stages of synaptic dysfunction, which could promote excitotoxicity. However, the possible reduction in SV recycling and clustering of SVs in the reserve pool due to sustained phosphorylation of SnpI at Ser9 could gradually lead to depletion of SVs and impaired neurotransmission. For further work, the functional effect of sustained phosphorylation of SnpI at Ser9 by Aß42 could be investigated by comparing the recycling of SVs in Aß42-exposed cultured hippocampal neurons that are WT or expressing a Ser9-phospho-deficient mutant of SnpIa.

3.3.4 VPA attenuates the disruptive effect of Aß42 oligomers on SnpI regulation

Since the data presented here revealed that Aß42 oligomers affect SnpI regulation, it was of interest to look for available drugs that could potentially interfere with this effect. VPA was selected as a candidate molecule because it has been shown to induce clustering of SnpI (Hall et al., 2002), as well as to restore physiological SV recycling that was reduced in neurons exposed to Aß42 (Williams and Bate, 2016). Treatment of neurons with VPA did not affect the physiological regulation of SnpI protein levels or phosphorylation. Remarkably however, the results showed that treatment of Aß42-exposed neurons with VPA restored physiological pSer9-SnpI levels in a concentration dependent manner, suggesting that VPA may act antagonistically of Aß42. Since this could occur through reduced kinase or increased phosphatase activity, the levels of pTyr307-PP2A were examined for Aß42/VPA-treated neurons. The data showed that VPA treatment did not affect the levels of inactivated PP2A. Therefore, it is plausible that VPA instead may restore the physiological regulation of SnpI in Aß-exposed neurons

by interfering with the maintained kinase activity of CAMKIV that is triggered by Aß42-mediated calcium influx (Park et al., 2017). There is very little evidence in the literature on whether VPA affects CAMK signalling, and given the data discussed here, it would be an interesting avenue to explore in future studies. One possible mechanism underlying the protective effect of VPA in SnpI regulation which warrants investigation, is downregulation of CAMK signalling and thus decreased SnpI phosphorylation at Ser9, through altered phosphoinositide signalling. The basis for this speculation stems from a study that showed constitutive CAMKIV hyperphosphorylation was reduced when phosphoinositide signalling was attenuated (Muller et al., 2011), and other studies which demonstrate VPA can also alter phosphoinositide signalling (Xu et al., 2007b, Chang et al., 2012). It is also possible that VPA may interfere with the other kinases responsible for phosphorylation Ser9 of SnpI such as PKA. Indeed, VPA has also been shown to downregulate PKA activity through inhibiting the accumulation of cAMP (Chang et al., 2010), thus highlighting another potential mechanism underpinning the antagonistic effect of VPA on Aß-mediated SnpI deregulation. In view of the protective effect of VPA on SnpI regulation and SV dynamics (Marsh et al., 2017, Williams and Bate, 2016), VPA may provide therapeutic benefit in AD, particularly during the early stages of Aß-mediated synaptic dysfunction, which is likely when SnpI deregulation is triggered. In support of this hypothesis, it was reported that memory deficits observed in transgenic AD mouse models were reduced to a greater extent when VPA treatment was used early (Qing et al., 2008).

3.3.5 Conclusion

To conclude, the work in this chapter highlights a novel mechanism for how accumulation of intraneuronal Aß42 can contribute to synaptic dysfunction during the early stages of AD. The evidence suggests that Aß42 deregulates SnpI phosphorylation through altered CAMK signalling, leading to sustained CAMKIV kinase activity. It also highlights a novel therapeutic mode of action for VPA in AD, since VPA treatment can attenuate the effect of Aß42 on SnpI. From this data, a model can be proposed to summarise how SnpI deregulation can affect SV dynamics that may contribute to the

reported defects in neurotransmission and SV pool organisation and how VPA may interfere with this. This model is illustrated in Figure 3-6.

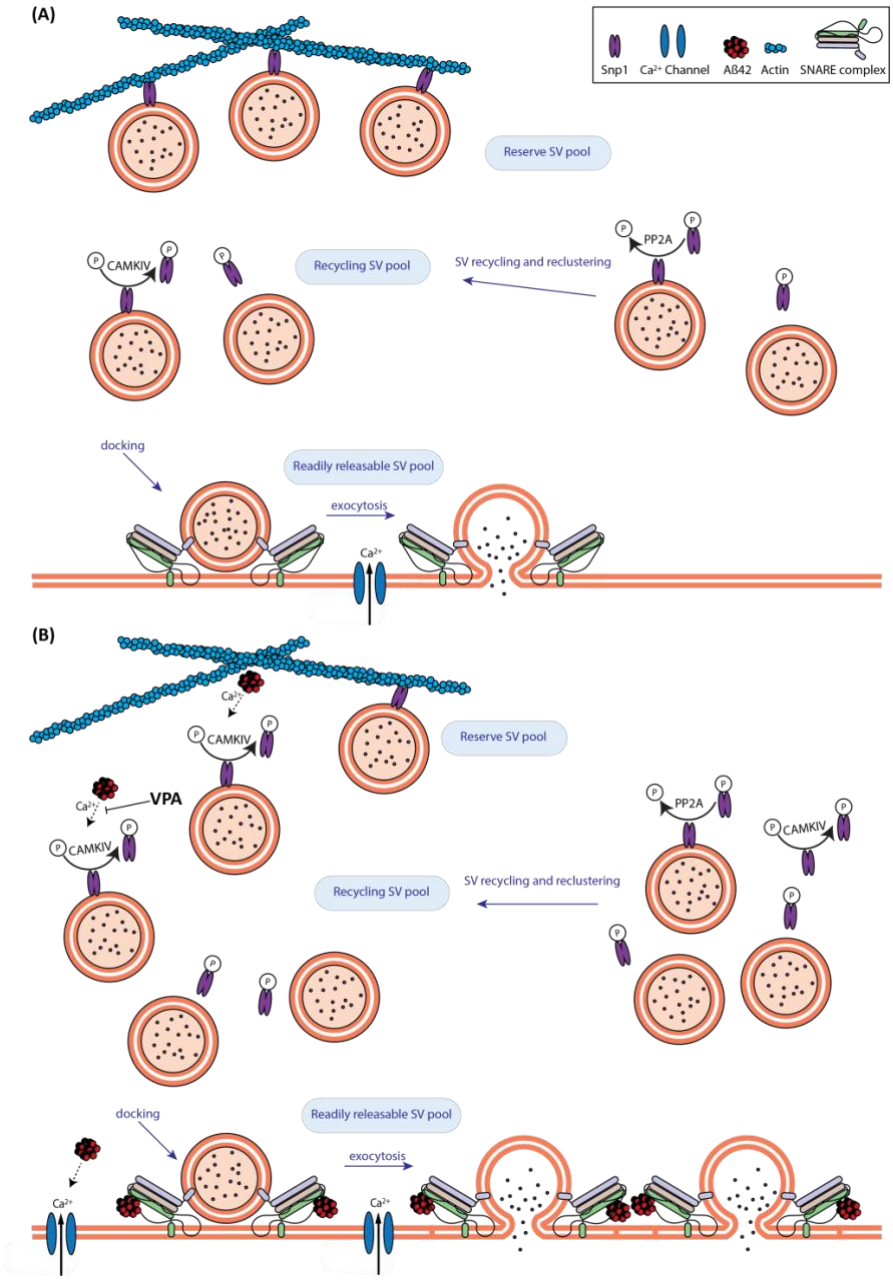

Figure 3-6 Model illustrating the early effects of Aß42-mediated deregulation of SnpI on SV dynamics and the therapeutic effect of VPA

(A) Physiological SV dynamics involves a balance between SV recycling and neurotransmitter release. SVs are released from the reserve pool to participate in neurotransmitter (NT) release following neuronal activity via CAMKIV-induced SnpI phosphorylation at Ser9. SVs dock via SNARE complex assembly and then fuse with the membrane following calcium influx, releasing NT. SVs are tethered back to the reserve pool following endocytosis via PP2A-mediated dephosphorylation of SnpI. (B) Aß oligomers disrupt SV recycling and enhance NT release. Aß increases the availability of SVs for NT release and reduces the reserve pool due to increased calcium influx and elevated CAMKIV/SnpI phosphorylation. The greater number of SVs in the RRP combined with an Aß-mediated increase in calcium influx results in aberrant neurotransmitter release. VPA abolishes this effect by attenuating Aß-induced phosphorylation of SnpI at Ser9, possibly through downregulating CAMK signaling. Image adapted from (Marsh and Alifragis, 2018).

Chapter 4 DEVELOPMENT OF APOE LENTIVIRAL VECTORS

4.1 INTRODUCTION

Whilst neuronal expression of apoE4 has been considered to be an additional contributor to AD pathology (Brecht et al., 2004b, Harris et al., 2004, Buttini et al., 2010), the processing and role of neuronally expressed apoE is still not fully understood. Hence the work in this thesis aimed to explore this by overexpressing apoE in suitable cell models. One such model is primary rat neuronal cultures, a commonly used *in vitro* model for neurodegeneration that has similar physiological properties of neuronal cells *in vivo* such as functional synapses, unlike neuroblastoma cell lines which are tumor-derived. However, a disadvantage is that primary neuronal cultures can contain non-neuronal cells such as astrocytes and glia, to varying degrees. Although drugs such as cytosine arabinoside (AraC) can be used to inhibit dividing cells, they often affect the viability of primary neurons in culture (Dessi et al., 1995). Whilst neuronal cultures can be made using either prenatal or early postnatal rodent embryos, prenatal tissue was used because there are fewer glial cells at this developmental stage compared to mature brain tissue. To further minimise the number of non-neuronal cells in culture, the meningens were removed during the isolation of the hippocampus from the brain. Specific culturing reagents were also used to promote survival of neuronal cells against other cell types. Culturing neurons in serum-free neurobasal media reduces the number of non-neuronal cells proliferating, whilst supplementing the media with B27 supports neuronal growth (Brewer et al., 1993). Collectively, this creates a more simplistic system to study neuronal function with minimal influence from other cell types.

Though primary neurons are an advantageous model system for neurodegeneration, they are infamously challenging to transfect (Karra and Dahm, 2010). Lentiviral vectors however, are an efficient Human immunodeficiency virus 1 (HIV-1)-based tool that enables gene delivery into both dividing and quiescent cells such as postmitotic neurons. They can transduce mature postmitotic neurons with high efficiency, yielding high expression levels and low toxicity, as reviewed in (Karra and Dahm, 2010). Thus, lentiviral vectors enable the expression of desired genes to allow for quantitative and biochemical analyses in mature neurons. Due to this, lentiviral vectors were developed

and used to express the three major human apoE isoforms in 18-21DIV primary hippocampal cultures, as evidenced by the results in this chapter, so that the fragmentation and cell biology of neuronally expressed apoE could be investigated in later chapters. Recombinant lentiviral vectors expressing apoE were generated using a third generation lentiviral system for improved biosafety as the *Tat* viral gene required for viral self-replication is absent in this system (Dull et al., 1998). Additionally, an integration-deficient lentiviral vector (IDLV) design was used to reduce the likelihood of gene dysregulation due to insertional mutagenesis, thus minimising the risk of virus-mediated effects on neuronal cell biology. Initially, the cDNA sequences for *APOE2*, *APOE3* and *APOE4* were subcloned into an IDLV transfer plasmid. The transfer plasmids were sequenced and functionality verified by transfection into HEK293T cells followed by western blotting for apoE protein. Lentiviral vectors containing the apoE transgene under the CMV promoter were then generated by calcium phosphate transfection of the transfer, regulatory, packaging and envelope constructs into HEK293T cells. The viral vectors were titrated by qPCR because they did not contain a fluorescence reporter required for titration by FACs analysis. Having established the number of transducing units/ml (TU/ml), the optimal ratio of lentiviral vector TU to number of cells/well that is required for efficient transduction (termed as MOI), was determined using GFP lentiviral vectors as an indicator. Finally, the functionality of the apoE-expressing vectors was confirmed by western blotting for apoE protein using lysate from mature primary neurons transduced with the apoE lentiviral vectors.

4.2 RESULTS

4.2.1 Verification of plasmid sequences by restriction mapping analysis

Plasmid sequence maps were not available for the pCMV-apoE2 and pCMV-apoE4 plasmids, however information sheets for these constructs (provided by Professor George Dickson) indicated that the cDNA sequences encoding apoE2 and apoE4 were inserted into the pCMV backbone using flanking *XbaI* linkers and that it contained the sequence for the apoE signalling peptide (example plasmid map shown in Figure 4-1, C). To confirm that this was the case and to determine if *XbaI* could be used to liberate the apoE cDNA, the pCMV-apoE2 and pCMV-apoE4 plasmids were digested with *XbaI* endonuclease. The result from the digestion showed that using *XbaI* could liberate a product around the expected size for apoE cDNA of approximately 1Kb (Figure 4-1, A and B). Two other products of sizes ~3.7Kb (expected backbone fragment) and 0.2Kb were observed, suggesting that the backbone contained a third *XbaI* cut site. Both pCMV-apoE2 and pCMV-apoE4 were then sequenced, which verified that the plasmids contained apoE2 and apoE4 cDNA (including the signalling peptide) flanked by *XbaI* restriction sites.

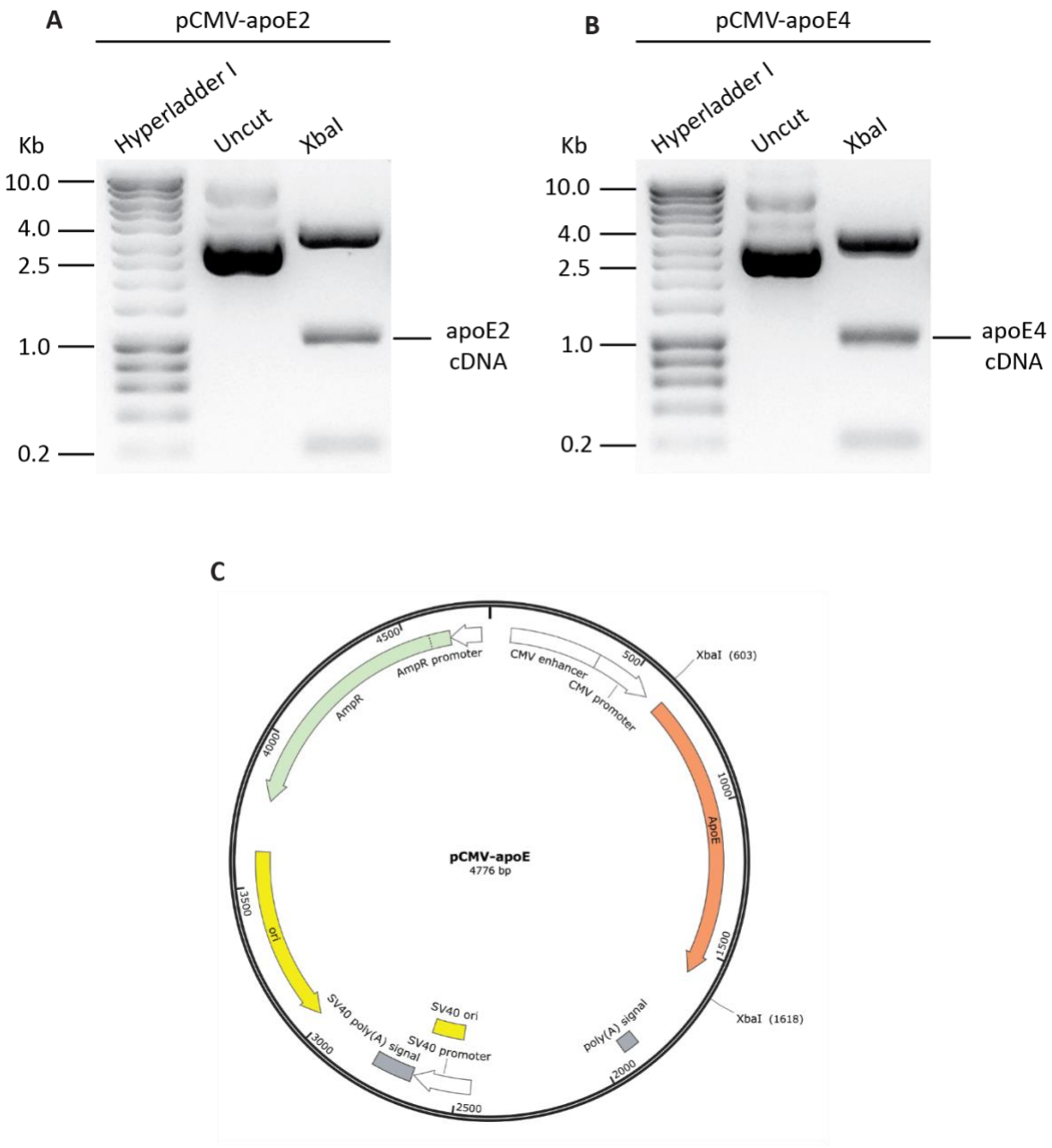

Figure 4-1 Restriction mapping analysis of pCMV-ApoE2 and pCMV-ApoE4 to confirm *XbaI* cut sites and plasmid maps

pCMV-apoE2 (A) and pCMV-apoE4 (B) were digested with XbaI to confirm presence of *XbaI* linkers flanking apoE2- and apoE4- cDNA. (C) A general plasmid map for the apoE-containing plasmids was generated detailing the *XbaI* linkers upstream and downstream of the apoE insert.

The backbone of the IDLV transfer plasmid (pRRL-CMV-Wpre) was examined by digestion with the *HindIII* endonuclease to assess the integrity of the plasmid. This endonuclease was selected due to the presence of restriction sites within some of the lentiviral elements (e.g. LTRs / Gag) that are crucial for the generation of the lentiviral vectors (plasmid map shown in Figure 4-2, A). The *HindIII* endonuclease was predicted to cut at six positions within the plasmid, resulting in the generation of six products listed in Figure 4-2 B, which were observed by gel electrophoresis of the digest products (Figure 4-2, C). Although the fragments of sizes ~584bp and ~553bp could not be clearly distinguished, they appeared as a thicker band, indicating two similar sized products. Next, pRRL-CMV-Wpre was digested with *XbaI* to confirm the presence of unique *XbaI* cut site located after the CMV promoter (Figure 4-2, A), as this was required for cloning of apoE cDNA. Examining the digestion products by gel electrophoresis showed a single band at approximately 7Kb (Figure 4-2, D), confirming one cut site for the *XbaI* endonuclease that linearised the plasmid.

A

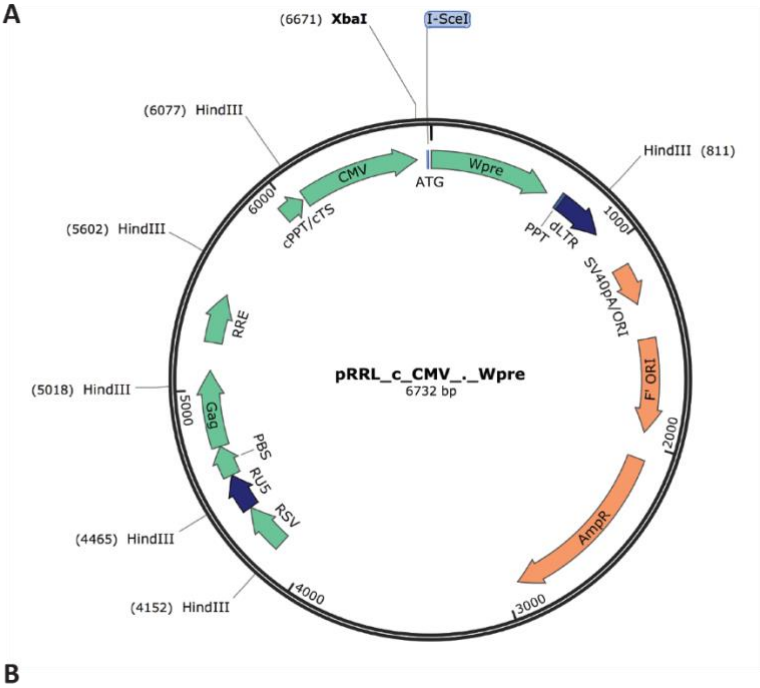

B

Restriction endonucleases	Predicted fragment sizes (bp)
HindIII-HF	3341, 1466, 594, 553, 475, 313
XbaI	6732

C

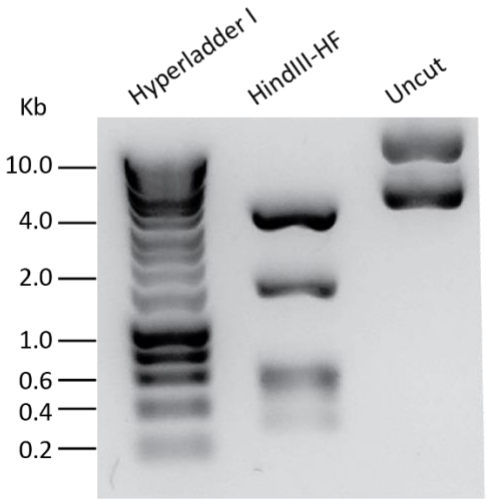

D

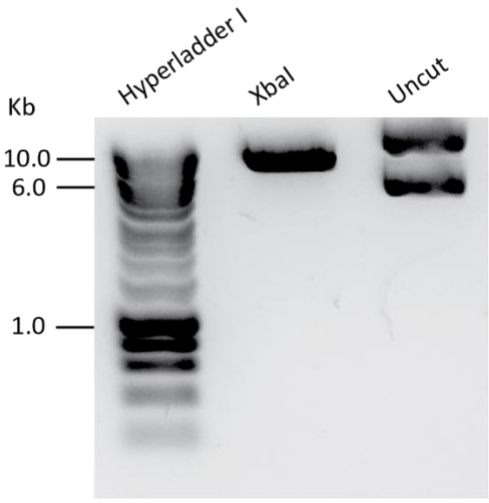

Figure 4-2 Plasmid map of pRRL-CMV-Wpre and restriction mapping analysis to check plasmid backbone
Plasmid map for pRRL-CMV-Wpre (A) and predicted fragment sizes for the *HindIII-HF* and *XbaI* restriction endonucleases (B). pRRL-CMV-Wpre was digested using HindIII-HF (C) to check plasmid backbone, as well as *XbaI* (D), to confirm unique cut site.

Since the pCMV6-ApoE3 plasmid (map shown in Figure 4-3, A) was composed of a different backbone to pCMV-ApoE2 and pCMV-ApoE4, different combinations of restriction endonucleases (listed in Figure 4-3, B) were used for restriction mapping analysis, but also to isolate the apoE3 cDNA for cloning (strategy described in 4.2.2.2). Digestion with *EcorI-HF* linearised the plasmid, showing a band of ~7Kb (Figure 4-3, C). A double digest using *EcorI-HF* and *XhoI* removed ~1.2Kb of sequence containing the apoE3 insert, leaving the backbone of ~5.8Kb. Digestion using the *BlpI* and *SbfI-HF* restriction endonucleases removed a fragment of apoE3 cDNA containing the SNPs that distinguish each isoform. Due to a second *BlpI* cut site in the Poly(A) sequence, another fragment of~708bp was generated. A triple digest was also carried out using *BlpI*, *SbfI-HF* and *XhoI* so that the additional fragment of~708bp could be further digested by *XhoI*, yielding two fragments of~379 and~329bp as observed by gel electrophoresis, and thus enabling better separation of the apoE3 cDNA fragment (Figure 4-3, C). Taken together, these digests confirmed the expected plasmid sequence.

A

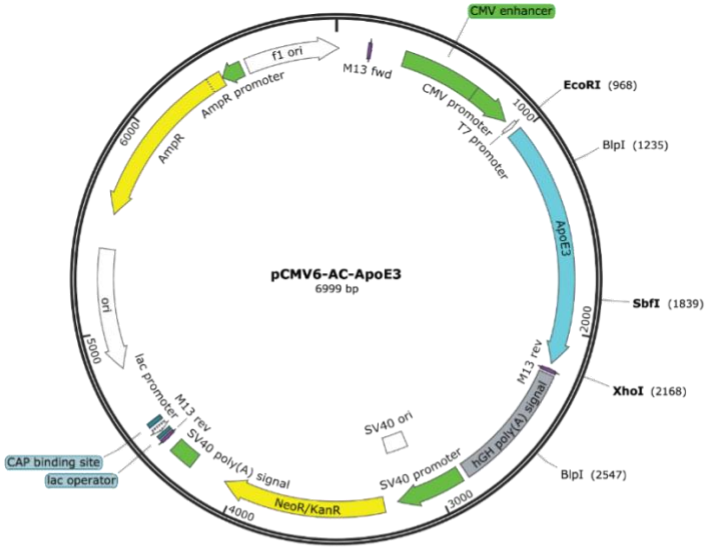

B

Restriction endonucleases	Predicted fragment sizes (bp)
EcoRI-HF	6999
EcoRI-HF + XhoI	5799, 1200
BlpI + SbfI-HF	5687, 604, 708
BlpI + XhoI + SbfI-HF	5687, 604, 379, 329

C

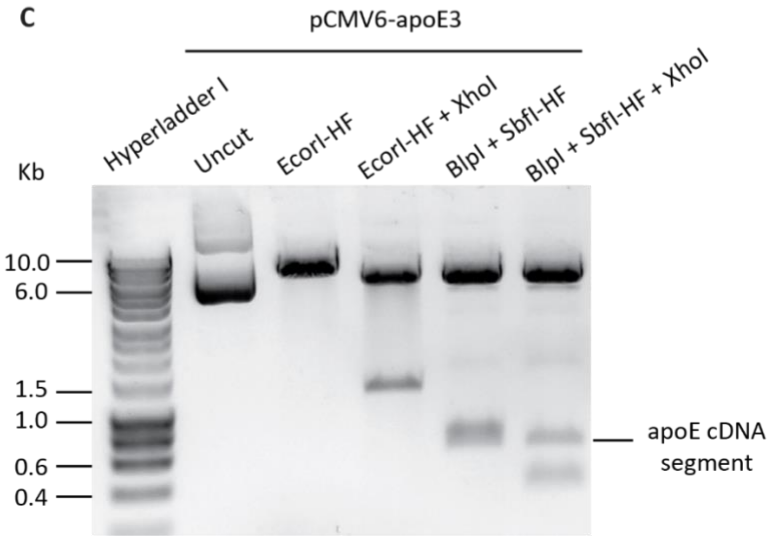

Figure 4-3 Plasmid maps of pCMV6-ApoE3 and restriction mapping analysis to check plasmid backbone

Plasmid map for pCMV6-AC-ApoE3 (A) and predicted fragment sizes following digestion using various combinations of restriction endonucleases (B). pCMV6-ApoE3 was digested by using different combinations of restriction endonucleases (C) to check plasmid backbone. The digest using *BlpI* + *SbfI* + *XhoI* confirmed that a region of apoE cDNA containing the SNPs could be isolated by gel electrophoresis.

4.2.2 Generation of IDLV transfer plasmids containing apoE cDNA

4.2.2.1 Generation of pRRL-CMV-ApoE2-Wpre and pRRL-CMV-ApoE4-Wpre plasmids

Following verification of the constructs, the apoE2 and apoE4 inserts were then cloned into the lentivirus transfer plasmid, as summarised in Figure 4-4. The cDNAs for apoE2 and apoE4 cDNA were liberated from pCMV-apoE2 and pCMV-apoE4 respectively, by digestion with *XbaI*. The *XbaI* endonuclease was also used to linearise the target plasmid, pRRL-CMV-Wpre. The digest products were separated by agarose gel electrophoresis and then extracted from the gel so that the apoE cDNAs could be ligated into the linearised pRRL-CMV-Wpre plasmid using different vector:insert ratios (1:1, 1:3, 1:5 and 1:10). The ligated products were transformed into Top10 E. Coli cells and random colonies were screened for a positive clone that contained the insert in the correct orientation. This was achieved by digesting the purified plasmid DNA from selected colonies with both *NdeI* and *BlpI* since the recognition sites of these endonucleases are located within the CMV promoter region and the 5'-end of the apoE cDNA respectively. A positive clone containing the apoE insert in the correct orientation within the lentivirus plasmid (Figure 4-5, A) would generate a fragment of 637bp after digestion. However, a plasmid containing apoE cDNA in the reverse orientation (Figure 4-5, B) would generate a larger fragment of 1189bp. The cloning of apoE cDNAs into the IDLV transfer plasmid was successful, as a band of ~637bp was observed for both pRRL-CMV-ApoE2_Wpre plasmids derived from clone A and clone B (Figure 4-6, B), and for pRRL-CMV-ApoE4_Wpre derived from clone B (Figure 4-6, C). An example IDLV transfer plasmid containing apoE4 in the reverse orientation was also generated, as indicated by the presence of a ~1189bp sized band in Figure 4-6 C. The apoE-IDLV transfer plasmid backbones were also validated using a variety of restriction endonucleases as listed in Figure 4-6 A. The predicted fragmentation patterns shown in Figure 4-6 A were observed for both pRRL-CMV-ApoE2-Wpre and pRRL-CMV-ApoE4 (Figure 4-6, B and C), confirming the presence and integrity of the lentiviral elements and the size of the plasmid. Sequencing both pRRL-CMV-ApoE2-Wpre and pRRL-CMV-ApoE4-Wpre confirmed that the cloning was successful and verified that the correct apoE isoforms were cloned.

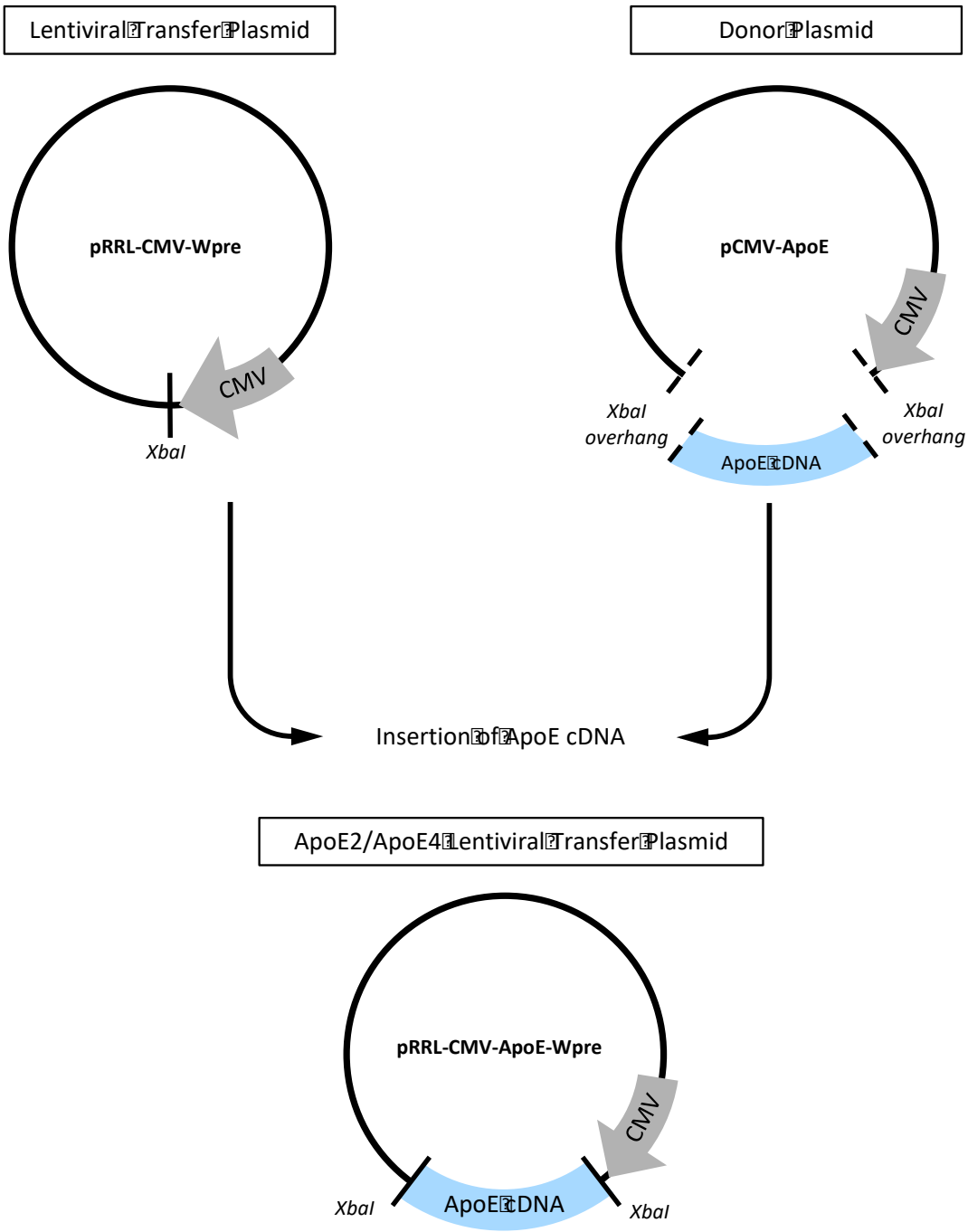

Figure 4-4 Cloning strategy used to create pRRL-CMV-ApoE2-Wpre and pRRL-CMV-ApoE4-Wpre constructs

The apoE2 or apoE4 insert was isolated and purified from the pCMV-apoE donor plasmid by digestion with *XbaI* since the apoE cDNA was flanked by *XbaI* recognition sites. The pRRL-CMV-Wpre backbone was linearised by digestion with *XbaI* aswell (recognition site present after the CMV promoter) so that the apoE cDNA could be ligated using the *XbaI* complementary ends. Ligation of the apoE cDNA with the lentiviral backbone generated an apoE containing lentiviral transfer plasmid.

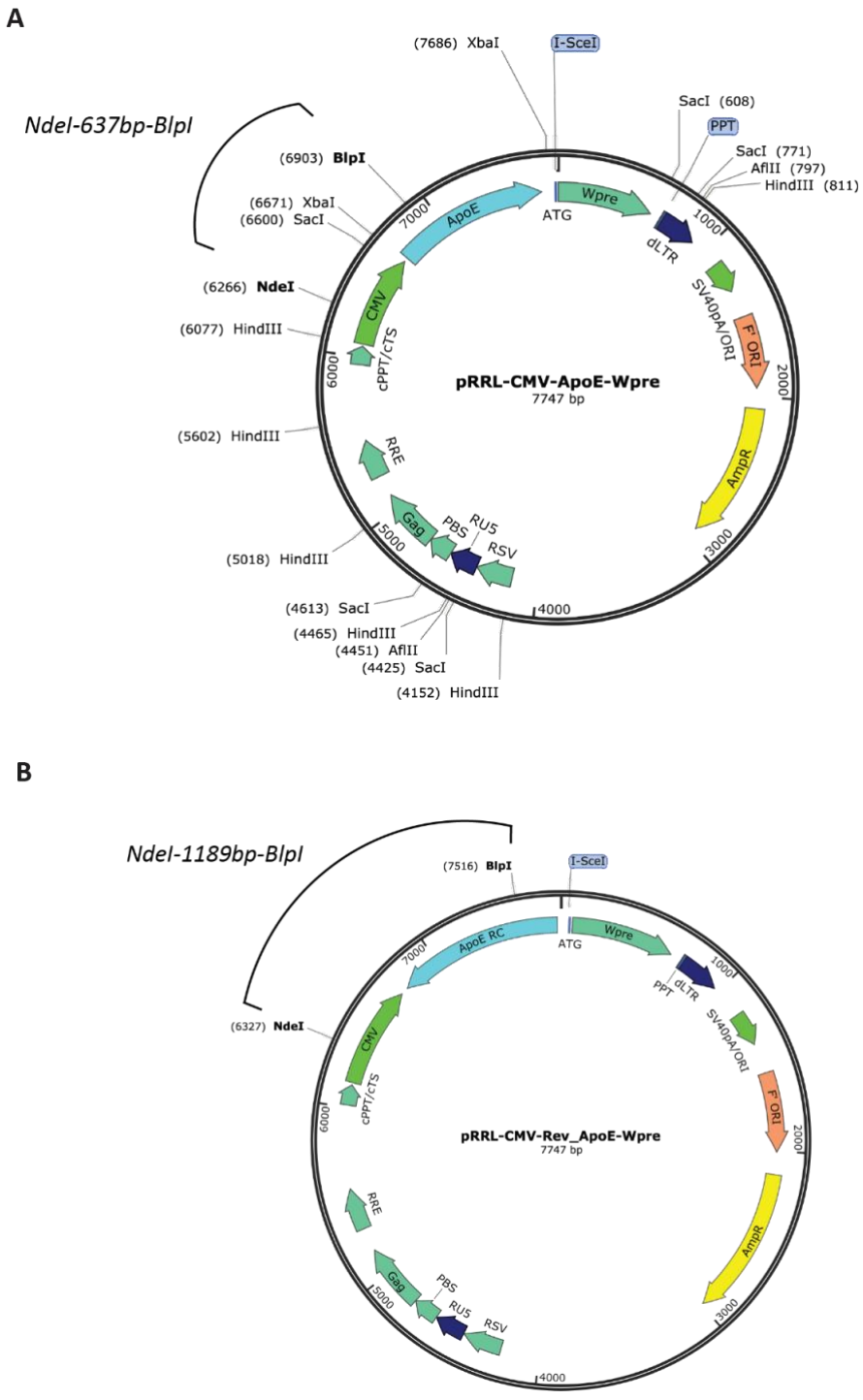

Figure 4-5 Plasmid maps showing the lentiviral transfer plasmid containing either apoE cDNA in the correct orientation (A) or apoE cDNA in the reverse orientation (B).

The purified apoE cDNA could be ligated into the lentiviral transfer plasmid in either direction since using *XbaI* sticky ends did not provide directionality for insertion. The apoE gene is driven by a CMV promoter and its expression is enhanced by the presence of a Woodchuck Hepatitis Virus (WHP) Posttranscriptional Regulatory Element (WPRE) sequence. A Central Polypurine tract (cPPT) sequence is also present for enhanced transduction in post-mitotic cells.

A

Restriction endonucleases	Predicted fragment sizes (bp)
NdeI + BlpI	7110, 637
HindIII-HF	3341, 2481, 584, 553, 475, 313
AflII	4093, 3654
SacI	3654, 1987, 1755, 188, 163
XbaI	6732, 1015

B

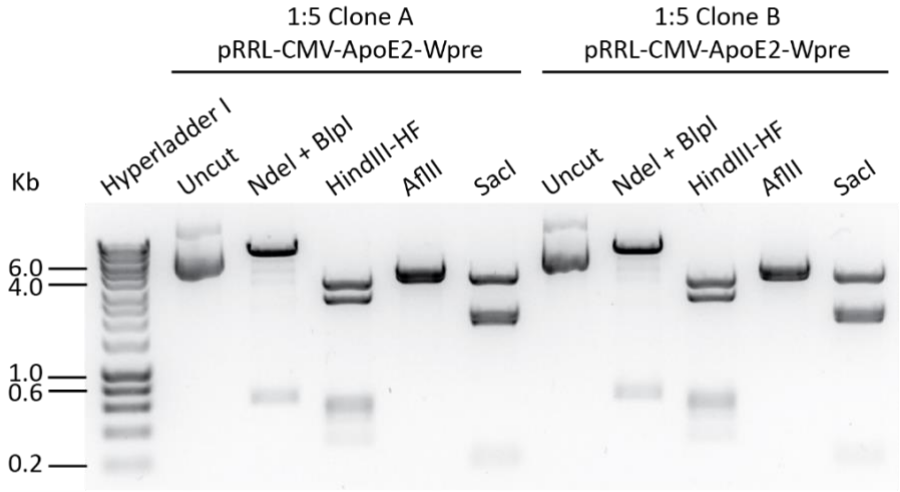

C

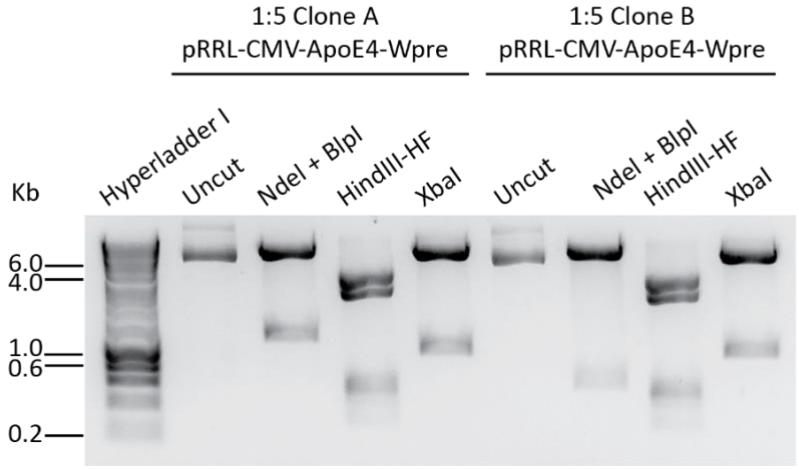

Figure 4-6 Restriction mapping analysis to identify clones containing pRRL-CMV-ApoE2-Wpre and pRRL-CMV-ApoE4-Wpre with apoE cDNA in the correct orientation.

(A) Table showing the predicted fragment sizes for the pRRL-CMV-ApoE-Wpre plasmid digested with combinations of restriction endonucleases, including a diagnostic co-digest using *NdeI* with *BlpI* to identify IDLV transfer plasmids containing apoE cDNA in the correct orientation. Representative gel electrophoresis images of restriction digests from plasmid DNA purified from E. Coli transformed with pRRL-CMV-ApoE2-Wpre (B) and pRRL-CMV-ApoE4-Wpre (C) to validate the plasmid backbone and to screen for positive clones.

4.2.2.2 Generation of pRRL-CMV-ApoE3-Wpre

An alternative strategy, summarised in Figure 4-7, was used to generate a lentivirus transfer plasmid containing apoE3 because the pCMV6-ApoE3 plasmid did not contain *XbaI* linkers. To create lentiviral transfer plasmids that contain the same sequence either side of the apoE insert, a fragment of the apoE4 cDNA within pRRL-CMV-ApoE4-Wpre was replaced with a fragment carrying the apoE3 specific sequences. Two restriction sites recognised by *BlpI* and *SbfI* flank a region of apoE cDNA containing the two polymorphisms that distinguish the apoE isoforms. Thus, the apoE4 fragment was removed from pRRL-CMV-ApoE4-Wpre by a double digest with *BlpI* and *SbfI*. Due to the presence of a second *BlpI* cut site within the Poly(A) signal of the pCMV6-ApoE3 plasmid, a *BlpI* and *SbfI* double digest produced two fragments that were similar in size (~604bp and ~708bp) and thus difficult to separate (Figure 4-3). It was therefore necessary to perform a triple digest so that the ~708bp fragment could be cleaved into smaller products, enabling isolation of the ~604bp apoE cDNA fragment. Since a recognition site for *XhoI* was identified in the ~708bp fragment, the apoE3 cDNA fragment was instead excised following a triple digest with *BlpI*, *SbfI* and *XhoI*. A ~604bp fragment containing the apoE3 sequence was liberated by *BlpI* and *SbfI* digestion and the second fragment (~708bp) was cleaved into two smaller fragments of ~329 and~379bp by *XhoI* digestion, as shown in Figure 4-3. Following separation of the digested products by agarose gel electrophoresis, the backbone of pRRL-CMV-ApoE4-Wpre and the apoE3 cDNA fragment (containing the SNPs) were purified and ligated together. The *BlpI* and *SbfI* complementary ends enabled directional insertion of apoE3 into the IDLV transfer plasmid. The ligation products were then transformed into Top10 E. Coli cells and a restriction digest was used to identify clones containing pRRL-CMV-ApoE3-Wpre (plasmid map shown in Figure 4-8 A). Plasmids derived from isolated bacterial colonies were transformed using different vector:insert ratios. These were then digested with *NdeI* and *BlpI*, which cut at unique restriction sites within the CMV promoter and apoE segment respectively. Successful ligation of apoE3 would result in two digest products (7110bp and 637bp), whereas a self-annealed vector would show a single band of 7143bp due to linearisation by *NdeI*. All pRRL-CMV-ApoE3-Wpre plasmids were positive for insertion of apoE3 cDNA as determined by detection of a fragment of ~637bp (Figure

4-8, C). A double digest with *BlpI* and *AflII* was used to check the LTR sequences and size of the construct. The expected fragment pattern and sizes as listed in Figure 4-8 B were observed (Figure 4-8, C). Sequencing of pRRL-CMV-ApoE3-Wpre confirmed that the cloning was successful and thus verified that the IDLV transfer plasmid contained cDNA encoding apoE3.

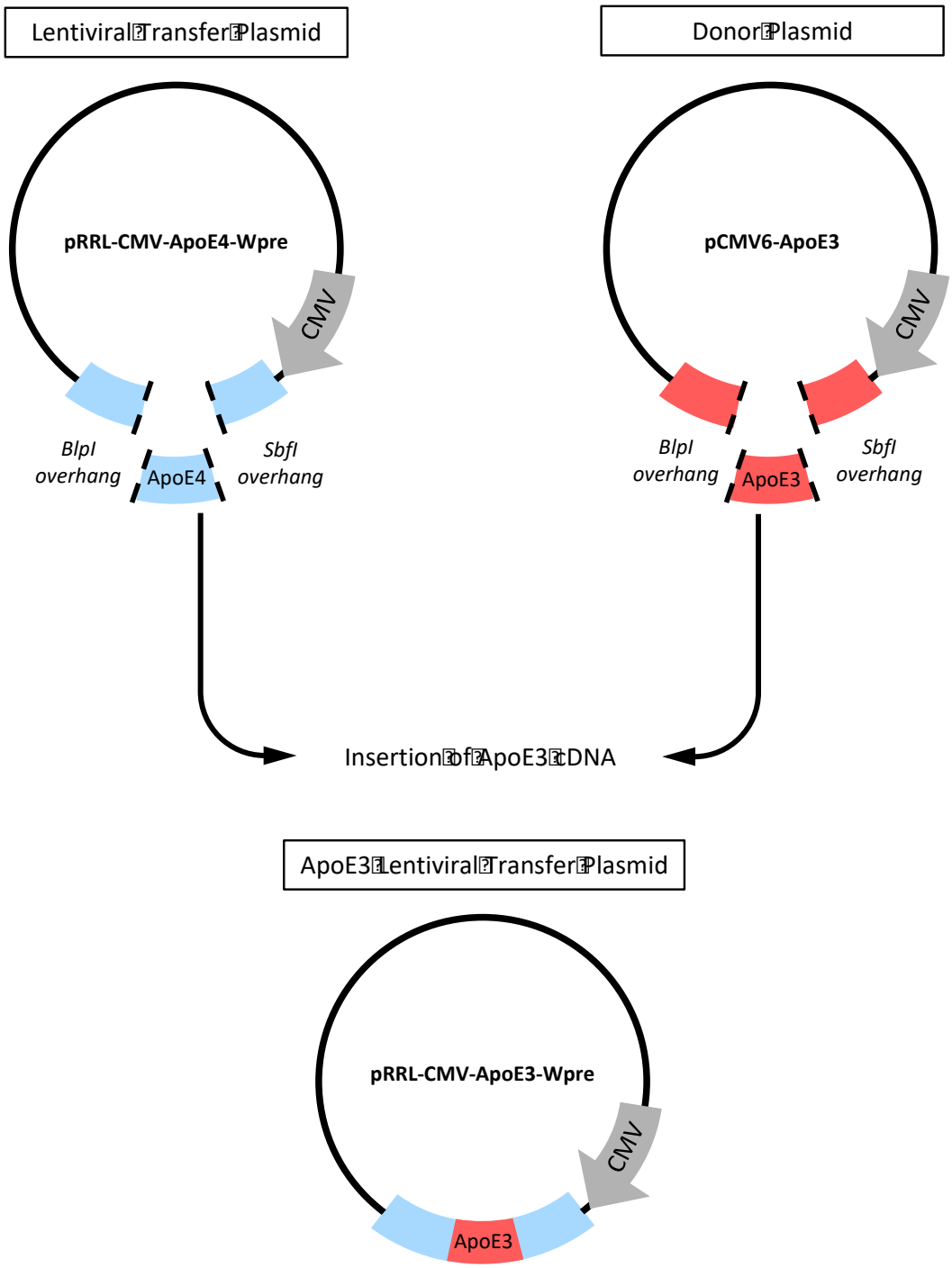

Figure 4-7 Cloning strategy used to create pRRL-CMV-ApoE3-Wpre

A fragment of the apoE3 cDNA containing the two SNPs was excised from the pCMV-AC-ApoE3 donor plasmid by a double digestion using *BlpI* with *SbfI* restriction endonucleases. XhoI was also used in this digestion to further cleave a byproduct from the donor plasmid backbone, enabling the isolation of the apoE3 cDNA segment. The apoE4 cDNA fragment was removed from pRRL-CMV-ApoE4-Wpre by digestion with *BlpI* and *SbfI* and the backbone was purified. The pRRL-CMV-ApoE3-Wpre was generated by ligation of the apoE3 cDNA fragment into the pRRL-CMV-ApoE-Wpre backbone in the correct orientation, as guided by the *BlpI* and *Sbf*I complementary-ends.

A

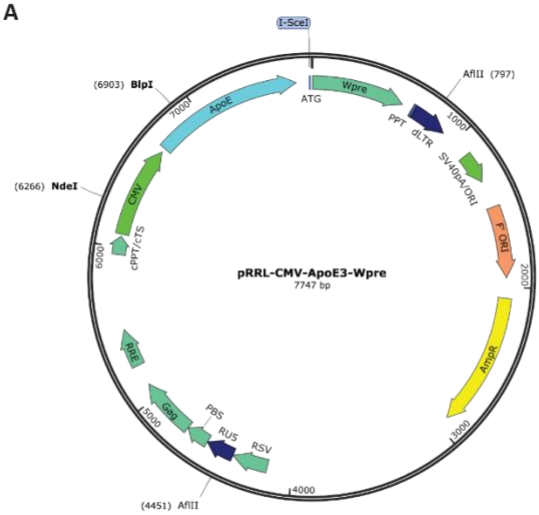

B

Restriction endonucleases	Predicted fragment sizes (bp)
NdeI + BlpI	7110, 637
AflII + BlpI	3654, 2452, 1641

C

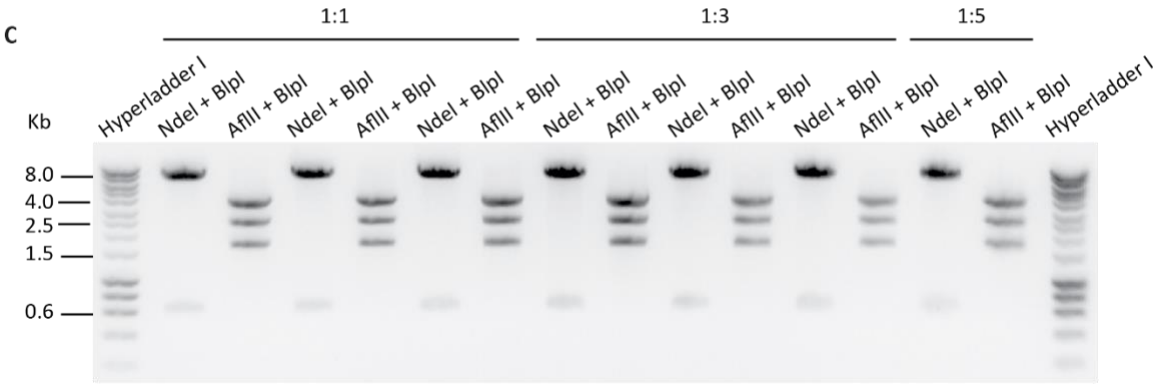

Figure 4-8 Restriction mapping analysis to identify clones containing pRRL-CMV-ApoE3-Wpre

(A) Plasmid map showing the IDLV transfer plasmid containing apoE3 cDNA. (B) Table showing the predicted fragment sizes resulting from digestion of pRRL-CMV-ApoE3-Wpre plasmid using combinations of restriction endonucleases, including the diagnostic co-digest using *NdeI* with *BlpI* to distinguish lentiviral transfer constructs containing apoE cDNA from re-ligated plasmids. (C) Gel electrophoresis image of restriction digests from plasmid DNA purified from E. Coli transformed with pRRL-CMV-ApoE3-Wpre to check the plasmid backbone and to screen for positive clones.

4.2.2.3 ApoE lentiviral transfer plasmids express apoE protein in transfected HEK293T cells

To confirm that the IDLV transfer plasmids containing apoE cDNA were functional, western blotting was performed using lysate from HEK293T cells transfected with pRRL-CMV-ApoE2-Wpre, pRRL-CMV-ApoE3-Wpre and pRRL-CMV-ApoE4-Wpre. Immunoblotting with rabbit anti- apoE 16H22L18 detected a band at ~34kDa indicating that all three constructs expressed full length apoE protein (Figure 4-9). This was not observed in the negative control, confirming that apoE was detected due to expression from the constructs. This result verified that all three IDLV transfer plasmids were indeed functional. Interestingly, less full length apoE4 was detected compared to apoE2 and apoE3, although equal amounts of protein were loaded for all samples (as shown by the actin loading control in Figure 4-9). It is possible that this could be due to enhanced degradation of apoE4 in HEK293T cells, poor transfection efficiency of pRRL-CMV-ApoE4-Wpre, or greater cell death due to apoE4 expression.

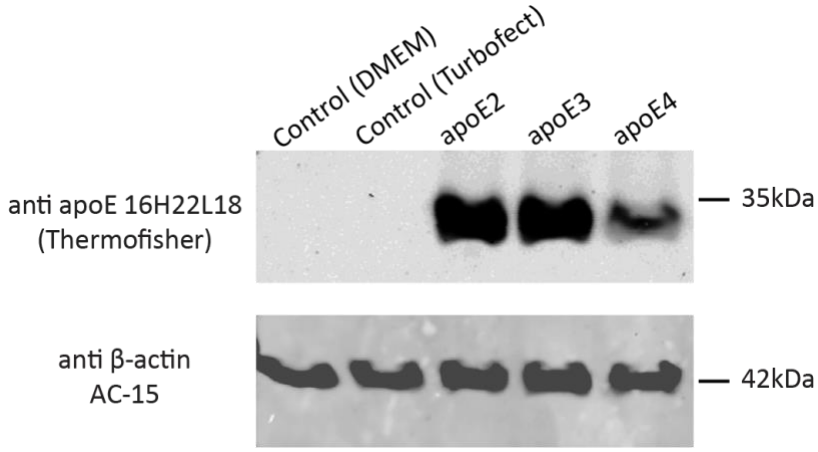

Figure 4-9 Western blots show that apoE-lentiviral plasmids express apoE protein in HEK293T cells
Western blots showing detection of full length apoE protein from HEK293T cells transfected with either pRRL-CMV-ApoE2-Wpre, pRRL-CMV-ApoE3-Wpre or pRRL-CMV-ApoE4-Wpre for 24 hours, and ß-actin to confirm equal loading of protein.

4.2.3 Transduction of primary neurons with GFP lentiviral vectors

The optimal MOI to use in mature primary neurons was established using lentiviral vectors expressing GFP under a CMV promoter (shown in Figure 4-10). Primary neurons were transduced at 18DIV using a range of MOIs: 10, 50, 100, 150 and 200 for a qualitative comparison of transduction efficiency. The neurons were imaged three days post transduction using brightfield microscopy and fluorescence microscopy (using the GFP channel and consistent exposure settings) to examine neuronal morphology and to detect GFP fluorescence. Figure 4-11 shows images of primary neurons transduced with different MOIs taken in the FITC and brightfield channels. GFP expression in neuronal cell bodies and neurite projections, as shown in the merged images, was observed to increase as MOI increased. At an MOI of 10, approximately less than 50% of neurons showed high GFP expression in the cell bodies, whereas at an MOI of 150, a substantial number of neurons (~90%) showed high levels of GFP signal in both cell bodies and neurite projections. An MOI of 200 however, appeared to be toxic since the GFP expression revealed retraction of the neurite projections. Moreover, GFP signal was apparent in smaller cell bodies resembling apoptotic cells. Since the fragmentation of apoE was to be characterised by western blotting, high expression levels of the transgene was desired so that less abundant fragments were likely to be detected. Therefore an MOI of 150 was selected for further experiments, since this showed the highest expression levels of GFP, whilst showing relatively healthy neuronal morphology.

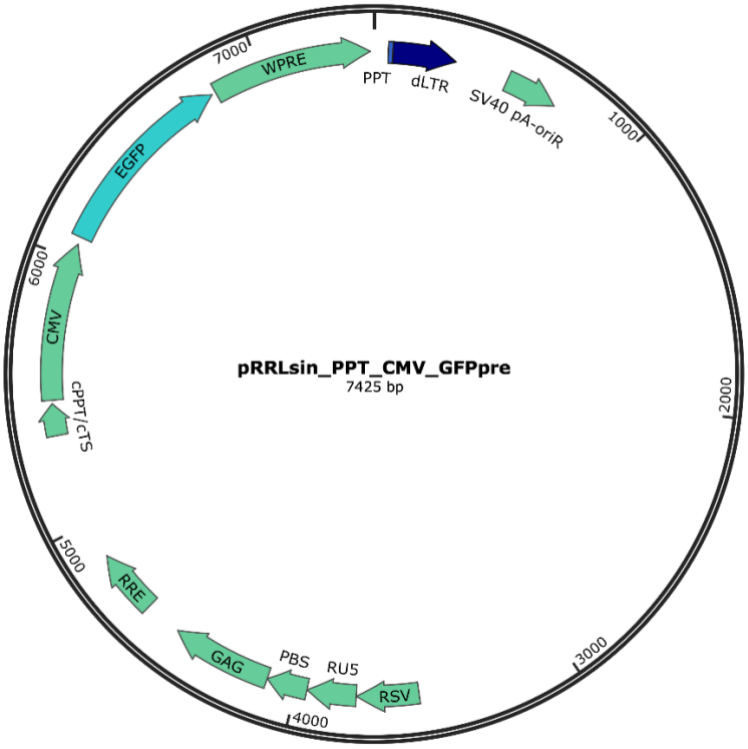

Figure 4-10 Plasmid map of the GFP-lentiviral transfer plasmid

The GFP gene is driven by a CMV promoter and GFP expression is enhanced by the presence of a Woodchuck Hepatitis Virus (WHP) Posttranscriptional Regulatory Element (WPRE) sequence. A Central Polyprune tract (cPPT) sequence is also present for enhanced transduction in post-mitotic cells.

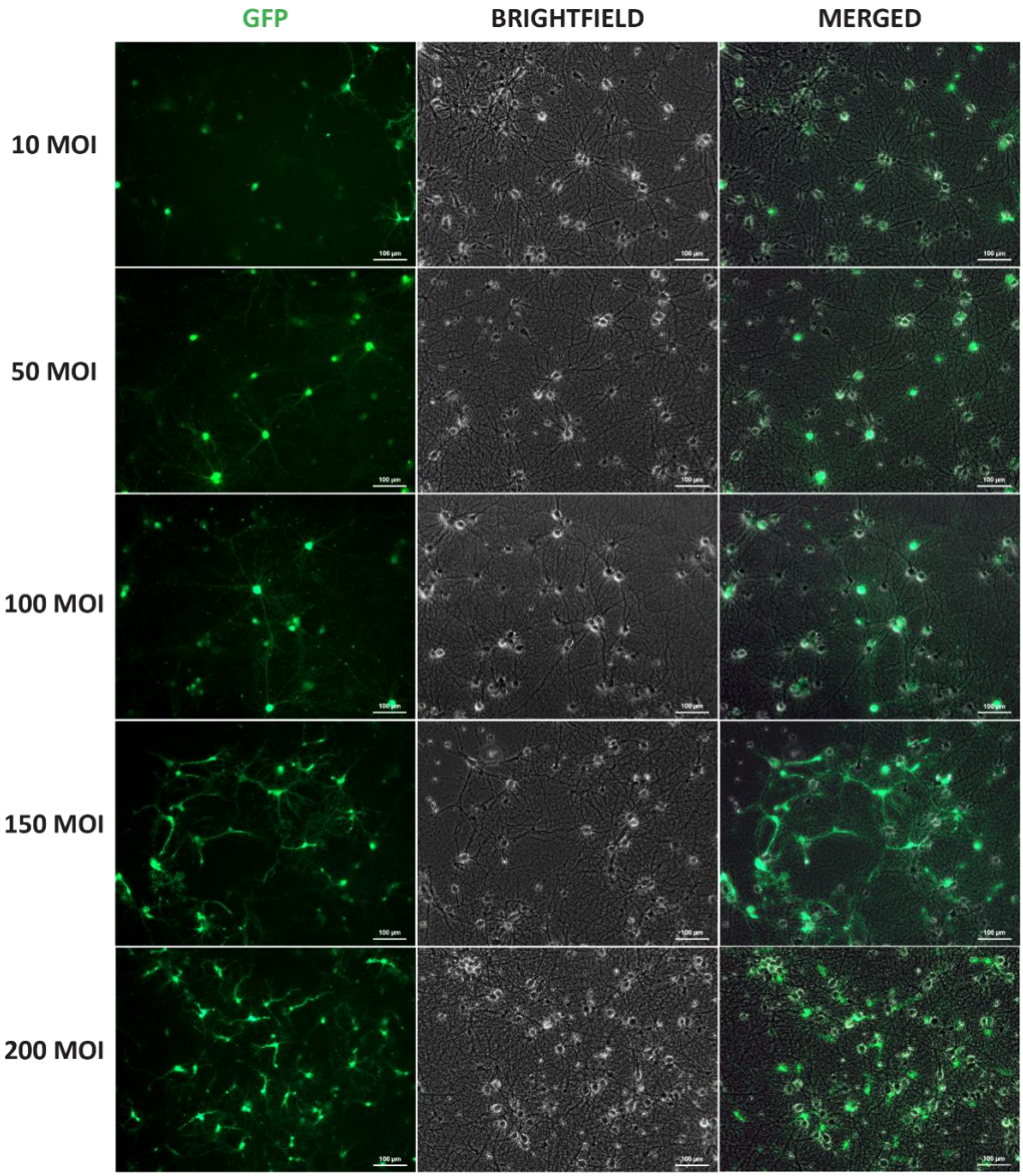

Figure 4-11 Comparison of transduction efficiency by GFP-expressing lentiviruses at increasing MOIs in primary neurons

Primary neurons were transduced at 18DIV with GFP-expressing lentiviral vectors at increasing MOIs: 10, 50, 100, 150 and 200 for a qualitative comparison of transduction efficiency and expression level throughout the neuron. Scale bar, 100µm.

4.2.4 ApoE-lentiviral vectors express apoE protein in transduced rat primary neurons

Following the generation and titration of apoE-lentiviral vectors, the functionality of the vectors was next assessed. To do so, primary hippocampal neurons were initially transduced at 18DIV for 72 hours using apoE-expressing lentiviral vectors at an MOI of 150. Western blotting was used to confirm the expression of apoE protein in transduced neurons. Full length apoE protein was detected in protein extracts of neurons transduced with lentiviral vectors expressing apoE2, apoE3 and apoE4 as shown in Figure 4-12. No apoE expression was detected in control non-transduced neurons, confirming that the presence of apoE was due to expression from the lentiviral vectors. This result verified that the apoE-lentiviral vectors were successfully produced and showed that they could transduce mature neurons with expression levels suitable for western blotting analysis at an MOI of 150.

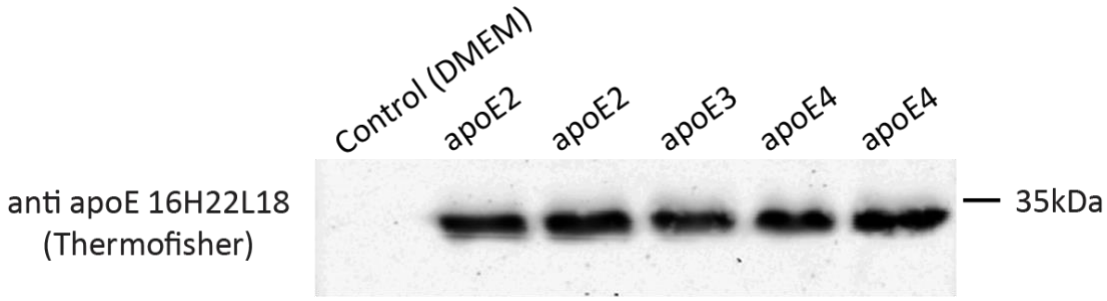

Figure 4-12 Western blots show apoE-expressing lentiviral vectors express apoE protein in transduced primary neurons

Western blot showing detection of full length apoE protein in protein extracts from 18DIV primary neurons transduced with lentiviral vectors expressing either apoE2, apoE3 or apoE4. These vectors were generated using the pRRL-CMV-ApoE2-Wpre, pRRL-CMV-ApoE3-Wpre or pRRL-CMV-ApoE4-Wpre lentiviral transfer plasmids.

4.3 DISCUSSION

Here, lentiviral vectors expressing apoE under the CMV promoter were generated so that the three major human apoE isoforms could be expressed in mature primary hippocampal cultures. This approach was chosen because gene delivery into postmitotic neurons by transfection techniques often requires freshly isolated neurons that yield low transfection efficiency and show high toxicity (Washbourne and McAllister, 2002, Karra and Dahm, 2010). Lentiviral vectors however, can transduce mature primary neurons with high transduction efficiency and little toxicity and result in high expression levels (Karra and Dahm, 2010, Royo et al., 2008). The data presented in this chapter shows that lentiviral transfer plasmids containing cDNA encoding either apoE2, apoE3, or apoE4 were successfully generated. Restriction mapping analysis and sequencing confirmed that apoE cDNA for all three isoforms was correctly inserted into the lentiviral transfer plasmid backbone. Furthermore, western blotting for apoE protein confirmed that the apoE constructs were functional.

The apoE lentiviral transfer plasmids were used as part of the third generation lentiviral packaging system to produce lentiviral vectors expressing apoE. Before the apoE lentiviral vectors could be used to transduce the neuronal cultures, the optimal MOI had to be determined. Since the apoE lentiviral vectors do not contain a reporter transgene, GFP lentiviral vectors were used for rapid comparison of transduction efficiencies at different MOIs in neuronal cultures by fluorescence microscopy. Typical MOIs used in several publications range from 1-10 (Ding and Kilpatrick, 2013, Denning et al., 2013). This is because these MOIs are based on titres derived by fluoresence microscopy or FACS and so are reflective of functional viral vector. Here however, high MOIs (10-200) were selected because the vector titres used to calculate the MOI were determined by qPCR analysis, which also accounts for incomplete and non-functional vectors. Although the GFP lentiviral vectors could have been titrated by flow cytometry analysis, qPCR analysis was carried out so that the titres would be comparable to those obtained for the apoE lentiviral vectors. Based on GFP fluorescence images in section 4.2.3, the optimum MOI for high expression levels in 18 DIV primary neurons was determined to be 150. Remarkably at this MOI, a transduction efficiency of approximately 90% was

observed. This was surprising since transduction efficiencies of this level are usually found in neurons transduced on the day of cell plating (0 DIV) or the day after (1 DIV) (Dittgen et al., 2004, Ding and Kilpatrick, 2013). Moreover, transduction efficiency has been shown to significantly decrease with increasing age of the primary neuronal culture (Wanisch et al., 2013). Nonetheless, the results indicated that this MOI was suitable for applications such as western blotting analysis, where high expression levels are required for sufficient detection of the protein. Indeed, transduction of mature primary neurons using apoE-expressing lentiviral vectors at an MOI of 150 resulted in detectable apoE expression for all apoE isoforms.

Collectively, this work in this chapter shows that apoE lentiviral vectors were successfully produced and that they could be used to express apoE protein at sufficient levels in mature primary neurons for western blotting analysis. Therefore, the apoE lentiviral vectors can be used to aid the study of apoE fragmentation and cell biology in primary neuronal cultures.

Chapter 5 CHARACTERISATION OF APOE PROCESSING IN CELL MODELS

5.1 INTRODUCTION

Increasing evidence suggests that intraneuronal full length apoE and its proteolytic fragments may be key players in AD pathology (Huang et al., 2004, Mahley et al., 2006, Mahley and Huang, 2012). This has led to the proposal of a model where fragmentation of apoE leads to a loss of protective function, but also a toxic gain of function (Rohn, 2013, Mahley and Huang, 2012). In this model, apoE expression in neurons is triggered by factors such as oxidative stress or Aß42-mediated neuronal dysfunction. Intraneuronal apoE protein then undergoes isoform-dependent proteolysis (apoE4>apoE3>apoE2) due to differential domain interaction, which produces bioactive and toxic fragments. It is thought that these fragments escape the secretory pathway, enter the cytosol and induce dysfunction in mitochondria and the cytoskeletal network (Huang et al., 2004, Mahley and Huang, 2012).

Although there is mounting evidence to support a role for neuron-specific proteolysis of apoE4 and AD pathology, there is very little available data to determine whether the contrasting, neuroprotective role of apoE2 is due to differential processing when expressed in neurons. So far, fragmentation of apoE has primarily been characterised using protein extracts from post-mortem brains of control and AD human patients (Jones et al., 2011, Elliott et al., 2011, Harris et al., 2003, Tamboli et al., 2014), as well as transgenic AD mouse models (Brecht et al., 2004b). Whilst the majority of these studies have shown that proteolysis of apoE4 is associated with greater fragmentation load when compared to apoE3, there is little conclusive evidence in the literature regarding the proteolytic susceptibility of apoE2. To date, only a single study has shown that apoE2 fragments also exist in human brain, however fragmentation load between isoforms was not compared (Conejero-Goldberg et al., 2014). One reason for the lack of studies including apoE2 is that the *APOE2* allele is rarer than the other two major isoforms, restricting the availability of brain tissue from patients with an *APOE2* genotype for experimentation. In consideration of this limitation, an alternative approach would be to use cell models to investigate the impact of apoE isoform on proteolytic susceptibility. Surprisingly though, the fragmentation profile of the three major apoE isoforms has not

been thoroughly explored in cell models either, although *in vitro* models are frequently used to investigate the functional roles of apoE. So far, only one *in vitro* study has compared the total level of fragments for all three apoE isoforms when expressed in mouse neuroblastoma cells (Wellnitz et al., 2005). In this study, western blotting using a C-terminus specific antibody revealed a single ~13kDa C-terminal fragment for all three apoE isoforms, which was more abundant for apoE4 expressing cells, followed by apoE3 and apoE2. Whilst this data supports the apoE proteolysis model, it does not provide information on the relative abundancy of other fragments.

The identity of apoE fragments also remains elusive. Whilst apoE fragments have been examined either by mass spectrometry or using N- and C- terminal specific antibodies (Castano et al., 1995, Wisniewski et al., 1995, Rohn et al., 2012, Tamboli et al., 2014, Wellnitz et al., 2005), there is still not a consensus regarding their composition. This is partly due to the wide variation in the source of apoE fragments, which range from spleen tissue through to fragments obtained via cleavage of recombinant apoE using thrombin or chymotrypsin (Castano et al., 1995, Wisniewski et al., 1995, Rohn et al., 2012, Tamboli et al., 2014). Even though conclusive proof of the apoE fragments existence and exact sequences is yet to be provided, several studies have used truncated versions of either apoE3 or apoE4 in order to understand the functions of these proteolytic fragments (Huang et al., 2001, Harris et al., 2003, Chang et al., 2005, Nakamura et al., 2009, Bien-Ly et al., 2011, Tanaka et al., 2006).

Here, three cell models were used to characterise fragmentation of apoE2, apoE3 and apoE4. These models were: N2a cells (a murine neuroblastoma cell line), SH-SY5Y cells (a human neuroblastoma cell line), and primary hippocampal rat neurons. N2a cells are from a mouse neuroblastoma and have a mixed neuronal-like and amoeboid morphology in the undifferentiated state. It has been reported that apoE-mediated toxicity in N2a cells is comparable to that observed in cultured primary neurons from NSE-apoE mice (Chen et al., 2011a). Moreover, N2a cells have been extensively used to study the effects of apoE and its fragments on mitochondrial and cytoskeletal function (Huang et al., 2001, Nakamura et al., 2009, Chang et al., 2005), indicating that they are

useful models for investigating the effects of intraneuronal apoE. For these reasons, N2a cells were considered as a suitable cell-based model to examine apoE processing. SH-SY5Y cells are a human-derived neuroblastoma cell line, which show two phenotypes in culture: neuronal-like cells and epithelial-like cells (Ross et al., 1983). Characterisation of this cell line by enzymatic assays revealed that whilst the neuronal-like cells exhibit markers of dopaminergic neurons (e.g. tyrosine hydroxylase positive), the epithelial-like cells lack neuronal markers (Ross et al., 1983). Despite the heterogeneity in cellular phenotype, there are benefits to using this cell line such as the expression of human protein isoforms (Kovalevich and Langford, 2013). SH-SY5Y cells are homozygous for *APOE3* and are reported to express apoE mRNA (Soulié et al., 1999). It is notable that fragmentation of endogenous apoE has also been observed in SH-SY5Y cells, which occurred in response to overexpression of wild type APP751 or the C-terminal domain of APP (C99) (Saul and Wirths, 2016). However, whether apoE cleavage is isoform-dependent in this cell line is unknown. It is also important to consider that neuroblastoma cells have drawbacks, such as the lack of mature neuronal structures that include synapses and axons. Primary neurons however, are one of the closest culture-based models to *in vivo* systems. Hence, comparing the neuroblastoma cell lines to primary neurons, enables evaluation of their use to model apoE processing and neurobiology of all three full length apoE isoforms. Furthermore, using multiple *in vitro* cell models enables an assessment of the reproducibility of the observations made about the effect of apoE isoform on apoE proteolysis *in vitro*. Expression of apoE in the N2a and SH-SY5Y cell lines was achieved by transient transfection with constructs expressing apoE2, apoE3 or apoE4 under a CMV promoter for 48 hours. Primary neurons however, were transduced using apoE-lentiviral vectors at an MOI of 150 for 72 hours as based on the high expression levels of GFP lentiviral vectors at this MOI and time point (shown in the previous chapter). Fragmentation of the 'protective' apoE2, the 'neutral' apoE3 and the 'toxic' apoE4 was then characterised in the different cell models to address:

1. The fragmentation pattern of each isoform – are there unique fragments that could confer protection or toxicity?

2. The susceptibility of each isoform to proteolysis – could the differential risk in AD be due to differences in fragment load?
3. The composition of apoE fragments - could the differential risk in AD be due to differences in fragment composition?

This is of importance because insights into apoE processing for each isoform may partially explain the differential effects these variants have in neurons. In addition, determining the identity of these fragments in a cellular context is a necessary first step to understanding how they may contribute to neuronal dysfunction and AD, or confer neuroprotection against AD.

5.2 RESULTS

5.2.1 Validation of anti- apoE antibody epitope sites in HEK293T cells

In order to thoroughly characterise apoE processing, the epitopes that the commercially available anti-apoE antibodies recognise were first validated by western blotting. Protein extracts used were from HEK293T cells transfected with constructs encoding full length or truncated versions of apoE3 (kindly gifted by Professor Tadafumi Hashimoto and Professor Bradley Hyman) for 24 hours. The truncated apoE constructs expressed either apoE3 NT (Δ192-299), apoE3 CT (Δ1-192), apoE3 Δ243-299, apoE3 Δ243-272 or apoE3 Δ273-299. A schematic illustration for each of these variants is shown in Figure 5-1. The truncated variants of apoE facilitated identification of the regions of apoE that these antibodies recognise. For example, antibodies against N-terminal apoE should only detect N-terminal fragments and vice versa. Additionally, the C-terminal truncations include deletions of either the lipid binding domain or the region after, both of which are specific epitopes for commercially available antibodies (anti-apoE 3H1 and anti-apoE E-8 respectively). Since not all epitopes were disclosed for some of the antibodies, it was imperative to determine as accurately as possible, the domains that these antibodies recognise (i.e. either the N- or C- terminus of apoE).

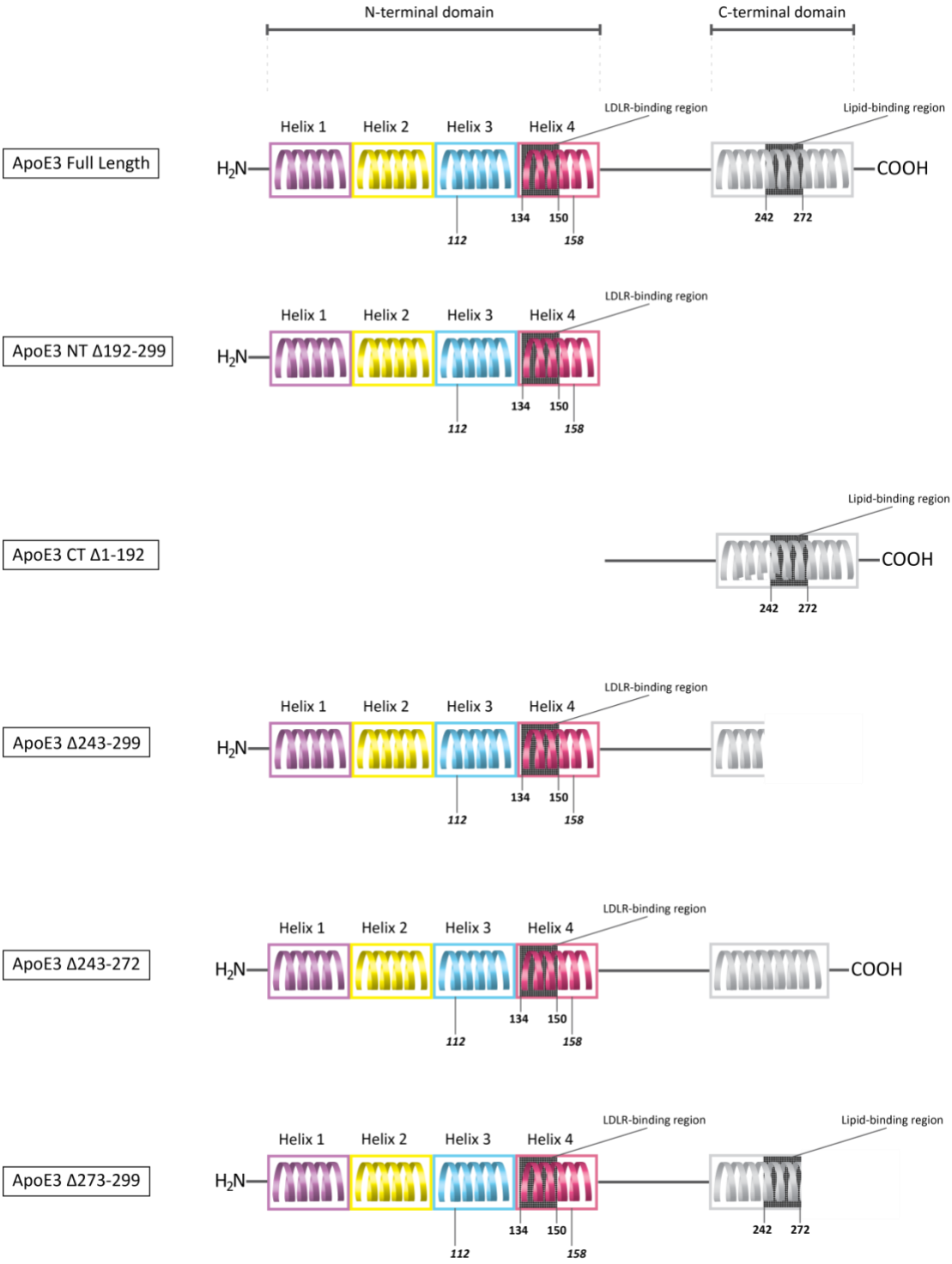

Figure 5-1 Schematic of full length apoE and truncated apoE variants

Illustrations showing the domain structure of full length apoE and the truncated apoE variants. ApoE3 full length is composed of an N-terminal domain containing 4 α-helix structures, followed by a hinge region and a C-terminal domain. The polymorphisms that distinguish the three major apoE isoforms are located within the N-terminus: at position 112 in Helix 3 and 158 in Helix 4. The LDLR-binding region (134-150aa) is within helix 4 of the N-terminus and the lipid-binding region (242-272aa) is within the C-terminal domain. The truncated apoE variants comprise different domains as depicted in the diagram.

Figure 5-2 shows western blots of anti- apoE antibodies that are specific for the N-terminus of apoE protein. Expectedly, rabbit anti- apoE SP+1-32aa (Aviva) detected full length apoE3 and truncated apoE3 variants containing the N-terminus (Figure 5-2, A). Additionally, this antibody did not detect a band for apoE3 CT (Δ1-192), thus confirming its specificity for the N-terminus of apoE. Likewise, only bands for N-terminal-containing apoE3 variants were detected by mouse anti- apoE WU E-4 suggesting that the epitope for this antibody is also located within the N-terminus of apoE (Figure 5-2, B). Surprisingly, rabbit anti- apoE 16H22L18 detected apoE3 NT (Δ192-299), apoE3 Δ243-299 and apoE3 Δ243-272 (Figure 5-2, C), even though these variants do not contain the advertised epitope of this antibody: the lipid-binding region (240-251aa) of apoE. Moreover, apoE3 Δ273-299 was detected, whilst apoE CT Δ1-192 was not. These findings indicate that the advertised epitope is incorrect and that antibody recognises a region within the N-terminal domain of apoE.

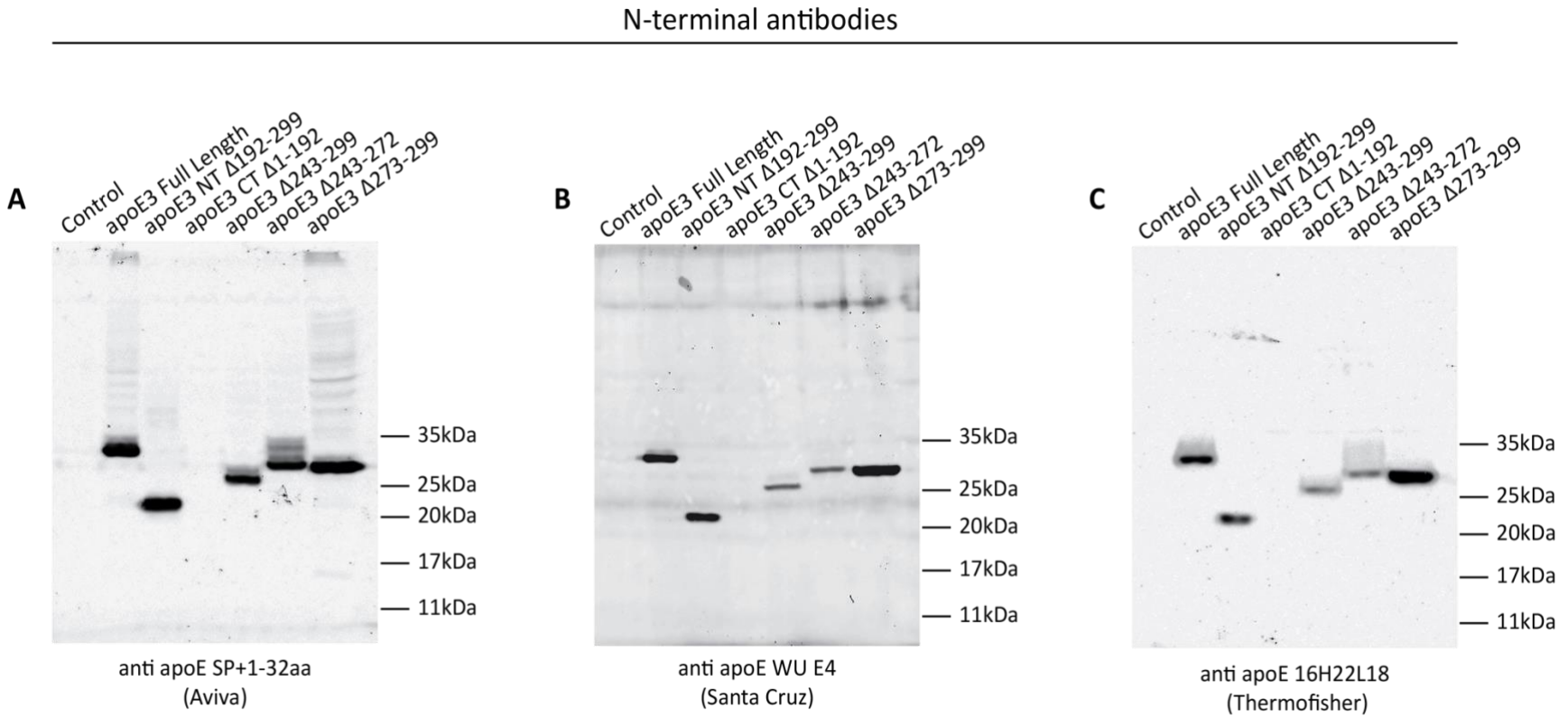

Figure 5-2 Western blots validate N-terminal specific anti- apoE antibodies

Western blots showing immunoreactivity of (A) anti- apoE SP+1-32aa (Aviva), (B) anti- apoE WU E-4 and (C) anti- apoE 16H22L18 antibodies to full length or N-terminal-containing truncated apoE3 protein expressed by transient transfection in HEK293T cells.

Figure 5-3 shows western blots of anti- apoE antibodies that are advertised as specific to the C-terminus of the apoE protein. The advertised epitope of mouse anti- apoE 3H1 is 243-272aa of apoE. Indeed, the antibody was specific to this region as shown by detection of a band for apoE3 Δ273-299 but not for apoE3 NT Δ192-299, apoE3 Δ243-272 and apoE3 Δ243-299; all variants in which the epitope is deleted (Figure 5-3, A). As anticipated, mouse anti- apoE 3H1 also detected full length apoE3 and apoE3 CT Δ1-192. Likewise, western blotting analysis confirmed the advertised epitope of the mouse anti-apoE E-8 as 272-299aa of apoE (Figure 5-3, B). This antibody detected full length apoE3 and the C-terminal variants containing 272-299aa: apoE3 CT Δ1-192 and apoE3 Δ243-272. However, no bands were detected when this epitope was not present, such as in apoE3 Δ243-299 and apoE3 Δ273-299, confirming the specificity of this antibody for the 272-299aa of apoE. Additionally, mouse anti- apoE E-8 did not detect apoE NT Δ192-299, confirming that it does not recognise any regions of the apoE N-terminus.

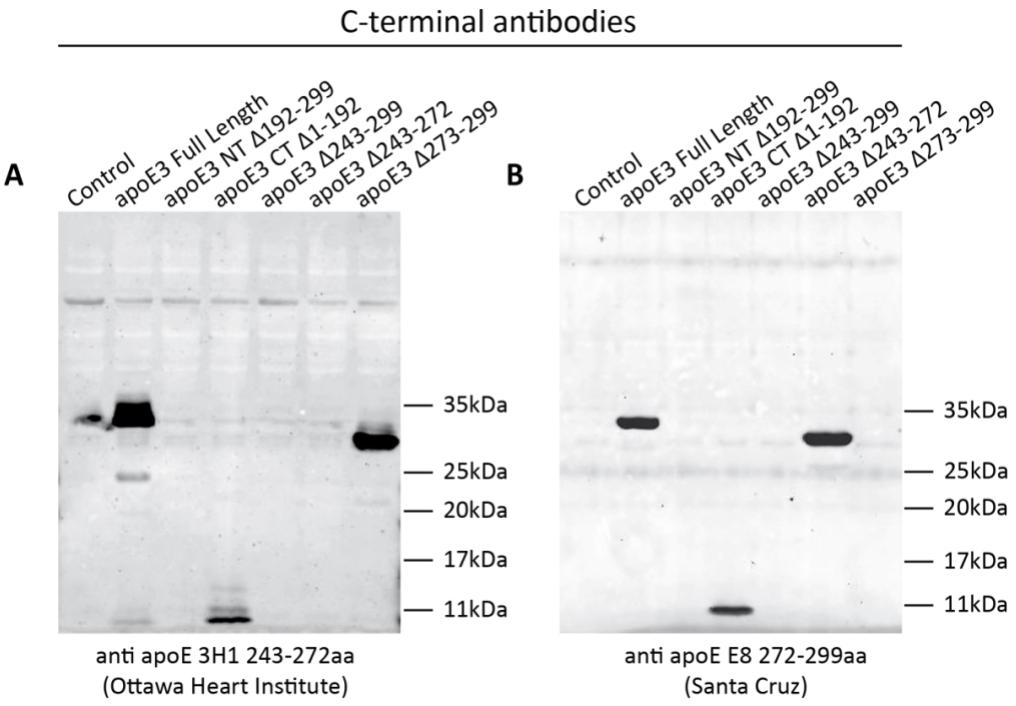

Figure 5-3 Western blots validate the epitopes of C-terminal anti- apoE antibodies

The epitopes of C terminal specific anti- apoE antibodies were verified by western blotting using full length and truncated apoE3 protein expressed by transient transfection in HEK293T cells. (A) Western blot showing immunoreactivity of anti- apoE 3H1 to full length or truncated apoE3 variants containing the epitope 243-272aa (apoE3 CT Δ1-191 and apoE3 Δ273-299 only). (B) Western blot showing immunoreactivity of anti- apoE E-8 to full length or truncated apoE3 variants containing epitope 273-299aa (apoE CT Δ1-191 and apoE Δ243-272 only).

The goat anti- apoE (Calbiochem) antibody raised against the full length apoE protein detected full length apoE3 and all truncated apoE3 variants (Figure 5-4). Notably, the signal for the ~10kDa apoE CT fragment appeared to be lower when using the goat-anti apoE (Calbiochem) compared to both mouse anti-apoE 3H1 (Figure 5-3, A) and mouse anti- apoE E-8 (Figure 5-3, B) for the same protein extracts, although the same amount of protein was loaded. Minor fragments were observed for apoE3 full length, apoE3 Δ243-272, apoE3 Δ243-299, and apoE3 Δ273-299, suggesting that apoE may be cleaved towards the amino-end of the protein in HEK293T cells. This greater range of apoE epitopes detected by goat anti-apoE (Calbiochem) antibody highlights its suitability over the other antibodies for comparing the proteolytic susceptibility and fragmentation profile of all three major isoforms by western blotting.

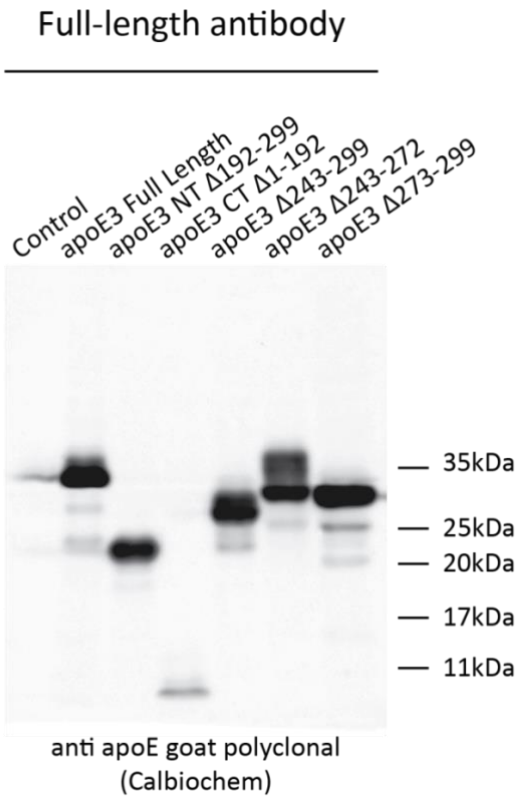

Figure 5-4 Western blot showing immunoreactivity of the polyclonal goat anti- apoE antibody to various regions of the N- and C-terminus of apoE

Goat anti- apoE (Calbiochem) detected full length and truncated apoE3 variants expressed by transient transfection in HEK293T cells, indicating that it exhibits immunoreactivity to both the N- and C-terminus of apoE.

Subsequently, the regions recognised by each antibody were identified and summarised in a schematic of the apoE protein shown in Figure 5-5.

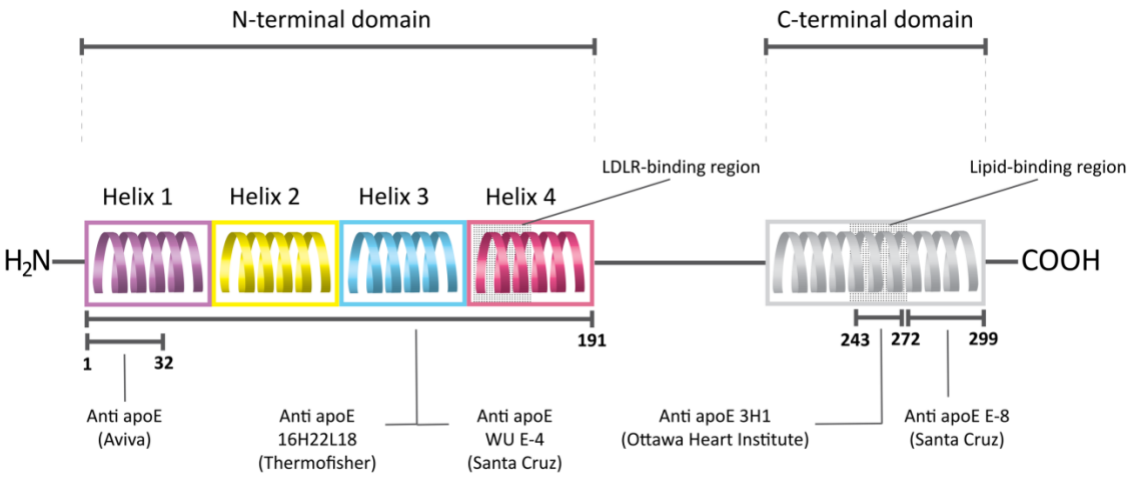

Figure 5-5 Diagram illustrating apoE domain structure and anti- apoE antibody epitopes
Anti- apoE (Aviva) recognises a region between the signalling peptide and the first 32 amino acids within Helix 1 of the N-terminus of apoE. Anti- apoE 16H22L18 and anti- apoE WU E-4 recognise a region within the N-terminus of apoE. Anti- apoE 3H1 recognises the lipid binding region (243-272aa) within the C-terminus whilst anti- apoE E-8 recognises the remaining residues after the lipid binding region (272-299aa).

5.2.2 Optimisation of western blotting for the detection of apoE fragments

5.2.2.1 Trialling different SDS PAGE systems to resolve apoE fragments

In order to examine the fragmentation pattern of apoE isoforms, it was first necessary to determine the optimal SDS PAGE system for clearly separating the fragments of apoE. To do so, hand-cast Tris-glycine gels of different acrylamide percentages and a pre-cast 10% Bis-Tris gel were used to separate protein extracts from apoE-transfected and control N2a cells. To ensure that the maximum range of apoE fragments were detected, all blots were probed with the goat anti- apoE (Calbiochem) antibody.

The blots from hand-cast Tris-glycine gels are shown in Figure 5-6; A-C. Since apoE has been shown to generate fragments ranging from 10kDa in size and upwards, a 12% Tris-glycine gel was first used because this acrylamide percentage is suitable for the separation of protein sizes ranging from ~10 to 70kDa. Five fragments that were ~10 to 30kDa in size were observed (Figure 5-6, A), and were comparable to those generated from murine apoE in 5XFAD mice detected by a C-terminal specific antibody (Saul and

Wirths, 2016). However, although the ~22-30kDa bands were clearly distinguishable, the lower molecular weight bands were not sharp, and were partly obscured by the excess SDS visible toward the end of the separation gel. Since this would make quantification of the relative amounts of each fragment problematic, a 4-20% Tris-glycine gradient gel was also trialled (Figure 5-6, B) in an attempt to separate the lower molecular weight bands from the SDS front. This gel percentage showed sharper lower molecular weight bands (~10 and ~14kDa) but poorly separated the higher molecular weight bands (~22-30kDa). Hence, to increase resolution of the high molecular weight bands too, the samples were next resolved on a 10-20% Tris-glycine gradient gel. Whilst this approach showed better separation of both the high and low molecular weight fragments, the ~10 and ~14kDa bands were still diffuse in comparison to the ~22-30kDa bands (Figure 5-6, C). In addition, the Tris-glycine gels consistently showed horizontal smearing of the full length apoE protein in lanes containing extracts from apoE-transfected N2a cells, but also control cells (Figure 5-6, A-C). Because of this, Tris-glycine gels were considered as unsuitable for quantification of the relative amount of apoE fragments in extracts from overexpression work.

To enhance separation/resolution of the lower molecular weight bands and to see if the smear was an artefact of using the Tris-glycine gels, a pre-cast 10% Bis-Tris NuPAGE protein gel using MES buffer was also trialled. The Bis-Tris SDS PAGE system was selected since the lower operating pH of 7.0, compared with 9.5 in Tris-glycine gels, is reported to promote sample integrity and gel stability. Moreover, using MES buffer in conjunction with a gel percentage of 10% is advertised as suitable for resolving proteins ranging from ~2.5-55kDa, which is ideal for resolving apoE fragments that are within this range. Surprisingly, immunoblotting for apoE revealed differences in the number of distinct fragments observed when using the 10% Bis-Tris gel (Figure 5-6, D) compared to the Tris-glycine gels (Figure 5-6, A-C). A total of ~6 distinct fragments were detected in the blots from using 10% Bis-Tris gels, compared to ~5 observed when using Tris-glycine gels. Interestingly, although the faint ~30kDa fragment was no longer visible, a strong ~32kDa fragment was detected, suggesting that the full-length band observed in the Tris-glycine gels likely represents both the ~32kDa fragment and full length apoE. Moreover,

an additional lower molecular weight band at ~17kDa was clearly visible, indicating that the ~14kDa band observed in the Tris-glycine gels likely comprised the ~14kDa and ~17kDa fragments. The horizontal smear observed the Tris-glycine gels was not apparent when using the 10% Bis-Tris gel, likely due to improved separation of both full length apoE and the ~32kDa fragment. Collectively, results from the use of the Bis-Tris gel system showed optimal separation of the apoE fragments and enabled quantitation of the relative intensities of each apoE fragment in subsequent work.

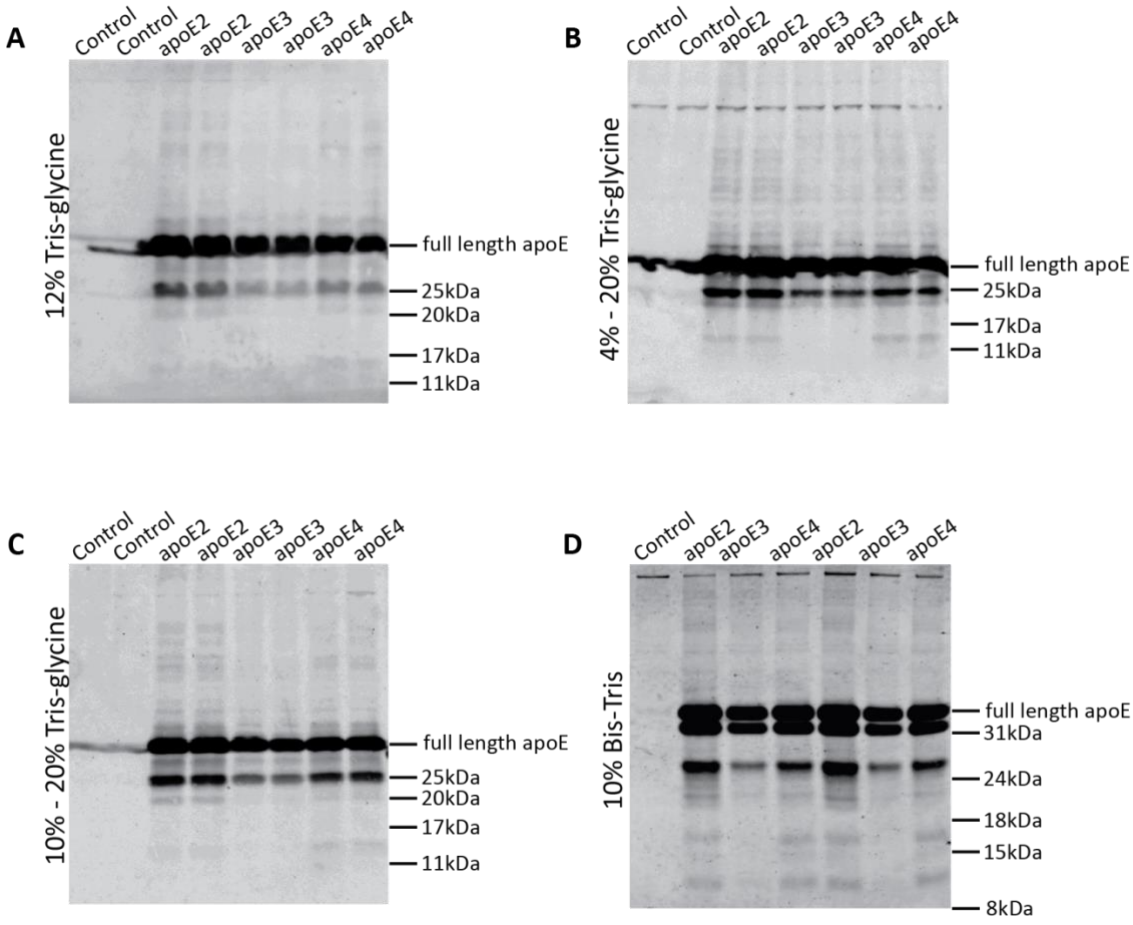

Figure 5-6 Separation of apoE full length protein and fragments using different acrylamide percentages and gel systems

Western blots showing the separation of apoE fragments from 20µg of apoE-transfected and control N2a cell extracts by SDS PAGE using different acrylamide percentages and gel systems: (A) 12% acrylamide Tris-glycine gel, (B) 4-20% acrylamide Tris-glycine gradient gel, (C) 10-20% acrylamide Tris-glycine gradient gel, and (D) 10% Bis-Tris gel using MES buffer.

5.2.2.2 Optimisation of the incubation time for primary anti- apoE antibodies in western blotting

Following optimisation of SDS PAGE for resolving the apoE fragments, the optimal incubation time for the goat anti- apoE (Calbiochem), rabbit anti- apoE SP+1-32aa (Aviva) and mouse anti- apoE E-8 antibodies was next determined. This was carried out because the time of primary antibody incubation during western blotting can affect the specificity and efficiency of staining. Blots showing protein extracts from control and apoE-transfected N2a cells were incubated with the anti- apoE antibodies for either 2 hours at room temperature (RTP) (Figure 5-7, A) or overnight at 4°C (Figure 5-7, B).

An incubation time of 2 hours at RTP resulted in detection of full length apoE protein from apoE-transfected N2a extracts for all antibodies. Both the polyclonal goat anti-apoE (Calbiochem) and the mouse anti- apoE E-8 antibody detected the~32kDa fragment, indicating that this was generated by a small cleavage at the N-terminus. No other fragments were detected by either the anti- N- or C-terminal specific apoE antibodies, suggesting that these fragments were deletions at both the N- and C-terminus of apoE. Intriguingly though, changing the incubation conditions to overnight at 4°C resulted in the detection of additional bands by the mouse anti- apoE E-8 antibody in lanes containing apoE-transfected N2a cell extracts. Since no additional bands were observed in lanes containing control N2a cell extracts, it is likely that these additional bands are apoE fragments generated from proteolysis of overexpressed full length apoE. This result suggests that an overnight incubation time at 4°C is necessary for optimal performance of the mouse anti- apoE E-8 antibody in detecting apoE and its proteolytic fragments. This contrasting data also highlights the importance for this optimisation step because the data obtained from a 2-hour incubation time would have otherwise incorrectly indicated that these fragments lacked the C-terminal end of the protein. On the other hand, no additional bands were detected by either the goat anti- apoE (Calbiochem) or rabbit anti- apoE SP+1-32aa (Aviva) antibodies as a result of the extended incubation time. Nonetheless, an overnight incubation period at 4°C was determined to be optimal for the panel of anti- apoE antibodies and this incubation step was used in subsequent western blotting experiments.

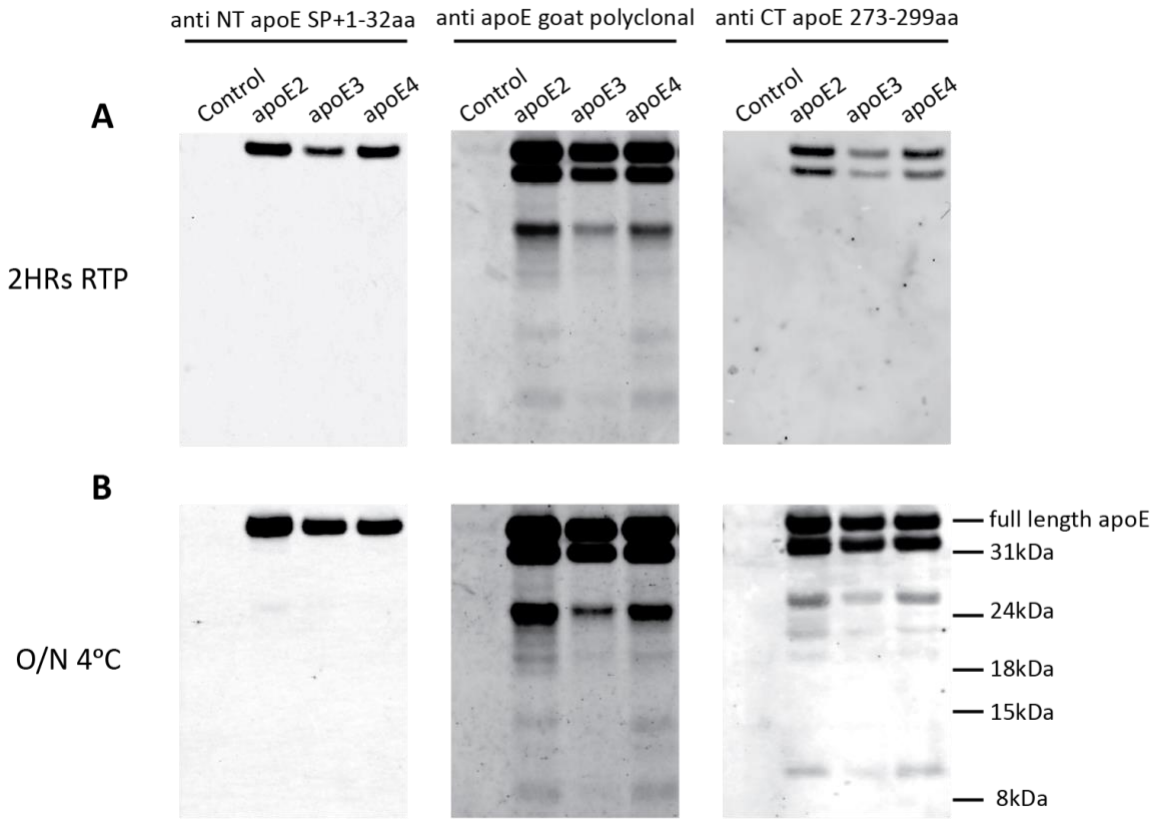

Figure 5-7 Optimisation of primary antibody incubation time during western blotting for the detection of apoE fragments

Western blots of protein extracts from apoE-overexpressing N2a cells, immunoblotted with anti- apoE SP+1-32aa (Aviva), goat anti- apoE (Calbiochem) or anti- apoE E-8 for either 2 hours at RTP (A) or overnight at 4°C (B). Increasing the incubation time from 2 hours (A) to overnight (B) for anti- apoE E-8 revealed additional apoE fragments.

5.2.3 Characterisation of apoE proteolysis susceptibility in cell models

Several lines of evidence have shown that apoE4 undergoes proteolysis more readily than apoE3, generating a greater amount of total fragments (Huang et al., 2001, Brecht et al., 2004b, Jones et al., 2011). However, the proteolytic susceptibility of the 'protective' apoE2 has not been examined comprehensively in human brains, transgenic models such as NSE-apoE mice or cell models. In view of this, N2a cells, SH-SY5Y cells and primary neurons were used to examine the fragmentation pattern and the proteolytic susceptibility of all apoE isoforms here. Equal amounts of protein from each cell model were separated using 10% Bis-Tris gels with MES buffer. Western blotting was carried out using a polyclonal goat anti- apoE (Calbiochem) due to its ability to consistently detect the largest number of fragments with a high degree of sensitivity in extracts from human brain and brain homogenates of transgenic AD models (Huang et al., 2001, Harris et al., 2003, Brecht et al., 2004b, Zhou et al., 2006, Jones et al., 2011). Also, since the epitope mapping data (shown in Figure 5-4) revealed that the goat anti-apoE (Calbiochem) antibody is not specific to either of the apoE termini, it is more likely to recognise additional intermediate cleavage products than the other anti- apoE antibodies. The signal intensity of full length apoE and apoE fragment bands were determined by selecting each band within discrete boxes in the Image Studio software 4.0 (LI-COR).

The percentage of total apoE fragments was calculated based on the following equation:

$$\%\, apoE = \frac{Sum\ of\ cleavage\ product\ intensity}{(Sum\ of\ cleavage\ product\ intensity + full\ length\ band\ intensity)} \times 100$$

The percentage of total apoE fragments for apoE2 and apoE4 was then measured against total apoE fragments for apoE3 as 100% to compare proteolysis susceptibility between the isoforms. Additionally, the relative size (kDa) of each fragment was determined by the Image Studio 4.0 software (LICOR), which based its size estimation according to the protein ladder sizes that were manually entered in the software.

5.2.3.1 ApoE is cleaved in an isoform-dependent manner

Figure 5-8 shows a representative western blot of apoE-transfected N2a cell extracts probed with goat anti- apoE (Calbiochem). Similar sized bands were detected for all isoforms (Figure 5-8, A), indicating that each isoform is processed similarly. Fragments observed were major bands of ~32 and ~26kDa, and minor bands ranging between ~10-22kDa. However, differences in the abundance of total fragments between the isoforms was revealed by densitometric analysis (p=0.0011) as displayed in the graph in Figure 5-8 B. As expected, apoE4-expressing N2a cells displayed a greater abundance of fragments compared to apoE3-expressing N2a cells (117.8%±3.7 apoE4 versus apoE3, p=0.0381). Surprisingly though, apoE2-expressing N2a cells accumulated a significantly greater amount of apoE fragments when compared to apoE3 as 100% (131.8%±6.8 apoE2 versus apoE3, p=0.0008). No statistical difference was observed for the total % of fragments between apoE2 and apoE4 (apoE2 versus apoE4, p=0.1073).

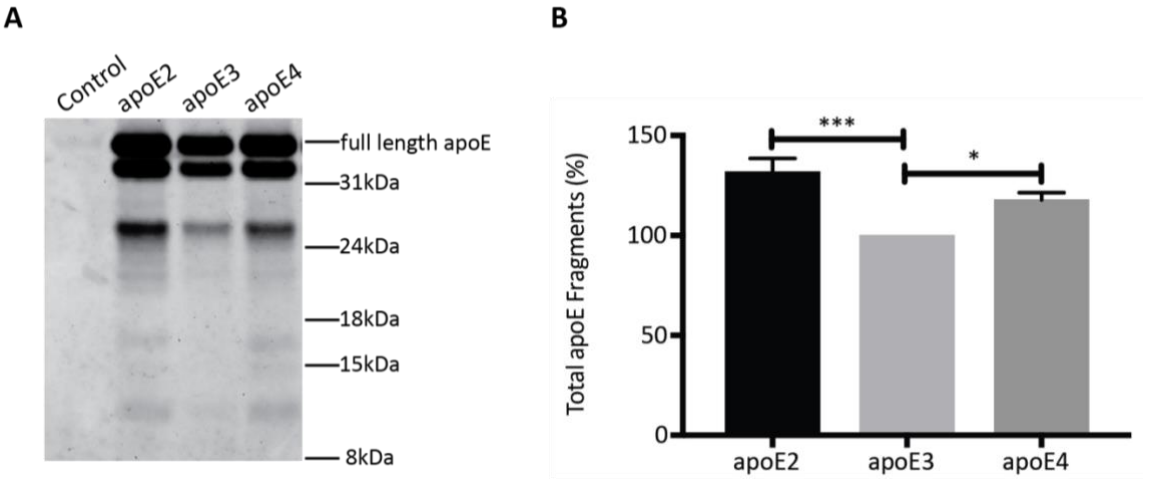

Figure 5-8 Isoform-specific apoE fragmentation in N2a cells

(A) Representative western blot of protein extracts from N2a cells transiently transfected with pCMV-ApoE2, pCMV4-ApoE3 and pCMV-ApoE4 constructs, showing full length apoE for all isoforms and up to 6 apoE fragments ranging from ~32-11kDa. (B) Quantification of blots revealed significant differences in total apoE fragment levels for both apoE2 (131.8%±6.8) and apoE4 (117.8%±3.7) compared against apoE3 as 100%, indicating cleavage occurs in the order of E2>E4>E3 in N2a cells. Data are mean ±SEM, and differences were assessed using one-way ANOVA followed by a Tukey's multiple comparisons test. *p<0.05; ***p<0.001; (n=5).

Figure 5-9 shows a representative western blot of apoE-transfected SH-SY5Y cell extracts probed with goat anti- apoE (Calbiochem). Consistent with observations of apoE

fragments from N2a cells, similar sized bands were detected for all isoforms (Figure 5-9, A). Fragments observed were major bands of ~32, ~26 and ~10kDa; and minor bands ranging between ~13-22kDa. Differences in the percentage of total fragments between apoE isoforms were also observed in SH-SY5Y cells ($p<0.0001$) as shown in the graph in Figure 5-9, B. Greater levels of fragments were observed for apoE2, followed by apoE4 when compared to apoE3 as 100% (157.1%±6.8 apoE2 versus apoE3, $p<0.0001$; 136%±7.0 apoE4 versus apoE3, $p=0.0012$). Surprisingly, a small statistical difference was also observed for apoE fragment levels between apoE2 and apoE4, as apoE2 showed a greater abundance of fragments (157.1%±6.8 apoE2 versus 136%±7.0 apoE4, $p=0.0455$).

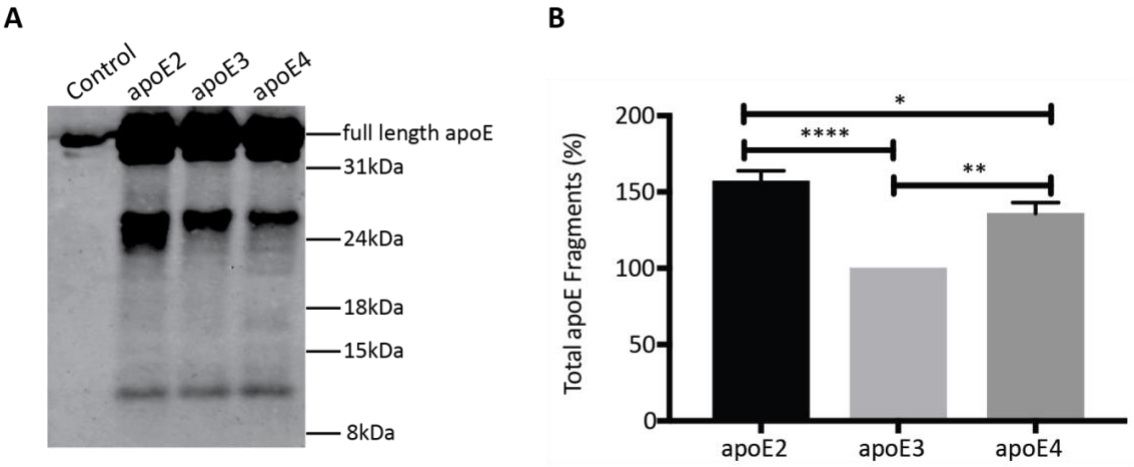

Figure 5-9 Isoform-specific apoE fragmentation in SH-SY5Y cells

(A) Representative western blot of protein extracts from SH-SY5Y cells transiently transfected with pCMV-ApoE2, pCMV4-ApoE3 and pCMV-ApoE4 constructs, showing apoE fragments ranging from ~32-11kDa. (B) Quantification of blots revealed significant differences in total apoE fragment levels for both apoE2 (157.1%±6.8) and apoE4 (136.0%±7.0) compared against apoE3 as 100%, indicating cleavage occurs in the order of E2>E4>E3 in SHSY5Y cells. Data are mean ±SEM, and differences were assessed using one-way ANOVA followed by a Tukey's multiple comparisons test. *p<0.05; **p<0.01; ****p<0.0001; (n=6).

Figure 5-10 shows a representative western blot of apoE-transduced primary neuron extracts probed with goat anti- apoE (Calbiochem). Similar sized bands were also observed for all apoE isoforms in this *in vitro* model (Figure 5-10, A), albeit at noticeably differing intensities. Fragments detected were major bands of ~26, ~22, ~15 and ~10kDa; and minor bands of ~32,~20,~18 and ~16-20kDa. Interestingly, the 18kDa band was more prominent in blots containing primary neuronal extracts but not in those from

neuroblastoma cell models. Differences in the percentage of total fragments between apoE isoforms were revealed by densitometric analysis (p=0.0002) as shown in the graph in Figure 5-10 B. In contrast to the cell lines, apoE4 showed the highest level of fragments in primary neurons when compared to both apoE3 and apoE2 (145.3%±6.4 apoE4 versus apoE3, p=0.0009; 145.3%±6.4 apoE4 versus 85.96%±4.2 apoE2, p=0.0002). Analysis of fragment levels in apoE2- and apoE3- overexpressing primary neurons however, did not reveal a statistically significant difference (85.96%±4.2 apoE2 versus apoE3, p=0.1408).

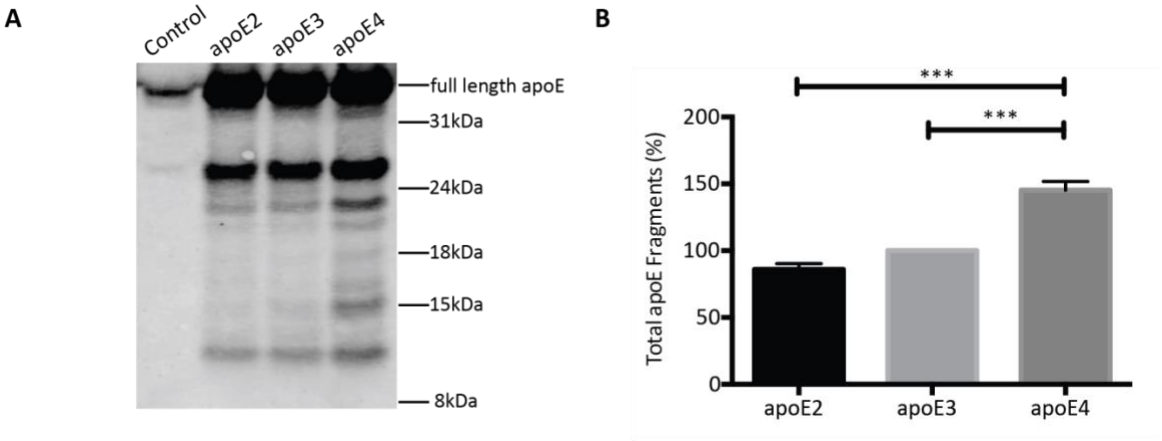

Figure 5-10 Isoform-specific apoE fragmentation in rat primary neurons

(A) Western blots of protein extracts from rat primary neurons transduced with apoE-expressing lentiviral vectors showed up to ~10 apoE fragments ranging from ~32-11kDa. (B) Quantification of blots revealed significant differences in total apoE fragment levels for apoE4 (145.3%±6.4) compared to apoE3 (100%) apoE2 (85.9%±4.2), indicating that cleavage occurs in the order of E4>E3>E2 in rat primary neurons. Data are mean ±SEM, and differences were assessed using one-way ANOVA followed by a Tukey's multiple comparisons test. ***p<0.001; (n=3).

5.2.4 Screen for N-terminal apoE fragments in cell models

The western blotting data using the goat anti- apoE (Calbiochem) antibody so far showed that similar fragments were generated for all the apoE isoforms *in vitro*, based on the patterning and size (kDa). However, whether they do indeed contain the same domains is not known. Here, western blotting using three N-terminal specific anti- apoE antibodies was carried out to screen for fragments containing the N-terminal domain in protein extracts from N2a cells, SH-SY5Y cells and primary neurons overexpressing the three major apoE isoforms.

5.2.4.1 ApoE fragments comprise N-terminal deletions

Figure 5-11 shows western blots of N2a extracts probed with N-terminal specific anti-apoE antibodies. Unexpectedly, rabbit anti- apoE (Aviva) which is raised against the first 50aa of the N-terminus (SP+1-32aa) detected only full length apoE (Figure 5-11, A). Likewise, rabbit anti- apoE 16H22L18 detected only full length apoE (Figure 5-11, B). Mouse anti- apoE WU E-4 however, detected both full length apoE and a ~32kDa fragment (Figure 5-11, C). Failure to detect the range of apoE fragments (~10-32kDa) reported in the literature and detected by goat anti- apoE in section 5.2.3.1 indicates that these fragments do not contain an intact N-terminus.

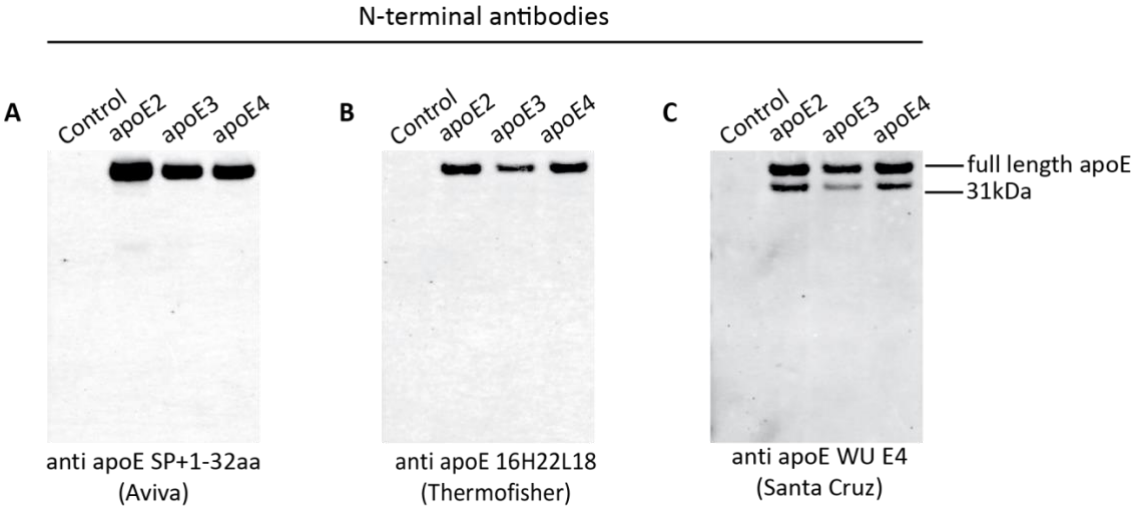

Figure 5-11 Fragments in N2a cells are not detected by anti- N-terminal specific apoE antibodies
Representative western blots of protein extracts from control and apoE-overexpressing N2a cells were probed using N-terminal specific anti- apoE antibodies. Anti- apoE SP+1-32aa (Aviva) (A) and anti- apoE 16H22L18 (B) detect only full length apoE protein, whereas anti- apoE WU E-4 (C) detects both full length apoE and a ~32kDa fragment. (n=5).

Similarly to N2a cells, western blots of extracts from apoE-transfected SH-SY5Y cells also indicated that the fragments are at least partially truncated at the N-terminus, since N-terminal specific anti- apoE antibodies detected only full length apoE (Figure 5-12 A, B and C). Interestingly though, mouse anti- apoE WU E-4 did not detect the ~32kDa fragment, suggesting that there may be cell-type dependent differences in the cleavage sites of apoE at the N-terminus.

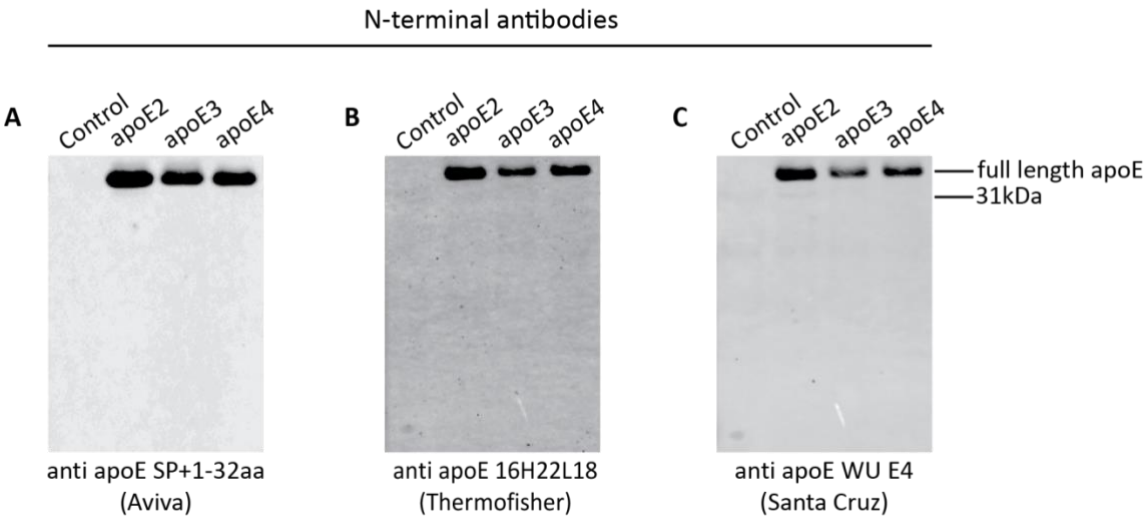

Figure 5-12 Fragments in SH-SY5Y cells are not detected by anti- N-terminal specific apoE antibodies
Representative western blots of protein extracts from SH-SY5Y cells transfected with either apoE2, apoE3 or apoE4- expressing plasmids were probed with N-terminal specific anti- apoE antibodies. (A) Anti- apoE SP+1-32aa (Aviva), (B) anti- apoE 16H22L18 and (C) anti- apoE WU E-4 detected only full length apoE protein for all isoforms. (n=6).

Western blots of extracts from apoE-overexpressing primary hippocampal neurons probed with N-terminal specific anti- apoE antibodies are shown in Figure 5-13. Consistent with western blotting data from the neuroblastoma cell lines, all three antibodies detected only full length apoE (Figure 5-13, A-C).

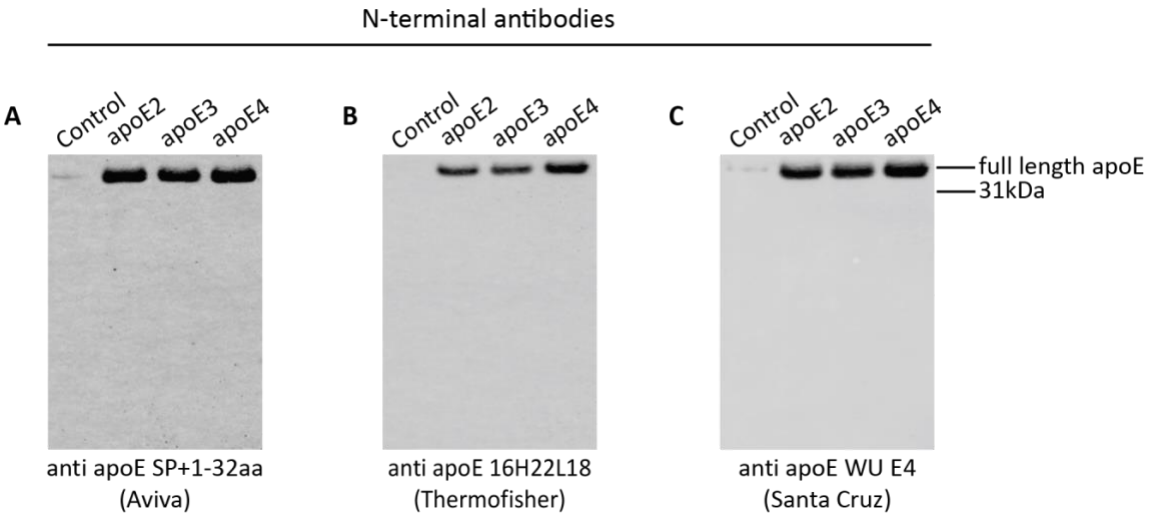

Figure 5-13 Fragments in primary neurons are not detected by anti- N-terminal specific apoE antibodies

Representative western blots of protein extracts from rat primary neurons transduced with apoE-expressing lentiviral vectors were probed using N-terminal specific anti- apoE antibodies. (A) Anti- apoE SP+1-32aa (Aviva), (B) anti- apoE 16H22L18 and (C) anti- apoE WU E-4 detected only full length apoE protein for all isoforms. (n=3).

Collectively, these data suggest that proteolysis of full length apoE involves cleavage within the vicinity of the first 32aa of apoE, at least, since this is the epitope for the anti-apoE SP+1-32aa (Aviva) antibody. Based on these data, apoE proteolysis *in vitro* does not lead to the generation of fragments with intact N-termini for any of the three major apoE isoforms.

5.2.5 Screen for apoE fragments containing either an intact or truncated C-terminus in cell models

Data in section 5.2.4 showed that apoE fragments may be produced through N-terminal cleavages, thus giving rise to the possibility that C-terminal fragments of apoE may exist. To test this hypothesis, two C-terminal specific antibodies were used. The mouse anti-apoE 3H1 antibody which recognises an epitope between 243-272aa (lipid binding domain) of apoE was selected since studies have shown that it can detect a wide range of fragments (~10-32kDa) in human brain tissue (Cho et al., 2001, Jones et al., 2011). The mouse anti- apoE E-8, which recognises an epitope within 272-299aa, was also used to enable identification of fragments with an intact C-terminus. Moreover, this antibody combination would also facilitate the identification of fragments with an exposed lipid

binding domain: those detected by mouse anti- apoE antibody 3H1 but not mouse anti-apoE E-8. This is of interest because exposure of this domain through C-terminal truncations is thought to be responsible for mitochondrial localisation and neurotoxicity (Mahley and Huang, 2012). For example, overexpression of a 1-272aa fragment of apoE has been shown to induce cytoskeletal and mitochondrial dysfunction in *in vitro* model systems, as well as induce neurodegeneration when expressed in transgenic rodent models (Huang et al., 2001, Nakamura et al., 2009, Harris et al., 2003).

5.2.5.1 ApoE fragments contain an intact C-terminus

Figure 5-14 shows western blots of control and apoE-transfected N2a cells probed with C-terminal specific anti- apoE antibodies. Mouse anti- apoE antibody 3H1 detected full length apoE and three major fragments of ~32, ~26 and ~10kDa (Figure 5-14, A). Additionally, a very faint fragment of ~20kDa was observed for apoE2, which was barely detectable for the other two isoforms. The anti- apoE E-8 antibody however, detected the ~20kDa fragment for all isoforms and other bands of similar sizes to those observed when using the other C-terminal specific antibody (see Figure 5-14, B), but generally with a stronger signal intensity. It is notable that the patterning and sizes of the bands detected by both C-terminal specific anti- apoE antibodies are similar to those observed when using the goat anti- apoE (Calbiochem) antibody.

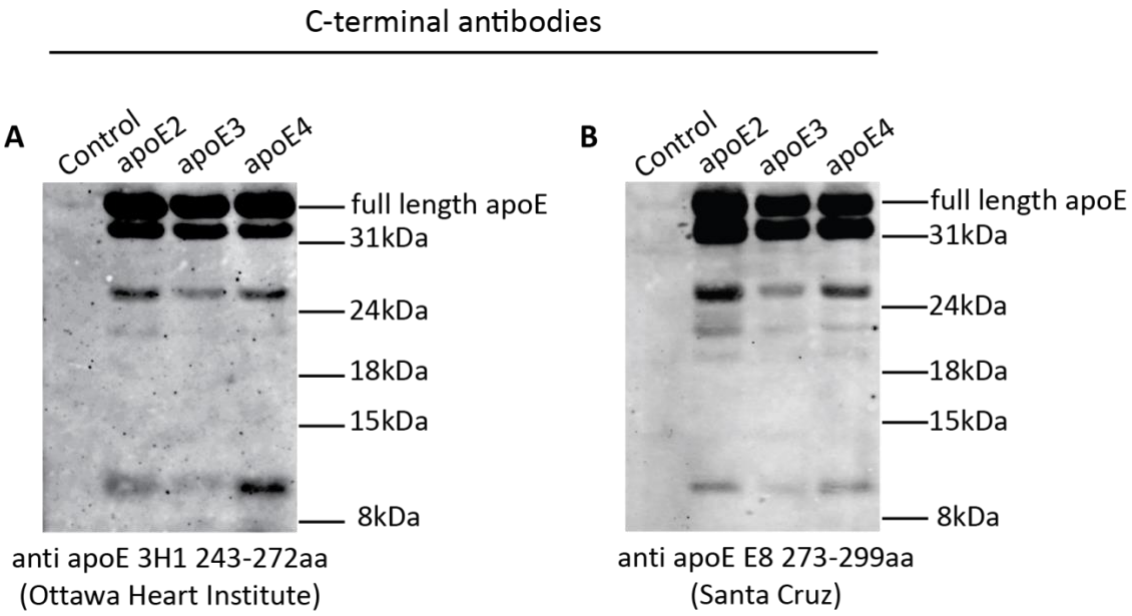

Figure 5-14 Anti- C-terminal specific apoE antibodies reveal fragments to be N-terminally truncated in apoE-overexpressing N2a cells

Representative western blots of protein extracts from N2a cells transfected with either apoE2-, apoE3- or apoE4- expressing plasmids were probed using C-terminal specific anti- apoE antibodies. Both (A) anti- apoE 3H1 and (B) anti- apoE E-8 detected full length apoE protein and several apoE fragments. (n=5).

Figure 5-15 shows western blots of apoE-overexpressing SH-SY5Y cells probed with the C-terminal specific anti- apoE antibodies. Mouse anti- apoE antibody 3H1 detected full length apoE and two fragments of ~32 and ~10kDa (Figure 5-15, A). Likewise, mouse anti- apoE E-8 detected these bands, but also a faint ~26kDa band and a nonspecific band, which was observed in the control lane (Figure 5-15, B).

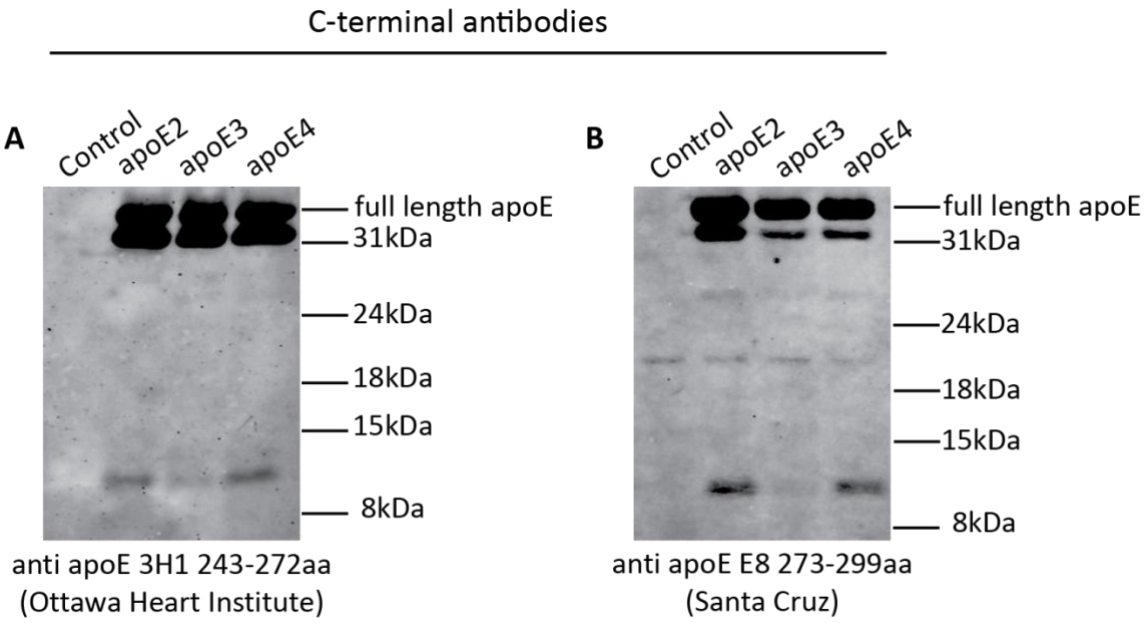

Figure 5-15 Anti- C-terminal specific apoE antibodies reveal fragments to be N-terminally truncated in transfected SH-SY5Y cells

Representative western blots of protein extracts from SH-SY5Y cells transiently transfected with either apoE2, apoE3 or apoE4 expressing constructs were probed using C-terminal specific anti- apoE antibodies. Both (A) anti- apoE 3H1 and (B) anti- apoE E-8 detected full length apoE protein, the ~32kDa fragment and the ~10kDa fragment. (B) anti- apoE E-8 also faintly detected the ~26kDa fragment. (n=6).

Figure 5-16 shows western blots of extracts from apoE-transduced primary neurons probed with the C-terminus specific apoE antibodies. Mouse anti- apoE antibody 3H1 detected full length apoE and six fragments for apoE4: three major fragments of ~26, ~22 and ~10kDa; and three faint fragments of ~32, ~20 and ~15kDa (Figure 5-16, A). Likewise, mouse anti- apoE E-8 detected these bands for apoE4. In contrast, both C-terminal antibodies barely detected the minor bands for apoE2 and apoE3, likely due to lower levels of these fragments for these isoforms.

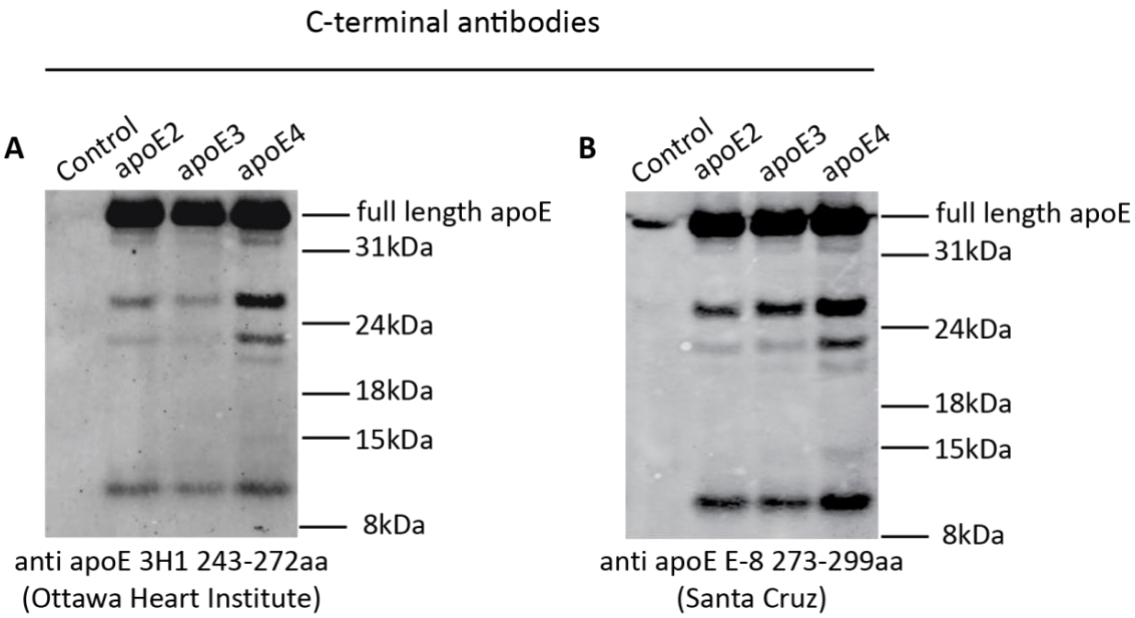

Figure 5-16 Anti- C-terminal specific apoE antibodies reveal majority of fragments to contain an intact C-terminus in transduced primary neurons

Representative western blots of protein extracts from rat primary neurons transduced with apoE-expressing lentiviral vectors were probed using C-terminal specific anti- apoE antibodies. Both (A) anti-apoE 3H1 and (B) anti- apoE E-8 detected full length apoE protein and a range of major and minor apoE fragments. (n=3).

Collectively, these data indicate that many of the apoE fragments detected by the goat anti- apoE (Calbiochem) antibody in each cell model are likely generated by sequential cleavage within the N-terminus, since they contain the 272-299aa epitope that is detected by the anti- apoE E-8 antibody. Furthermore, the western blotting data did not reveal the presence of a fragment with an exposed lipid binding domain in any of the cell models when overexpressing full length apoE, since the anti- apoE E-8 detected the same bands as the anti- apoE 3H1 antibody. Finally, qualitative comparisons of the fragments detected by both C-terminus specific antibodies in each cell model show that apoE fragmentation likely occurs to a greater extent in primary neurons, followed by N2a cells and the least fragmentation occurring in SH-SY5Y cells.

5.3 DISCUSSION

The work presented in this chapter provides a clearer understanding of apoE proteolysis in neurons and the identity of apoE fragments, which is pivotal to discovering how apoE fragments may contribute to AD pathology. This work involved: validating the epitopes of the commercially available anti- apoE antibodies, optimising conditions for anti- apoE antibodies for western blotting and characterisation of intracellular apoE fragmentation. To do so, apoE2, apoE3 and apoE4 were expressed in N2a cells, SH-SY5Y cells and primary rat neurons since cell models are extensively used to model apoE neurobiology, but little is known about the fragmentation profile of apoE *in vitro*.

5.3.1 Epitope mapping and optimisation of commercial anti- apoE antibodies

To unambiguously identify apoE fragment composition, the epitopes of the commercially available anti- apoE antibodies used throughout this work were first validated. Results showed that all antibodies were specific to the regions advertised except for the rabbit anti- apoE 16H22L18. Although it is advertised as an antibody that binds to the lipid-binding domain (240-251aa) of apoE, it instead recognised a region within the N-terminus of apoE. This result was significant since the use of this antibody would have produced conflicting data when compared with the mouse anti- apoE 3H1, which is indeed specific to 243-272aa of apoE. In addition, the specificity of the mouse anti- apoE 3H1 antibody for 243-272aa shown here is in line with an earlier study which also demonstrated that this antibody recognises a region within 243-272aa of apoE (Weisgraber et al., 1986). Overall, these data highlight the necessity to validate the epitopes of antibodies when using them to determine protein fragment composition.

After verifying the specificity for the anti- apoE antibodies, the effect of incubation time for a number of anti- apoE antibodies was examined to determine optimal conditions for apoE fragment detection. The results showed that incubation time and temperature were crucial for accurate observation of apoE fragments, since less abundant fragments were only detected by mouse anti-apoE E-8 following an overnight incubation at 4°C. Incubation for 2 hours at room temperature revealed only abundant fragments, which would have otherwise falsely indicated that the other fragments did contain intact C-

termini. This result shows the importance of antibody optimisation for examining apoE fragmentation.

5.3.2 ApoE proteolysis is isoform- and cell- dependent

Characterisation of apoE fragmentation using the goat anti- apoE (Calbiochem) antibody showed that isoform-specific cleavage of apoE does occur, and that this is cell-dependent. There was scant evidence to suggest that apoE isoforms are differentially cleaved in a manner that produces unique fragments. However, these data showed significant differences in proteolytic susceptibility between isoforms. Interestingly, this occurred in the order of apoE2>apoE4>apoE3 for the N2a and SH-SY5Y cell lines, and apoE4>apoE3>apoE2 in primary neurons. The data from the cell lines was unexpected since the apoE proteolysis model proposes that apoE4 should be the most susceptible to cleavage followed by apoE3 and apoE2 due to isoform-associated differences in protein structure (Huang et al., 2004). The basis for this hypothesis is that the presence of an arginine residue at position 112 in apoE4 causes greater N-/C-terminal domain interaction due to a salt bridge formation between Arg61 and Glu255. Since apoE2 and apoE3 have a cysteine at position 112, the inter-domain interaction is thought to be reduced (Dong and Weisgraber, 1996, Hatters et al., 2005). Although the data from the primary neurons support this model, the greater abundance of fragments for apoE2 compared with the other two apoE isoforms in the neuroblastoma cells does not. It is notable though, that a greater abundance of apoE2 fragments has been observed in human plasma when compared to the other two isoforms (Xu et al., 2015a). In view of this and studies which have detected apoE fragments in the culture media of apoE-overexpressing cells (Wellnitz et al., 2005, Munoz et al., 2018), it is conceivable that the differing levels of intraneuronal fragments for each isoform may also involve differences in secretion versus retention of fragments. To determine if this is the case, the profile and levels of fragments secreted by apoE-overexpressing cells could be assessed by western blotting in further work. It is also possible that vulnerability of apoE to proteolysis may not be entirely due to the native protein structure, but could involve cell-dependent post-translational modifications (PTMs) that affect the structural features of apoE and its processing. In fact, other researchers have proposed that

glycosylation of apoE may be able to confer secondary polymorphism to the genetic isoforms (Zannis and Breslow, 1981) and protect apoE from proteolysis (Wernette-Hammond et al., 1989). Intriguingly, multiple glycosylation sites have been identified across apoE in subsequent studies (Halim et al., 2013, Nilsson et al., 2009, Lee et al., 2010), however it is still not fully understood how these modifications affect apoE structure and function. It is notable though, that a recent structural study found that inter-domain interactions were mediated by residues within the hinge region and the C-terminus of apoE, both of which contain several sites for glycosylation (Williams et al., 2015). In addition to the increasing evidence suggesting an effect of glycosylation on apoE structure, glycosylation has also been shown to affect its function. Mutation of an apoE glycosylation site (Thr194) was observed to impair its binding affinity to Aß42 (Sugano et al., 2008), likely due to alterations in structure. In addition, a study investigating the role of apoE in the Niemann Pick Type C (NPC) cholesterol storage disorder observed changes in the glycan profile of apoE prior to the onset of neurological abnormalities in an animal model of the disease (Chua et al., 2010), indicating that there may be a link between altered apoE glycosylation and CNS pathology. However, this study did not examine whether this altered the fragmentation profile of apoE. Therefore, even though glycosylation affects the function of apoE, whether it also directly alters its proteolytic susceptibility remains an elusive, but intriguing possibility. It is also possible that differential glycosylation of the apoE isoforms may affect their respective fragmentation profiles on western blots due to altering the mass and thus mobility of apoE fragments in SDS-PAGE. Of note, Chua and colleagues examined the glycan profile of apoE in total brain homogenate from NPC rodent models by performing a lectin-ELISA using a panel of biotinylated lectins (Chua et al., 2010), glycoproteins that have distinct sugar-binding specificities. This approach could also be used in future work to determine whether the glycan profile of apoE differs between isoforms, but also between cell models; providing more insight into the basis of the differential proteolytic susceptibility of the apoE isoforms in the three cell model systems observed here.

Detection of fragments using goat anti- apoE (Calbiochem) revealed similarities in the fragmentation pattern of apoE between cell models. Importantly, this pattern resembles the apoE fragment profile found in murine apoE in APP/PS1K1 mice (Saul and Wirths, 2016) and in human brains of AD patients (Huang et al., 2001, Zhou et al., 2006, Jones et al., 2011). This indicates that the proteolytic processing of the three major apoE isoforms *in vitro* is similar to processing of apoE *in vivo* and thus supports the use of these cell models to investigate apoE proteolytic processing. Having established the fragmentation profile of the three major apoE isoforms in N2a cells, SH-SY5Y cells and primary neurons, the composition of the apoE fragments was next addressed.

5.3.3 ApoE fragment characterisation reveals fragments are likely to be N-terminally truncated

The work in sections 5.2.4 and 5.2.5 set out to characterise the composition of these fragments *in vitro*. Determining the composition of these fragments is necessary to better guide future studies using artificial truncated variants of apoE to either explore how apoE fragments contribute to Alzheimer's disease pathology, or in the case of apoE2, to use as possible therapeutic compounds. Initially, a screen using a panel of N-terminal specific anti- apoE antibodies was used to identify which of the fragments detected using the goat anti- apoE (Calbiochem) contained an intact N-terminus (if any). Unexpectedly, all of the N-terminal specific antibodies failed to detect fragments from any of the apoE isoforms in each model system, with the exception of a ~32kDa band revealed by mouse anti- apoE WU E-4 in N2a cells. Although the binding specificities of these antibodies were mapped to the N-terminus in section 5.2.1, only the exact epitope of rabbit anti- apoE (Aviva) was known (SP+32aa). Therefore, this data suggests that the fragments observed using the goat anti- apoE (Calbiochem) either do not contain the first 32aa or that the antibody epitopes are occluded. For the first scenario, a very small portion of apoE containing the first 32aa would need to be initially cleaved and either degraded or secreted since smaller fragments (<4kDa) weren't detected by any of the three antibodies. Interestingly, there is evidence from sequencing studies that have identified apoE fragments which are truncated at position 32, thus supporting this hypothesis (Jahn et al., 2011, Lonn et al., 2018). There is also evidence from a structural study to support the alternative scenario. The amino-terminus of apoE4 has been shown

to adopt a molten globule structure (Morrow et al., 2002), which could affect accessibility of antibodies to their respective epitopes. Nonetheless, failure to detect N-terminal apoE fragments was surprising because such fragments have been detected in extracts from human AD brains by antibodies that recognise the amino portion of apoE (Cho et al., 2001, Jones et al., 2011). Indeed, the use of two such antibodies (mouse anti-apoE 6C5 and mouse anti- apoE 1D7 from Ottawa Heart Institute) revealed high molecular weight fragments ranging between ~22-32kDa in extracts from human AD brain (Cho et al., 2001, Jones et al., 2011). The data from these studies suggest that many of the high molecular weight fragments detected (between ~22 and 26kDa) contained an intact N-terminal since these antibodies are reported to recognise residues 1-15 and 140-160 respectively (Weisgraber et al., 1986). However, these studies also showed that fragments of similar sizes were detected by mouse anti- apoE 3H1 (recognising the lipid binding domain), thus indicating that these proteolytic products must be cleaved after position 272aa. However, cleavage of apoE only after the lipid binding domain would generate fragments of ~31kDa or more. This suggests that either the reported epitope of the anti- apoE 6C5 is incorrect, or that the fragments detected by both the anti- apoE 6C5 and anti- apoE 3H1 antibodies are different in composition but are of similar size. Nonetheless, there are other studies which lend support to the notion that fragments generated *in vitro* may be N-terminally truncated. For example, only full length apoE and a ~32kDa fragment were detected by mouse anti- apoE 6C5 in apoE4-expressing N2a cells (Huang et al., 2001). Additionally, reduced binding of recombinant apoE to mouse anti- apoE 6C5, which was used as an anchor antibody in a solid phase apoE sandwich immunometric assay, was proposed to be the result of amino-terminal proteolysis (Raffai et al., 1995).

Although the data indicated that apoE is cleaved at the N-terminus, it was still plausible that apoE could be truncated at the C-terminus too. Indeed, it has been postulated by other researchers that apoE fragments are cleaved after the lipid binding domain within the C-terminus (Huang and Mahley, 2014, Mahley and Huang, 2012). The basis for this stems from earlier work using human brain samples. Fragments detected by goat anti-apoE (Calbiochem) were not detected using an antibody against 272-299aa of apoE in

either human AD brains or mice expressing apoE under an NSE promoter (Huang et al., 2001, Brecht et al., 2004b). This observation led to a vast number of studies using a range of truncated variants of apoE with an exposed lipid binding domain (x-272aa) which could induce neuronal dysfunction (Harris et al., 2003, Chang et al., 2005, Nakamura et al., 2009, Huang et al., 2001). The most toxic of these was reported to be apoE4 1-272aa, and it was suggested that the presence and exposure of the lipid binding domain seemed necessary for toxicity (Chang et al., 2005). Moreover, apoE4 variants were found to be more toxic than the apoE3 versions, and since these fragments contained the SNPs, it provided an explanation for the increased risk for AD associated with the *APOE4* gene. It is notable though that the identity of a fragment containing an exposed lipid binding domain had not yet been conclusively determined, likely due to the lack of commercially available antibodies at the time to distinguish between fragments with an intact or truncated C-terminus. Additionally, it was not known whether apoE2 also generates these fragments, and if so, if they would be neuroprotective. Therefore, western blotting using antibodies against the lipid binding domain (243-272aa) of apoE and the region after (272-299aa) were used here to confirm that these fragments were C-terminally truncated and to identify the generation of a fragment containing an exposed lipid binding domain. The range of fragments detected by the anti- apoE 3H1 is consistent with that shown in western blots using protein extracts from human AD brains (Cho et al., 2001, Jones et al., 2011). Notably, both the anti- apoE 3H1 and the anti- apoE E-8 antibodies detected fragments of similar sizes to those revealed by the goat anti- apoE (Calbiochem) antibody, suggesting that the majority of apoE fragments do contain the last 27aa and are thus generated by proteolysis of apoE within the N-terminus. This observation also suggests that the absence of fragments detected by the N-terminal specific anti- apoE antibodies (in section 5.2.4) was not solely due to cleavage of apoE within 1-32aa of the N-terminus, but rather due to progressive N-terminal cleavages. The range of fragments detected by the anti- apoE E-8 antibody however, contrasts with western blots from other studies that used an in-house made antibody against the same epitope (272-299aa) (Huang et al., 2001, Harris et al., 2003, Brecht et al., 2004b), which suggest that apoE fragments are truncated at the C-terminus of apoE. It is plausible that this discrepancy could be

due to low immunoreactivity or sensitivity of the in-house generated antibody. Moreover, it is notable that although the anti- apoE (272-299aa) antibody used by these researchers was produced by passing the goat anti- apoE antibody through a column of beads bound to apoE3 1-272aa and apoE4 1-272aa, the specificity and reactivity of the unbound fraction of antibody for 272-299aa of apoE was not demonstrated. Importantly, a fragment containing an exposed lipid binding domain was not observed in any of the three cell models, for any apoE isoform, suggesting that human apoE is not cleaved within the end of the C-terminus. To validate the finding that apoE fragments contain intact C-termini *in vitro*, apoE fragments in lysates from the apoE-overexpressing cells could be isolated by immunoprecipitation and sequenced by mass spectrometry in future work. It would also be of interest to confirm that apoE is cleaved at the N-terminus in the human brain, by western blotting analysis of protein extracts from post-mortem AD human brains using the panel of commercially available antibodies used in this chapter.

In support of the data presented in this chapter, there is also a significant body of evidence within the literature to support that apoE fragments contain an intact C-terminus and are thus N-terminally truncated. For example, Saul and co-workers observed a range of C-terminal fragments in AD mouse models by using an anti- apoE antibody raised against the C-terminus of murine apoE (Saul and Wirths, 2016), supporting the existence of C-terminal fragments *in vivo*. As for *in vitro* work, Wellnitz et al sequenced a ~13kDa fragment derived from apoE-transfected N2a cells and determined that it contained residues 182-299 (Wellnitz et al., 2005). Interestingly, there is also evidence from much earlier work for the existence of C-terminal apoE fragments in human tissue. Microsequencing analysis of fibrillar amyloid A from spleen tissue of human patients revealed the presence of a 216-299aa C-terminal apoE fragment (Castano et al., 1995). ApoE fragments of similar sequence identity (193-299aa and 216-299aa) have also been identified in amyloid fibrils isolated from AD brain tissue (Wisniewski et al., 1995), providing further evidence to implicate C-terminal apoE fragments in amyloid plaque pathology. Furthermore, Aizawa and colleagues found that amyloid plaques stained only with antibodies against the C-terminus of apoE, and not N-

terminal antibodies that recognise a region within the first 100aa of apoE (Aizawa et al., 1997). As a result, they proposed that the fragments observed in amyloid plaques were truncated within the first 100aa of apoE, a conclusion that also lends support to the data presented in this chapter.

5.3.4 A role for differential proteolysis of apoE and N-terminally truncated apoE fragments in AD

Collectively, these data add clear evidence to the theory that apoE fragments are generated by cleavage within the N-terminus of apoE and that these fragments may contribute to AD pathology. An interesting question arises from this data: how do carboxyl-fragments account for isoform-specific toxic effects if the SNPs are in the amino-terminal portion of apoE? It is important to consider that many of the larger and abundant apoE fragments could still include the SNPs, which are at positions 112 and 158, and thus form isoform-specific structures that could account for differences in toxicity. For instance, cleavage up to 111aa of apoE could generate an SNP-containing carboxyl fragment spanning between 112-299aa of approximately 22kDa, as based on the average of every amino acid being equal to 0.11kDa. Hence, it is possible that apoE fragments of 22kDa and above in size could have different structures. Interestingly, the data here demonstrate that N-terminally truncated fragments of such sizes exist in cell models and are likely similar to fragments of similar size observed in extracts from CSF and human AD brain (Marques et al., 1996). Following this notion, the major ~26kDa fragment observed in all three model systems using the goat anti- apoE (Calbiochem) and C-terminal specific anti- apoE antibodies likely also contains these SNPs. It is probable that this fragment is generated by cleavage within the second α-helix (42-71aa) of apoE which is interesting because it has been reported that deletion of residues 1-71 increases the structural variance between apoE4 and apoE3 (Chou et al., 2005), supporting the possibility of isoform-specific differences between N-terminally truncated apoE fragments. Intriguingly, Chou and colleagues also identified that deletion of the first two α-helices for apoE4 promoted concentration-dependent aggregation of apoE4, raising the possibility that apoE4 may also induce toxicity in neurons through accumulating as aggregates. In support of this, high and low molecular weight apoE fragments have been observed in Triton-insoluble protein fractions from human AD

brain tissue (Jones et al., 2011). Interestingly, this property could also partially explain earlier work by Huang and colleagues which found that N2a cells overexpressing an 81-272aa fragment of apoE displayed a greater number of tangle-like structures than N2a cells overexpressing a 1-272aa apoE fragment (Huang et al., 2001). In consideration of these findings, it can be reasonably assumed that cleavage within the N-terminus of apoE4 can result in a toxic-gain of function and may contribute to AD pathology.

Although similar fragments are generated for each isoform, the differential proteolytic susceptibility of each apoE isoform as based on differing levels of fragments generated, could also contribute to the differential effects of each isoform in AD. Indeed, the data in this chapter showed that apoE4 undergoes proteolysis more readily in primary neurons, indicating that fragments could accumulate at a faster rate which could result in increased toxicity. Further to this, the concentration of fragments has been shown to affect the propensity of self-assembly in a sedimentation velocity study of apoE isoforms (Chou et al., 2005). Therefore, it is possible that a greater load of apoE fragments as seen for apoE4 in primary neurons, could be associated with increased amyloidogenic potential that may be a factor in its reported toxic-gain of function. It is also important to note that increased proteolysis of apoE could lead to a loss of protective function (e.g. mediating lipid redistribution during neuronal repair), as has been proposed by Rohn et al (Rohn, 2013).

5.3.5 Conclusion

To conclude, the data presented in this chapter is the first to address the proteolytic susceptibility profile and composition of apoE fragments for all three major human apoE isoforms in N2a cells, SH-SY5Y cells and primary neurons. The data showed that levels of apoE fragments were produced in an isoform and cell-dependent manner, which could account for variations in toxic gain or loss of protective function for each isoform in these cell models. Of note, apoE processing in primary neurons was more similar to published *in vivo* work and so may be the most suitable *in vitro* model for apoE neurobiology. In addition, the data indicated that apoE2, apoE3 and apoE4 fragments are predominately C-terminal fragments of varying length. Furthermore, considering the

sizes of the fragments and using this to estimate the position of cleavage sites, it is possible to speculate that the structure of some of these fragments and thus the effects on neuronal function may differ for each isoform due to the presence of SNPs. Overall this work highlights the necessity for future studies to investigate the structure and function of N-terminally truncated apoE fragments. Such studies will help to uncover the mechanisms by which C-terminal apoE fragments contribute to AD pathology and may lead to new therapies.

Chapter 6 THE ROLE OF INTRANEURONAL APOE

6.1 INTRODUCTION

Having confirmed that the three major apoE isoforms undergo isoform-dependent proteolysis in the previous chapter, the work presented in this chapter compared the impact of the three apoE isoforms on downstream effects associated with expression and proteolysis of apoE in neurons (Mahley and Huang, 2012). One key step associated with the toxic gain of function for apoE4 in the apoE proteolysis model is the translocation of apoE fragments from the secretory pathway to the cytosol of the neuron, which is thought to be a prerequisite for cytoskeletal and mitochondrial dysfunction and thus toxicity (Chang et al., 2005, Mahley and Huang, 2012). Whilst the translocation of apoE4 fragments from the secretory pathway to the cytosol has been shown to require the receptor binding region, mitochondrial dysfunction and the formation of p-Tau inclusions *in vitro* has been demonstrated to require exposure of the lipid binding region (Chang et al., 2005, Huang et al., 2001). Moreover, it is notable that much of the evidence supporting a toxic role for intraneuronal apoE4 stems mostly from studies showing that C-terminally truncated variants of this protein (particularly the 1-272aa fragment) induce neuronal dysfunction and toxicity (Huang et al., 2001, Harris et al., 2003, Chang et al., 2005, Nakamura et al., 2009). However, the existence of a fragment with an exposed lipid binding region was not supported by the work presented in the previous chapter, which instead indicated that fragments of apoE2, apoE3 and apoE4 are generated by N-terminal cleavages. In view of this, it was first necessary to determine whether the toxic effects associated with apoE4 could be reproduced and confirmed as isoform specific in the three neuronal model systems used in the previous chapter. In doing so, this work also extended upon previous studies since these did not include the apoE2 isoform (Huang et al., 2001, Harris et al., 2003, Chang et al., 2005, Nakamura et al., 2009).

One well studied aspect of apoE4-mediated cytoskeletal dysfunction is the deregulation and destabilisation of the microtubule network, which is supported by studies showing that neuroblastoma cells exposed to or expressing apoE4 exhibit impaired neurite outgrowth and microtubule depolymerisation (Nathan et al., 1995, Nathan et al., 1994,

Bellosta et al., 1995). Increasing data indicates that apoE4 and its fragments contribute to this by disrupting the function of tau, which is partly responsible for the stabilisation and polymerisation of microtubules. For instance, studies have shown that neuronal expression of full length apoE4 *in vivo* or the 1-272aa apoE fragment *in vitro* promote tau hyperphosphorylation, and induce and co-localise with p-Tau inclusions (Huang et al., 2001, Brecht et al., 2004b, Tesseur et al., 2000b, Tesseur et al., 2000a). In view of these findings, the first two aims of this section were to (i) determine whether C-terminal fragments could be observed in the cytosol for each apoE isoform and (ii) determine whether expression and proteolysis of apoE4 affected the organisation and regulation of tau as reported in the literature, and to confirm that this was also specific to the apoE4 isoform.

The work here next investigated the neuroprotective role of apoE expression in neurons by examining the relationship between apoE and vimentin, an intermediate filament (IF) protein that has recently been implicated in the neuronal repair response (Levin et al., 2009). Vimentin is a cytoplasmic protein that is primarily expressed by vascular endothelial cells and some glial cells in the mature, healthy brain (Bignami et al., 1982, Schnitzer et al., 1981). It is also expressed in developing neurons to initiate and promote dendritic branching (Boyne et al., 1996, Levin et al., 2009), but is then replaced by neurofilament proteins once neurons become post-mitotic (Cochard and Paulin, 1984). Intriguingly, neurons re-express vimentin in AD-relevant brain regions showing pathologies such as amyloid plaques and NFTs, as revealed by enhanced staining for vimentin in brain tissue from AD donors and AD transgenic mice (Levin et al., 2009). Furthermore, it was also shown that traumatic injury to brain tissue of adult mice resulted in increased vimentin expression in neurons (Levin et al., 2009). Levin and collaborators suggested that this could be a protective response that enables injured neurons to delay dendritic and synapse loss, thus implicating vimentin expression as part of the very poorly understood repair response mechanism in neurons. Similarly, apoE expression in neurons has also been shown to occur in response to neuronal injury or stress (Xu et al., 2006b, Boschert et al., 1999), raising the possibility of a connection between neuronal apoE and vimentin expression that may contribute to neuronal

repair. Therefore, the third aim of the work presented in this chapter was to (iii) determine whether neuronal apoE expression was associated with vimentin upregulation, and to what extent this was an isoform specific effect.

Finally, to investigate whether apoE expression and proteolysis in neurons leads to an isoform-dependent toxic or protective gain of function, neuronal viability and survival was assessed. Although apoE4 has been associated with a toxic gain of function when expressed in neurons, only a single study to date has directly tested whether neuronal expression of apoE4 does indeed reduce neuronal viability *in vitro* (Chang et al., 2005). Notably in the study by Chang and collaborators, full length apoE4 expression in neuroblastoma cells was found not to be toxic, whereas expression of the 1-272aa fragment of apoE4 was. Furthermore, whilst apoE2 is considered neuroprotective due to the association of an *APOE2* genotype with a decreased risk for AD (Chartier-Hariln et al., 1994, Corder et al., 1994), it is not known whether expression and proteolysis of apoE2 in neurons contributes to this neuroprotective effect, or alternatively, also triggers a toxic gain of function. Hence the fourth aim of the work presented here was to (iv) determine if neuronal viability and survival was affected by neuronal apoE expression in the three cell models and whether this was isoform-dependent.

6.2 RESULTS

6.2.1 Immunocytochemical analysis of apoE distribution in N2a cells

The data presented in the previous chapter showed that antibodies specific to the N-terminus of apoE detected only full length apoE protein in western blots, whereas antibodies specific to the C-terminus of apoE detected a wide range of fragments. Therefore, to determine whether fragments translocate to the cytosol and to provide insight for fragment-related functions, immunocytochemistry was used to examine whether the fragments containing an intact C-terminus were distributed in subcellular compartments where full length was not. This was done by double immunolabelling apoE-transfected N2a cells using antibodies specific to the N- and C-terminus of apoE followed by imaging with a confocal microscope. Immunolabelling was carried out in N2a cells transfected with all three major apoE isoforms to determine if the staining distribution differed between isoforms.

There was no clear evidence for differences in the subcellular distribution of either the N- or C-terminus of apoE in cells co-stained with anti- apoE 16H22L18 and anti- apoE E-8 antibodies for all three isoforms of apoE (Figure 6-1). Immunolabelling with both antibodies revealed a granular distribution throughout the cell soma and strong punctate perinuclear staining for all isoforms of apoE. However, although the distribution of full length apoE (staining by the N-terminal specific antibody) was observed throughout the cytoplasm, immunoreactivity appeared to be stronger when staining with the C-terminal specific antibody. To test whether this was an artefact of the N-terminal specific antibody, N2a cells were also labelled using the two other N-terminus specific antibodies: anti- apoE SP+32aa (Aviva) and anti- apoE WU E-4. Both these antibodies revealed similar cytoplasmic and perinuclear distribution of apoE (shown in Figure 6-2) that also appeared to co-localise more than the staining between the N- and C-terminal specific antibodies (Figure 6-2 compared to Figure 6-1). This suggests that it is possible that there may be increased cytoplasmic labelling for C-terminal apoE, although this was inconclusive based on the limited resolution of this method. Finally, control cells showed negligible staining for all antibodies used here, which is indicative that the staining for apoE by each antibody is specific to apoE.

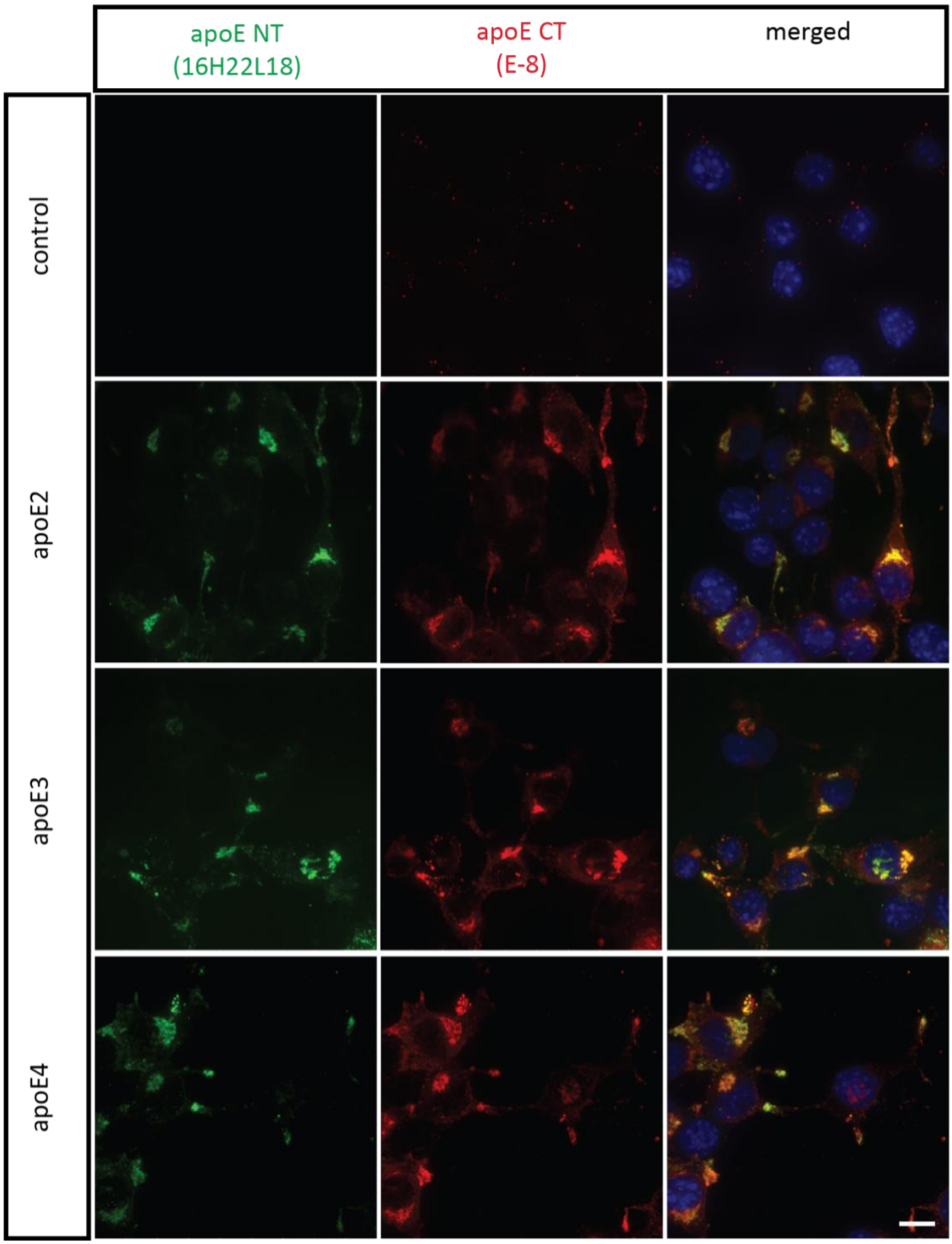

Figure 6-1 Immunofluorescence images showing the distribution of apoE N- and C- terminal specific staining in N2a cells

Representative images of immunolabelling with an N-terminus specific and a C-terminus specific antibody of apoE in N2a cells transfected with apoE2, apoE3 and apoE4 for 48 hours and fixed with FA. Extensive co-localisation was observed. Scale bar = 10µm.

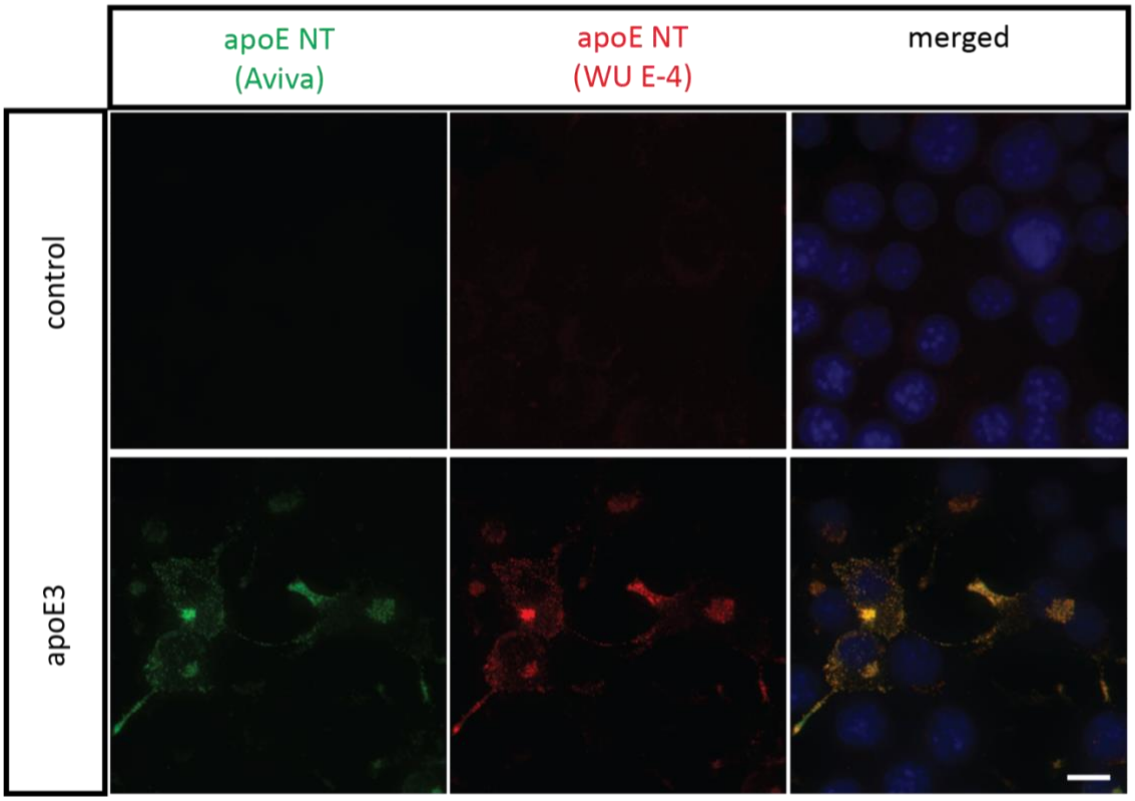

Figure 6-2 Immunofluorescence images showing the distribution of apoE N-terminus specific staining in N2a cells

Representative images of immunolabelling with two N-terminus specific antibodies of apoE in N2a cells transfected with apoE2, apoE3 and apoE4 for 48 hours and fixed with FA; n=3. Extensive co-localisation was observed. Scale bar = 10µm.

6.2.2 The effect of apoE overexpression on endogenous p-Tau organisation and regulation

6.2.2.1 Validating phosphospecificity of the anti pThr181-Tau antibody

Since the anti- pThr181-Tau AT270 antibody has been used in studies reporting apoE-induced tau hyperphosphorylation (Huang et al., 2001, Hoe et al., 2006), this antibody was also used in the present study to investigate whether apoE overexpression affects the organisation and regulation of p-Tau. However, the phosphospecificity of the anti-pThr181-Tau AT270 antibody for the phosphorylated form of tau was first confirmed. Usually protein lysate is treated with phosphatases after extraction and then western blotting performed, however protease and phosphatase inhibitors were used in the lysis buffer to minimise dephosphorylation of Tau due to lysis. Hence to ensure the specificity of the anti- pThr181-Tau AT270 antibody for the phosphorylated form of tau, lamba phosphatase treatment (LPP) was used to remove phosphate groups from proteins

transferred onto nitrocellulose blots after SDS PAGE. Lysate used was from control mature primary neurons since they endogenously express tau protein. Control primary neuron lysate from three independent cultures were loaded in duplicate so that the blots could be cut into two after transfer to enable comparison of identical blots that were untreated or treated with LPP. Due to limited available protocols for this approach, two protocols were trialled. Blots were either treated with LPP before blocking with 5% BSA (Figure 6-3, A) or after blocking with 5% BSA (Figure 6-3, B). The blots were then immunolabelled using anti- pThr181-Tau AT270, anti- pSer9-SnpI (weakly labels pSer9-SnpII) as a positive control for antibody phosphospecificity, and anti- actin as a loading control. On untreated blots, the anti- pThr181-Tau AT270 antibody detected various isoforms of Tau ranging from 52-63kDa (Figure 6-3, A and B, untreated blot). The anti-pSer9-SnpI antibody did not detect pSer9-SnpI, likely due to very low basal phosphorylation of this protein without induced-neuronal activity, but it did however detect low levels of pSer9-SnpII (Figure 6-3, A and B, untreated blot). Treating the blot with LPP before blocking resulted in reduced signal for both phospho-antibodies (Figure 6-3, A), whereas treatment after blocking eliminated the signal (Figure 6-3, B). This data confirms that the antibody for pThr181-Tau is phosphospecific.

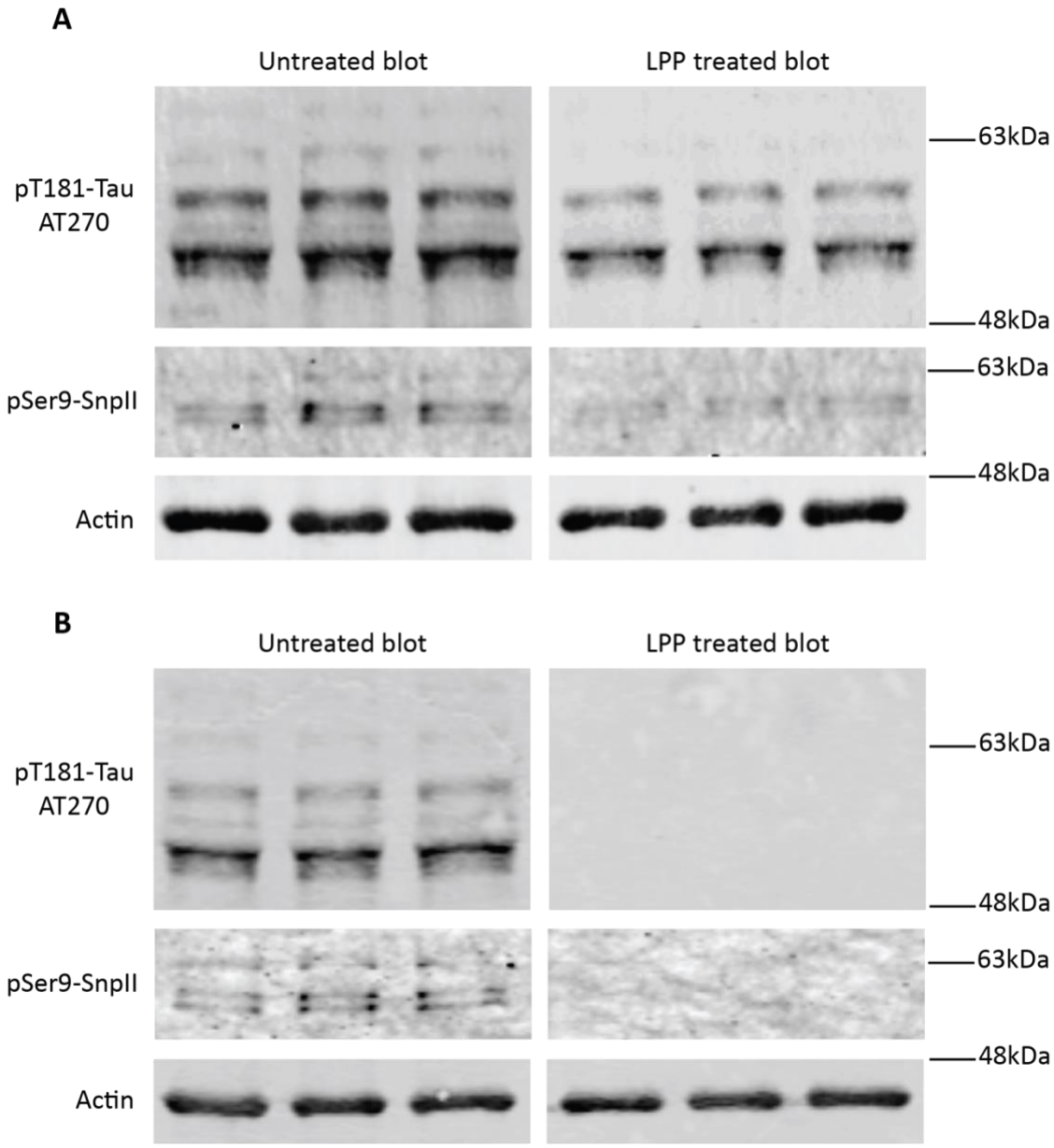

Figure 6-3 Western blots of primary neuron lysate showing phospho-specificity of anti- pThr181-Tau antibody

Western blots of primary neuron protein extracts probed with antibodies for tau phosphorylated at threonine 181, SynapsinII at Ser9 (positive control) and actin (loading control) before (A) and after (B) blocking the blot with 5% BSA. Both untreated blots reveal detection of pThr181-Tau, pSer9-SnpII and actin (A and B). Lambda phosphatase (LPP) treatment of duplicate blot before blocking reduces the signal for both pThr181-Tau and pSer9-SnpII (A). LPP treatment of duplicate blot after blocking completely eliminates detection of pThr181-Tau and pSer9-SnpII (B), confirmining that both antibodies are phosphospecific.

6.2.2.2 Comparing the effects of different fixatives on apoE and pThr181-Tau staining in N2a cells

Prior to assessing the effect of apoE isoform on the intracellular organisation of pThr-181-Tau, the effect of fixative on the staining pattern of apoE and pThr-181-Tau in control and apoE3-transfected N2a cells was carried out. Control and apoE3-expressing N2a cells were fixed using methanol or FA and then immunolabelled using anti- pThr181 Tau AT270 and anti- apoE (Calbiochem) to determine the optimal fixation method (Figure 6-4). The staining of pThr181-Tau was similar in cells fixed with FA and methanol (Figure 6-4 A compared with B), although methanol fixation did appear to enhance its cytoplasmic staining. The staining for apoE however, was remarkably altered when N2a cells were fixed with methanol. The labelling of apoE appeared more diffused and the strong perinuclear staining was no longer distinguishable (Figure 6-4, B compared with A). Therefore, FA was used as the fixative for subsequent immunofluorescence experiments involving staining for apoE.

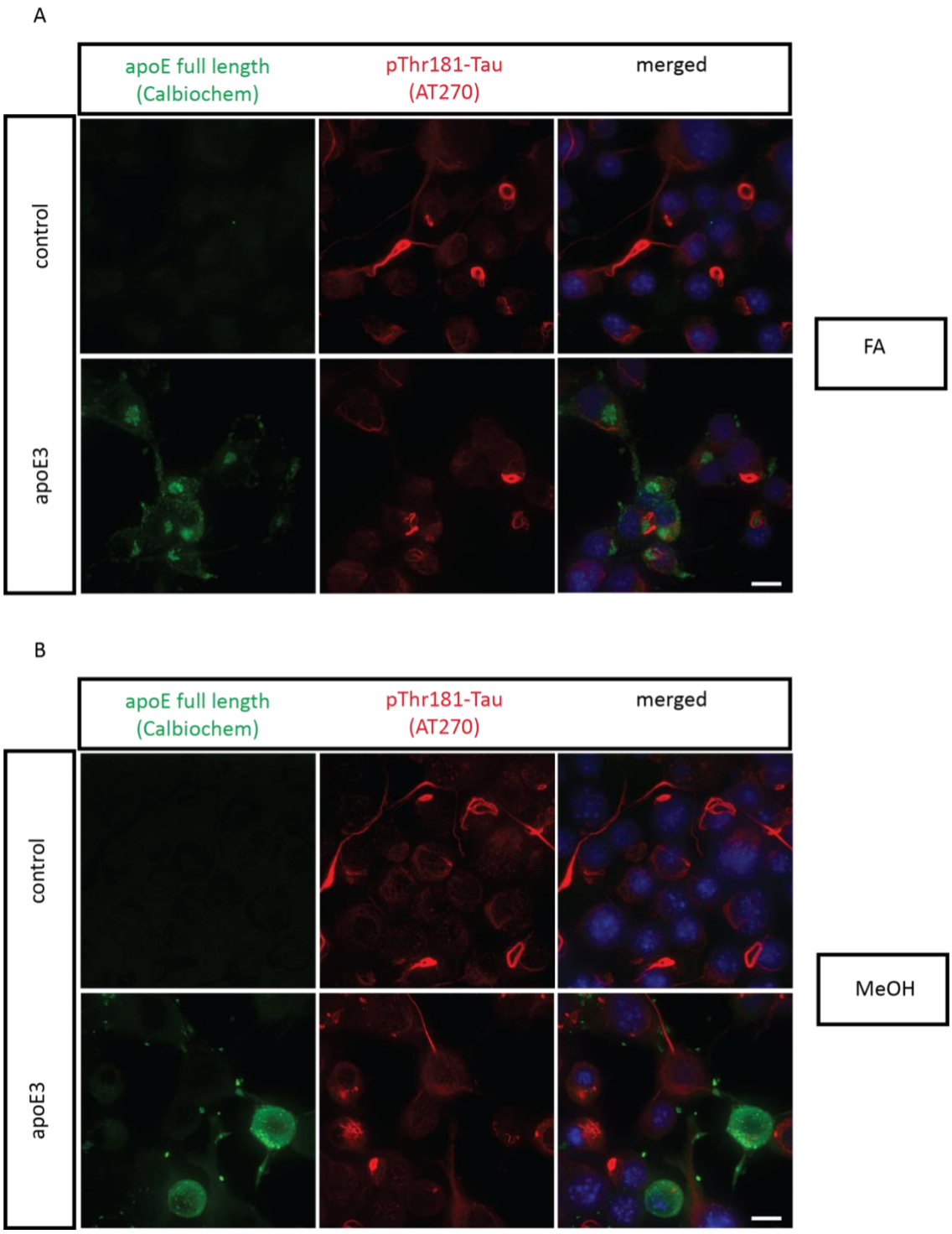

Figure 6-4 Immunofluorescence images showing apoE and pThr181-Tau staining in N2a cells fixed with either formaldehyde or methanol

Representative immunofluorescence images of formaldehyde- (A) and methanol- (B) fixed control and apoE3-expressing N2a cells double immunolabelled for apoE (green) and Tau phosphorylated at Thr181 (red) using goat anti- apoE (Calbiochem) and mouse anti- pThr181-Tau AT270 antibodies respectively. Scale bar = 10µm.

6.2.2.3 ApoE does not co-localise with pThr181-Tau in N2a cells

it has been demonstrated that GFP-tagged full length apoE4 and C-terminally truncated apoE4 (1-272aa) induce and co-localise with p-Tau containing inclusions to a greater extent than apoE3 when expressed in N2a cells (Huang et al., 2001). Since the data in the previous chapter indicated that C-terminally truncated fragments are not generated, and that apoE fragments are instead N-terminally truncated, the present study investigated whether the findings reported by Huang and colleagues could be reproduced under the same conditions used in the previous chapter. Furthermore, since the Huang et al. study did not include apoE2, it was of interest to determine the effect of this isoform on the subcellular organisation of pThr181-Tau in N2a cells. To do so, apoE-transfected N2a cells were immunolabelled using goat anti- apoE (Calbiochem) (Figure 6-5, green staining) to detect full length apoE and its fragments, and anti- pThr181-Tau AT270 (Figure 6-5, red staining) to detect hyperphosphorylated 'tangle-like' inclusions. (Huang et al., 2001).

Surprisingly, the immunolabelling revealed intense staining for pThr181-Tau that resembled the reported 'tangle-like' structures (Huang et al., 2001) in both, control and apoE-transfected N2a cells. This suggests that this structure may not be the pathological form of tau in N2a cells, or that this staining is not specific to p-Tau. Immunolabelling also revealed diffused cytoplasmic staining of pThr181-Tau that was stronger in apoE-transfected cells compared to control cells, which could suggest increased pThr181-Tau levels. This did not appear to be dependent on apoE isoform. Remarkably though, apoE staining for all three isoforms did not appear to co-localise with either the cytoplasmic or tangle-like staining of pThr181-Tau. Instead, the tangle-like structures of pThr181-Tau appeared to wrap or cage around the intense apoE staining proximal to the nucleus.

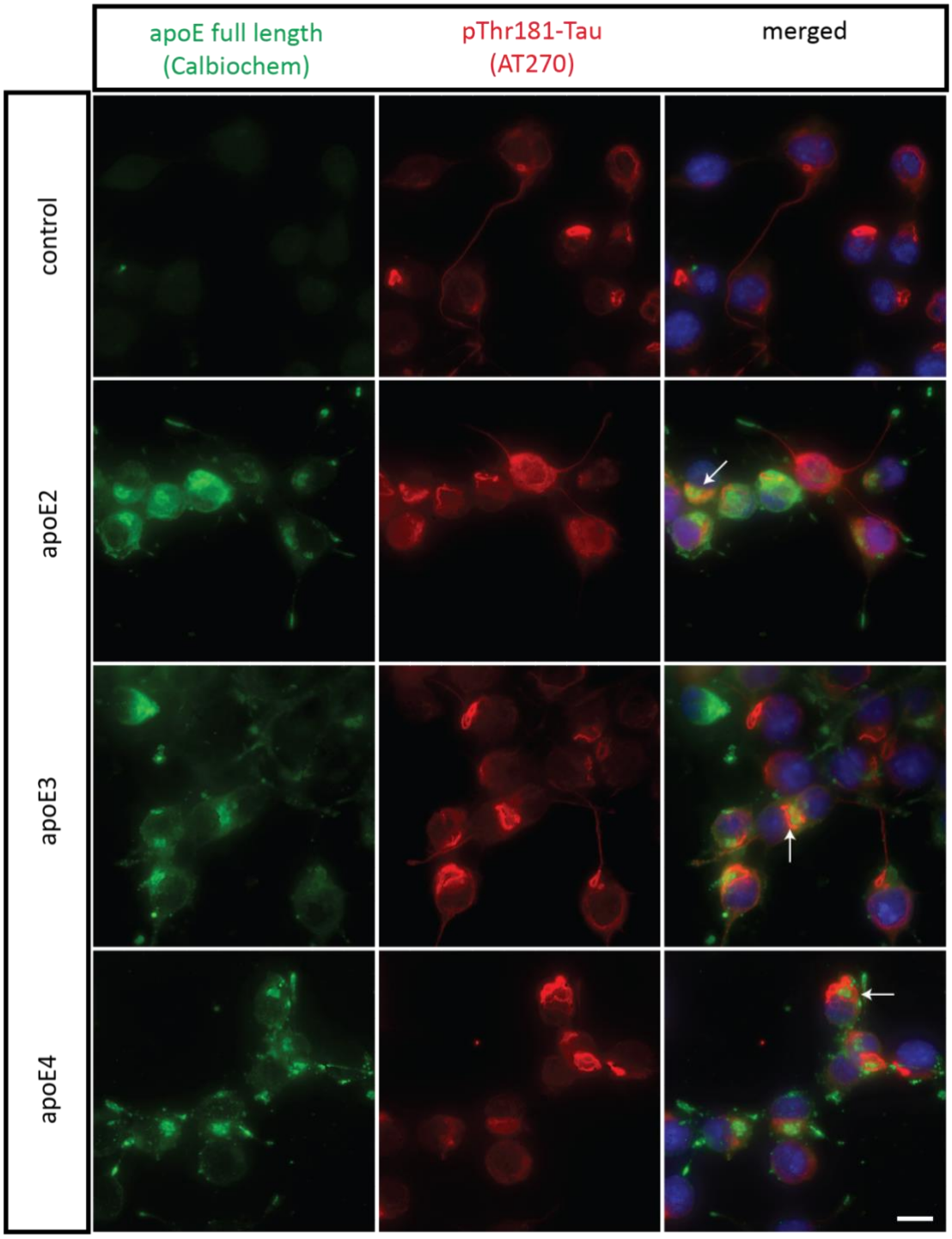

Figure 6-5 Immunofluorescence images showing the localisation of different human apoE isoforms and pThr181-Tau in N2a cells

Representative immunofluorescence images of N2a cells transfected with either human apoE2, apoE3 or apoE4 for 48 hours (n=3), fixed with FA and co-stained for apoE (green) and p-Tau (red) using goat anti-apoE (Calbiochem) and mouse anti- pThr181 Tau AT270 antibodies. No co-localisation was observed between apoE and pThr181-Tau in apoE-transfected cells for any isoform. However, pThr181-Tau cage-like structures surrounding the perinuclear region of apoE was apparent for all isoforms of apoE, as indicated by the white arrows. Scale bar = 10µm.

6.2.2.4 ApoE affects tau phosphorylation in an isoform-dependent manner in vitro

Although full length apoE did not appear to co-localise with pThr181-Tau in N2a cells, the diffused cytoplasmic staining for pThr181-Tau seemed to be stronger in apoE-transfected cells than in control N2a cells. This raised the possibility that apoE overexpression may affect the levels of pThr181-Tau. To investigate if this was case, western blotting was carried out using anti- pThr181-Tau AT270, anti- Tau-1, anti- Tau D-8, and anti- actin antibodies for all three cell models overexpressing apoE under the same conditions used previously.

Western blots showed very weak detection (near background levels) of tau isoforms phosphorylated at Thr181 (Figure 6-6, A;~52-63kDa bands) and Tau-1 (Figure 6-6, B;~52-63kDa bands) for all conditions in N2a cells, which did not allow for reliable quantitation. Immunoblotting using anti- Tau D-8 did not detect any bands (data not shown). These findings were surprising considering the intense staining that was observed by immunofluorescence in N2a cells labelled with anti- pThr181-Tau AT270. Immunoblotting for actin as a loading control revealed strong bands in each lane suggesting that the protein quality and amount loaded was adequate for western blotting analysis. Despite the weak labelling for p-Tau (~52-63kDa bands), the anti-pThr181-Tau AT270 antibody strongly detected high molecular weight bands within 100kDa-180kDa of size (Figure 6-6, A). These bands were not detected by anti- Tau-1, indicating that they may be nonspecific. As a result, whether apoE overexpression affected endogenous p-Tau/total tau levels in N2a cells could not be confidently determined.

Western blotting analysis of pThr181-Tau and total tau levels in SH-SY5Y cells was also not conclusive. Immunoblotting using the anti- pThr181-Tau AT270 antibody revealed faint bands for all conditions in SH-SY5Y cells (Figure 6-7, A; ~52-58kDa bands). Whilst the anti- Tau-1 antibody failed to recognise total tau in this cell line, immunoblotting using anti- Tau D-8 (Santa Cruz) showed that there were low levels of total tau for all conditions (Figure 6-7, B; ~52-58kDa bands). In addition, a strong band of ~135kDa was also detected by anti- pThr181-Tau AT270 in all extracts (Figure 6-7, A), but not by anti-

Tau D-8 (Figure 6-7, B). This suggests that it is likely a non-specific band, similar to those observed in N2a cells.

Finally, these experiments were repeated with extracts from primary neurons. High levels of pThr181-Tau and total tau isoforms were detected in these extracts (Figure 6-8, A and B respectively; ~52-63kDa bands). Notably, high molecular weight bands (~135-180kDa) were also detected by anti- pThr181-Tau AT270 (Figure 6-8, A; top blot) but not by anti- Tau-1 (Santa Cruz). Since the signal for the pThr181-Tau and tau bands were strong enough, densitometric analysis was carried out. The levels of pThr181-Tau and total tau were determined by normalising the ratios of pThr181-tau/actin and total tau/actin to control neurons (Figure 6-9). Densitometric analysis (shown in Figure 6-9, A) showed a significant increase in ~52kDa pThr181-Tau levels in extracts from primary neurons overexpressing apoE3 and apoE4 (134.6%±8.9 apoE3 versus control, p=0.0188; 145.3%±8.0 apoE4 versus control, p=0.004), whereas extracts from primary neurons overexpressing apoE2 showed that similar levels of ~52kDa pThr181-Tau to control neurons (112.2%±3.5 apoE2 versus control, p>0.05). The levels of pThr181-Tau in protein extracts from apoE4-overexpressing neurons were also significantly different to those from apoE2-overexpressing neurons (p=0.0237). Collectively this data suggests that apoE overexpression induces tau phosphorylation at the Thr181 site of the ~52kDa tau variant in an isoform dependent manner (E4>E3, whilst apoE2 does not exert an effect). This was not the case for ~58kDa pThr181-Tau though. The levels of ~58kDa pThr181-Tau (shown in Figure 6-9, B) in neurons overexpressing the three apoE isoforms were similar to control neurons (102.8%±8.1 apoE2, 119%±3.8 apoE3 and 113.8%±2.8 apoE4; p>0.05). Since the other tau variants were near background levels, the difference in the pThr181-Tau levels of these variants between conditions could not be calculated. Total tau levels (~52kDa band) in primary neuron lysates were also assessed following normalisation against actin (Figure 6-9C). The data revealed no significant in the levels of total tau (113.1%±27.4 apoE2, 117.6%±20.1 apoE3 and 130%±18.4 apoE4; p>0.05) suggesting that apoE overexpression in neuronal cultures for 3 days does not affect total tau levels, and therefore indicates that the increase in pThr181-Tau levels is due to increased phosphorylation at this site.

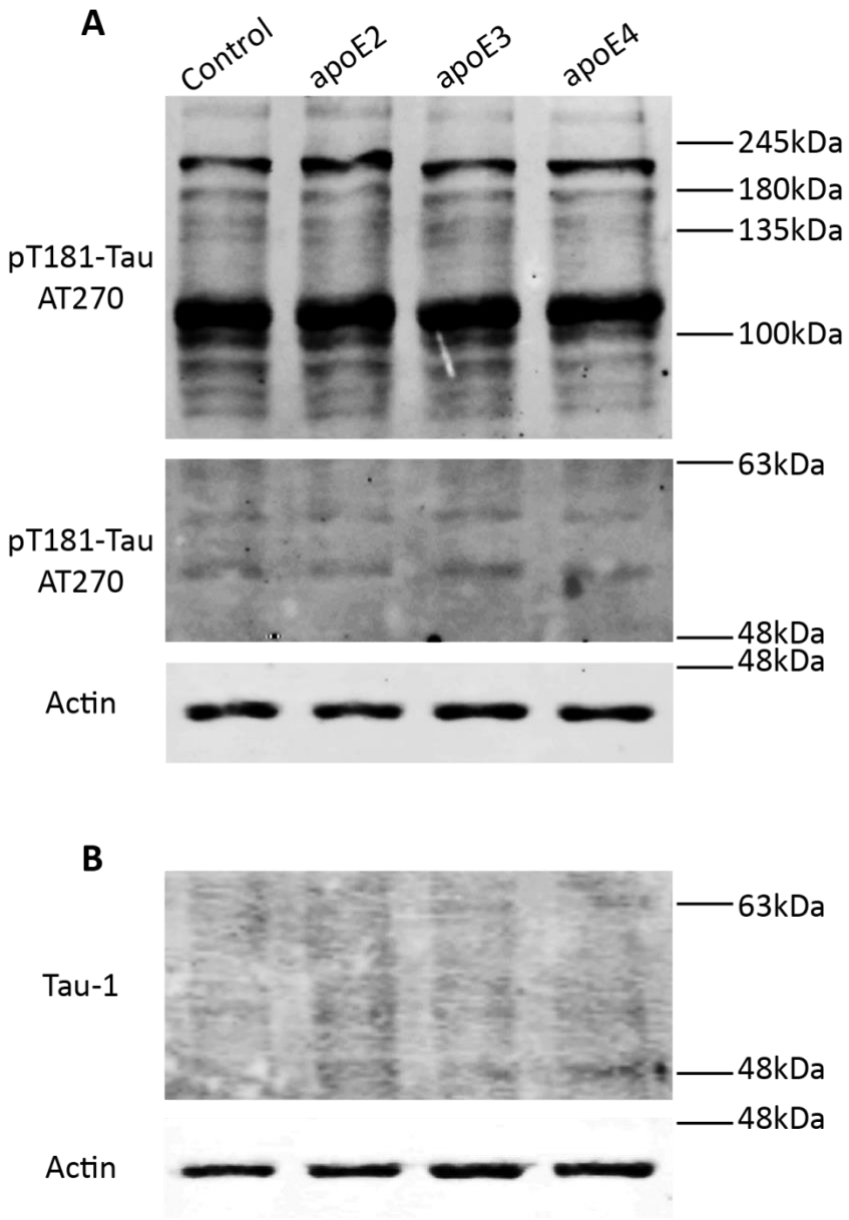

Figure 6-6 Western blots of pThr181-Tau and total tau from protein extracts of apoE-transfected N2a cells

N2a cells were transiently transfected with pCMV-ApoE plasmids for 48 hours and protein was harvested for western blotting analysis; n=3. (A) Immunoblotting using anti- pThr181-Tau AT270 revealed faint bands for pThr181-Tau isoforms ranging from 52-63kDa but also intense bands of approximately 110kDa and 215kDa. (B) Immunoblotting using anti- Tau-1 detected low levels of endogenous tau in N2a cells. Both blots were also labelled for actin to use as a loading control.

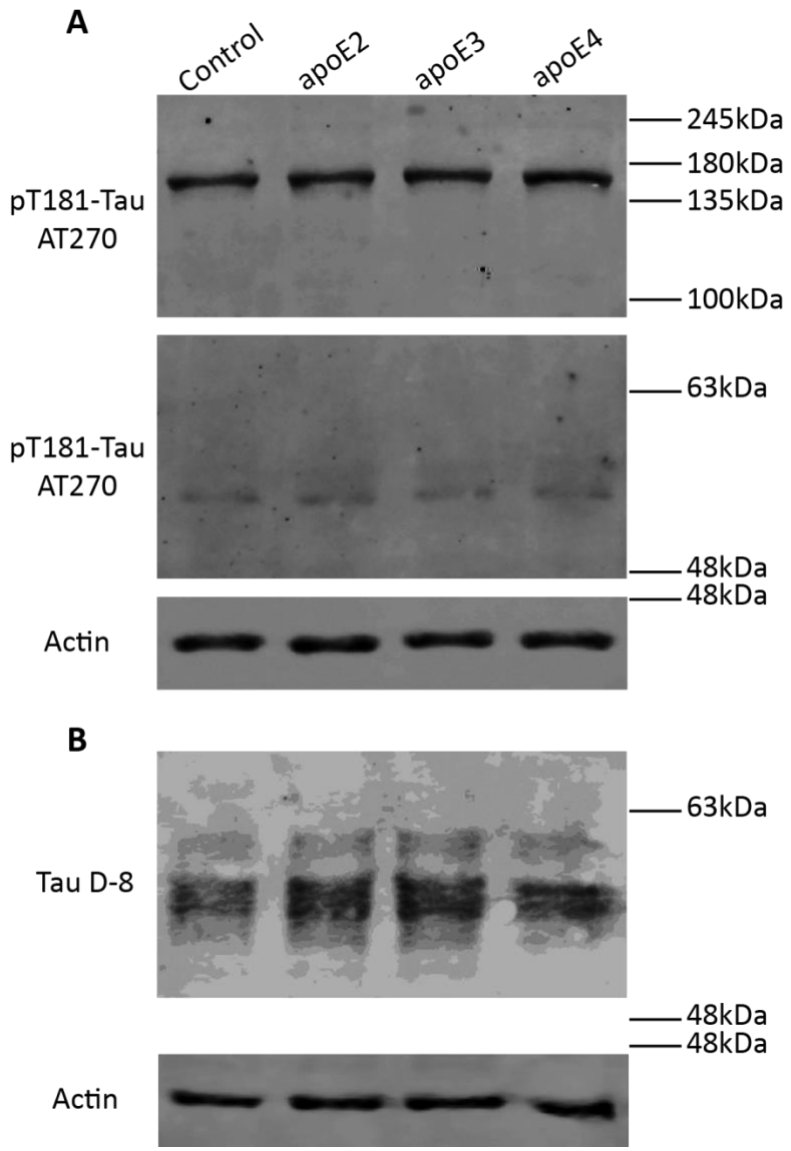

Figure 6-7 Western blots of pThr181-Tau and total tau from protein extracts of apoE-transfected SH-SY5Y cells

SH-SY5Y cells were transiently transfected with pCMV-ApoE constructs for 48 hours and protein was harvested for western blotting analysis; n=3. (A) Immunoblotting using anti- pThr181-Tau AT270 revealed faint bands for pThr181-Tau isoforms ranging from 52-58kDa but also an intense band of approximately 150kDa. (B) Immunoblotting using anti- Tau D-8 showed that low levels of endogenous tau is expressed in SH-SY5Y cells. Both blots were also labelled for actin to use as a loading control.

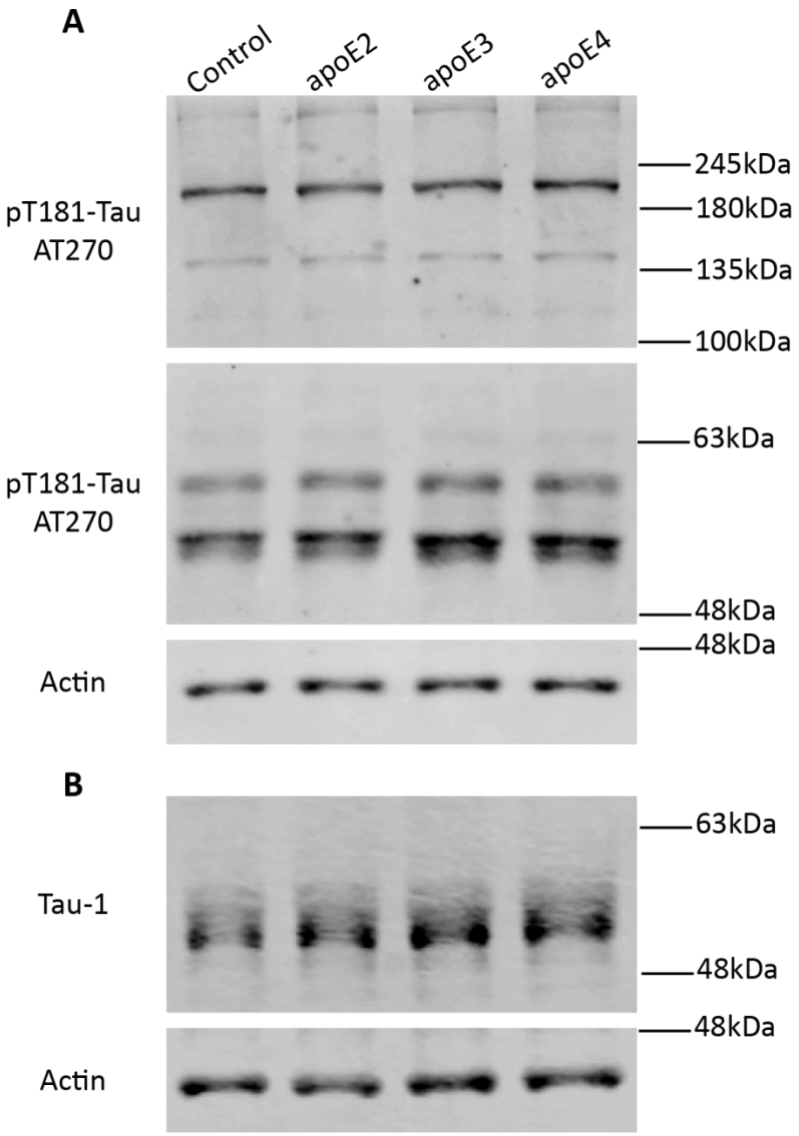

Figure 6-8 Western blots of pThr181-Tau and total tau from protein extracts of primary neurons transduced with apoE lentiviral vectors

Primary neurons were transduced using apoE lentiviral vectors at an MOI of 150 for 3 days and protein was harvested for western blotting analysis; n=3. (A) Immunoblotting using anti- pThr181-Tau AT270 revealed pThr181-Tau isoforms ranging from 52-74kDa but also bands of approximately 135kDa and 215kDa. (B) Immunoblotting using anti- Tau-1 revealed the doublet band of approximately 52-58kDa. Both blots were also labelled for actin to use as a loading control for quantitiation.

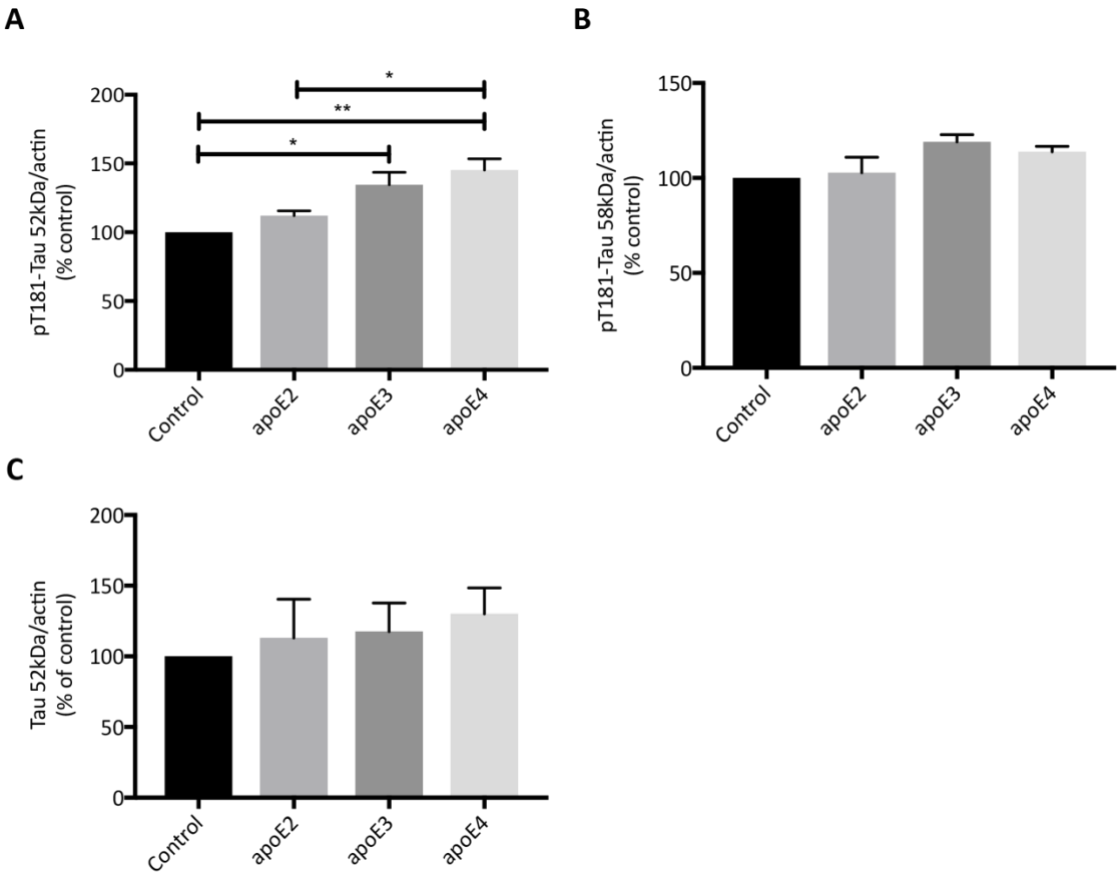

Figure 6-9 Bar charts showing quantitation of pThr181-Tau (52kDa and 58kDa) and total tau levels in lysates of primary neurons transduced with apoE-expressing lentiviral vectors for 3 days

The intensity of pThr181-Tau, total tau and actin bands were quantified by densitometric analysis and the levels of pThr181-Tau and total tau were calculated as a percentage of control levels as 100%. (A) Bar chart showing that the levels of ~52kDa pThr181-Tau (normalised to actin) significantly increase ($p<0.05$) in apoE3- and apoE4- overexpressing neurons, whereas apoE2-overexpressing neurons display similar levels to control neurons. (B) Bar chart showing that levels of ~58kDa pThr181-Tau (normalised to actin) are similar in apoE2-, apoE3- and apoE4- overexpressing neurons to control neurons. (C) Bar chart showing that levels of ~52kDa total tau (normalised to actin) are similar in apoE2-, apoE3- and apoE4-overexpressing neurons. Data are mean ±SEM, and differences were assessed using one-way ANOVA followed by a Tukey's multiple comparisons test. *$p<0.05$; **$p<0.01$; n=3.

6.2.2.5 Cell model dependent effects of apoE overexpression on GSK3 kinase phosphorylation

The GSK3 kinase is one of many kinases that modulates tau function through phosphorylation events at several sites across the protein, including the Thr181 site (Sperber et al., 1995). Since the previous section showed that tau was phosphorylated at the Thr181 site to a greater extent in apoE3- and apoE4- overexpressing primary neurons, the aim of the work presented in this section was to determine whether apoE overexpression alters the levels of inactive GSK3, which could in turn affect the phosphate content at Thr181 of tau. Phosphorylation of GSK3ß at Ser9 and GSK3α at Ser21 is associated with inhibition of kinase activity, whilst a decrease in the phosphorylated form of GSK3 indirectly indicates enhanced kinase activity (Sutherland et al., 1993). Here, the levels of phosphorylated GSK3 were quantified from western blots of protein extracts from N2a cells, SH-SY5Y cells and primary neurons overexpressing apoE isoforms as previously described. Immunoblotting was carried out using an antibody that detects GSK3ß phosphorylated at Ser9.

Western blots of N2a cell extracts (Figure 6-10, A) detected pSer9-GSK3ß at ~46kDa for all conditions, as well as another band at ~51kDa that likely represents GSK3α phosphorylated at Ser21 due to epitope sequence similarity. Quantification of pSer9-GSK3ß levels (Figure 6-10, B) revealed a significant reduction in protein extracts from apoE3- and apoE4- transfected N2a cells compared to control cells (60.6%±7.6 apoE3, $p=0.0041$ and 59.8%±5.8 apoE4, $p=0.0036$). The levels of pSer9-GSK3ß in apoE2-transfected N2a cells were similar to control (100.0%±5.3 apoE2, $p>0.05$), and so were also significantly different to the levels for the other two isoforms (apoE2 versus apoE3, $p=0.004$ and apoE2 versus apoE4, $p=0.0035$). A reduction in pSer21-GSK3α levels was also observed in apoE3- and apoE4- transfected N2a cells compared to control cells (66.24%±10.7 apoE3, $p=0.0252$ and 67.85%±4.6 apoE4, $p=0.0322$), but not in apoE2-transfected N2a cells (103.5%±5.6 apoE2, $p>0.05$). This suggests that in N2a cells, the activity of both GSK3ß and GSK3α is elevated by the expression of apoE3 or apoE4, but not apoE2.

Western blots of SH-SY5Y cell extracts also revealed bands corresponding to pSer9-GSK3ß and pSer21-GSK3α in all lanes (Figure 6-11, A). However, quantitation did not show significantly altered levels of pSer9-GSK3ß (Figure 6-11, B; 87.4%±4.0 apoE2, 96.3%±6.7 apoE3 and 92.7%±6.5 apoE4; $p>0.05$) or pSer21-GSK3α (Figure 6-11, C; 89.6%±5.2 apoE2, 93.1%±5.7 apoE3 and 102.0%±4.8 apoE4; $p>0.05$) when any of the three apoE isoforms were overexpressed. This suggests that apoE expression does not affect the kinase activity of either pSer9-GSK3ß and pSer21-GSK3α in SH-SY5Y cells.

pSer9-GSK3ß and pSer21-GSK3α were also detected by western blotting of lysate from primary neurons overexpressing the three major apoE isoforms (Figure 6-12, A). Quantitation did not reveal any significant differences in the levels of pSer9-GSK3ß between apoE-overexpressing neurons and control neurons (Figure 6-12, B; 97.1%±9.6 apoE2, 90.45%±7.8 apoE3 and 82.1%±8.9 apoE4; $p>0.05$). Likewise, no significant difference was observed in the levels of pSer21-GSK3α (Figure 6-12, B; 108.1%±16.6 apoE2, 99.8%±14.3 apoE3 and 89.5%±12.9 apoE4; $p>0.05$). These data indicate that neuronal apoE expression does not affect the kinase activity of pSer9-GSK3ß and pSer21-GSK3α, which is consistent with that observed in SH-SY5Y cells. Hence the decrease in pSer9-GSK3ß and pSer21-GSK3α levels in N2a cells appears to be a cell-dependent effect.

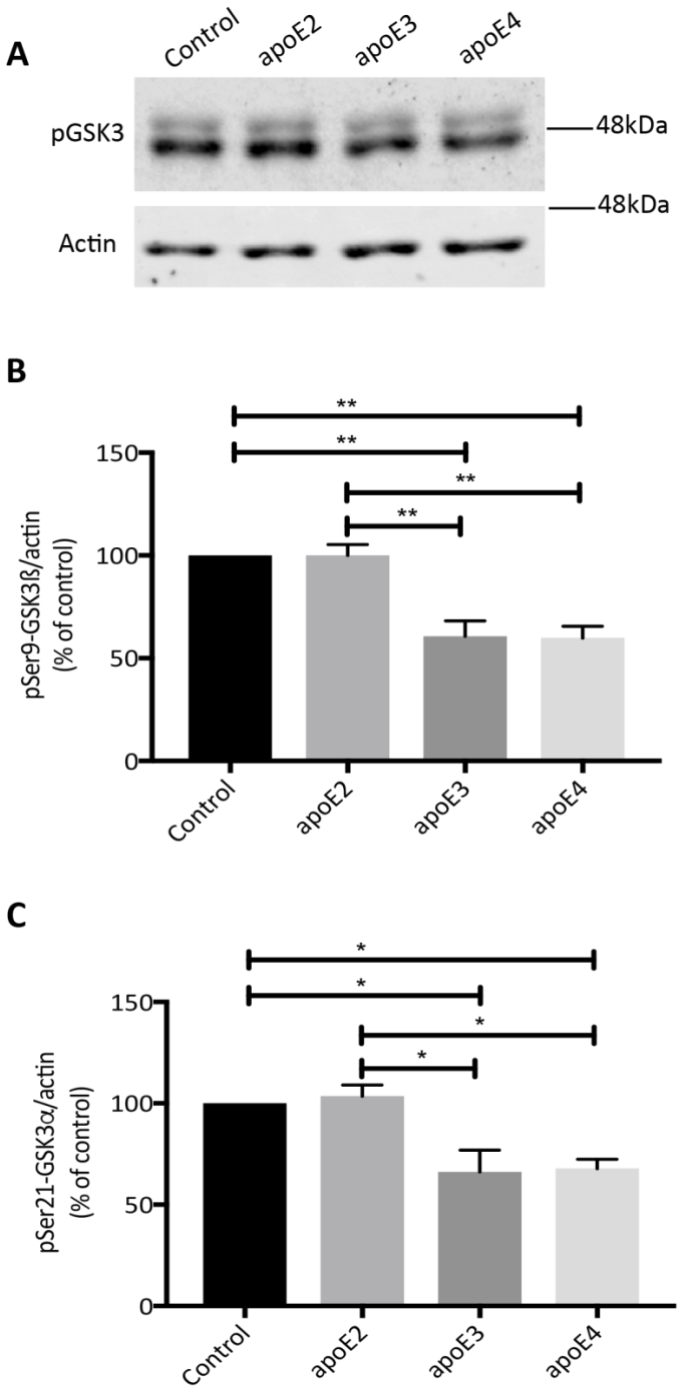

Figure 6-10 Western blotting analysis of pSer9-GSK3ß and pSer21-GSK3α levels in lysates of apoE-transfected N2a cells

(A) Immunoblotting using anti- pSer9-GSK3ß revealed bands corresponding to pSer9-GSK3ß at ~46kDa and pSer21-GSK3α at ~51kDa in lysates of control N2a cells and N2a cells overexpressing apoE2, apoE3 and apoE4 for 48 hours. Blots were also labelled for actin as a loading control. Quantitation of pSer9-GSK3ß levels (B) and pSer21-GSK3α levels (C) showed a significant reduction in apoE3- and apoE4-transfected N2a cells, but not in apoE2-transfected N2a cells. Data are mean ±SEM, and differences were assessed using one-way ANOVA followed by a Tukey's multiple comparisons test where $p<0.05$ is significant. *$p<0.05$; **$p<0.01$; n=3.

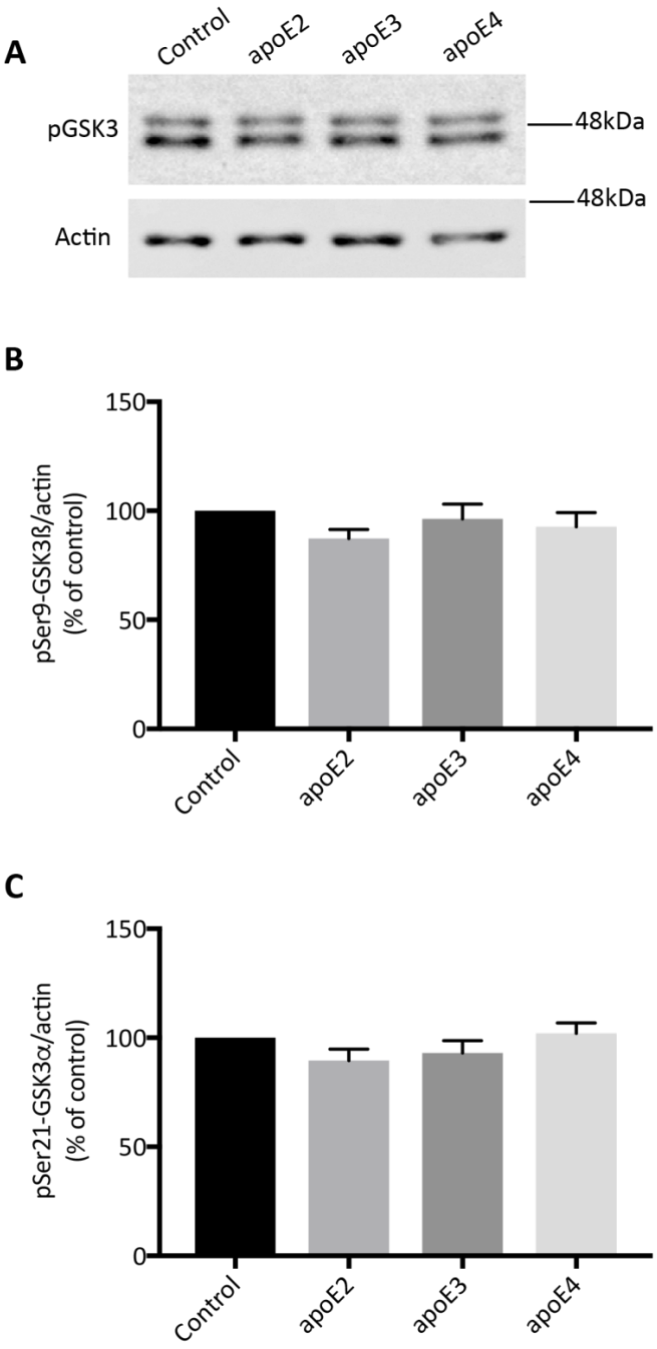

Figure 6-11 Western blotting analysis of pSer9-GSK3ß and pSer21-GSK3α levels in lysates of apoE-transfected SH-SY5Y cells

(A) Immunoblotting using anti- pSer9-GSK3ß (cell signalling) reveals bands corresponding to pSer9-GSK3ß at ~46kDa and pSer21-GSK3α at ~51kDa in lysates of control SH-SY5Y cells and SH-SY5Y cells transfected with apoE-expressing plasmids for 48 hours. Blots were also labelled for actin as a loading control. Quantitation of pSer9-GSK3ß levels (B) and pSer21-GSK3α levels (C) showed no significant differences between control and apoE-expressing SH-SY5Y cells. Data are mean ±SEM, and differences were assessed using one-way ANOVA followed by a Tukey's multiple comparisons test where $p<0.05$ is significant; n=3.

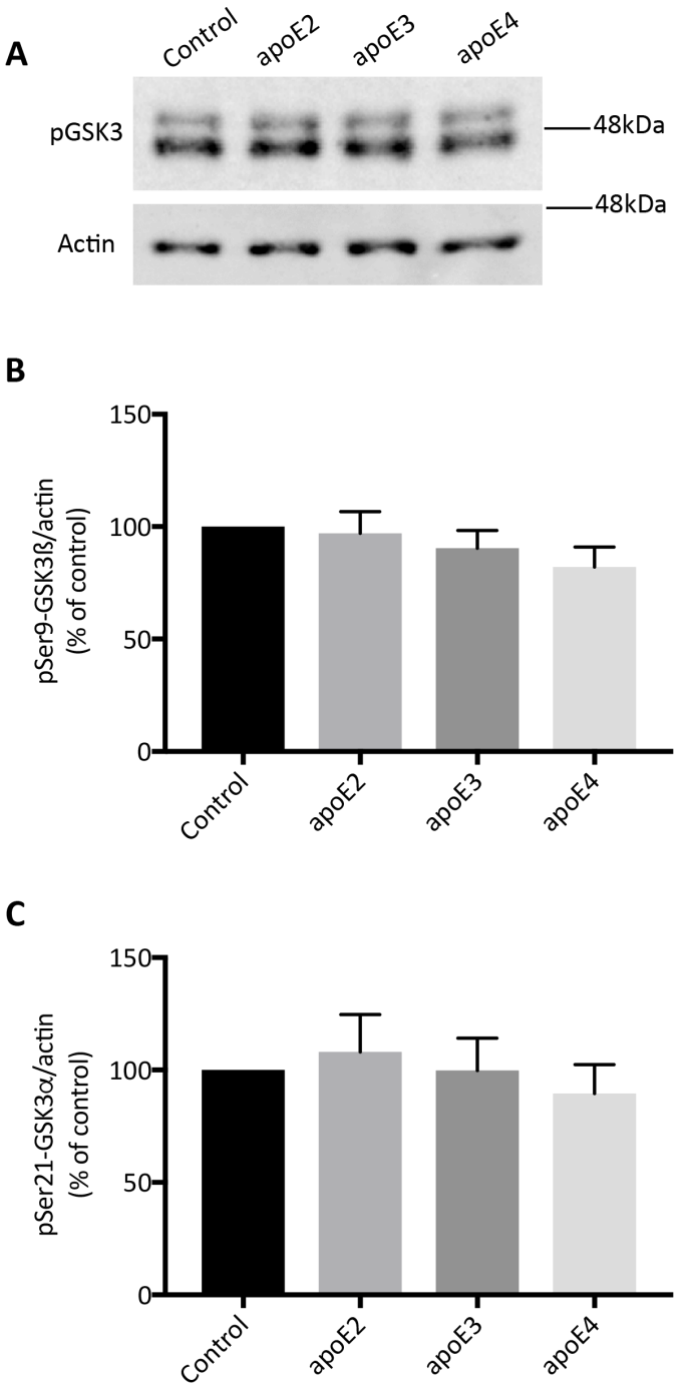

Figure 6-12 Western blotting analysis of pSer9-GSK3ß and pSer21-GSK3α levels in lysates of primary neurons transduced with apoE-expressing lentiviral vectors

(A) Immunoblotting using anti- pSer9-GSK3ß (cell signalling) revealed bands corresponding to pSer9-GSK3ß at ~46kDa and pSer21-GSK3α at ~51kDa in lysates of control primary neurons and primary neurons transduced with apoE lentiviral vectors (150MOI) for 3 days. Blots were also labelled for actin as a loading control. Quantitation of pSer9-GSK3ß levels (B) and pSer21-GSK3α levles (C) revealed that there were no significant differences between control and apoE-expressing primary neurons. Data are mean ±SEM, and differences were assessed using one-way ANOVA followed by a Tukey's multiple comparisons test where $p<0.05$ is significant; n=3.

6.2.3 ApoE overexpression in neurons enhances vimentin expression in an isoform and cell dependent manner

Although expression of apoE and vimentin in neurons has been proposed to play a role in the repair response of stressed or injured neurons, it is not known whether there is a relationship between the two. To investigate this, the levels of vimentin were examined in neuronal cell models overexpressing either apoE2, apoE3 or apoE4. The levels of vimentin were calculated as a percentage of the control (as 100%) from the ratios of vimentin/actin band intensity values for each condition.

Unfortunately, western blots of N2a cell extracts using anti- vimentin did not reveal bands (not shown), although this was unsurprising since this commercially available antibody is reported as unreactive to mouse vimentin.

Western blots of SH-SY5Y cell extracts did however, reveal bands of approximately 58kDa all conditions (Figure 6-13, A). Quantification of vimentin levels did not reveal any statistical differences in SH-SY5Y cells overexpressing apoE2, apoE3, or apoE4 (Figure 6-13, B; 82.7%±18.4 apoE2, 78.8%±10.8 apoE3 and 117.0%±13.0 apoE4; $p>0.05$), suggesting that total vimentin levels are unaffected by apoE overexpression in SH-SY5Y cells under these conditions.

Bands corresponding to vimentin were also detected on western blots of primary neuronal extracts, which appeared to increase in intensity for neurons overexpressing apoE2 and apoE4 protein, but not apoE3 (Figure 6-14, A). Quantification of vimentin levels (Figure 6-14, B) confirmed a significant increase in apoE2- and apoE4-transduced primary neurons compared to control cells (239.9%±18.6 apoE2, $p=0.0024$ and 208.8%±23.7 apoE4, $p=0.0109$). Although vimentin levels were marginally increased in neurons overexpressing apoE3 compared to control neurons, this was not significant (132.9%±19.0 apoE3, $p=0.5852$). The levels of vimentin in apoE2-overexpressing neurons were also found to be significantly greater when compared to apoE3-overexpressing neurons ($p=0.0120$). These results suggest that both apoE2 and apoE4 expression in primary neurons may induce expression of vimentin, whilst apoE3 expression does not.

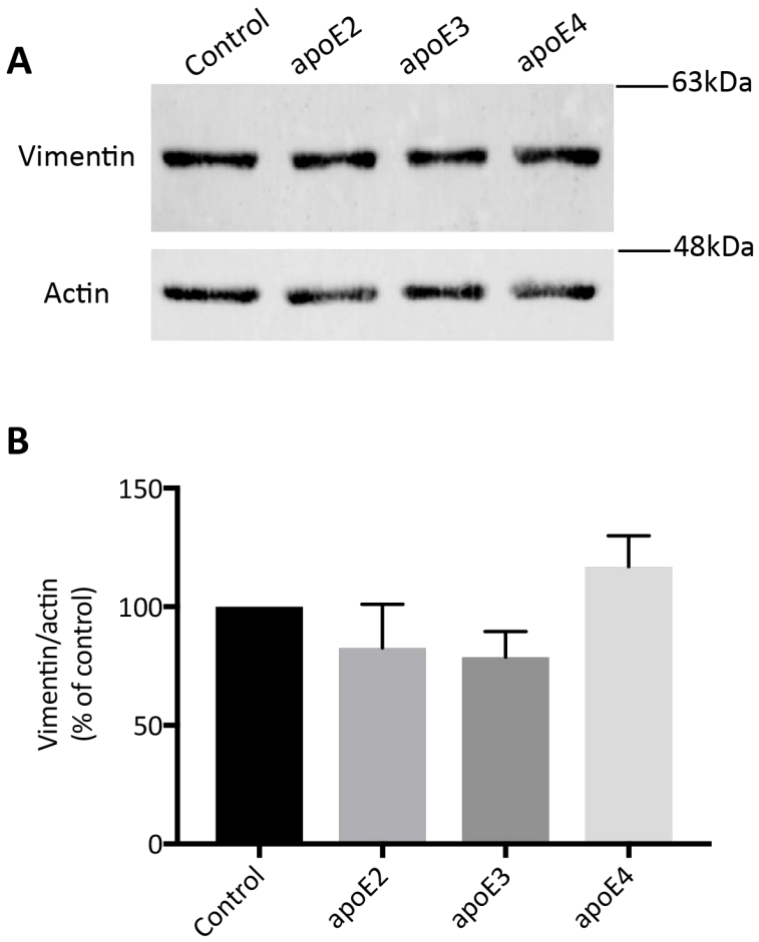

Figure 6-13 Western blotting analysis of vimentin levels in lysates of apoE-transfected SH-SY5Y cells
(A) Immunoblotting using anti- vimentin revealed bands corresponding to vimentin at ~58kDa in lysates of control SH-SY5Y cells and SH-SY5Y cells transfected with apoE2, apoE3 and apoE4 constructs for 48 hours. Blots were also labelled for actin to use as a loading control. (B) Quantitation of vimentin levels did not show significant differences between control and apoE-expressing SH-SY5Y cells. Data are mean ±SEM, and differences were assessed using one-way ANOVA followed by a Tukey's multiple comparisons test where $p<0.05$ is significant; (n=3).

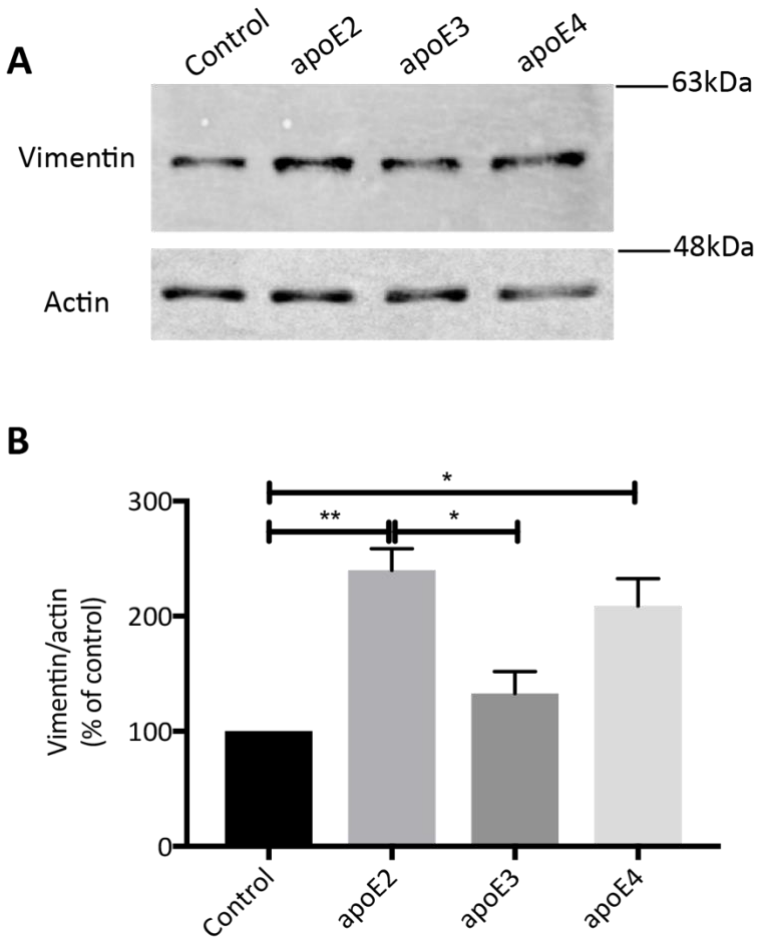

Figure 6-14 Western blotting analysis of vimentin levels in lysates of primary neurons transduced with apoE-expressing lentiviral vectors

(A) Immunoblotting using anti- vimentin revealed bands corresponding to vimentin at ~58kDa in lysates of control primary neurons and primary neurons transduced with apoE2, apoE3 and apoE4 lentiviral vectors (150 MOI) for 3 days. Blots were also labelled for actin to use as a loading control. (A) Quantitation of vimentin levels revealed significant increases of vimentin protein in apoE2- and apoE4-overexpressing primary neurons compared to control neurons, whilst this was not the case for apoE3-overexpressing neurons. The levels of vimentin in neurons overexpressing apoE2 were also significantly greater when compared to apoE3-transduced neurons. Data are mean ±SEM, and differences were assessed using one-way ANOVA followed by a Tukey's multiple comparisons test where $p<0.05$ is significant. *$p<0.05$; **$p<0.01$; (n=3 per condition).

6.2.4 The effect of apoE overexpression on cell viability *in vitro*

Whether apoE expression and proteolysis in neuronal cell models leads to an isoform-dependent toxic or protective gain of function is still not fully established. Therefore, the effect of full length apoE overexpression on cell viability of N2a cells, SH-SY5Y cells and primary neuronal cultures was explored by using an MTT reduction assay, where a reduction in MTT indicates a loss of viable cells. Both N2a and SH-SY5Y cells were transfected with plasmids overexpressing apoE2, apoE3 or apoE4 under a CMV promoter for 48 hours. MTT reduction values were normalised to control cells transfected with an empty plasmid (pCIS backbone) to discount toxicity due to transfection reagent and introduction of plasmid DNA into the cell. Primary neurons were transduced with apoE-expressing lentiviral vectors for 3 days, at an MOI of 50 to reduce the likelihood of toxicity that may accompany high protein expression observed when using an MOI of 150.

Bar charts showing the effect of apoE overexpression on the viability of N2a cells, SH-SY5Y cells and primary neurons are shown in Figure 6-15, where MTT reduction levels are normalised to control values where control is 100%. In N2a cells, MTT reduction was similar between all conditions (Figure 6-15, A; 93.28%±2.1 apoE2, 98.55%±5.3 apoE3 and 97.11%±2.6 apoE4; $p>0.05$). In contrast, significant differences were observed for MTT reduction values in SH-SY5Y cells as shown in Figure 6-15, B. Both apoE2- and apoE3-transfected SH-SY5Y cells displayed significantly greater MTT reduction levels compared to control cells (Figure 6-15, B; 125.2%±9.3 apoE2, $p=0.0277$ and 128.6%±2.9 apoE3, $p=0.0140$), whereas apoE4-transfected cells did not (Figure 6-15, B; 99.8%±1.1 apoE4, $p>0.05$). MTT reduction levels were also significantly greater in SH-SY5Y cells overexpressing apoE2 and apoE3 when compared to apoE4 (apoE2 versus apoE4, $p=0.0268$ and apoE3 versus apoE4, $p=0.0136$). In primary neurons, MTT reduction levels were similar between control neurons and neurons overexpressing apoE2, apoE3 and apoE4 for 3 days (Figure 6-15, C; 101.7%±1.7 apoE2, 101.2%±3.0 apoE3 and 100.9%±3.9 apoE4; $p>0.05$). Collectively apoE overexpression did not appear to be toxic in any of the three cell models since no significant decreases in MTT levels were observed. This suggests that neuronal expression of full length apoE, irrespective of isoform, does not

result in toxicity under these conditions. Surprisingly though, apoE2 and apoE3 expression seemed to enhance cell viability in SH-SY5Y cells, as indicated by the significant increases in MTT reduction levels. This result also highlights another cell dependent effect of apoE expression since an effect was only observed in the human neuroblastoma cell line.

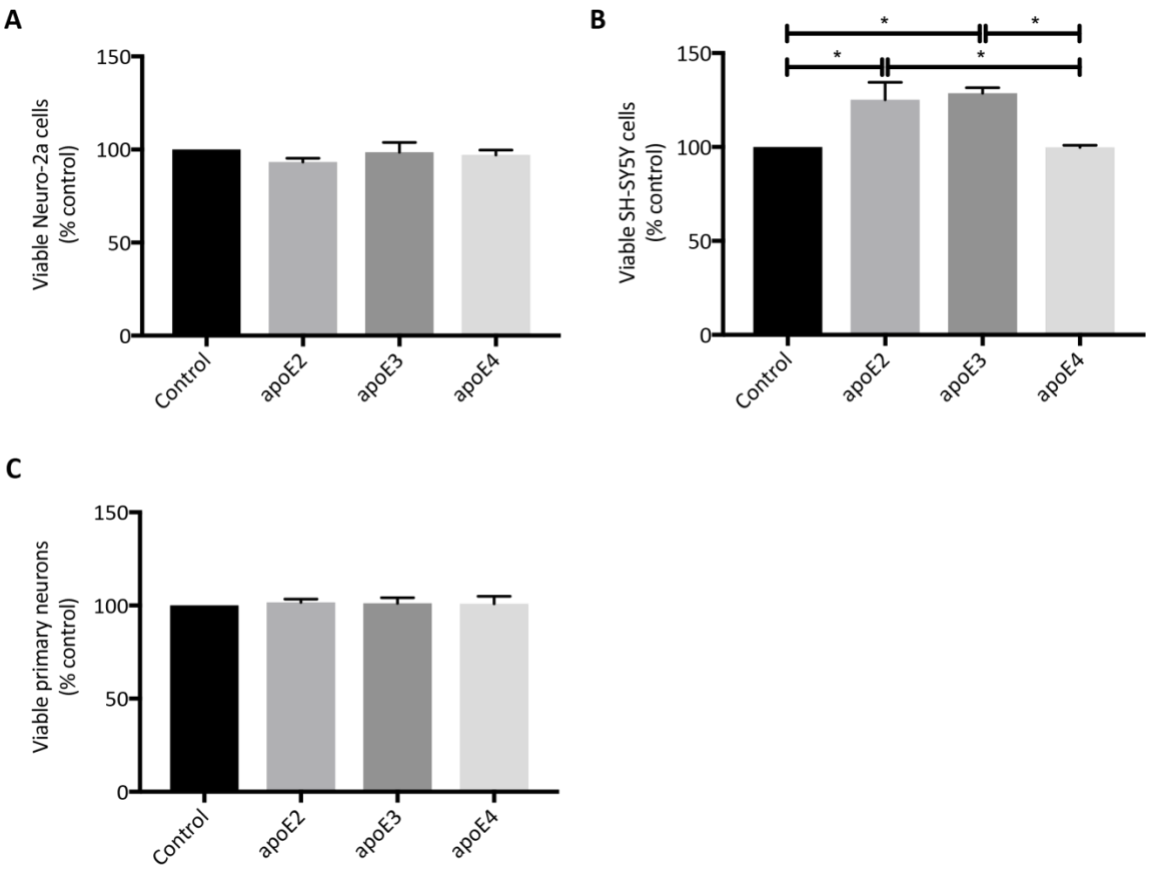

Figure 6-15 Graphs showing the effect of apoE2, apoE3 and apoE4 overexpression on cell viability as based on the MTT reduction assay

(A) Bar chart showing MTT reduction values normalised to control for N2a cells transfected with an empty pCIS construct (control) or pCMV-apoE constructs expressing apoE2, apoE3 and apoE4 for 48 hours (n=6). Cell viability did not appear to affected by apoE overexpression of any isoform, as indicated by similar MTT reduction levels. (B) Bar chart showing MTT reduction values normalised to control for SH-SY5Y cells transfected with an empty pCIS construct (control) or pCMV-apoE constructs expressing apoE2, apoE3 and apoE4 for 48 hours (n=3). Cell viability was enhanced by overexpression of apoE2 and apoE3, as indicated by increased MTT reduction levels. Overexpression of apoE4 however did not affect cell viability. (C) Bar chart showing MTT reduction values as a percentage of control for primary neurons transduced with apoE2, apoE3 and apoE4 lentiviral vectors at an MOI of 50 for 3 days (n=3). Cell viability appeared similar between control neurons and neurons overexpressing all three apoE isoforms affected by apoE overexpression of any isoform. Data are mean ±SEM, and differences were assessed using a one-way ANOVA followed by a Tukey's multiple comparisons test where $p<0.05$ is significant. *$p<0.05$.

6.2.5 The effect of apoE overexpression on apoptosis *in vitro*

To further examine and validate whether apoE expression is toxic or neuroprotective to neurons, a cell death assay was performed for all three cell models using the Nuclear-ID Blue/Red cell viability reagent (Enzo). This assay enables dead cells to be distinguished from the total population of cells in culture by using a combination of two fluorescent

nucleic acid dyes. The blue fluorescent dye is cell-permeable and stains the nucleus, whilst the red fluorescent dye is cell-impermeable in healthy cells, but can stain the nucleus of dead cells since they have compromised cellular membranes. The ratio of live/dead cell populations was determined by FACS analysis for apoE-transfected N2a and SH-SY5Y cells (shown in Figure 6-16 and Figure 6-17). This method provides a measure of cell populations according to their fluorescence, which in this case, involves sorting cells labelled either with both fluorescent dyes compared to cells labelled with the blue fluorescent dye alone. Although cells can be fixed for FACS analysis, fixation was not used here to ensure that cells were not falsely labelled with the red dye due to compromised cellular membrane integrity from the fixation process. Since creating single cell suspensions from primary neuronal cultures can be challenging, the number of dead primary neurons was assessed by live fluorescence microscopy instead of FACS (see Figure 6-18). This approach involved counting the number of dead cells compared to the total number of cells using the NUCLEAR-ID cell viability assay and ImageJ. The ratio of dead cells for each condition was then calculated by the number of dead cells over the total number of cells, and this ratio was then normalised to the ratio of the control. Statistical comparisons between control and apoE-expressing cells were made by one-way ANOVA followed by a Tukey's multiple comparison post-hoc test. A students t-test was used to statistically compare control and ethanol treated cells.

Representative FACs plots for live/dead cell populations of N2a cells overexpressing apoE isoforms or treated with ethanol as a positive control are shown in Figure 6-16, A. In these plots, live N2a cells (with blue fluorescence) are shown in Q4 whereas dead cells (with blue/red fluorescence) are in Q2. The ratio of dead cells (normalised to the control) is depicted in the bar charts in Figure 6-16, B and C. As expected, treatment of N2a cells with ethanol resulted in a statistically significant 18.27±1.35 fold increase in dead cells compared to control N2a cells ($p=0.0002$). In contrast, the ratio of dead cells was not significantly different in N2a cells overexpressing the three major apoE isoforms (1.35±0.15 for apoE2, 1.12±0.11 for apoE3 and 1.00±0.10 for apoE4, $p>0.05$). These data suggest that overexpression of full length apoE2, apoE3 and apoE4 does not confer

either toxicity or neuroprotection in N2a cells, consistent with observations from the MTT assay.

Representative FACs plots for live/dead cell populations of SH-SY5Y cells overexpressing apoE isoforms or treated with ethanol as a positive control are shown in Figure 6-17, A. Like for N2a cells, live SH-SY5Y cells (with blue fluorescence) are shown in Q4 whereas dead cells (with blue/red fluorescence) are in Q2. The ratio of dead cells (normalised to the control) is shown in the bar charts in Figure 6-17, B and C. Exposure of SH-SY5Y cells to ethanol also resulted in a significant increase of dead cells (17.38±2.30 fold-change, $p=0.002$). A reduction in the ratio of dead cells was observed for SH-SY5Y cells overexpressing apoE2 and apoE3, however this was only significant for the apoE2 isoform (0.62±0.05 apoE2, $p=0.0041$ and 0.81±0.04, $p=0.1420$). Moreover, the ratio of dead cells was similar between control SH-SY5Y cells and cells overexpressing apoE4 (1.001±0.08, $p>0.05$). A significant difference was also observed between apoE2- and apoE4- transfected SH-SY5Y cells ($p=0.0041$). These results are similar to those observed for the MTT assay, whereby apoE2 seems to mediate neuroprotection in SH-SY5Y cells. Although the neuroprotective effect of apoE3 observed in the MTT assay was not found here. Similarly, the apoE4 isoform did not induce toxicity, nor mediate neuroprotection.

Representative fluorescence microscopy images of primary neurons transduced with apoE2, apoE3 and apoE4 lentiviral vectors for 3 days are shown in Figure 6-18, A. The left panel shows total cells in culture (blue-fluorescence), the middle panel shows dead cells (red-fluorescence) and the right panel is a merge of both images. Statistical analysis of the ratio of dead primary neurons did not reveal any significant differences between conditions (Figure 6-18, B; 1.29±0.14 apoE2, 1.38±0.14 apoE3 and 1.33±0.12 apoE4; $p>0.05$), suggesting that overexpression of full length apoE2, apoE3 and apoE4 for 3 days in primary neurons does not affect cell survival under these conditions.

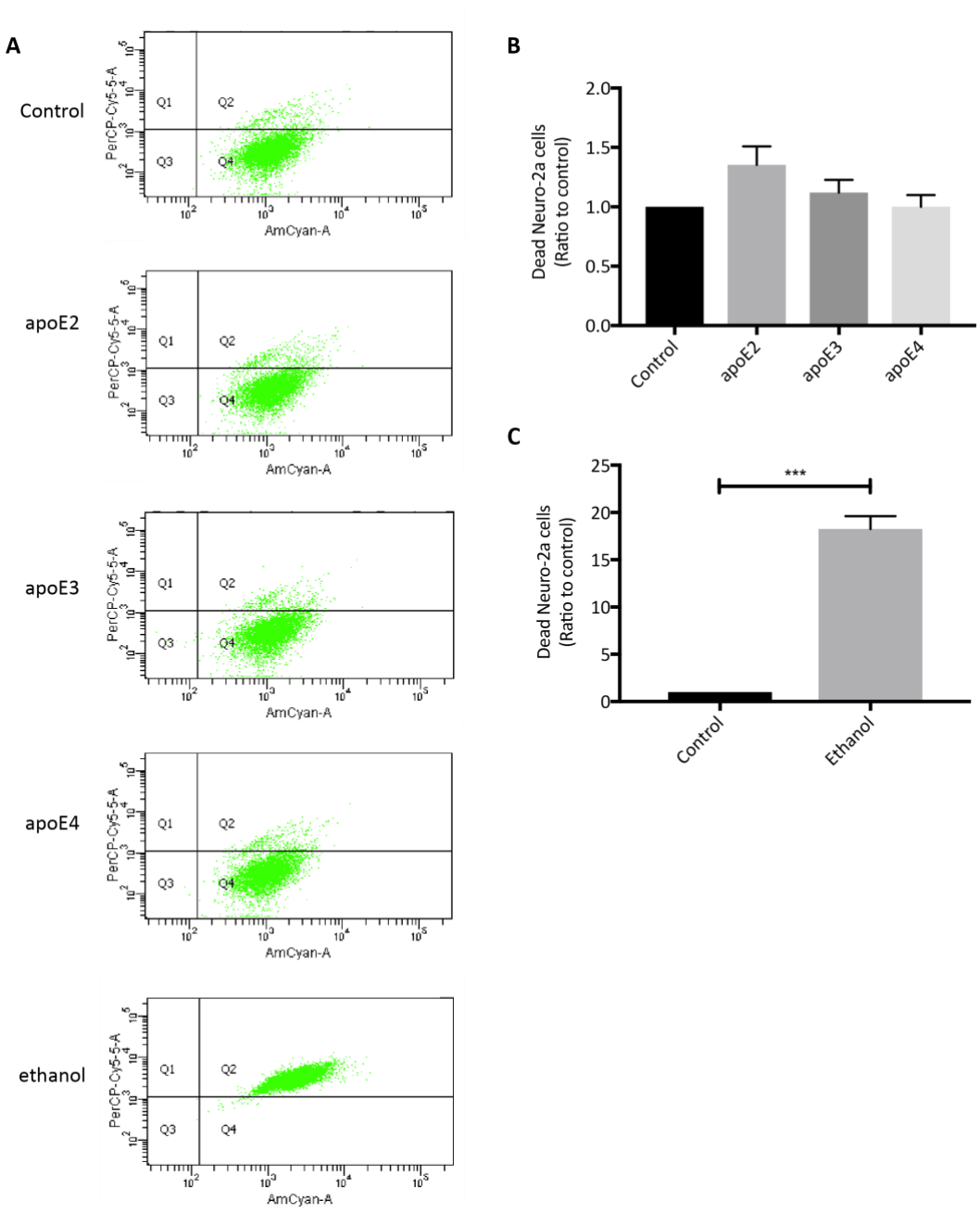

Figure 6-16 FACS analysis of live/dead cell populations of apoE-transfected N2a cells

(A) Representative FACS plots of live and dead cell populations in apoE-transfected or ethanol treated N2a cells, as based on blue fluorescense for live cells (AmCyan-A channel) and red fluorescence for dead cells (PerCP-Cy5-5-A channel). (B) Bar chart showing the ratio of dead cells for apoE-overexpressing N2a cells relative to control cells. The ratio of dead cells for each condition was not significantly different from control N2a cells. (C) Bar chart showing a significant increase in the ratio of dead N2a cells after ethanol treatment. Data are mean ±SEM, and differences were assessed using a one-way ANOVA followed by a Tukey's multiple comparisons test in (B) or a students T-test in (C), where $p<0.05$ is significant. n=3 per condition. ***$p<0.001$.

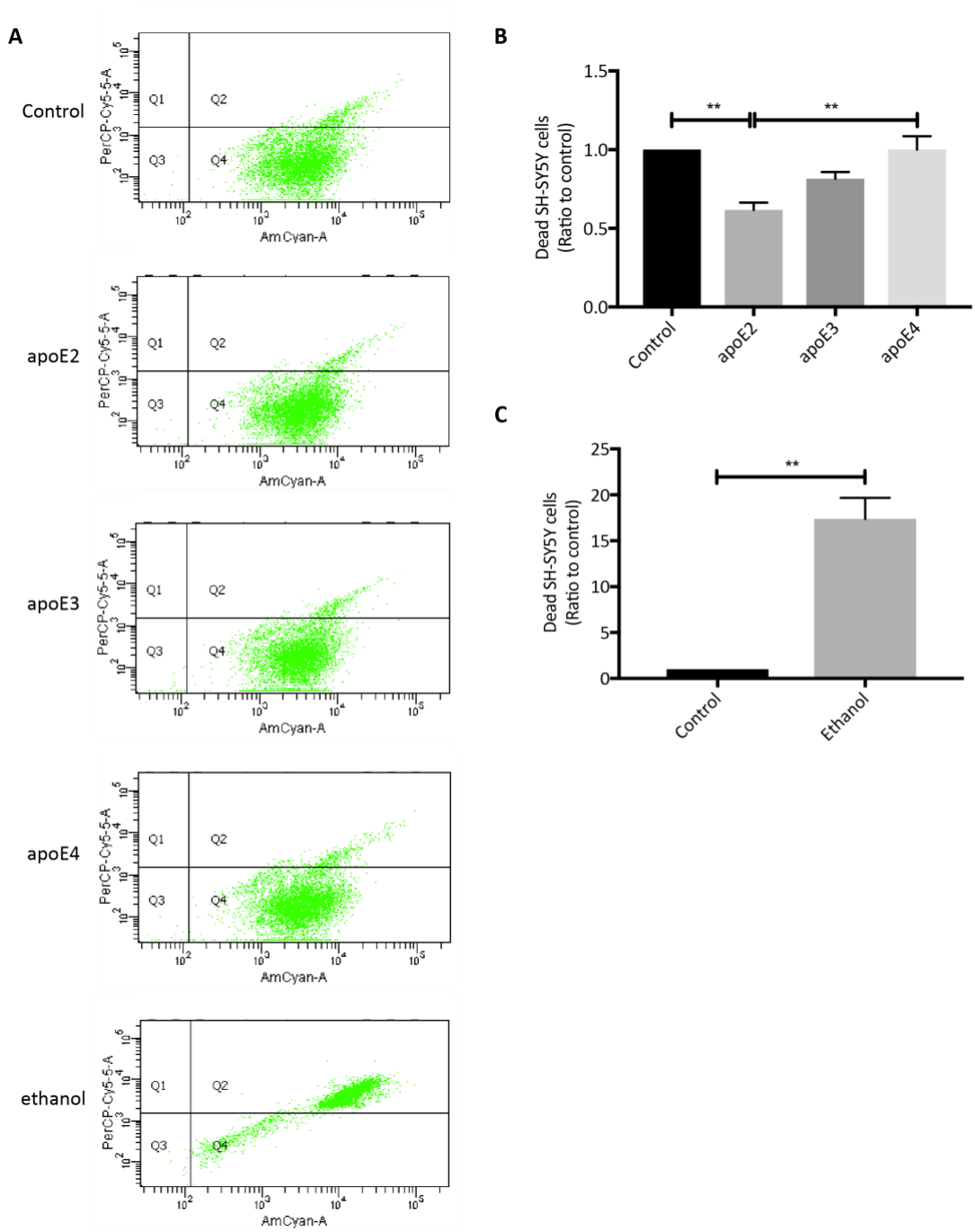

Figure 6-17 FACS analysis of live/dead cell populations of apoE-transfected SH-SY5Y cells

A) Representative FACS plots of live and dead cell populations in apoE-transfected or ethanol treated SH-SY5Y cells, as based on blue fluorescense for live cells (AmCyan-A channel) and red fluorescence for dead cells (PerCP-Cy5-5-A channel). (B) Bar chart showing the ratio of dead cells for apoE-overexpressing SH-SY5Y cells normalised to control cells. The ratio of dead apoE2-overexpressing SH-SY5Y cells was significantly lower compared to control SH-SY5Y cells and apoE4-overexpressing SH-SY5Y cells. In contrast, overexpression of apoE3 and apoE4 did not affect the ratio of dead SH-SY5Y cells compared to control SH-SY5Y cells. (C) Bar chart showing a significant increase in dead SH-SY5Y cells after ethanol treatment. Data are mean ±SEM, and differences were assessed using a one-way ANOVA followed by a Tukey's multiple comparisons test in (B) or a students T-test in (C), where $p<0.05$ is significant; n=3. **$p<0.01$.

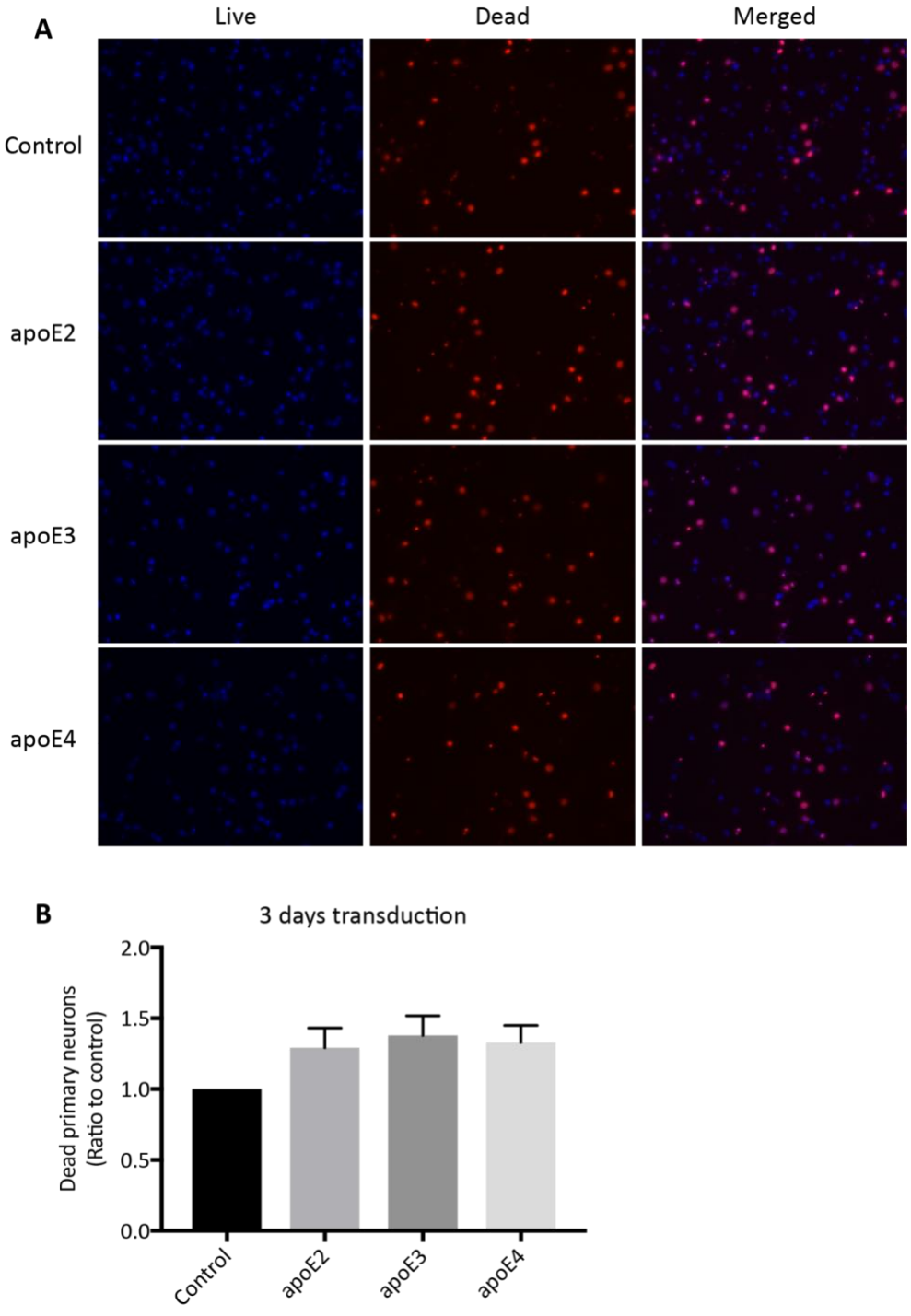

Figure 6-18 Fluorescence microscopy based quantitation of live/dead cell populations of primary neurons transduced with apoE lentiviral vectors for 3 days

(A) Representative fluorescence microscopy images of control neurons and apoE2-, apoE3- and apoE4-transduced neurons showing dead cells (red fluorescence) and total cells in culture (blue fluorescence). (B) Bar chart shows a small increase in neuronal death when cultures express either of the apoE isoforms, although this was not significant. Data are mean ±SEM, and differences were assessed using a one-way ANOVA followed by a Tukey's multiple comparisons test where $p<0.05$ is significant; n=3.

6.3 DISCUSSION

6.3.1 Subcellular distribution of apoE and insights into apoE function

The staining distribution of apoE was examined to determine whether N-terminally truncated apoE fragments generated in apoE-overexpressing N2a cells localised to the cytoplasm without full length apoE, and to see if apoE isoform influenced this. The immunolabelling data showed additional cytoplasmic staining for the C-terminal specific antibody, suggesting that apoE fragments with an intact C-terminus may indeed accumulate in the cytosol. However, these results should be treated with caution because this finding could also be a result of a weaker signal from the antibody specific to the N-terminus of apoE. Nevertheless, there is evidence in the literature to support accumulation of C-terminal apoE fragments in the cytosol. For instance, an electron microscopy study that used an antibody specific for lipid binding region within the C-terminus of apoE (3H1) revealed a cytoplasmic distribution of apoE in human cortical neurons from post-mortem AD brain tissue (Han et al., 1994a). Considering that some of these fragments may also contain the receptor binding region (135-150aa) that is thought to be required for fragment translocation (Chang et al., 2005), it is plausible that a portion of N-terminally truncated fragments that retain this region would translocate to the cytoplasm. Therefore, under the conditions used here, fragments of apoE appear to localise to the cytoplasm as posited in the proteolysis hypothesis, whereby they may affect cellular function. Interestingly, the staining of cytoplasmic apoE did not appear more pronounced for apoE2- or apoE4- transfected N2a cells despite western blotting showing isoform-specific differences in fragment load (apoE2>apoE4>apoE3). This could be attributed to the similar abundance of the major ~26kDa fragment for all three apoE variants, and because the varying load of low molecular weight fragments were less abundant. Nonetheless, the majority of C- and N-terminus specific staining appeared co-localised, suggesting that most of the staining is representative of either full length apoE or N-terminally truncated fragments of apoE that are within close proximity to full length apoE.

The distribution of intracellular apoE in apoE-transfected N2a cells is similar to observations of apoE staining in a variety of cells including primary human neurons,

HepG2 cells and N2a cells (Dekroon and Armati, 2001, Sabaretnam et al., 2009, DeMattos et al., 1999). Interestingly, the work here also showed that this pattern was similar for all three isoforms of apoE, suggesting that the distribution of neuronally expressed apoE and its fragments is not isoform-dependent under basal conditions. The immunolabelling for apoE was primarily concentrated in the perinuclear region, but diffuse and granular cytoplasmic staining and granular staining in the neurite extensions was also observed. It has been suggested that the perinuclear localisation of apoE in N2a cells is associated with the Golgi network (Chang et al., 2005). This is likely the case since studies have demonstrated co-localisation between perinuclear apoE and markers of the Golgi network in Hep2G cells and primary neuronal cultures (Sabaretnam et al., 2009, Dekroon and Armati, 2001). This is unsurprising though, since the Golgi apparatus is a site of major protein synthesis and modification. It is therefore likely that the intense staining within this region could be reflective of high protein overexpression within the Golgi network due to the use of a CMV promoter. Indeed, this region of apoE likely represents newly synthesised apoE protein since perinuclear staining for apoE was also detected by the N-terminus specific antibody that was shown by western blotting in the previous chapter to only detect full length apoE. An alternative hypothesis however, is that the granular perinuclear staining of apoE could be partially composed of dispersed protein aggregates. This hypothesis stems from similarities between the staining pattern of apoE to dispersed aggregates of a prion protein called CyPRP that is juxtanuclear in N2a cells (Grenier et al., 2006, Beaudoin et al., 2008). Further to this, N-terminal deletions of apoE have been shown to enhance the aggregation properties of the protein (Chou et al., 2005). Although this region shows co-localisation between the N- and C- terminus of apoE, immunofluorescence in conjunction with confocal microscopy does not provide sufficient resolution to distinguish between full length apoE and C-terminal fragments that are in close proximity. Hence, future investigation into whether this region of apoE accumulation does indeed contain small aggregates of C-terminal fragments is warranted. On the other hand, the punctate staining pattern of apoE in N2a cells has also been suggested to be vesicle-bound apoE in the secretory pathway (DeMattos et al., 1999), which is also likely here since the apoE secretory signalling peptide sequence was included in the apoE-overexpression plasmids. The localisation of

apoE in neurites of N2a cells was an interesting observation as studies have shown that both exogenous application or expression of apoE can affect neurite outgrowth (Nathan et al., 1995, Bellosta et al., 1995). Hence, it is conceivable that apoE localised to neurites may contribute to this effect.

Notably, other techniques that provide greater resolution could be used in future work to acquire more information on the subcellular localisation of full length apoE and fragments. For instance, double-label immunoelectron microscopy of apoE-overexpressing cells could be used. In this technique, antibodies to the N- and C-terminus of apoE could be detected by secondary antibodies conjugated to colloidal gold nanoparticles of different diameter (Hagiwara et al., 2010). Under the scenario where C-terminal fragments are recognised by smaller sized gold nanoparticles, subcellular localisation of the smaller electron-dense spots would reveal more precisely which compartments the C-terminal apoE fragments distribute to. In addition, subcellular fractionation of protein lysate from apoE-overexpressing cells and western blotting using a panel of terminal specific anti-apoE antibodies could also be used. This approach could facilitate identifying the localisation of specific fragments in a range of subcellular compartments, such as cytosolic, membrane bound and nuclear compartments (Baghirova et al., 2015). Further work using such methodologies to explore which intracellular compartments apoE localises to could prove informative in elucidating the cellular functions of full length apoE and apoE fragments in neurons.

6.3.2 Does neuronal expression of apoE affect organisation of endogenous p-Tau?

Whilst the western blotting data in the previous chapter showed that the physiological proteolysis of apoE2, apoE3 and apoE4 results in substantial fragment load, the immunofluorescence data here indicated that N-terminally truncated fragments of apoE may accumulate in the cytosol. Hence, it was plausible that the cytosolic apoE fragments may mediate deregulation of tau and promote cytoskeletal dysfunction as suggested in the apoE proteolysis model (Mahley and Huang, 2012). However, although it has been shown in an earlier study that expression of full length apoE4 and C-terminally apoE4 (1-272aa) can affect the regulation and organisation of tau in N2a cells (Huang et al., 2001),

the data presented in this chapter did not support a direct association between apoE and pThr181-Tau staining in N2a cells. Strong pThr181-Tau staining and tangle-like structures were observed in control N2a cells, which was surprising since this suggested that the basal levels of pThr181-Tau that are incorporated into perceived NFT like structures were high in this cell line. Moreover, staining for apoE and pThr181-Tau did not reveal any co-localisation in apoE-transfected N2a cells, irrespective of apoE isoform, which initially appeared to conflict with the proposed apoE proteolysis model. However, it is notable that in the study by Huang et al., full length apoE4 co-localised with tau 'tangles' in only a small percentage (~2.7%) of N2a cells, whilst apoE3 did not associate with tau at all (Huang et al., 2001). It is also noteworthy that a later independent study found that expression of GFP-tagged full length apoE4 (lacking the signalling peptide) did not induce intracellular apoE-inclusions in N2a cells at all (Ljungberg et al., 2002), which is in accordance with the observations here. Hence there is little evidence to support that expression and physiological proteolysis of full length apoE in N2a cells leads to apoE/p-Tau inclusion formation. Considering this, the lack of association between the three isoforms of apoE and pThr181-Tau observed here is not entirely unexpected. Furthermore, it was a C-terminally truncated form of apoE (1-272aa) that significantly induced and co-localised with p-Tau inclusions in N2a cells (Huang et al., 2001). However, in the previous chapter it was revealed that the proteolytic fragments of apoE2, apoE3 and apoE4 in all three cell models were N-terminally truncated fragments with intact C-termini. This confirms that the 1-272aa apoE fragment that induces and co-distributes with p-Tau inclusions in the Huang et al. study is not produced in the cell models overexpressing apoE here, and is thus one likely explanation for the lack of association between apoE and pThr181-Tau staining in the apoE-transfected N2a cells. This data also indicates that N-terminally truncated apoE fragments do not lead to the formation of apoE-containing tangle-like structures in N2a cells.

Intriguingly, pThr181-Tau staining frequently appeared to partially surround the intense perinuclear staining of apoE in transfected N2a cells, for all apoE isoforms, indicating a structural rearrangement of pThr181-Tau. Although p-Tau has not been implicated in

the protective response to aggresome formation, this staining pattern is similar to the juxtanuclear cage-like staining of cytoskeletal proteins such as vimentin that encase aggresomes in cells (Johnston et al., 1998, Beaudoin et al., 2008). This supports the intriguing possibility that apoE may exist as small aggregates within this region. This hypothesis could be investigated in future work by immunostaining apoE-transfected N2a cells with antibodies specific to apoE and aggresome markers such as vimentin and γ-tubulin.

6.3.3 Does neuronal expression of apoE affect regulation of endogenous p-Tau?

To further investigate whether apoE expression in neurons affects the phosphorylation of tau as reported in the literature, the levels of pThr181-Tau were examined by western blotting analysis. Surprisingly, pThr181-Tau and total tau protein were barely detectable in both control and apoE-overexpressing N2a and SH-SY5Y cells, suggesting that these cell lines may express very low levels of endogenous tau protein. A search in the literature revealed similar reports of very low levels of endogenous tau in both SH-SY5Y cells and N2a cells in studies using either immunofluorescence or western blotting techniques (Biernat et al., 2002, Bretteville et al., 2012, Khlistunova et al., 2006, Ljungberg et al., 2002). This appeared to be the case for a variety of total tau and p-Tau specific antibodies including the anti- pThr181-Tau AT270 antibody (Bretteville et al., 2012), which is consistent with the western blotting data for N2a and SH-SY5Y cells presented in this chapter. Furthermore, intense HMW bands were detected by the pThr181-Tau antibody in both cell lines, but not by the total tau antibodies used, indicating that they are likely nonspecific. This observation raised the possibility that the immunofluorescence staining in N2a cells may not be specific to pThr181-Tau. Intriguingly, it was reported by Ljungberg and colleagues that the tangle-like structures formed by overexpression of apoE4 1-272aa, but also by C-terminally truncated fragments of apoE2 and apoE3 in N2a cells, do not contain tau but instead neurofilament protein (Ljungberg et al., 2002). In this earlier study, immunolabelling using a different antibody specific for tau (DAKO) showed that overexpressed tau does not co-localise with apoE-containing tangle-like structures in N2a cells overexpressing the C-terminally truncated apoE fragments. In view of these findings and that the anti-

pThr181-Tau antibody revealed intense staining in control cells, it was considered that that the anti- pThr181-Tau antibody may not specific for tau in N2a cells. Nonetheless, these data imply that neuroblastoma cells may express low levels of tau or have lower basal levels of tau phosphorylated at a variety of sites including the Thr181 site, which was probed for here. Because of this, it was not possible to assess the effect of apoE overexpression on pThr181-Tau or total tau levels in the WT neuroblastoma cells under the conditions used here. Therefore, co-expressing human tau with apoE should be considered in future work exploring the effect of apoE expression on tau in the N2a and SH-SY5Y cell models. On the other hand, pThr181-Tau and pan tau were detected on western blots of primary neuron extracts at levels that were quantifiable. The levels of ~52kDa pThr181-Tau were significantly increased in an isoform-dependent manner (apoE4>apoE3, apoE2 similar to control) in primary neurons. This suggests that neuronal expression of apoE4 and apoE3 to a lesser extent, may induce phosphorylation of tau at the Thr181 site. This finding is in accordance with *in vivo* studies that show apoE expression is associated with increased levels of p-Tau in an isoform-dependent manner (apoE4>apoE3) (Liraz et al., 2013, Brecht et al., 2004b). Overexpression of apoE2 in primary neurons however, did not affect pThr181-Tau levels, showing for the first time that apoE2 overexpression in neuronal cultures is not associated with increased phosphorylation of tau at this site. This finding also further supports the notion that apoE2 does not exert a toxic gain of function in neurons. In addition, overexpression of the three major apoE isoforms did not significantly increase the levels of total tau, confirming that the increases in pThr181-Tau levels in apoE3- and apoE4- overexpressing neurons is due to increased phosphate content at Thr181 and not total tau levels. Although the evidence here indicates that neuronal expression of apoE may affect the regulation of tau phosphorylation at the Thr181Pro motif, the functional implications of this are not so clear. This is because regulation of tau function is a complex process that involves a vast array of post translational modifications that includes, for example: phosphorylation, glycosylation, glycation, oxidation and proteolysis (truncation) (Mietelska-Porowska et al., 2014). Nevertheless, phosphorylation of tau at sites shown to be affected in AD such as Thr181, are thought to decrease its affinity for microtubules and subsequently, reduce microtubule polymerisation and stabilisation (Alonso et al.,

1994, Li et al., 2007). Hence increased phosphorylation of tau by apoE expression in neurons, which is supported by the data presented here, could contribute to microtubule dysfunction as posited in the apoE proteolysis model (Mahley and Huang, 2012). Indeed, studies have also shown that application and expression of apoE can affect microtubule organisation and neurite outgrowth *in vitro* (Nathan et al., 1995, Bellosta et al., 1995). Furthermore, transgenic mice expressing human apoE in neurons of the CNS display tau hyperphosphorylation and prominent axonal defects that are thought to be associated with cytoskeletal dysfunction (Tesseur et al., 2000a, Tesseur et al., 2000b). However, although the Thr181 phospho-epitope is associated with AD, increased pThr181-Tau levels do not necessarily indicate that tau is pathological in this cell model under the conditions used. Indeed, ablation of phosphorylation sites in a drosophila model revealed that there is not a single essential phosphorylation site for neurodegeneration, suggesting instead that alterations at multiple sites are required for tau pathology (Steinhilb et al., 2007). This highlights the need for further study of how other phospho-epitopes of tau are affected in neuronal cell models expressing the three major apoE isoforms. Nevertheless, the data here supports a role for apoE in the regulation of tau and shows that apoE-transduced primary neurons can be used to investigate the relationship between apoE and p-Tau. Therefore, apoE-transduced primary neurons appear to be a suitable model to explore which other phospho-epitopes of tau are affected by apoE expression, the mechanisms underlying apoE-induced phosphorylation of tau and for investigation into the functional implications related to this.

How apoE overexpression affects tau phosphorylation was also addressed in this chapter. The phosphorylation status of tau involves a careful balance between kinase and phosphatase activity, and either could be affected in apoE3- and apoE4- overexpressing primary neurons. Here, the activity state of a candidate tau kinase GSK3 was examined because this kinase targets the Thr181 site of tau amongst others, and changes in its kinase activity have been strongly implicated in AD pathology (Sperber et al., 1995, Hooper et al., 2008). The data revealed similar levels of inactive GSK3 in control primary neurons and apoE-overexpressing neurons, suggesting that the increase in pThr181-Tau

levels is not due to alleviating the inhibition of GSK3 activity. In agreement with this finding, an earlier *in vivo* study similarly showed that inactive GSK3 levels were also unaffected by neuronal expression of human apoE in transgenic rodent models (Harris et al., 2004). It is notable though that some studies have demonstrated apoE-mediated alterations in GSK3 signalling in neuroblastoma cells and primary neuronal cultures (Cedazo-Mínguez et al., 2003, Hoe et al., 2006). One possible explanation for these differences is that recombinant apoE was exogenously applied to cultured cells in these experiments, and so the changes in GSK signalling were likely receptor mediated. This contrasts to the approach used in the work here, whereby apoE was overexpressed in the three cell models by use of either lentiviral vector transduction or transfection techniques. Although secretion of apoE in the cell models is likely, the levels secreted into the medium may be insufficient to induce significant alterations in receptor mediated signalling that affect GSK3 activity. Indeed, Hoe et al demonstrated that inhibition of GSK3 signalling in primary neurons by application of recombinant apoE occurred only at concentrations higher than physiological levels (Hoe et al., 2006), supporting this notion and the lack of effect on GSK activity status here. Taken together, these data suggest that the increased pThr181-Tau levels in primary neurons likely occurs through alternative mechanisms that may include increased activity of other kinases or reduced phosphatase activity. In fact, there is evidence to suggest that recombinant apoE does affect other tau-associated kinases (Hoe et al., 2005, Hoe et al., 2006), however whether neuronal apoE expression mediates similar effects is currently not known and could be explored in further work. Furthermore, a recent study showed a reduction in the active form of PP2A, a key tau phosphatase, that was associated with apoE expression (apoE4>apoE3) in a glioblastoma cell line (Theendakara et al., 2017). In consideration of this, it is possible that the increase in pThr181-Tau levels in apoE3- and apoE4- overexpressing neurons could be contributed to by apoE-mediated downregulation of PP2A activity, which warrants further investigation. It was also considered that the differential effects of apoE isoforms on tau phosphorylation in the primary neuronal model may be associated with their affinity for binding to tau. Indeed, *in vitro* experiments have shown that the greater binding between apoE3 and tau is associated with reduced tau phosphorylation compared to apoE4, which has been

proposed to occur due to structural protection from kinase action (Strittmatter et al., 1994a, Strittmatter et al., 1994b). However, since levels of pThr181-Tau in apoE3 overexpressing neurons were greater than levels in control neurons, it is unlikely that a tau-apoE interaction underlies this increase because on this basis, apoE3 overexpression should prevent tau phosphorylation. Although the levels of endogenous tau were barely detectable by western blotting in the neuroblastoma cell lines, the levels of inactive GSK3 were examined in these cell models. The levels of inactive GSK3 were not significantly altered in the SH-SY5Y cell line when either of the apoE isoforms were overexpressed, which is consistent with that observed in the primary neurons. However, the data unexpectedly revealed a significant reduction in inactive GSK3 levels in apoE3- and apoE4- overexpressing N2a cells, which is indicative of an increase in GSK3 activity and suggests that apoE-mediated effects on GSK3-related cell signalling may be cell-dependent. On this basis, one would expect to observe significant increases in the levels of tau phosphorylated at epitopes targeted by GSK3 in N2a cells. This could be explored in future experiments by co-expressing human apoE and human tau in N2a cells and performing western blotting analysis using antibodies specific to tau phospho-epitopes targeted by GSK3. As for how these cell-dependent differences arise is uncertain, but they could involve differences in the levels of apoE-related receptors at the cell surface of N2a cells compared to the other cell models. Furthermore, it is also possible that modifications of apoE protein in N2a cells may differ to the other cell models as discussed in the previous chapter as a possible reason for cell-dependent variations in apoE processing, which could alter the functions of apoE. Because of this, it would also be interesting to investigate whether there are cell-specific modifications of apoE in future experiments.

6.3.4 A possible relationship between neuronal expression of apoE and vimentin

Although expression of apoE and vimentin has been observed in neurons that are stressed or injured and has been proposed to occur as part of the neuronal repair response mechanism (Boschert et al., 1999, Xu et al., 2006b, Xu et al., 2008, Levin et al., 2009), it was not known whether the expression of these two proteins were linked. The data in Figure 6-14 show for the first time that expression of apoE is associated with increased expression of vimentin in primary neuronal cultures, suggesting that neuronal

apoE expression may act as a trigger for re-expression of vimentin to contribute to neuronal repair. However, the data also showed that the effect of apoE on vimentin expression was isoform dependent whereby increased vimentin levels occurred in the order of apoE2>apoE4, whilst apoE3 had no effect. This is puzzling when considering that apoE2 is thought to confer neuroprotection whilst apoE4 is associated with toxicity. One possible explanation for the differential effect on vimentin by apoE stems from another aspect of the apoE proteolysis model where apoE4 increases the risk for AD due to a loss of protective function compared to the other two variants. On this basis, one would expect to see a greater protective response in the order of apoE2>apoE3>apoE4, which is partially supported by the data here when considering vimentin expression as an indicator of protective response. However, apoE3 did not affect vimentin levels in primary neurons, which could suggest that this variant plays a more neutral role. Nonetheless, the data here reveal a relationship between apoE and vimentin expression. It also suggests a new potential role for apoE in affecting the IF network and modulating the neuronal repair response, two hypotheses which warrant further investigation.

The data also showed that the effect of neuronal apoE expression on vimentin levels is dependent on the cell model used. Whilst the data showed increased vimentin levels in apoE2- and apoE4- overexpressing primary neurons, no differences were observed in SH-SY5Y cells. One possible explanation for this is that the regulation of vimentin expression between these cell models is likely different since the SH-SY5Y cell line is a proliferating neuroblastoma cell, whereas the 18-21DIV primary neuronal model likely contains relatively mature post-mitotic neurons (Sapoznik et al., 2006). Evidence for this proposal comes from studies which have shown that vimentin is readily expressed in neuronal precursors to initiate neuritogenesis (Shea, 1990, Boyne et al., 1996, Levin et al., 2009), but is then downregulated when neurons are mature (Cochard and Paulin, 1984), thus indicating that differentiation status plays a key part in the regulation of vimentin expression. Therefore, this data indicates that a mature neuronal model may be required to explore the role of apoE on vimentin expression, and possibly other components of the IF network.

6.3.5 Is neuronal expression of apoE neurotoxic or neuroprotective?

The three major isoforms of apoE have been associated with different effects on neuronal viability such that apoE2 is thought to be neuroprotective, apoE3 neutral or a little protective and apoE4 neurotoxic. Whilst it has been proposed that neuron-specific proteolysis of apoE4 contributes to a toxic gain and loss of protective function, this was not reflected in the data from the viability (section 6.2.4) or cell death assay (section 6.2.5). Overexpression of apoE4 in all three cell models did not significantly reduce cell viability or increase the number of apoptotic cells, suggesting that overexpression and proteolysis of apoE4 in neurons does not induce toxicity under physiological conditions. These data are surprising because apoE4 fragments are thought to promote toxicity, partly through cytoskeletal and mitochondrial dysfunction, yet the apoE4 fragments generated *in vitro* here did not appear to induce significant toxicity. An important question arises from this data: if fragments are generated *in vitro*, why was toxicity not observed here? It is notable that many of the *in vitro* studies of apoE-related neurotoxicity supporting this working model are based on overexpression of C-terminally truncated apoE4 (Chang et al., 2005), or application of full length/truncated apoE4 in cell cultures (Marques et al., 1996, Tolar et al., 1999, Veinbergs et al., 2002, Persson et al., 2017). Hence, these studies do not directly test whether neuronal apoE4 expression and the physiological generation of apoE4 fragments leads to a toxic gain of function. Whilst conclusive evidence for the existence of such fragments remains to be seen in the literature, the data from the previous chapter showed that apoE may be N-terminally cleaved instead. Therefore, the results from the published *in vitro* studies may not be an accurate representation of the role of neuronal apoE4 and fragments *in vivo*. Interestingly, the only study in the literature that tested whether overexpression of full length apoE4 affects neuronal viability showed that MTT reduction was not significantly affected in N2a cells (Chang et al., 2005), supporting the data presented here. In consideration of the hypothesised protective function of apoE expression in neurons and that the majority of apoE protein observed by western blotting is full length (see previous chapter), it is possible that full length apoE4 may act antagonistically to neurotoxic apoE4 fragments (if any). In support of this, application of full length apoE4 was shown to confer protection against toxicity induced by a dimeric peptide (141-

149aa) of apoE4 in embryonic chick sympathetic neurons, in a concentration dependent manner. To test this hypothesis, future work could compare the effect of overexpressing N-terminally truncated apoE4 fragments with and without full length apoE4 on neuronal viability and survival. Another possibility is that the cellular environment may influence whether apoE expression is toxic. For instance, pH levels have been shown to affect the structure and aggregation properties of apoE (Garai et al., 2011), raising the possibility that changes in cellular environment (such as pH levels) could also influence the structural and functional properties of intraneuronal apoE. In support of the hypothesis that apoE4 has differential effects relating to cellular state, a recent study showed that application of apoE4 to N2a-APP cells only promoted apoptosis when N2a-APP cells were injured by application of ethanol (Li and Cheng, 2018). Considering that apoE expression is reported to occur in neurons following a form of injury such as from oxidative stress, this may be a key factor to include in future *in vitro* studies exploring the role of intraneuronal apoE in AD. Nonetheless, there is also *in vivo* data showing that expression of apoE4 in CNS neurons of transgenic mice is associated with enhanced neurodegeneration with and without excitotoxic triggers (Buttini et al., 2010, Zhang et al., 2012, Raber et al., 1998, Tesseur et al., 2000a). One explanation for why apoE4 has this effect *in vivo* is that these rodents are ageing, and so can accumulate cellular stress over time in a manner that could alter the properties of apoE4 as described above. Indeed, cognitive deficits and markers of neurodegeneration associated with apoE4 expression in neurons has been shown to increase with age in NSE-apoE4 mice, but not in NSE-apoE3 and wild-type mice (Buttini et al., 1999, Raber et al., 1998). Overexpression of full length apoE3 did not affect cell viability or survival in any of the three cell models used, which is in accordance with independently published data showing that apoE3 overexpression does not affect N2a cell viability (DeMattos et al., 1999). This result supports the notion that apoE3 expression has a more neutral/ slightly protective effect in neurons, although whether this is the case under conditions of cellular stress *in vitro* remains to be confirmed. Overall, the findings discussed here highlight that additional work should be carried out to determine whether different forms of cellular stress/damage (e.g. oxidative, genotoxic and proteotoxic stress) affect

apoE processing and function in neuronal cell models, and to explore how this affects neuronal viability and survival.

Intriguingly, both the MTT and cell death assays revealed an increase in SH-SY5Y cell viability and survival when apoE2 was overexpressed, which is the first direct *in vitro* evidence to support the hypothesis that this isoform is neuroprotective. It is notable though that apoE2 also displayed the greatest fragmentation load in the SH-SY5Y cell line, suggesting that the load of fragments may not necessarily be the major factor for apoE-related toxicity. This finding also supports the hypothesis that the fragments generated from each isoform may differ structurally and so have different effects, which in this case, may confer neuroprotective properties, although this remains to be confirmed. As for why a neuroprotective effect was observed only in SH-SY5Y cells could be attributed to it being a human neuroblastoma cell line, indicating that it may be important for human protein orthologues to be present to study the protective role of human apoE2 and to determine interacting partners of this isoform. Furthermore, this cell-dependent observation suggests that the neuroprotective effect of apoE2 may go beyond its reported role in ameliorating oxidative stress such as through its antioxidant activity and ability to bind the toxic lipid peroxidation product, 4-hydroxynonenal (HNE) (Miyata and Smith, 1996, Pedersen et al., 2000). In view of this finding, it would be of interest to validate the neuroprotective effect of apoE2 in another cell model such as iPSC-derived neurons. Further work could also involve investigating the molecular mechanisms underpinning the neuroprotective properties of apoE2.

6.3.6 Conclusion

Although there was no conclusive evidence to support that apoE induces the formation of tangle-like structures containing apoE and p-Tau, the data showed that apoE expression and proteolysis in primary neurons was associated with increased tau phosphorylation at Thr181 in an isoform-dependent manner (apoE4>apoE3), which is consistent with published studies. The work here is also the first to show that overexpression of apoE2 in primary neuronal cultures does not promote tau phosphorylation at Thr181, supporting the hypothesis that apoE2 does not deregulate tau and induce cytoskeletal dysfunction. A novel isoform-specific effect of apoE

expression (apoE2>apoE4, no effect for apoE3) on the upregulation of vimentin was also observed in primary neurons, indicating that neuronal apoE expression may affect the IF network and modulate the repair response of injured or stressed neurons. Surprisingly, none of the isoforms were found to be toxic to neurons despite evidence supporting the cytosolic localisation of N-terminally truncated fragments and increased levels of pThr181-Tau. Therefore, these findings indicate that the cytosolic localisation of fragments and the increased phosphorylation at the Thr181 site of tau does not necessarily confer toxicity. Moreover, these data suggest that conditions of cellular stress may be required to model the toxic gain of function associated with apoE4 expression and proteolysis, since the physiological generation of fragments was not sufficient to induce toxicity. Remarkably though, the data presented here show for the first time that expression of apoE2 is neuroprotective in human neuroblastoma cells. Whilst the protective mechanisms are unknown, this result reveals that a human neuronal model, such as SH-SY5Y cells, may be more suitable for elucidating the protective functions of neuronally expressed apoE2 in AD. This data also indicates that the trigger of apoE2 expression after injury or stress in human neurons may contribute to decreased risk for AD. Collectively, the data demonstrate that the effects of apoE on neuronal function and viability are isoform-dependent, and support the hypothesis that this is likely due to either structural differences in the full length protein and/or the fragments generated.

Chapter 7 FINAL DISCUSSION

7.1 Project 1: Role of Aß42 and VPA in SnpI regulation

Extensive research has revealed that Aß42 oligomers contribute to synaptic dysfunction during the early stages of AD, partly through deregulating SV dynamics and thus neurotransmitter release (Kelly and Ferreira, 2007, Parodi et al., 2010, Russell et al., 2012, Park et al., 2013, Park et al., 2017, Park and Chang, 2018). Therefore, the work presented in chapter 3 was carried out to investigate the molecular basis of Aß42-mediated disruption to SV dynamics and synaptic function by determining whether Aß42 oligomers deregulate SnpI, a key SV-associated protein. The data confirmed that Aß42 does indeed deregulate SnpI by promoting sustained phosphorylation of SnpI at Ser9, an effect which has since been replicated in recent studies (Park et al., 2017, Park and Chang, 2018). Because the data also suggested that the phosphatase activity of PP2A was unaffected by Aß42 oligomers, the deregulation of SnpI was hypothesised to occur through maintained CAMKIV kinase activity instead. This hypothesis has been confirmed in later independent studies demonstrating that Aß42 oligomers induce autonomous CAMKIV activity (Park et al., 2017, Park and Chang, 2018). In addition, Park and co-workers showed that the autonomous CAMKIV activity was due to Aß42 oligomers triggering an increase in cytosolic calcium through extracellular calcium influx and calcium release from mitochondria. Interestingly, it was also shown that Aß42-mediated calcium release from mitochondria alone was sufficient to induce sustained phosphorylation of SnpI at Ser9 (Park and Chang, 2018). Importantly, this finding highlights a molecular mechanism that may partly underlie the deleterious effects of intraneuronal Aß42 oligomers on SV-associated proteins that are regulated by calcium-signalling like SnpI, and thus SV dynamics and synaptic function.

Since phosphorylation of SnpI at Ser9 has been suggested to modulate the availability of SVs to participate in neurotransmitter release via reversible tethering and clustering of SVs from the recycling pool to the reserve pool (Hosaka et al., 1999, Fiumara et al., 2004, Ceccaldi et al., 1995, Bloom et al., 2003), it was hypothesised that the maintained phosphorylation of SnpI induced by Aß42 oligomers could contribute to the deregulation of SV dynamics. Indeed, dissociation of SnpI from SVs due to phosphorylation at Ser9

could increase the availability of SVs for neurotransmitter release during the early stages of Aß42-mediated synaptic dysfunction and thus contribute to the reported increased release probability of SVs and aberrant neurotransmitter release triggered by Aß oligomers *in vitro* (Parodi et al., 2010, Puzzo et al., 2008, Russell et al., 2012). On the other hand, prolonged phosphorylation of SnpI at Ser9 by autonomous CAMKIV activity could contribute to defective SV recycling and lead to SV pool depletion as reported in the literature (Williams and Bate, 2016, Kelly and Ferreira, 2007, Parodi et al., 2010). However, these hypotheses remain to be confirmed. Nevertheless, two recent studies have demonstrated by using a quantum dot-based single-SV tracking assay and fluorescence recovery after photobleaching (FRAP) experiments, that the maintained phosphorylation of SnpI at Ser9 by CAMKIV autonomous kinase activity inhibits intersynaptic vesicle trafficking in Aß42-exposed cultured rat hippocampal neurons (Park et al., 2017, Park and Chang, 2018). In these studies, overexpression of a phospho-deficient mutant of SnpI or using an inhibitor of CAMKK, blocked the inhibition of intersynaptic vesicle trafficking, confirming that phosphorylation of SnpI at Ser9 has a direct effect on the lateral sharing of SVs between neighbouring synapses. Interestingly, inhibition of CAMKK signalling was also shown to block the inhibitory effect of Aß42 oligomers on chemically induced LTP in rat hippocampal cultures (Park et al., 2017). In view of these findings, Park and co-workers proposed that phosphorylation of Snp at Ser9 and subsequently inhibition of intersynaptic vesicle trafficking mediated by Aß42 oligomers may partly contribute to the Aß42-induced defects in synaptic plasticity (Park et al., 2017). Taken together, these studies support the hypothesis that the deregulation of SnpI phosphorylation at Ser9 could have a substantial impact on SV dynamics and as a result, may contribute to synaptic dysfunction in AD. It is therefore reasonable to suggest that SnpI may be a suitable candidate target for therapeutic intervention in AD. However, it is notable that Aß42 oligomers have also been reported to directly interact with proteins involved in SV docking and fusion and therefore neurotransmitter release, such as synaptophysin (Russell et al., 2012) and syntaxin Ia (Yang et al., 2015). In addition, Aß42 oligomers have been shown to indirectly affect proteins involved in endocytosis, such as dynamin I, through interfering with signalling mechanisms (Kelly et al., 2005, Kelly and Ferreira, 2006a, Kelly and Ferreira, 2007). It is therefore likely that

the mechanisms underpinning the effect of Aß42 oligomers on synaptic function involve an additive disruption to multiple aspects of SV dynamics through affecting several key SV-associated proteins that regulate this process. Hence future studies are needed to improve our understanding of the temporal effects of Aß42 oligomers on SV dynamics and presynaptic function so that an effective therapeutic treatment can be found for the early stages of AD. One such therapeutic treatment could involve the use of VPA, a compound that has been shown to have therapeutic benefit in transgenic AD mouse models (Qing et al., 2008, Hu et al., 2011b, Noh and Seo, 2014) and to prevent Aß42-induced reduction in SV recycling (Williams and Bate, 2016). Although the molecular basis of the protective effect of VPA on SV recycling is still not fully understood, the work presented in chapter 3 showed for the first time that VPA could abolish the sustained phosphorylation of SnpI at Ser9 in Aß42-exposed cultured hippocampal neurons. This prompted the hypothesis that the molecular mechanisms underpinning the protective role of VPA may involve attenuating the disruptive effect of Aß42 oligomers on SnpI regulation and subsequently SV dynamics. It is also possible that VPA may disrupt other SV-associated proteins, although this remains to be tested. Interestingly, VPA has been reported to suppress Aß-induced elevations of intracellular calcium in cultured rat hippocampal neurons (Mark et al., 1995). Hence it is possible that this compound could attenuate the disruptive effect of Aß oligomers on SV-associated proteins by blocking Aß oligomers from altering calcium signalling. VPA has also been shown to inhibit cyclin-dependent kinase 5 (Cdk5) (Hu et al., 2011a), an important kinase that has numerous presynaptic substrates, including SnpI (Matsubara et al., 1996) and dynamin I (Tan et al., 2003), and has been shown to regulate SV endocytosis (Tan et al., 2003, Tomizawa et al., 2003, Nguyen and Bibb, 2003) and the release of SVs from the resting pool to participate in neurotransmitter release (Kim and Ryan, 2010, Verstegen et al., 2014). It is therefore likely that VPA affects multiple aspects of SV dynamics, raising the need to further explore the effect of VPA on SV-associated proteins and the SV life cycle to evaluate its use as a therapeutic treatment to combat synaptic dysfunction in the early stages of AD.

7.2 Project 2: Role of apoE isoform on apoE processing and function in neurons

In this thesis, the role of apoE expression and proteolysis on neuronal function and viability was assessed for the three major isoforms of apoE (apoE2, apoE3 and apoE4) in an effort to understand their differential effects on the risk for AD. Although the expression and proteolysis of apoE4 in neurons has been proposed to result in a toxic gain of function and thus increase the risk for AD (Huang et al., 2004, Mahley et al., 2006, Mahley and Huang, 2012), the impact of proteolysis on the role of the 'protective' apoE2 isoform in neurons has been largely understudied. To address this, the three major apoE isoforms were expressed in neuronal cell models so that the fragmentation (profile, load and composition of fragments) of each isoform could be characterised and their effect on cytoskeletal-associated proteins and neuronal viability could be assessed. Together, these data also enabled an assessment of the relationship between the fragmentation of each isoform and their effects on neurons, as discussed here.

Importantly, the data in this thesis show for the first time, a comprehensive analysis of the fragmentation of apoE2 when expressed in neuronal cell models. Examination of the fragmentation profile for each apoE isoform *in vitro* did not reveal any unique apoE fragments. This indicates that the differential effects that these isoforms have on neuronal function may instead be due to differences in the levels of fragments generated, and/or the structure of fragments (containing SNPs) and the full length protein. Indeed, the proteolytic susceptibility of apoE was shown to be isoform-dependent, but surprisingly, also cell-dependent. The proteolytic susceptibility of each isoform in primary neurons followed the order of apoE4>apoE3>apoE2, consistent with the proposed proteolysis model that posits that apoE4 is more susceptible to proteolytic cleavage due to a stronger domain interaction that is induced by the presence of Arg112. It is notable that this work provides the first direct evidence that the apoE2 isoform is the least susceptible to cleavage in primary neurons, a hypothesis which has previously only been inferred in the literature on the basis of structural studies of domain interaction (Mahley and Huang, 2012, Dong et al., 1994, Xu et al., 2004). Furthermore, the fragmentation load for each isoform in primary neurons is consistent

with that found in *APOE*-genotyped human AD brains and NSE-apoE mice brain extracts (apoE4>apoE3) (Harris et al., 2003, Jones et al., 2011, Tamboli et al., 2014, Brecht et al., 2004b), indicating that apoE processing in this *in vitro* model is comparable to processing of apoE *in vivo*. In contrast, the apoE fragmentation load for each apoE isoform in the neuroblastoma cells followed the order of apoE2>apoE4>apoE3, raising the prospect that the proteolytic susceptibility of apoE may involve other factors such as PTMs (Zannis and Breslow, 1981, Wernette-Hammond et al., 1989). Although, it should not be discounted that isoform-specific variation in the secretion of apoE fragments may underlie the differences in the levels of intracellular fragments, as studies have reported the presence of apoE fragments in extracellular fractions (Wellnitz et al., 2005, Munoz et al., 2018). Examination of fragment composition using a panel of commercially available antibodies to specific regions of apoE also provided evidence to support the hypothesis that fragments of apoE containing the SNPs may be generated. Thus, fragment load and fragment structure may play a role in the differential effects that these isoforms have on neuronal function. In addition, this work revealed that apoE fragments contain an intact C-terminus and are thus generated by sequential cleavage within the N-terminal domain. This finding is of importance because numerous studies have used C-terminally truncated apoE4 fragments or N-terminal apoE4 fragments to investigate the role of apoE4 proteolysis in neuronal dysfunction and thus AD (Huang et al., 2001, Harris et al., 2003, Chang et al., 2005, Nakamura et al., 2009, Bien-Ly et al., 2011, Tanaka et al., 2006). As such, the data presented here suggests that these fragments may not exist *in vivo* and that the findings from these studies may not be an entirely accurate representation of the function of apoE fragments in the human brain. The data also highlight that work exploring the role of apoE fragments truncated at the N-terminus may provide a more accurate insight into the function of these fragments. However, it would be better to approach this line of investigation following the identification of the amino acid sequence of such fragments.

Investigating the effect of apoE isoform on the levels and regulation of cytoskeletal-associated proteins as an indicator of a toxic or protective gain of function revealed isoform-specific increases in tau phosphorylation at Thr181 (apoE4>apoE3, no effect for

apoE2) and vimentin expression (apoE2>apoE4, no effect for apoE3) in primary neurons. The isoform-dependent effect on tau phosphorylation is consistent with that observed in the literature (Tesseur et al., 2000b, Brecht et al., 2004b, Lin et al., 2018, Wang et al., 2018) and suggests that apoE4 may contribute to AD pathology through the deregulation of tau and thus microtubule network disruption. Interestingly, the data also showed a relationship between vimentin expression, which has been proposed to be involved in the neuronal repair response (Levin et al., 2009), and apoE expression in an isoform-dependent manner. This supports the hypothesis that expression of apoE in neurons may be triggered as part of the neuronal repair response in stressed or injured neurons, although it is unclear why no effect was observed for apoE3. This result also indicates that apoE expression in neurons may affect the IF network in addition to the microtubule network and may modulate the repair response in injured or stressed neurons, although this remains to be verified. Surprisingly, none of the isoforms were found to be toxic despite substantial fragment load observed for all the isoforms, cytosolic localisation of fragments and apoE4- / apoE3- mediated increases in the levels of tau phosphorylated at Thr181 that mirrored the level of fragments generated. These findings suggest that full length apoE and its fragments are not inherently toxic *in vitro* and that phosphorylation of tau at Thr181 is not necessarily representative of toxic tau. However, one important aspect to consider about the work here, is that modelling apoE4-mediated toxicity in culture is a more simplistic approach than expressing apoE4 *in vivo*, which incorporates longer expression times and age-dependent alterations at the cellular and molecular level. Hence it is possible that prolonged expression of apoE and/or additional factors such as cellular stress may be required to initiate the reported gain of toxic function for apoE4 *in vitro*, and possibly, to observe subsequent tau-mediated toxicity (if it all). Indeed, although neuronal apoE4 expression *in vivo* has been demonstrated to induce neurodegeneration (Tesseur et al., 2000a, Tesseur et al., 2000b, Brecht et al., 2004a), it is important to note that these effects were age-dependent, presenting in aged transgenic mice and worsening over time. Of note, the work in this thesis is also the first to demonstrate that apoE2 expression and proteolysis promotes cell viability and survival of SH-SY5Y cells, thus supporting the hypothesis that this isoform may play a neuroprotective role in AD. Although the mechanisms underlying this

remain to be determined, it is unlikely that this effect involves vimentin expression because vimentin levels were unchanged by apoE2 expression in SH-SY5Y cells. Since this neuroprotective effect was restricted to SH-SY5Y cells, it is possible that human-derived neuronal cell models may be required to investigate protective role of apoE2 *in vitro*. In addition, since SH-SY5Y cells expressing apoE2 showed the greatest abundance of fragments compared to the other two isoforms, proteolysis of apoE may not necessarily result in a loss of protective function. In fact, it is conceivable that apoE2 fragments may confer neuroprotection, an intriguing possibility that remains to be confirmed. Taken together, it is plausible that expression and proteolysis of apoE2 in human neurons following stress or injury may partially underlie the decreased risk for AD associated with the *APOE2* genotype. In conclusion, these findings support the hypothesis that the differential effects of each apoE isoform on neuronal function and the risk for AD are likely linked to structural differences in the full-length protein and/or fragments. Additionally, these findings highlight that research into the role of apoE2 expression and proteolysis in neurons may be a promising avenue for identifying new therapies for AD.

Bibliography

ABRAMOV, E., DOLEV, I., FOGEL, H., CICCOTOSTO, G. D., RUFF, E. & SLUTSKY, I. 2009. Amyloid-beta as a positive endogenous regulator of release probability at hippocampal synapses. *Nat Neurosci,* 12**,** 1567-76.

ADI 2018. World Alzheimer Report 2018 - The state of the art of dementia research: New frontiers. *Alzheimer's disease international*.

AHMED, M., DAVIS, J., AUCOIN, D., SATO, T., AHUJA, S., AIMOTO, S., ELLIOTT, J. I., VAN NOSTRAND, W. E. & SMITH, S. O. 2010a. Structural conversion of neurotoxic amyloid-beta(1-42) oligomers to fibrils. *Nat Struct Mol Biol,* 17**,** 561-567.

AHMED, M., DAVIS, J., AUCOIN, D., SATO, T., AHUJA, S., AIMOTO, S., ELLIOTT, J. I., VAN NOSTRAND, W. E. & SMITH, S. O. 2010b. Structural conversion of neurotoxic amyloid-beta(1-42) oligomers to fibrils. *Nat Struct Mol Biol,* 17**,** 561-7.

AIZAWA, Y., FUKATSU, R., TAKAMARU, Y., TSUZUKI, K., CHIBA, H., KOBAYASHI, K., FUJII, N. & TAKAHATA, N. 1997. Amino-terminus truncated apolipoprotein E is the major species in amyloid deposits in Alzheimer's disease-affected brains: a possible role for apolipoprotein E in Alzheimer's disease. *Brain Research,* 768**,** 208-214.

ALESHKOV, S., ABRAHAM, C. R. & ZANNIS, V. I. 1997. Interaction of nascent ApoE2, ApoE3, and ApoE4 isoforms expressed in mammalian cells with amyloid peptide beta (1-40). Relevance to Alzheimer's disease. *Biochemistry,* 36**,** 10571-80.

ALONSO, A. C., ZAIDI, T., GRUNDKE-IQBAL, I. & IQBAL, K. 1994. Role of abnormally phosphorylated tau in the breakdown of microtubules in Alzheimer disease. *Proc Natl Acad Sci U S A,* 91**,** 5562-6.

AMANATKAR, H. R., PAPAGIANNOPOULOS, B. & GROSSBERG, G. T. 2017. Analysis of recent failures of disease modifying therapies in Alzheimer's disease suggesting a new methodology for future studies. *Expert Rev Neurother,* 17**,** 7-16.

ANDREW, R. J., KELLETT, K. A., THINAKARAN, G. & HOOPER, N. M. 2016. A Greek Tragedy: The Growing Complexity of Alzheimer Amyloid Precursor Protein Proteolysis. *J Biol Chem,* 291**,** 19235-44.

AOKI, K., UCHIHARA, T., SANJO, N., NAKAMURA, A., IKEDA, K., TSUCHIYA, K. & WAKAYAMA, Y. 2003. Increased Expression of Neuronal Apolipoprotein E in Human Brain With Cerebral Infarction. *Stroke,* 34**,** 875-881.

ARENDT, T. 2009. Synaptic degeneration in Alzheimer's disease. *Acta Neuropathol,* 118**,** 167-79.

BAGHIROVA, S., HUGHES, B. G., HENDZEL, M. J. & SCHULZ, R. 2015. Sequential fractionation and isolation of subcellular proteins from tissue or cultured cells. *MethodsX,* 2**,** 440-5.

BALDELLI, P., FASSIO, A., VALTORTA, F. & BENFENATI, F. 2007. Lack of synapsin I reduces the readily releasable pool of synaptic vesicles at central inhibitory synapses. *The Journal of neuroscience : the official journal of the Society for Neuroscience,* 27**,** 13520-13531.

BALES, K. R., LIU, F., WU, S., LIN, S., KOGER, D., DELONG, C., HANSEN, J. C., SULLIVAN, P. M. & PAUL, S. M. 2009. Human APOE isoform-dependent effects on brain beta-amyloid levels in PDAPP transgenic mice. *J Neurosci,* 29**,** 6771-9.

BAO, F., ARAI, H., MATSUSHITA, S., HIGUCHI, S. & SASAKI, H. 1996. Expression of apolipoprotein E in normal and diverse neurodegenerative disease brain. *Neuroreport,* 7**,** 1733-9.

BAUM, L., CHEN, L., NG, H. K., CHAN, Y. S., MAK, Y. T., WOO, J., CHIU, H. F. & PANG, C. P. 1998. Low density lipoprotein receptor related protein gene exon 3 polymorphism association with Alzheimer's disease in Chinese. *Neurosci Lett,* 247**,** 33-6.

BAUMGART, M., SNYDER, H. M., CARRILLO, M. C., FAZIO, S., KIM, H. & JOHNS, H. 2015. Summary of the evidence on modifiable risk factors for cognitive decline and dementia: A population-based perspective. *Alzheimers Dement,* 11**,** 718-26.

BEAUDOIN, S., GOGGIN, K., BISSONNETTE, C., GRENIER, C. & ROUCOU, X. 2008. Aggresomes do not represent a general cellular response to protein misfolding in mammalian cells. *BMC Cell Biol,* 9**,** 59.

BELL, R. D., SAGARE, A. P., FRIEDMAN, A. E., BEDI, G. S., HOLTZMAN, D. M., DEANE, R. & ZLOKOVIC, B. V. 2007. Transport pathways for clearance of human Alzheimer's amyloid beta-peptide and apolipoproteins E and J in the mouse central nervous system. *J Cereb Blood Flow Metab,* 27**,** 909-18.

BELLOSTA, S., NATHAN, B. P., ORTH, M., DONG, L. M., MAHLEY, R. W. & PITAS, R. E. 1995. Stable expression and secretion of apolipoproteins E3 and E4 in mouse neuroblastoma cells produces differential effects on neurite outgrowth. *J Biol Chem,* 270**,** 27063-71.

BENFENATI, F., VALTORTA, F., BAHLER, M. & GREENGARD, P. 1989. Synapsin I, a neuron-specific phosphoprotein interacting with small synaptic vesicles and F-actin. *Cell Biol Int Rep,* 13**,** 1007-21.

BETTHAUSER, T. J., CODY, K. A., ZAMMIT, M. D., MURALI, D., CONVERSE, A. K., BARNHART, T. E., STONE, C. K., ROWLEY, H. A., JOHNSON, S. C. & CHRISTIAN, B. T. 2019. In Vivo Characterization and Quantification of Neurofibrillary Tau PET Radioligand (18)F-MK-6240 in Humans from Alzheimer Disease Dementia to Young Controls. *J Nucl Med,* 60**,** 93-99.

BIEN-LY, N., ANDREWS-ZWILLING, Y., XU, Q., BERNARDO, A., WANG, C. & HUANG, Y. 2011. C-terminal-truncated apolipoprotein (apo) E4 inefficiently clears amyloid-beta (Abeta) and acts in concert with Abeta to elicit neuronal and behavioral deficits in mice. *Proceedings of the National Academy of Sciences of the United States of America,* 108**,** 4236-41.

BIERNAT, J., WU, Y. Z., TIMM, T., ZHENG-FISCHHOFER, Q., MANDELKOW, E., MEIJER, L. & MANDELKOW, E. M. 2002. Protein kinase MARK/PAR-1 is required for neurite outgrowth and establishment of neuronal polarity. *Mol Biol Cell,* 13**,** 4013-28.

BIGNAMI, A., RAJU, T. & DAHL, D. 1982. Localization of vimentin, the nonspecific intermediate filament protein, in embryonal glia and in early differentiating neurons. In vivo and in vitro immunofluorescence study of the rat embryo with vimentin and neurofilament antisera. *Dev Biol,* 91**,** 286-95.

BILELLO, M., DOSHI, J., NABAVIZADEH, S. A., TOLEDO, J. B., ERUS, G., XIE, S. X., TROJANOWSKI, J. Q., HAN, X. & DAVATZIKOS, C. 2015. Correlating Cognitive Decline with White Matter Lesion and Brain Atrophy Magnetic Resonance Imaging Measurements in Alzheimer's Disease. *J Alzheimers Dis,* 48**,** 987-94.

BLACKER, D., WILCOX, M. A., LAIRD, N. M., RODES, L., HORVATH, S. M., GO, R. C., PERRY, R., WATSON, B., JR., BASSETT, S. S., MCINNIS, M. G., ALBERT, M. S., HYMAN, B. T.

& TANZI, R. E. 1998. Alpha-2 macroglobulin is genetically associated with Alzheimer disease. *Nat Genet,* 19**,** 357-60.

BLENNOW, K. 2017. A Review of Fluid Biomarkers for Alzheimer's Disease: Moving from CSF to Blood. *Neurol Ther,* 6**,** 15-24.

BLOOM, O., EVERGREN, E., TOMILIN, N., KJAERULFF, O., LOW, P., BRODIN, L., PIERIBONE, V. A., GREENGARD, P. & SHUPLIAKOV, O. 2003. Colocalization of synapsin and actin during synaptic vesicle recycling. *J Cell Biol,* 161**,** 737-47.

BORCHELT, D. R., THINAKARAN, G., ECKMAN, C. B., LEE, M. K., DAVENPORT, F., RATOVITSKY, T., PRADA, C. M., KIM, G., SEEKINS, S., YAGER, D., SLUNT, H. H., WANG, R., SEEGER, M., LEVEY, A. I., GANDY, S. E., COPELAND, N. G., JENKINS, N. A., PRICE, D. L., YOUNKIN, S. G. & SISODIA, S. S. 1996. Familial Alzheimer's disease-linked presenilin 1 variants elevate Abeta1-42/1-40 ratio in vitro and in vivo. *Neuron,* 17**,** 1005-13.

BOSCHERT, U., MERLO-PICH, E., HIGGINS, G., ROSES, A. D. & CATSICAS, S. 1999. Apolipoprotein E expression by neurons surviving excitotoxic stress. *Neurobiol Dis,* 6**,** 508-514.

BOUR, A., GROOTENDORST, J., VOGEL, E., KELCHE, C., DODART, J. C., BALES, K., MOREAU, P. H., SULLIVAN, P. M. & MATHIS, C. 2008. Middle-aged human apoE4 targeted-replacement mice show retention deficits on a wide range of spatial memory tasks. *Behav Brain Res,* 193**,** 174-82.

BOYLES, J. K., PITAS, R. E., WILSON, E., MAHLEY, R. W. & TAYLOR, J. M. 1985. Apolipoprotein E associated with astrocytic glia of the central nervous system and with nonmyelinating glia of the peripheral nervous system. *J Clin Invest,* 76**,** 1501-13.

BOYNE, L. J., FISCHER, I. & SHEA, T. B. 1996. Role of vimentin in early stages of neuritogenesis in cultured hippocampal neurons. *Int J Dev Neurosci,* 14**,** 739-48.

BRAAK, H. & BRAAK, E. 1991. Neuropathological stageing of Alzheimer-related changes. *Acta Neuropathol,* 82**,** 239-59.

BRAAK, H. & BRAAK, E. 1995. Staging of Alzheimer's disease-related neurofibrillary changes. *Neurobiol Aging,* 16**,** 271-8; discussion 278-84.

BRECHT, W. J., HARRIS, F. M., CHANG, S., TESSEUR, I., YU, G.-Q. Q., XU, Q., DEE FISH, J., WYSS-CORAY, T., BUTTINI, M., MUCKE, L., MAHLEY, R. W. & HUANG, Y. 2004a. Neuron-specific apolipoprotein e4 proteolysis is associated with increased tau phosphorylation in brains of transgenic mice. *J Neurosci,* 24**,** 2527-2534.

BRECHT, W. J., HARRIS, F. M., CHANG, S., TESSEUR, I., YU, G. Q., XU, Q., DEE FISH, J., WYSS-CORAY, T., BUTTINI, M., MUCKE, L., MAHLEY, R. W. & HUANG, Y. 2004b. Neuron-specific apolipoprotein e4 proteolysis is associated with increased tau phosphorylation in brains of transgenic mice. *J Neurosci,* 24**,** 2527-34.

BRETTEVILLE, A., MARCOUILLER, F., JULIEN, C., EL KHOURY, N. B., PETRY, F. R., POITRAS, I., MOUGINOT, D., LEVESQUE, G., HEBERT, S. S. & PLANEL, E. 2012. Hypothermia-induced hyperphosphorylation: a new model to study tau kinase inhibitors. *Sci Rep,* 2**,** 480.

BREWER, G. J., TORRICELLI, J. R., EVEGE, E. K. & PRICE, P. J. 1993. Optimized survival of hippocampal neurons in B27-supplemented Neurobasal, a new serum-free medium combination. *J Neurosci Res,* 35**,** 567-76.

BRITO-MOREIRA, J., PAULA-LIMA, A. C., BOMFIM, T. R., OLIVEIRA, F. B., SEPULVEDA, F. J., DE MELLO, F. G., AGUAYO, L. G., PANIZZUTTI, R. & FERREIRA, S. T. 2011. Abeta

oligomers induce glutamate release from hippocampal neurons. *Curr Alzheimer Res,* 8**,** 552-62.

BUERGER, K., ZINKOWSKI, R., TEIPEL, S. J., TAPIOLA, T., ARAI, H., BLENNOW, K., ANDREASEN, N., HOFMANN-KIEFER, K., DEBERNARDIS, J., KERKMAN, D., MCCULLOCH, C., KOHNKEN, R., PADBERG, F., PIRTTILA, T., SCHAPIRO, M. B., RAPOPORT, S. I., MOLLER, H. J., DAVIES, P. & HAMPEL, H. 2002. Differential diagnosis of Alzheimer disease with cerebrospinal fluid levels of tau protein phosphorylated at threonine 231. *Arch Neurol,* 59**,** 1267-72.

BUTTINI, M., MASLIAH, E., YU, G.-Q., PALOP, J. J., CHANG, S., BERNARDO, A., LIN, C., WYSS-CORAY, T., HUANG, Y. & MUCKE, L. 2010. Cellular source of apolipoprotein E4 determines neuronal susceptibility to excitotoxic injury in transgenic mice. *The American journal of pathology,* 177**,** 563-569.

BUTTINI, M., ORTH, M., BELLOSTA, S., AKEEFE, H., PITAS, R. E., WYSS-CORAY, T., MUCKE, L. & MAHLEY, R. W. 1999. Expression of Human Apolipoprotein E3 or E4 in the Brains of Apoe ⁒… / ⁒… Mice : Isoform-Specific Effects on Neurodegeneration. 19**,** 4867-4880.

CACCAMO, A., ODDO, S., SUGARMAN, M. C., AKBARI, Y. & LAFERLA, F. M. 2005. Age- and region-dependent alterations in Abeta-degrading enzymes: implications for Abeta-induced disorders. *Neurobiol Aging,* 26**,** 645-54.

CARPENTIER, M., ROBITAILLE, Y., DESGROSEILLERS, L., BOILEAU, G. & MARCINKIEWICZ, M. 2002. Declining expression of neprilysin in Alzheimer disease vasculature: possible involvement in cerebral amyloid angiopathy. *J Neuropathol Exp Neurol,* 61**,** 849-56.

CARRILLO-MORA, P., LUNA, R. & COLÍN-BARENQUE, L. 2014. Amyloid beta: multiple mechanisms of toxicity and only some protective effects? *Oxidative medicine and cellular longevity,* 2014**,** 795375.

CASTANO, E. M., PRELLI, F., PRAS, M. & FRANGIONE, B. 1995. Apolipoprotein E carboxyl-terminal fragments are complexed to amyloids A and L. Implications for amyloidogenesis and Alzheimer's disease. *J Biol Chem,* 270**,** 17610-5.

CASTELLANO, J. M., KIM, J., STEWART, F. R., JIANG, H., DEMATTOS, R. B., PATTERSON, B. W., FAGAN, A. M., MORRIS, J. C., MAWUENYEGA, K. G., CRUCHAGA, C., GOATE, A. M., BALES, K. R., PAUL, S. M., BATEMAN, R. J. & HOLTZMAN, D. M. 2011. Human apoE isoforms differentially regulate brain amyloid-beta peptide clearance. *Sci Transl Med,* 3**,** 89ra57.

CECCALDI, P. E., GROHOVAZ, F., BENFENATI, F., CHIEREGATTI, E., GREENGARD, P. & VALTORTA, F. 1995. Dephosphorylated synapsin I anchors synaptic vesicles to actin cytoskeleton: An analysis by videomicroscopy. *Journal of Cell Biology,* 128**,** 905-912.

CEDAZO-MÍNGUEZ, A., POPESCU, B. O., BLANCO-MILLÁN, J. M., AKTERIN, S., PEI, J.-J., WINBLAD, B. & COWBURN, R. F. 2003. Apolipoprotein E and beta-amyloid (1-42) regulation of glycogen synthase kinase-3beta. *Journal of neurochemistry,* 87**,** 1152-1164.

CERF, E., GUSTOT, A., GOORMAGHTIGH, E., RUYSSCHAERT, J. M. & RAUSSENS, V. 2011. High ability of apolipoprotein E4 to stabilize amyloid-beta peptide oligomers, the pathological entities responsible for Alzheimer's disease. *Faseb j,* 25**,** 1585-95.

CESCA, F., BALDELLI, P., VALTORTA, F. & BENFENATI, F. 2010. The synapsins: key actors of synapse function and plasticity. *Prog Neurobiol,* 91**,** 313-348.

CHANG, P., CHANDLER, K. E., WILLIAMS, R. S. B. & WALKER, M. C. 2010. Inhibition of long-term potentiation by valproic acid through modulation of cyclic AMP. *Epilepsia,* 51**,** 1533-1542.

CHANG, P., ORABI, B., DERANIEH, R., DHAM, M., HOELLER, O., SHIMSHONI, J., YAGEN, B., BIALER, M., GREENBERG, M., WALKER, M. & WILLIAMS, R. 2012. The antiepileptic drug valproic acid and other medium-chain fatty acids acutely reduce phosphoinositide levels independently of inositol in Dictyostelium. 124**,** 115-124.

CHANG, S., RAN MA, T., MIRANDA, R. D., BALESTRA, M. E., MAHLEY, R. W. & HUANG, Y. 2005. Lipid- and receptor-binding regions of apolipoprotein E4 fragments act in concert to cause mitochondrial dysfunction and neurotoxicity. *Proceedings of the National Academy of Sciences of the United States of America,* 102**,** 18694-9.

CHARTIER-HARILN, M.-C., PARFITT, M., LEGRAIN, S., PÉREZ-TUR, J., BROUSSEAU, T., EVANS, A., BERR, C., VLDAL, O., ROQUES, P., GOURLET, V., FRUCHART, J.-C., DELACOURTE, A., ROSSOR, M. & AMOUYEL, P. 1994. Apolipoprotein E, ε4 allele as a major risk factor for sporadic early and late-onset forms of Alzheimer's disease: analysis of the 19q13.2 chromosomal region. *Human Molecular Genetics,* 3**,** 569-574.

CHEN, H.-K., JI, Z.-S., DODSON, S. E., MIRANDA, R. D., ROSENBLUM, C. I., REYNOLDS, I. J., FREEDMAN, S. B., WEISGRABER, K. H., HUANG, Y. & MAHLEY, R. W. 2011a. Apolipoprotein E4 domain interaction mediates detrimental effects on mitochondria and is a potential therapeutic target for Alzheimer disease. *The Journal of biological chemistry,* 286**,** 5215-21.

CHEN, J., LI, Q. & WANG, J. 2011b. Topology of human apolipoprotein E3 uniquely regulates its diverse biological functions. *Proc Natl Acad Sci U S A,* 108**,** 14813-8.

CHEN, J., MARTIN, B. L. & BRAUTIGAN, D. L. 1992. Regulation of protein serine-threonine phosphatase type-2A by tyrosine phosphorylation. *Science,* 257**,** 1261-4.

CHO, H. S., HYMAN, B. T., GREENBERG, S. M. & REBECK, G. W. 2001. Quantitation of apoE domains in Alzheimer disease brain suggests a role for apoE in Abeta aggregation. *Journal of neuropathology and experimental neurology,* 60**,** 342-349.

CHOU, C. Y., LIN, Y. L., HUANG, Y. C., SHEU, S. Y., LIN, T. H., TSAY, H. J., CHANG, G. G. & SHIAO, M. S. 2005. Structural variation in human apolipoprotein E3 and E4: secondary structure, tertiary structure, and size distribution. *Biophys J,* 88**,** 455-66.

CHUA, C. C., LIM, M. L. & WONG, B. S. 2010. Altered apolipoprotein E glycosylation is associated with Abeta(42) accumulation in an animal model of Niemann-Pick Type C disease. *J Neurochem,* 112**,** 1619-26.

CLERX, L., JACOBS, H. I., BURGMANS, S., GRONENSCHILD, E. H., UYLINGS, H. B., ECHAVARRI, C., VISSER, P. J., VERHEY, F. R. & AALTEN, P. 2013. Sensitivity of different MRI-techniques to assess gray matter atrophy patterns in Alzheimer's disease is region-specific. *Curr Alzheimer Res,* 10**,** 940-51.

COCHARD, P. & PAULIN, D. 1984. Initial expression of neurofilaments and vimentin in the central and peripheral nervous system of the mouse embryo in vivo. *J Neurosci,* 4**,** 2080-94.

CONEJERO-GOLDBERG, C., GOMAR, J. J., BOBES-BASCARAN, T., HYDE, T. M., KLEINMAN, J. E., HERMAN, M. M., CHEN, S., DAVIES, P. & GOLDBERG, T. E. 2014. APOE2 enhances neuroprotection against Alzheimer's disease through multiple molecular mechanisms. *Molecular Psychiatry,* 19**,** 1243-1250.

CORDER, E. H., SAUNDERS, A. M., RISCH, N. J., STRITTMATTER, W. J., SCHMECHEL, D. E., GASKELL, P. C., JR., RIMMLER, J. B., LOCKE, P. A., CONNEALLY, P. M., SCHMADER, K. E. & ET AL. 1994. Protective effect of apolipoprotein E type 2 allele for late onset Alzheimer disease. *Nat Genet,* 7**,** 180-4.

CORDER, E. H., SAUNDERS, A. M., STRITTMATTER, W. J., SCHMECHEL, D. E., GASKELL, P. C., SMALL, G. W., ROSES, A. D., HAINES, J. L. & PERICAK-VANCE, M. A. 1993. Gene dose of apolipoprotein E type 4 allele and the risk of Alzheimer's disease in late onset families. *Science,* 261**,** 921-923.

CORK, L. C., STERNBERGER, N. H., STERNBERGER, L. A., CASANOVA, M. F., STRUBLE, R. G. & PRICE, D. L. 1986. Phosphorylated neurofilament antigens in neurofibrillary tangles in Alzheimer's disease. *J Neuropathol Exp Neurol,* 45**,** 56-64.

CRUCHAGA, C., HALLER, G., CHAKRAVERTY, S., MAYO, K., VALLANIA, F. L., MITRA, R. D., FABER, K., WILLIAMSON, J., BIRD, T., DIAZ-ARRASTIA, R., FOROUD, T. M., BOEVE, B. F., GRAFF-RADFORD, N. R., ST JEAN, P., LAWSON, M., EHM, M. G., MAYEUX, R. & GOATE, A. M. 2012. Rare variants in APP, PSEN1 and PSEN2 increase risk for AD in late-onset Alzheimer's disease families. *PLoS One,* 7**,** e31039.

CRUTCHER, K. A., CLAY, M. A., SCOTT, S. A., TIAN, X., TOLAR, M. & HARMONY, J. A. 1994. Neurite degeneration elicited by apolipoprotein E peptides. *Exp Neurol,* 130**,** 120-6.

CRUTCHER, K. A., LILLEY, H. N., ANTHONY, S. R., ZHOU, W. & NARAYANASWAMI, V. 2010. Full-length apolipoprotein E protects against the neurotoxicity of an apoE-related peptide. *Brain Research,* 1306**,** 106-115.

CRUTS, M., THEUNS, J. & VAN BROECKHOVEN, C. 2012. Locus-specific mutation databases for neurodegenerative brain diseases. *Hum Mutat,* 33**,** 1340-4.

CUMMINGS, J., RITTER, A. & ZHONG, K. 2018. Clinical Trials for Disease-Modifying Therapies in Alzheimer's Disease: A Primer, Lessons Learned, and a Blueprint for the Future. *J Alzheimers Dis,* 64**,** S3-s22.

CUMMINGS, J. A., MULKEY, R. M., NICOLL, R. A. & MALENKA, R. C. 1996. Ca2+ signaling requirements for long-term depression in the hippocampus. *Neuron,* 16**,** 825-33.

CUMMINGS, J. L., MORSTORF, T. & ZHONG, K. 2014. Alzheimer's disease drug-development pipeline: few candidates, frequent failures. *Alzheimers Res Ther,* 6**,** 37.

CUTLER, R. G., KELLY, J., STORIE, K., PEDERSEN, W. A., TAMMARA, A., HATANPAA, K., TRONCOSO, J. C. & MATTSON, M. P. 2004. Involvement of oxidative stress-induced abnormalities in ceramide and cholesterol metabolism in brain aging and Alzheimer's disease. *Proc Natl Acad Sci U S A,* 101**,** 2070-5.

CZERNIK, A. J., PANG, D. T. & GREENGARD, P. 1987. Amino acid sequences surrounding the cAMP-dependent and calcium/calmodulin-dependent phosphorylation sites in rat and bovine synapsin I. *Proc Natl Acad Sci U S A,* 84**,** 7518-22.

DAFNIS, I., RAFTOPOULOU, C., MOUNTAKI, C., MEGALOU, E., ZANNIS, V. I. & CHRONI, A. 2018. ApoE isoforms and carboxyl-terminal truncated apoE4 forms affect neuronal BACE1 levels and Abeta production independently of their cholesterol efflux capacity. *Biochem J*.

DAHL, D., SELKOE, D. J., PERO, R. T. & BIGNAMI, A. 1982. Immunostaining of neurofibrillary tangles in Alzheimer's senile dementia with a neurofilament antiserum. *J Neurosci,* 2**,** 113-9.

DAHLGREN, K. N., MANELLI, A. M., STINE, W. B., JR., BAKER, L. K., KRAFFT, G. A. & LADU, M. J. 2002. Oligomeric and fibrillar species of amyloid-beta peptides differentially affect neuronal viability. *J Biol Chem,* 277**,** 32046-53.

DAMKE, H., BABA, T., WARNOCK, D. E. & SCHMID, S. L. 1994. Induction of mutant dynamin specifically blocks endocytic coated vesicle formation. *J Cell Biol,* 127**,** 915-34.

DAVIES, C. A., MANN, D. M., SUMPTER, P. Q. & YATES, P. O. 1987. A quantitative morphometric analysis of the neuronal and synaptic content of the frontal and temporal cortex in patients with Alzheimer's disease. *J Neurol Sci,* 78**,** 151-64.

DAY, R. J., MCCARTY, K. L., OCKERSE, K. E., HEAD, E. & ROHN, T. T. 2016. Proteolytic Cleavage of Apolipoprotein E in the Down Syndrome Brain. 7**,** 267-277.

DE FELICE, F. G., WU, D., LAMBERT, M. P., FERNANDEZ, S. J., VELASCO, P. T., LACOR, P. N., BIGIO, E. H., JERECIC, J., ACTON, P. J., SHUGHRUE, P. J., CHEN-DODSON, E., KINNEY, G. G. & KLEIN, W. L. 2008. Alzheimer's disease-type neuronal tau hyperphosphorylation induced by A beta oligomers. *Neurobiol Aging,* 29**,** 1334-47.

DE STROOPER, B. 2003. Aph-1, Pen-2, and Nicastrin with Presenilin generate an active gamma-Secretase complex. *Neuron,* 38**,** 9-12.

DE STROOPER, B., IWATSUBO, T. & WOLFE, M. S. 2012. Presenilins and γ-secretase: structure, function, and role in Alzheimer Disease. *Cold Spring Harbor perspectives in medicine,* 2**,** a006304.

DE STROOPER, B. & KARRAN, E. 2016. The Cellular Phase of Alzheimer's Disease. *Cell,* 164**,** 603-615.

DE STROOPER, B., SAFTIG, P., CRAESSAERTS, K., VANDERSTICHELE, H., GUHDE, G., ANNAERT, W., VON FIGURA, K. & VAN LEUVEN, F. 1998. Deficiency of presenilin-1 inhibits the normal cleavage of amyloid precursor protein. *Nature,* 391**,** 387.

DEANE, R., SAGARE, A., HAMM, K., PARISI, M., LANE, S., FINN, M. B., HOLTZMAN, D. M. & ZLOKOVIC, B. V. 2008. apoE isoform-specific disruption of amyloid beta peptide clearance from mouse brain. *J Clin Invest,* 118**,** 4002-13.

DEANE, R., WU, Z., SAGARE, A., DAVIS, J., DU YAN, S., HAMM, K., XU, F., PARISI, M., LARUE, B., HU, H. W., SPIJKERS, P., GUO, H., SONG, X., LENTING, P. J., VAN NOSTRAND, W. E. & ZLOKOVIC, B. V. 2004. LRP/amyloid beta-peptide interaction mediates differential brain efflux of Abeta isoforms. *Neuron,* 43**,** 333-44.

DEHOUCK, B., FENART, L., DEHOUCK, M. P., PIERCE, A., TORPIER, G. & CECCHELLI, R. 1997. A new function for the LDL receptor: transcytosis of LDL across the blood-brain barrier. *J Cell Biol,* 138**,** 877-89.

DEKOSKY, S. T. & SCHEFF, S. W. 1990. Synapse loss in frontal cortex biopsies in Alzheimer's disease: correlation with cognitive severity. *Ann Neurol,* 27**,** 457-64.

DEKROON, R. M. & ARMATI, P. J. 2001. Synthesis and processing of apolipoprotein E in human brain cultures. *Glia,* 33**,** 298-305.

DEMATTOS, R. B., THORNGATE, F. E. & WILLIAMS, D. L. 1999. A test of the cytosolic apolipoprotein E hypothesis fails to detect the escape of apolipoprotein E from the endocytic pathway into the cytosol and shows that direct expression of apolipoprotein E in the cytosol is cytotoxic. *The Journal of neuroscience : the official journal of the Society for Neuroscience,* 19**,** 2464-2473.

DENNING, W., DAS, S., GUO, S., XU, J., KAPPES, J. C. & HEL, Z. 2013. Optimization of the transductional efficiency of lentiviral vectors: effect of sera and polycations. *Molecular biotechnology,* 53**,** 308-14.

DESHPANDE, A., MINA, E., GLABE, C. & BUSCIGLIO, J. 2006. Different conformations of amyloid beta induce neurotoxicity by distinct mechanisms in human cortical neurons. *J Neurosci,* 26**,** 6011-8.

DESSI, F., POLLARD, H., MOREAU, J., BEN-ARI, Y. & CHARRIAUT-MARLANGUE, C. 1995. Cytosine arabinoside induces apoptosis in cerebellar neurons in culture. *J Neurochem,* 64**,** 1980-7.

DICKSON, T. C., SAUNDERS, H. L. & VICKERS, J. C. 1997. Relationship between apolipoprotein E and the amyloid deposits and dystrophic neurites of Alzheimer's disease. *Neuropathol Appl Neurobiol,* 23**,** 483-91.

DIETSCHY, J. M. 2009. Central nervous system: cholesterol turnover, brain development and neurodegeneration. *Biol Chem,* 390**,** 287-93.

DING, B. & KILPATRICK, D. L. 2013. Lentiviral vector production, titration, and transduction of primary neurons. *Methods in molecular biology (Clifton, N.J.),* 1018**,** 119-31.

DITTGEN, T., NIMMERJAHN, A., KOMAI, S., LICZNERSKI, P., WATERS, J., MARGRIE, T. W., HELMCHEN, F., DENK, W., BRECHT, M. & OSTEN, P. 2004. Lentivirus-based genetic manipulations of cortical neurons and their optical and electrophysiological monitoring in vivo. *Proc Natl Acad Sci U S A,* 101**,** 18206-11.

DONG, L. M. & WEISGRABER, K. H. 1996. Human apolipoprotein E4 domain interaction. Arginine 61 and glutamic acid 255 interact to direct the preference for very low density lipoproteins.

DONG, L. M., WILSON, C., WARDELL, M. R., SIMMONS, T., MAHLEY, R. W., WEISGRABER, K. H. & AGARD, D. A. 1994. Human apolipoprotein E. Role of arginine 61 in mediating the lipoprotein preferences of the E3 and E4 isoforms. *J Biol Chem,* 269**,** 22358-65.

DRZEZGA, A., GRIMMER, T., HENRIKSEN, G., MUHLAU, M., PERNECZKY, R., MIEDERER, I., PRAUS, C., SORG, C., WOHLSCHLAGER, A., RIEMENSCHNEIDER, M., WESTER, H. J., FOERSTL, H., SCHWAIGER, M. & KURZ, A. 2009. Effect of APOE genotype on amyloid plaque load and gray matter volume in Alzheimer disease. *Neurology,* 72**,** 1487-94.

DRZEZGA, A., RIEMENSCHNEIDER, M., STRASSNER, B., GRIMMER, T., PELLER, M., KNOLL, A., WAGENPFEIL, S., MINOSHIMA, S., SCHWAIGER, M. & KURZ, A. 2005. Cerebral glucose metabolism in patients with AD and different APOE genotypes. *Neurology,* 64**,** 102-7.

DU, Y., NI, B., GLINN, M., DODEL, R. C., BALES, K. R., ZHANG, Z., HYSLOP, P. A. & PAUL, S. M. 1997. alpha2-Macroglobulin as a beta-amyloid peptide-binding plasma protein. *J Neurochem,* 69**,** 299-305.

DUARA, R., LOEWENSTEIN, D. A., POTTER, E., APPEL, J., GREIG, M. T., URS, R., SHEN, Q., RAJ, A., SMALL, B., BARKER, W., SCHOFIELD, E., WU, Y. & POTTER, H. 2008. Medial temporal lobe atrophy on MRI scans and the diagnosis of Alzheimer disease. *Neurology,* 71**,** 1986-92.

DUBOIS, B., FELDMAN, H. H., JACOVA, C., HAMPEL, H., MOLINUEVO, J. L., BLENNOW, K., DEKOSKY, S. T., GAUTHIER, S., SELKOE, D., BATEMAN, R., CAPPA, S., CRUTCH, S., ENGELBORGHS, S., FRISONI, G. B., FOX, N. C., GALASKO, D., HABERT, M. O., JICHA,

G. A., NORDBERG, A., PASQUIER, F., RABINOVICI, G., ROBERT, P., ROWE, C., SALLOWAY, S., SARAZIN, M., EPELBAUM, S., DE SOUZA, L. C., VELLAS, B., VISSER, P. J., SCHNEIDER, L., STERN, Y., SCHELTENS, P. & CUMMINGS, J. L. 2014. Advancing research diagnostic criteria for Alzheimer's disease: the IWG-2 criteria. *Lancet Neurol,* 13**,** 614-29.

DULL, T., ZUFFEREY, R., KELLY, M., MANDEL, R. J., NGUYEN, M., TRONO, D. & NALDINI, L. 1998. A third-generation lentivirus vector with a conditional packaging system. *J Virol,* 72**,** 8463-71.

EDELMANN, L., HANSON, P. I., CHAPMAN, E. R. & JAHN, R. 1995. Synaptobrevin binding to synaptophysin: a potential mechanism for controlling the exocytotic fusion machine. *Embo j,* 14**,** 224-31.

ELLIOTT, D. A., TSOI, K., HOLINKOVA, S., CHAN, S. L., KIM, W. S., HALLIDAY, G. M., RYE, K.-A. & GARNER, B. 2011. Isoform-specific proteolysis of apolipoprotein-E in the brain. *Neurobiology of aging,* 32**,** 257-71.

FARRIS, W., MANSOURIAN, S., CHANG, Y., LINDSLEY, L., ECKMAN, E. A., FROSCH, M. P., ECKMAN, C. B., TANZI, R. E., SELKOE, D. J. & GUENETTE, S. 2003. Insulin-degrading enzyme regulates the levels of insulin, amyloid beta-protein, and the beta-amyloid precursor protein intracellular domain in vivo. *Proc Natl Acad Sci U S A,* 100**,** 4162-7.

FERRER, I., MARTINEZ, A., BOLUDA, S., PARCHI, P. & BARRACHINA, M. 2008. Brain banks: benefits, limitations and cautions concerning the use of post-mortem brain tissue for molecular studies. *Cell Tissue Bank,* 9**,** 181-94.

FIUMARA, F., GIOVEDI, S., MENEGON, A., MILANESE, C., MERLO, D., MONTAROLO, P. G., VALTORTA, F., BENFENATI, F. & GHIRARDI, M. 2004. Phosphorylation by cAMP-dependent protein kinase is essential for synapsin-induced enhancement of neurotransmitter release in invertebrate neurons. *J Cell Sci,* 117**,** 5145-54.

FORNASIERO, E. F., RAIMONDI, A., GUARNIERI, F. C., ORLANDO, M., FESCE, R., BENFENATI, F. & VALTORTA, F. 2012. Synapsins Contribute to the Dynamic Spatial Organization of Synaptic Vesicles in an Activity-Dependent Manner. *Journal of Neuroscience,* 32**,** 12214-12227.

FRIEDEN, C. & GARAI, K. 2012. Structural differences between apoE3 and apoE4 may be useful in developing therapeutic agents for Alzheimer's disease. *Proc Natl Acad Sci U S A,* 109**,** 8913-8.

FRIEDEN, C. & GARAI, K. 2013. Concerning the structure of apoE. *Protein science : a publication of the Protein Society,* 22**,** 1820-5.

FRIEDLAND, R. P., BRUN, A. & BUDINGER, T. F. 1985. Pathological and positron emission tomographic correlations in Alzheimer's disease. *Lancet,* 1**,** 228.

FRISONI, G. B., FOX, N. C., JACK, C. R., JR., SCHELTENS, P. & THOMPSON, P. M. 2010. The clinical use of structural MRI in Alzheimer disease. *Nat Rev Neurol,* 6**,** 67-77.

FRYER, J. D., SIMMONS, K., PARSADANIAN, M., BALES, K. R., PAUL, S. M., SULLIVAN, P. M. & HOLTZMAN, D. M. 2005. Human apolipoprotein E4 alters the amyloid-beta 40:42 ratio and promotes the formation of cerebral amyloid angiopathy in an amyloid precursor protein transgenic model. *J Neurosci,* 25**,** 2803-10.

GARAI, K., BABAN, B. & FRIEDEN, C. 2011. Self-association and stability of the ApoE isoforms at low pH: implications for ApoE-lipid interactions. *Biochemistry,* 50**,** 6356-64.

GARAI, K., VERGHESE, P. B., BABAN, B., HOLTZMAN, D. M. & FRIEDEN, C. 2014. The binding of apolipoprotein E to oligomers and fibrils of amyloid-beta alters the kinetics of amyloid aggregation. *Biochemistry,* 53**,** 6323-31.

GATZ, M., REYNOLDS, C. A., FRATIGLIONI, L., JOHANSSON, B., MORTIMER, J. A., BERG, S., FISKE, A. & PEDERSEN, N. L. 2006. Role of genes and environments for explaining Alzheimer disease. *Arch Gen Psychiatry,* 63**,** 168-74.

GAUGLER, J., JAMES, B., JOHNSON, T., SCHOLZ, K. & WEUVE, J. 2016. 2016 Alzheimer's disease facts and figures. *Alzheimers Dement,* 12**,** 459-509.

GLENNER, G. G. & WONG, C. W. 1984. Alzheimer's disease: initial report of the purification and characterization of a novel cerebrovascular amyloid protein. *Biochem Biophys Res Commun,* 120**,** 885-90.

GONG, J. S., KOBAYASHI, M., HAYASHI, H., ZOU, K., SAWAMURA, N., FUJITA, S. C., YANAGISAWA, K. & MICHIKAWA, M. 2002. Apolipoprotein E (ApoE) isoform-dependent lipid release from astrocytes prepared from human ApoE3 and ApoE4 knock-in mice. *J Biol Chem,* 277**,** 29919-26.

GRABRUCKER, A., VAIDA, B., BOCKMANN, J. & BOECKERS, T. M. 2009. Synaptogenesis of hippocampal neurons in primary cell culture. *Cell Tissue Res,* 338**,** 333-41.

GRENIER, C., BISSONNETTE, C., VOLKOV, L. & ROUCOU, X. 2006. Molecular morphology and toxicity of cytoplasmic prion protein aggregates in neuronal and non-neuronal cells. *J Neurochem,* 97**,** 1456-66.

GRIMMER, T., GOLDHARDT, O., GUO, L. H., YOUSEFI, B. H., FORSTER, S., DRZEZGA, A., SORG, C., ALEXOPOULOS, P., FORSTL, H., KURZ, A. & PERNECZKY, R. 2014. LRP-1 polymorphism is associated with global and regional amyloid load in Alzheimer's Disease in humans in-vivo. *Neuroimage Clin,* 4**,** 411-6.

GRIMMER, T., THOLEN, S., YOUSEFI, B. H., ALEXOPOULOS, P., FORSCHLER, A., FORSTL, H., HENRIKSEN, G., KLUNK, W. E., MATHIS, C. A., PERNECZKY, R., SORG, C., KURZ, A. & DRZEZGA, A. 2010. Progression of cerebral amyloid load is associated with the apolipoprotein E epsilon4 genotype in Alzheimer's disease. *Biol Psychiatry,* 68**,** 879-84.

GRUNDKE-IQBAL, I., IQBAL, K., TUNG, Y. C., QUINLAN, M., WISNIEWSKI, H. M. & BINDER, L. I. 1986. Abnormal phosphorylation of the microtubule-associated protein tau (tau) in Alzheimer cytoskeletal pathology. *Proc Natl Acad Sci U S A,* 83**,** 4913-7.

GUSTAFSON, D. R., SKOOG, I., ROSENGREN, L., ZETTERBERG, H. & BLENNOW, K. 2007. Cerebrospinal fluid beta-amyloid 1-42 concentration may predict cognitive decline in older women. *J Neurol Neurosurg Psychiatry,* 78**,** 461-4.

HAASS, C., HUNG, A. Y., SCHLOSSMACHER, M. G., TEPLOW, D. B. & SELKOE, D. J. 1993. beta-Amyloid peptide and a 3-kDa fragment are derived by distinct cellular mechanisms. *J Biol Chem,* 268**,** 3021-4.

HAGIWARA, H., AOKI, T., SUZUKI, T. & TAKATA, K. 2010. Double-label immunoelectron microscopy for studying the colocalization of proteins in cultured cells. *Methods Mol Biol,* 657**,** 249-57.

HALIM, A., RUETSCHI, U., LARSON, G. & NILSSON, J. 2013. LC-MS/MS characterization of O-glycosylation sites and glycan structures of human cerebrospinal fluid glycoproteins. *J Proteome Res,* 12**,** 573-84.

HALL, A. C., BRENNAN, A., GOOLD, R. G., CLEVERLEY, K., LUCAS, F. R., GORDON-WEEKS, P. R. & SALINAS, P. C. 2002. Valproate regulates GSK-3-mediated axonal remodeling and synapsin I clustering in developing neurons. *Mol Cell Neurosci,* 20**,** 257-70.

HAMPEL, H., BUERGER, K., ZINKOWSKI, R., TEIPEL, S. J., GOERNITZ, A., ANDREASEN, N., SJOEGREN, M., DEBERNARDIS, J., KERKMAN, D., ISHIGURO, K., OHNO, H., VANMECHELEN, E., VANDERSTICHELE, H., MCCULLOCH, C., MOLLER, H. J., DAVIES, P. & BLENNOW, K. 2004. Measurement of phosphorylated tau epitopes in the differential diagnosis of Alzheimer disease: a comparative cerebrospinal fluid study. *Arch Gen Psychiatry,* 61**,** 95-102.

HAN, S. H., EINSTEIN, G., WEISGRABER, K. H., STRITTMATTER, W. J., SAUNDERS, A. M., PERICAK-VANCE, M., ROSES, A. D. & SCHMECHEL, D. E. 1994a. Apolipoprotein E is localized to the cytoplasm of human cortical neurons: a light and electron microscopic study. *J Neuropathol Exp Neurol,* 53**,** 535-44.

HAN, S. H., HULETTE, C., SAUNDERS, A. M., EINSTEIN, G., PERICAK-VANCE, M., STRITTMATTER, W. J., ROSES, A. D. & SCHMECHEL, D. E. 1994b. Apolipoprotein E is present in hippocampal neurons without neurofibrillary tangles in Alzheimer's disease and in age-matched controls. *Experimental Neurology.*

HARDY, J. & ALLSOP, D. 1991. Amyloid deposition as the central event in the aetiology of Alzheimer's disease. *Trends Pharmacol Sci,* 12**,** 383-8.

HARDY, J. A. & HIGGINS, G. A. 1992. Alzheimer's disease: the amyloid cascade hypothesis. *Science,* 256**,** 184-5.

HARNEY, S. C., ROWAN, M. & ANWYL, R. 2006. Long-term depression of NMDA receptor-mediated synaptic transmission is dependent on activation of metabotropic glutamate receptors and is altered to long-term potentiation by low intracellular calcium buffering. *J Neurosci,* 26**,** 1128-32.

HARRIS, F. M., BRECHT, W. J., XU, Q., MAHLEY, R. W. & HUANG, Y. 2004. Increased tau phosphorylation in apolipoprotein E4 transgenic mice is associated with activation of extracellular signal-regulated kinase. Modulation by zinc. *Journal of Biological Chemistry,* 279**,** 44795-44801.

HARRIS, F. M., BRECHT, W. J., XU, Q., TESSEUR, I., KEKONIUS, L., WYSS-CORAY, T., FISH, J. D., MASLIAH, E., HOPKINS, P. C., SCEARCE-LEVIE, K., WEISGRABER, K. H., MUCKE, L., MAHLEY, R. W. & HUANG, Y. 2003. Carboxyl-terminal-truncated apolipoprotein E4 causes Alzheimer's disease-like neurodegeneration and behavioral deficits in transgenic mice. *Proceedings of the National Academy of Sciences of the United States of America,* 100**,** 10966-10971.

HARTMAN, R. E., WOZNIAK, D. F., NARDI, A., OLNEY, J. W., SARTORIUS, L. & HOLTZMAN, D. M. 2001. Behavioral phenotyping of GFAP-apoE3 and -apoE4 transgenic mice: apoE4 mice show profound working memory impairments in the absence of Alzheimer's-like neuropathology. *Exp Neurol,* 170**,** 326-44.

HASHIMOTO, T., SERRANO-POZO, A., HORI, Y., ADAMS, K. W., TAKEDA, S., BANERJI, A. O., MITANI, A., JOYNER, D., THYSSEN, D. H., BACSKAI, B. J., FROSCH, M. P., SPIRES-JONES, T. L., FINN, M. B., HOLTZMAN, D. M. & HYMAN, B. T. 2012. Apolipoprotein E, Especially Apolipoprotein E4, Increases the Oligomerization of Amyloid Peptide. *Journal of Neuroscience,* 32**,** 15181-15192.

HATTERS, D. M., BUDAMAGUNTA, M. S., VOSS, J. C. & WEISGRABER, K. H. 2005. Modulation of apolipoprotein E structure by domain interaction: Differences in lipid-bound and lipid-free forms. *Journal of Biological Chemistry,* 280**,** 34288-34295.

HATTERS, D. M., PETERS-LIBEU, C. A. & WEISGRABER, K. H. 2006. Apolipoprotein E structure: insights into function. *Trends Biochem Sci,* 31**,** 445-54.

HAUGH, M. C., PROBST, A., ULRICH, J., KAHN, J. & ANDERTON, B. H. 1986. Alzheimer neurofibrillary tangles contain phosphorylated and hidden neurofilament epitopes. *J Neurol Neurosurg Psychiatry,* 49**,** 1213-20.

HIRONO, N., MORI, E., ISHII, K., IKEJIRI, Y., IMAMURA, T., SHIMOMURA, T., HASHIMOTO, M., YAMASHITA, H. & SASAKI, M. 1998. Hypofunction in the posterior cingulate gyrus correlates with disorientation for time and place in Alzheimer's disease. *J Neurol Neurosurg Psychiatry,* 64**,** 552-4.

HO, L., FUKUCHI, K. & YOUNKIN, S. G. 1996. The alternatively spliced Kunitz protease inhibitor domain alters amyloid beta protein precursor processing and amyloid beta protein production in cultured cells. *J Biol Chem,* 271**,** 30929-34.

HOE, H.-S., FREEMAN, J. & REBECK, G. W. 2006. Apolipoprotein E decreases tau kinases and phospho-tau levels in primary neurons. *Molecular neurodegeneration,* 1**,** 18.

HOE, H. S., HARRIS, D. C. & REBECK, G. W. 2005. Multiple pathways of apolipoprotein E signaling in primary neurons. *Journal of Neurochemistry,* 93**,** 145-155.

HOLLENBACH, E., ACKERMANN, S., HYMAN, B. T. & REBECK, G. W. 1998. Confirmation of an association between a polymorphism in exon 3 of the low-density lipoprotein receptor-related protein gene and Alzheimer's disease. *Neurology,* 50**,** 1905-7.

HOLTZMAN, D. M., BALES, K. R., WU, S., BHAT, P., PARSADANIAN, M., FAGAN, A. M., CHANG, L. K., SUN, Y. & PAUL, S. M. 1999. Expression of human apolipoprotein E reduces amyloid-beta deposition in a mouse model of Alzheimer's disease. *J Clin Invest,* 103**,** R15-r21.

HOOPER, C., KILLICK, R. & LOVESTONE, S. 2008. The GSK3 hypothesis of Alzheimer's disease. *Journal of Neurochemistry,* 104**,** 1433-1439.

HOSAKA, M., HAMMER, R. E. & SUDHOF, T. C. 1999. A phospho-switch controls the dynamic association of synapsins with synaptic vesicles. *Neuron,* 24**,** 377-87.

HOSHI, M., SATO, M., MATSUMOTO, S., NOGUCHI, A., YASUTAKE, K., YOSHIDA, N. & SATO, K. 2003. Spherical aggregates of beta-amyloid (amylospheroid) show high neurotoxicity and activate tau protein kinase I/glycogen synthase kinase-3beta. *Proc Natl Acad Sci U S A,* 100**,** 6370-5.

HSIA, A. Y., MASLIAH, E., MCCONLOGUE, L., YU, G. Q., TATSUNO, G., HU, K., KHOLODENKO, D., MALENKA, R. C., NICOLL, R. A. & MUCKE, L. 1999. Plaque-independent disruption of neural circuits in Alzheimer's disease mouse models. *Proc Natl Acad Sci U S A,* 96**,** 3228-33.

HSIEH, H., BOEHM, J., SATO, C., IWATSUBO, T., TOMITA, T., SISODIA, S. & MALINOW, R. 2006. AMPAR removal underlies Abeta-induced synaptic depression and dendritic spine loss. *Neuron,* 52**,** 831-43.

HU, J.-P., XIE, J.-W., WANG, C.-Y., WANG, T., WANG, X., WANG, S.-L., TENG, W.-P. & WANG, Z.-Y. 2011a. Valproate reduces tau phosphorylation via cyclin-dependent kinase 5 and glycogen synthase kinase 3 signaling pathways. *Brain research bulletin,* 85**,** 194-200.

HU, J. P., XIE, J. W., WANG, C. Y., WANG, T., WANG, X., WANG, S. L., TENG, W. P. & WANG, Z. Y. 2011b. Valproate reduces tau phosphorylation via cyclin-dependent kinase 5 and glycogen synthase kinase 3 signaling pathways. *Brain Res Bull,* 85**,** 194-200.

HUANG, Y. 2010. Aß-independent roles of apolipoprotein E4 in the pathogenesis of Alzheimer's disease. *Trends in Molecular Medicine,* 16**,** 287-294.

HUANG, Y. 2011. Roles of apolipoprotein E4 (ApoE4) in the pathogenesis of Alzheimer's disease: lessons from ApoE mouse models. *Biochem Soc Trans,* 39**,** 924-32.

HUANG, Y., LIU, X. Q., WYSS-CORAY, T., BRECHT, W. J., SANAN, D. A. & MAHLEY, R. W. 2001. Apolipoprotein E fragments present in Alzheimer's disease brains induce neurofibrillary tangle-like intracellular inclusions in neurons. *Proceedings of the National Academy of Sciences of the United States of America,* 98**,** 8838-8843.

HUANG, Y. & MAHLEY, R. W. 2014. Apolipoprotein E: Structure and function in lipid metabolism, neurobiology, and Alzheimer's diseases. *Neurobiology of Disease,* 72**,** 3-12.

HUANG, Y., WEISGRABER, K. H., MUCKE, L. & MAHLEY, R. W. 2004. Apolipoprotein E: diversity of cellular origins, structural and biophysical properties, and effects in Alzheimer's disease. *Journal of molecular neuroscience : MN,* 23**,** 189-204.

HUANG, Y. A., ZHOU, B., WERNIG, M. & SUDHOF, T. C. 2017. ApoE2, ApoE3, and ApoE4 Differentially Stimulate APP Transcription and Abeta Secretion. *Cell,* 168**,** 427-441.e21.

HUGHES, S. R., KHORKOVA, O., GOYAL, S., KNAEBLEIN, J., HEROUX, J., RIEDEL, N. G. & SAHASRABUDHE, S. 1998. α(2)-macroglobulin associates with β-amyloid peptide and prevents fibril formation. *Proc Natl Acad Sci U S A,* 95**,** 3275-80.

HUNT, D. L. & CASTILLO, P. E. 2012. Synaptic plasticity of NMDA receptors: mechanisms and functional implications. *Curr Opin Neurobiol,* 22**,** 496-508.

HUTTNER, W. B., SCHIEBLER, W., GREENGARD, P. & DE CAMILLI, P. 1983. Synapsin I (protein I), a nerve terminal-specific phosphoprotein. III. Its association with synaptic vesicles studied in a highly purified synaptic vesicle preparation. *J Cell Biol,* 96**,** 1374-88.

HUYNH, T. V., DAVIS, A. A., ULRICH, J. D. & HOLTZMAN, D. M. 2017. Apolipoprotein E and Alzheimer's disease: the influence of apolipoprotein E on amyloid-beta and other amyloidogenic proteins. *J Lipid Res,* 58**,** 824-836.

IBANEZ, V., PIETRINI, P., ALEXANDER, G. E., FUREY, M. L., TEICHBERG, D., RAJAPAKSE, J. C., RAPOPORT, S. I., SCHAPIRO, M. B. & HORWITZ, B. 1998. Regional glucose metabolic abnormalities are not the result of atrophy in Alzheimer's disease. *Neurology,* 50**,** 1585-93.

IGNATIUS, M. J., GEBICKE-HARTER, P. J., SKENE, J. H., SCHILLING, J. W., WEISGRABER, K. H., MAHLEY, R. W. & SHOOTER, E. M. 1986. Expression of apolipoprotein E during nerve degeneration and regeneration. *Proc Natl Acad Sci U S A,* 83**,** 1125-9.

INNERARITY, T. L., FRIEDLANDER, E. J., RALL, S. C., JR., WEISGRABER, K. H. & MAHLEY, R. W. 1983. The receptor-binding domain of human apolipoprotein E. Binding of apolipoprotein E fragments. *J Biol Chem,* 258**,** 12341-7.

IWATA, N., TSUBUKI, S., TAKAKI, Y., SHIROTANI, K., LU, B., GERARD, N. P., GERARD, C., HAMA, E., LEE, H. J. & SAIDO, T. C. 2001. Metabolic regulation of brain Abeta by neprilysin. *Science,* 292**,** 1550-2.

JACK, C. R., JR., WISTE, H. J., LESNICK, T. G., WEIGAND, S. D., KNOPMAN, D. S., VEMURI, P., PANKRATZ, V. S., SENJEM, M. L., GUNTER, J. L., MIELKE, M. M., LOWE, V. J., BOEVE, B. F. & PETERSEN, R. C. 2013. Brain beta-amyloid load approaches a plateau. *Neurology,* 80**,** 890-6.

JACOBSEN, J. S., WU, C. C., REDWINE, J. M., COMERY, T. A., ARIAS, R., BOWLBY, M., MARTONE, R., MORRISON, J. H., PANGALOS, M. N., REINHART, P. H. & BLOOM, F.

E. 2006. Early-onset behavioral and synaptic deficits in a mouse model of Alzheimer's disease. *Proc Natl Acad Sci U S A,* 103**,** 5161-6.

JAHN, H., WITTKE, S., ZURBIG, P., RAEDLER, T. J., ARLT, S., KELLMANN, M., MULLEN, W., EICHENLAUB, M., MISCHAK, H. & WIEDEMANN, K. 2011. Peptide fingerprinting of Alzheimer's disease in cerebrospinal fluid: identification and prospective evaluation of new synaptic biomarkers. *PLoS One,* 6**,** e26540.

JAIN, S., YOON, S. Y., LEUNG, L., KNOFERLE, J. & HUANG, Y. 2013. Cellular Source-Specific Effects of Apolipoprotein (Apo) E4 on Dendrite Arborization and Dendritic Spine Development. *PLoS ONE,* 8**,** 1-14.

JARRETT, J. T., BERGER, E. P. & LANSBURY, P. T., JR. 1993. The carboxy terminus of the beta amyloid protein is critical for the seeding of amyloid formation: implications for the pathogenesis of Alzheimer's disease. *Biochemistry,* 32**,** 4693-7.

JIN, M., SHEPARDSON, N., YANG, T., CHEN, G., WALSH, D. & SELKOE, D. J. 2011. Soluble amyloid beta-protein dimers isolated from Alzheimer cortex directly induce Tau hyperphosphorylation and neuritic degeneration. *Proceedings of the National Academy of Sciences of the United States of America,* 108**,** 5819-24.

JOHNSON, S. A., MCNEILL, T., CORDELL, B. & FINCH, C. E. 1990. Relation of neuronal APP-751/APP-695 mRNA ratio and neuritic plaque density in Alzheimer's disease. *Science,* 248**,** 854-7.

JOHNSTON, J. A., WARD, C. L. & KOPITO, R. R. 1998. Aggresomes: a cellular response to misfolded proteins. *J Cell Biol,* 143**,** 1883-98.

JONES, P. B., ADAMS, K. W., ROZKALNE, A., SPIRES-JONES, T. L., HSHIEH, T. T., HASHIMOTO, T., VON ARMIN, C. A. F., MIELKE, M., BACSKAI, B. J. & HYMAN, B. T. 2011. Apolipoprotein E: Isoform specific differences in tertiary structure and interaction with amyloid-?? in human Alzheimer brain. *PLoS ONE,* 6.

JONSSON, T., ATWAL, J. K., STEINBERG, S., SNAEDAL, J., JONSSON, P. V., BJORNSSON, S., STEFANSSON, H., SULEM, P., GUDBJARTSSON, D., MALONEY, J., HOYTE, K., GUSTAFSON, A., LIU, Y., LU, Y., BHANGALE, T., GRAHAM, R. R., HUTTENLOCHER, J., BJORNSDOTTIR, G., ANDREASSEN, O. A., JONSSON, E. G., PALOTIE, A., BEHRENS, T. W., MAGNUSSON, O. T., KONG, A., THORSTEINSDOTTIR, U., WATTS, R. J. & STEFANSSON, K. 2012. A mutation in APP protects against Alzheimer's disease and age-related cognitive decline. *Nature,* 488**,** 96-9.

JOVANOVIC, J. N., SIHRA, T. S., NAIRN, A. C., HEMMINGS, H. C., JR., GREENGARD, P. & CZERNIK, A. J. 2001. Opposing changes in phosphorylation of specific sites in synapsin I during Ca2+-dependent glutamate release in isolated nerve terminals. *J Neurosci,* 21**,** 7944-53.

KANEKIYO, T., XU, H. & BU, G. 2014. ApoE and Aβ in Alzheimer's disease: Accidental encounters or partners? *Neuron,* 81**,** 740-754.

KANG, D. E., PIETRZIK, C. U., BAUM, L., CHEVALLIER, N., MERRIAM, D. E., KOUNNAS, M. Z., WAGNER, S. L., TRONCOSO, J. C., KAWAS, C. H., KATZMAN, R. & KOO, E. H. 2000. Modulation of amyloid beta-protein clearance and Alzheimer's disease susceptibility by the LDL receptor-related protein pathway. *J Clin Invest,* 106**,** 1159-66.

KANG, D. E., SAITOH, T., CHEN, X., XIA, Y., MASLIAH, E., HANSEN, L. A., THOMAS, R. G., THAL, L. J. & KATZMAN, R. 1997. Genetic association of the low-density lipoprotein receptor-related protein gene (LRP), an apolipoprotein E receptor, with late-onset Alzheimer's disease. *Neurology,* 49**,** 56-61.

KANG, J., LEMAIRE, H. G., UNTERBECK, A., SALBAUM, J. M., MASTERS, C. L., GRZESCHIK, K. H., MULTHAUP, G., BEYREUTHER, K. & MULLER-HILL, B. 1987. The precursor of Alzheimer's disease amyloid A4 protein resembles a cell-surface receptor. *Nature,* 325**,** 733-6.

KANG, J. & MULLER-HILL, B. 1990. Differential splicing of Alzheimer's disease amyloid A4 precursor RNA in rat tissues: PreA4(695) mRNA is predominantly produced in rat and human brain. *Biochem Biophys Res Commun,* 166**,** 1192-200.

KANG, M. K., LEE, J., NGUYEN, A. H. & SIM, S. J. 2015. Label-free detection of ApoE4-mediated β-amyloid aggregation on single nanoparticle uncovering Alzheimer's disease. *Biosensors & bioelectronics,* 72**,** 197-204.

KARCH, C. M. & GOATE, A. M. 2015. Alzheimer's disease risk genes and mechanisms of disease pathogenesis. *Biological psychiatry,* 77**,** 43-51.

KARRA, D. & DAHM, R. 2010. Transfection Techniques for Neuronal Cells. *Journal of Neuroscience,* 30**,** 6171-6177.

KELLY, B. L. & FERREIRA, A. 2006a. beta-Amyloid-induced dynamin 1 degradation is mediated by N-methyl-D-aspartate receptors in hippocampal neurons. *J Biol Chem,* 281**,** 28079-89.

KELLY, B. L. & FERREIRA, A. 2006b. β-amyloid-induced dynamin 1 degradation is mediated by N-methyl-D-aspartate receptors in hippocampal neurons. *Journal of Biological Chemistry,* 281**,** 28079-28089.

KELLY, B. L. & FERREIRA, A. 2007. Beta-amyloid disrupted synaptic vesicle endocytosis in cultured hippocampal neurons. *Neuroscience,* 147**,** 60-70.

KELLY, B. L., VASSAR, R. & FERREIRA, A. 2005. Beta-amyloid-induced dynamin 1 depletion in hippocampal neurons. A potential mechanism for early cognitive decline in Alzheimer disease. *J Biol Chem,* 280**,** 31746-53.

KEVENAAR, J. T. & HOOGENRAAD, C. C. 2015. The axonal cytoskeleton: from organization to function. *Front Mol Neurosci,* 8**,** 44.

KHLISTUNOVA, I., BIERNAT, J., WANG, Y., PICKHARDT, M., VON BERGEN, M., GAZOVA, Z., MANDELKOW, E. & MANDELKOW, E. M. 2006. Inducible expression of Tau repeat domain in cell models of tauopathy: aggregation is toxic to cells but can be reversed by inhibitor drugs. *J Biol Chem,* 281**,** 1205-14.

KIM, J., YOON, H., BASAK, J. & KIM, J. 2014. Apolipoprotein E in synaptic plasticity and Alzheimer's disease: potential cellular and molecular mechanisms. *Molecules and cells,* 37**,** 767-776.

KIM, S. H. & RYAN, T. A. 2010. CDK5 serves as a major control point in neurotransmitter release. *Neuron,* 67**,** 797-809.

KIM, Y. G. & LEE, Y. I. 2012. Differential Expressions of Synaptogenic Markers between Primary Cultured Cortical and Hippocampal Neurons. *Exp Neurobiol,* 21**,** 61-7.

KINOSHITA, A., FUKUMOTO, H., SHAH, T., WHELAN, C. M., IRIZARRY, M. C. & HYMAN, B. T. 2003. Demonstration by FRET of BACE interaction with the amyloid precursor protein at the cell surface and in early endosomes. *J Cell Sci,* 116**,** 3339-46.

KIRSCHNER, D. A., ABRAHAM, C. & SELKOE, D. J. 1986. X-ray diffraction from intraneuronal paired helical filaments and extraneuronal amyloid fibers in Alzheimer disease indicates cross-beta conformation. *Proc Natl Acad Sci U S A,* 83**,** 503-7.

KLYUBIN, I., WALSH, D. M., LEMERE, C. A., CULLEN, W. K., SHANKAR, G. M., BETTS, V., SPOONER, E. T., JIANG, L., ANWYL, R., SELKOE, D. J. & ROWAN, M. J. 2005.

Amyloid beta protein immunotherapy neutralizes Abeta oligomers that disrupt synaptic plasticity in vivo. *Nat Med,* 11**,** 556-61.

KOFFIE, R. M., HASHIMOTO, T., TAI, H. C., KAY, K. R., SERRANO-POZO, A., JOYNER, D., HOU, S., KOPEIKINA, K. J., FROSCH, M. P., LEE, V. M., HOLTZMAN, D. M., HYMAN, B. T. & SPIRES-JONES, T. L. 2012. Apolipoprotein E4 effects in Alzheimer's disease are mediated by synaptotoxic oligomeric amyloid-β. *Brain,* 135**,** 2155-2168.

KOFFIE, R. M., HYMAN, B. T. & SPIRES-JONES, T. L. 2011. Alzheimer's disease: synapses gone cold. *Mol Neurodegener,* 6**,** 63.

KOVACS, D. M. 2000. α2-Macroglobulin in late-onset Alzheimer's disease. *Experimental Gerontology,* 35**,** 473-479.

KOVALEVICH, J. & LANGFORD, D. 2013. Considerations for the use of SH-SY5Y neuroblastoma cells in neurobiology. *Methods Mol Biol,* 1078**,** 9-21.

KUHN, P. H., WANG, H., DISLICH, B., COLOMBO, A., ZEITSCHEL, U., ELLWART, J. W., KREMMER, E., ROSSNER, S. & LICHTENTHALER, S. F. 2010. ADAM10 is the physiologically relevant, constitutive alpha-secretase of the amyloid precursor protein in primary neurons. *Embo j,* 29**,** 3020-32.

LADU, M. J., FALDUTO, M. T., MANELLI, A. M., REARDON, C. A., GETZ, G. S. & FRAIL, D. E. 1994. Isoform-specific binding of apolipoprotein E to beta-amyloid. *J Biol Chem,* 269**,** 23403-6.

LADU, M. J., GILLIGAN, S. M., LUKENS, J. R., CABANA, V. G., REARDON, C. A., VAN ELDIK, L. J. & HOLTZMAN, D. M. 1998. Nascent astrocyte particles differ from lipoproteins in CSF. *J Neurochem,* 70**,** 2070-81.

LALAZAR, A., WEISGRABER, K. H., RALL, S. C., JR., GILADI, H., INNERARITY, T. L., LEVANON, A. Z., BOYLES, J. K., AMIT, B., GORECKI, M., MAHLEY, R. W. & ET AL. 1988. Site-specific mutagenesis of human apolipoprotein E. Receptor binding activity of variants with single amino acid substitutions. *J Biol Chem,* 263**,** 3542-5.

LAMBERT, J. C., WAVRANT-DE VRIEZE, F., AMOUYEL, P. & CHARTIER-HARLIN, M. C. 1998a. Association at LRP gene locus with sporadic late-onset Alzheimer's disease. *Lancet,* 351**,** 1787-8.

LAMBERT, M. P., BARLOW, A. K., CHROMY, B. A., EDWARDS, C., FREED, R., LIOSATOS, M., MORGAN, T. E., ROZOVSKY, I., TROMMER, B., VIOLA, K. L., WALS, P., ZHANG, C., FINCH, C. E., KRAFFT, G. A. & KLEIN, W. L. 1998b. Diffusible, nonfibrillar ligands derived from Abeta1-42 are potent central nervous system neurotoxins. *Proc Natl Acad Sci U S A,* 95**,** 6448-53.

LAMMICH, S., KOJRO, E., POSTINA, R., GILBERT, S., PFEIFFER, R., JASIONOWSKI, M., HAASS, C. & FAHRENHOLZ, F. 1999. Constitutive and regulated alpha-secretase cleavage of Alzheimer's amyloid precursor protein by a disintegrin metalloprotease. *Proc Natl Acad Sci U S A,* 96**,** 3922-7.

LEE, Y., KOCKX, M., RAFTERY, M. J., JESSUP, W., GRIFFITH, R. & KRITHARIDES, L. 2010. Glycosylation and sialylation of macrophage-derived human apolipoprotein E analyzed by SDS-PAGE and mass spectrometry: evidence for a novel site of glycosylation on Ser290. *Mol Cell Proteomics,* 9**,** 1968-81.

LEMERE, C. A., LOPERA, F., KOSIK, K. S., LENDON, C. L., OSSA, J., SAIDO, T. C., YAMAGUCHI, H., RUIZ, A., MARTINEZ, A., MADRIGAL, L., HINCAPIE, L., ARANGO, J. C., ANTHONY, D. C., KOO, E. H., GOATE, A. M., SELKOE, D. J. & ARANGO, J. C. 1996. The E280A presenilin 1 Alzheimer mutation produces increased A beta 42 deposition and severe cerebellar pathology. *Nat Med,* 2**,** 1146-50.

LESNE, S., KOH, M. T., KOTILINEK, L., KAYED, R., GLABE, C. G., YANG, A., GALLAGHER, M. & ASHE, K. H. 2006. A specific amyloid-beta protein assembly in the brain impairs memory. *Nature,* 440**,** 352-7.

LEVIN, E. C., ACHARYA, N. K., SEDEYN, J. C., VENKATARAMAN, V., D'ANDREA, M. R., WANG, H. Y. & NAGELE, R. G. 2009. Neuronal expression of vimentin in the Alzheimer's disease brain may be part of a generalized dendritic damage-response mechanism. *Brain Res,* 1298**,** 194-207.

LI, B., CHOHAN, M. O., GRUNDKE-IQBAL, I. & IQBAL, K. 2007. Disruption of microtubule network by Alzheimer abnormally hyperphosphorylated tau. *Acta Neuropathol,* 113**,** 501-11.

LI, J. & CHENG, J. 2018. Apolipoprotein E4 exacerbates ethanol-induced neurotoxicity through augmentation of oxidative stress and apoptosis in N2a-APP cells. *Neurosci Lett,* 665**,** 1-6.

LI, S., HONG, S., SHEPARDSON, N. E., WALSH, D. M., SHANKAR, G. M. & SELKOE, D. 2009. Soluble oligomers of amyloid Beta protein facilitate hippocampal long-term depression by disrupting neuronal glutamate uptake. *Neuron,* 62**,** 788-801.

LI, S., JIN, M. B., KOEGLSPERGER, T., SHEPARDSON, N. E., SHANKAR, G. M. & SELKOE, D. 2011. Soluble Aβ Oligomers Inhibit Long-Term Potentiation through a Mechanism Involving Excessive Activation of Extrasynaptic NR2B-Containing NMDA Receptors. *J. Neuroscience,* 31**,** 6627-6638.

LI, Y. C. & KAVALALI, E. T. 2017. Synaptic Vesicle-Recycling Machinery Components as Potential Therapeutic Targets. *Pharmacol Rev,* 69**,** 141-160.

LIN, Y. T., SEO, J., GAO, F., FELDMAN, H. M., WEN, H. L., PENNEY, J., CAM, H. P., GJONESKA, E., RAJA, W. K., CHENG, J., RUEDA, R., KRITSKIY, O., ABDURROB, F., PENG, Z., MILO, B., YU, C. J., ELMSAOURI, S., DEY, D., KO, T., YANKNER, B. A. & TSAI, L. H. 2018. APOE4 Causes Widespread Molecular and Cellular Alterations Associated with Alzheimer's Disease Phenotypes in Human iPSC-Derived Brain Cell Types. *Neuron*.

LIRAZ, O., BOEHM-CAGAN, A. & MICHAELSON, D. M. 2013. ApoE4 induces Abeta42, tau, and neuronal pathology in the hippocampus of young targeted replacement apoE4 mice. *Mol Neurodegener,* 8**,** 16.

LIU, D. D., YANG, Q. & LI, S. T. 2013. Activation of extrasynaptic NMDA receptors induces LTD in rat hippocampal CA1 neurons. *Brain Res Bull,* 93**,** 10-6.

LIU, M., KUHEL, D. G., SHEN, L., HUI, D. Y. & WOODS, S. C. 2012. Apolipoprotein E does not cross the blood-cerebrospinal fluid barrier, as revealed by an improved technique for sampling CSF from mice. *Am J Physiol Regul Integr Comp Physiol,* 303**,** R903-8.

LJUNGBERG, M. C., DAYANANDAN, R., ASUNI, A., RUPNIAK, T. H., ANDERTON, B. H. & LOVESTONE, S. 2002. Truncated apoE forms tangle-like structures in a neuronal cell line. *Neuroreport,* 13**,** 867-70.

LONN, J., LJUNGGREN, S., KLARSTROM-ENGSTROM, K., DEMIREL, I., BENGTSSON, T. & KARLSSON, H. 2018. Lipoprotein modifications by gingipains of Porphyromonas gingivalis. *J Periodontal Res*.

LOVE, J. E., DAY, R. J., GAUSE, J. W., BROWN, R. J., PU, X., THEIS, D. I., CARAWAY, C. A., POON, W. W., RAHMAN, A. A., MORRISON, B. E. & ROHN, T. T. 2017. Nuclear uptake of an amino-terminal fragment of apolipoprotein E4 promotes cell death

and localizes within microglia of the Alzheimer's disease brain. *Int J Physiol Pathophysiol Pharmacol,* 9**,** 40-57.

LU, W., MAN, H., JU, W., TRIMBLE, W. S., MACDONALD, J. F. & WANG, Y. T. 2001. Activation of synaptic NMDA receptors induces membrane insertion of new AMPA receptors and LTP in cultured hippocampal neurons. *Neuron,* 29**,** 243-54.

LUND, E. G., XIE, C., KOTTI, T., TURLEY, S. D., DIETSCHY, J. M. & RUSSELL, D. W. 2003. Knockout of the cholesterol 24-hydroxylase gene in mice reveals a brain-specific mechanism of cholesterol turnover. *J Biol Chem,* 278**,** 22980-8.

LUSCHER, C. & MALENKA, R. C. 2012. NMDA receptor-dependent long-term potentiation and long-term depression (LTP/LTD). *Cold Spring Harb Perspect Biol,* 4.

LY, S., ALTMAN, R., PETRLOVA, J., LIN, Y., HILT, S., HUSER, T., LAURENCE, T. A. & VOSS, J. C. 2013. Binding of apolipoprotein E inhibits the oligomer growth of amyloid-beta peptide in solution as determined by fluorescence cross-correlation spectroscopy. *J Biol Chem,* 288**,** 11628-35.

MADDALENA, A., PAPASSOTIROPOULOS, A., MULLER-TILLMANNS, B., JUNG, H. H., HEGI, T., NITSCH, R. M. & HOCK, C. 2003. Biochemical diagnosis of Alzheimer disease by measuring the cerebrospinal fluid ratio of phosphorylated tau protein to beta-amyloid peptide42. *Arch Neurol,* 60**,** 1202-6.

MAHLEY, R. W. 2016a. Apolipoprotein E: from cardiovascular disease to neurodegenerative disorders. *Journal of Molecular Medicine*.

MAHLEY, R. W. 2016b. Central Nervous System Lipoproteins: ApoE and Regulation of Cholesterol Metabolism. *Arterioscler Thromb Vasc Biol,* 36**,** 1305-15.

MAHLEY, R. W. & HUANG, Y. 2012. Apolipoprotein e sets the stage: response to injury triggers neuropathology. *Neuron,* 76**,** 871-85.

MAHLEY, R. W., WEISGRABER, K. H. & HUANG, Y. 2006. Apolipoprotein E4: a causative factor and therapeutic target in neuropathology, including Alzheimer's disease. *Proceedings of the National Academy of Sciences of the United States of America,* 103**,** 5644-5651.

MAHLEY, R. W., WEISGRABER, K. H. & INNERARITY, T. L. 1979. Interaction of plasma lipoproteins containing apolipoproteins B and E with heparin and cell surface receptors. *Biochim Biophys Acta,* 575**,** 81-91.

MALONEY, J. A., BAINBRIDGE, T., GUSTAFSON, A., ZHANG, S., KYAUK, R., STEINER, P., VAN DER BRUG, M., LIU, Y., ERNST, J. A., WATTS, R. J. & ATWAL, J. K. 2014. Molecular mechanisms of Alzheimer disease protection by the A673T allele of amyloid precursor protein. *J Biol Chem,* 289**,** 30990-1000.

MARK, R. J., ASHFORD, J. W., GOODMAN, Y. & MATTSON, M. P. 1995. Anticonvulsants attenuate amyloid beta-peptide neurotoxicity, Ca2+ deregulation, and cytoskeletal pathology. *Neurobiol Aging,* 16**,** 187-98.

MARQUER, C., DEVAUGES, V., COSSEC, J. C., LIOT, G., LECART, S., SAUDOU, F., DUYCKAERTS, C., LEVEQUE-FORT, S. & POTIER, M. C. 2011. Local cholesterol increase triggers amyloid precursor protein-Bace1 clustering in lipid rafts and rapid endocytosis. *Faseb j,* 25**,** 1295-305.

MARQUES, M. A., TOLAR M FAU - HARMONY, J. A., HARMONY JA FAU - CRUTCHER, K. A. & CRUTCHER, K. A. 1996. A thrombin cleavage fragment of apolipoprotein E exhibits isoform-specific neurotoxicity.

MARR, R. A., ROCKENSTEIN, E., MUKHERJEE, A., KINDY, M. S., HERSH, L. B., GAGE, F. H., VERMA, I. M. & MASLIAH, E. 2003. Neprilysin gene transfer reduces human amyloid pathology in transgenic mice. *J Neurosci,* 23**,** 1992-6.

MARSH, J. & ALIFRAGIS, P. 2018. Synaptic dysfunction in Alzheimer's disease: the effects of amyloid beta on synaptic vesicle dynamics as a novel target for therapeutic intervention. *Neural Regen Res,* 13**,** 616-623.

MARSH, J., BAGOL, S. H., WILLIAMS, R. S. B., DICKSON, G. & ALIFRAGIS, P. 2017. Synapsin I phosphorylation is dysregulated by beta-amyloid oligomers and restored by valproic acid. *Neurobiol Dis,* 106**,** 63-75.

MARUYAMA, M., HIGUCHI, M., TAKAKI, Y., MATSUBA, Y., TANJI, H., NEMOTO, M., TOMITA, N., MATSUI, T., IWATA, N., MIZUKAMI, H., MURAMATSU, S., OZAWA, K., SAIDO, T. C., ARAI, H. & SASAKI, H. 2005. Cerebrospinal fluid neprilysin is reduced in prodromal Alzheimer's disease. *Ann Neurol,* 57**,** 832-42.

MASLIAH, E., MALLORY, M., ALFORD, M., DETERESA, R., HANSEN, L. A., MCKEEL, D. W., JR. & MORRIS, J. C. 2001. Altered expression of synaptic proteins occurs early during progression of Alzheimer's disease. *Neurology,* 56**,** 127-9.

MASTERS, C. L., BATEMAN, R., BLENNOW, K., ROWE, C. C., SPERLING, R. A. & CUMMINGS, J. L. 2015. Alzheimer's disease. *Nat Rev Dis Primers,* 1**,** 15056.

MASTERS, C. L., SIMMS, G., WEINMAN, N. A., MULTHAUP, G., MCDONALD, B. L. & BEYREUTHER, K. 1985. Amyloid plaque core protein in Alzheimer disease and Down syndrome. *Proc Natl Acad Sci U S A,* 82**,** 4245-9.

MATSUBARA, M., KUSUBATA, M., ISHIGURO, K., UCHIDA, T., TITANI, K. & TANIGUCHI, H. 1996. Site-specific phosphorylation of synapsin I by mitogen-activated protein kinase and Cdk5 and its effects on physiological functions. *J Biol Chem,* 271**,** 21108-13.

MAUCH, D. H., NAGLER, K., SCHUMACHER, S., GORITZ, C., MULLER, E. C., OTTO, A. & PFRIEGER, F. W. 2001. CNS synaptogenesis promoted by glia-derived cholesterol. *Science,* 294**,** 1354-7.

MAWUENYEGA, K. G., SIGURDSON, W., OVOD, V., MUNSELL, L., KASTEN, T., MORRIS, J. C., YARASHESKI, K. E. & BATEMAN, R. J. 2010. Decreased clearance of CNS beta-amyloid in Alzheimer's disease. *Science,* 330**,** 1774.

MCDONALD, C. R., MCEVOY, L. K., GHARAPETIAN, L., FENNEMA-NOTESTINE, C., HAGLER, D. J., JR., HOLLAND, D., KOYAMA, A., BREWER, J. B. & DALE, A. M. 2009. Regional rates of neocortical atrophy from normal aging to early Alzheimer disease. *Neurology,* 73**,** 457-65.

MCLEAN, C. A., CHERNY, R. A., FRASER, F. W., FULLER, S. J., SMITH, M. J., KONRAD, V., BUSH, A. I. & MASTERS, C. L. 1999. Soluble pool of Aβ amyloid as a determinant of severity of neurodegeneration in Alzheimer's disease. *Annals of Neurology,* 46**,** 860-866.

MENENDEZ-GONZALEZ, M., PEREZ-PINERA, P., MARTINEZ-RIVERA, M., CALATAYUD, M. T. & BLAZQUEZ MENES, B. 2005. APP processing and the APP-KPI domain involvement in the amyloid cascade. *Neurodegener Dis,* 2**,** 277-83.

MICHIKAWA, M., FAN, Q. W., ISOBE, I. & YANAGISAWA, K. 2000. Apolipoprotein E exhibits isoform-specific promotion of lipid efflux from astrocytes and neurons in culture. *J Neurochem,* 74**,** 1008-16.

MIETELSKA-POROWSKA, A., WASIK, U., GORAS, M., FILIPEK, A. & NIEWIADOMSKA, G. 2014. Tau protein modifications and interactions: their role in function and dysfunction. *Int J Mol Sci,* 15**,** 4671-713.

MINAGAWA, H., GONG, J. S., JUNG, C. G., WATANABE, A., LUND-KATZ, S., PHILLIPS, M. C., SAITO, H. & MICHIKAWA, M. 2009. Mechanism underlying apolipoprotein E (ApoE) isoform-dependent lipid efflux from neural cells in culture. *J Neurosci Res,* 87**,** 2498-508.

MINOSHIMA, S., GIORDANI, B., BERENT, S., FREY, K. A., FOSTER, N. L. & KUHL, D. E. 1997. Metabolic reduction in the posterior cingulate cortex in very early Alzheimer's disease. *Ann Neurol,* 42**,** 85-94.

MIYATA, M. & SMITH, J. D. 1996. Apolipoprotein E allele–specific antioxidant activity and effects on cytotoxicity by oxidative insults and β–amyloid peptides. *Nature Genetics,* 14**,** 55.

MOIR, R. D., LYNCH, T., BUSH, A. I., WHYTE, S., HENRY, A., PORTBURY, S., MULTHAUP, G., SMALL, D. H., TANZI, R. E., BEYREUTHER, K. & MASTERS, C. L. 1998. Relative increase in Alzheimer's disease of soluble forms of cerebral Abeta amyloid protein precursor containing the Kunitz protease inhibitory domain. *J Biol Chem,* 273**,** 5013-9.

MORELLI, L., LLOVERA, R. E., MATHOV, I., LUE, L. F., FRANGIONE, B., GHISO, J. & CASTANO, E. M. 2004. Insulin-degrading enzyme in brain microvessels: proteolysis of amyloid {beta} vasculotropic variants and reduced activity in cerebral amyloid angiopathy. *J Biol Chem,* 279**,** 56004-13.

MORROW, J. A., HATTERS, D. M., LU, B., HOCHTL, P., OBERG, K. A., RUPP, B. & WEISGRABER, K. H. 2002. Apolipoprotein E4 forms a molten globule. A potential basis for its association with disease. *J Biol Chem,* 277**,** 50380-5.

MOSCONI, L., HERHOLZ, K., PROHOVNIK, I., NACMIAS, B., DE CRISTOFARO, M. T., FAYYAZ, M., BRACCO, L., SORBI, S. & PUPI, A. 2005. Metabolic interaction between ApoE genotype and onset age in Alzheimer's disease: implications for brain reserve. *J Neurol Neurosurg Psychiatry,* 76**,** 15-23.

MOSCONI, L., NACMIAS, B., SORBI, S., DE CRISTOFARO, M. T., FAYAZZ, M., TEDDE, A., BRACCO, L., HERHOLZ, K. & PUPI, A. 2004a. Brain metabolic decreases related to the dose of the ApoE e4 allele in Alzheimer's disease. *J Neurol Neurosurg Psychiatry,* 75**,** 370-6.

MOSCONI, L., PERANI, D., SORBI, S., HERHOLZ, K., NACMIAS, B., HOLTHOFF, V., SALMON, E., BARON, J. C., DE CRISTOFARO, M. T., PADOVANI, A., BORRONI, B., FRANCESCHI, M., BRACCO, L. & PUPI, A. 2004b. MCI conversion to dementia and the APOE genotype: a prediction study with FDG-PET. *Neurology,* 63**,** 2332-40.

MUCKE, L., MASLIAH, E., YU, G. Q., MALLORY, M., ROCKENSTEIN, E. M., TATSUNO, G., HU, K., KHOLODENKO, D., JOHNSON-WOOD, K. & MCCONLOGUE, L. 2000. High-level neuronal expression of abeta 1-42 in wild-type human amyloid protein precursor transgenic mice: synaptotoxicity without plaque formation. *J Neurosci,* 20**,** 4050-8.

MUCKE, L. & SELKOE, D. J. 2012. Neurotoxicity of amyloid beta-protein: synaptic and network dysfunction. *Cold Spring Harb Perspect Med,* 2**,** a006338.

MULLER, M., CARDENAS, C., MEI, L., CHEUNG, K. H. & FOSKETT, J. K. 2011. Constitutive cAMP response element binding protein (CREB) activation by Alzheimer's disease

presenilin-driven inositol trisphosphate receptor (InsP3R) Ca2+ signaling. *Proc Natl Acad Sci U S A,* 108**,** 13293-8.

MUNOZ, S. S., LI, H., RUBERU, K., CHU, Q., SAGHATELIAN, A., OOI, L. & GARNER, B. 2018. The serine protease HtrA1 contributes to the formation of an extracellular 25-kDa apolipoprotein E fragment that stimulates neuritogenesis. *J Biol Chem,* 293**,** 4071-4084.

MYLLYKANGAS, L., POLVIKOSKI, T., SULKAVA, R., VERKKONIEMI, A., CROOK, R., TIENARI, P. J., PUSA, A. K., NIINISTO, L., O'BRIEN, P., KONTULA, K., HARDY, J., HALTIA, M. & PEREZ-TUR, J. 1999. Genetic association of alpha2-macroglobulin with Alzheimer's disease in a Finnish elderly population. *Ann Neurol,* 46**,** 382-90.

NAKAMURA, A., KANEKO, N., VILLEMAGNE, V. L., KATO, T., DOECKE, J., DORE, V., FOWLER, C., LI, Q. X., MARTINS, R., ROWE, C., TOMITA, T., MATSUZAKI, K., ISHII, K., ISHII, K., ARAHATA, Y., IWAMOTO, S., ITO, K., TANAKA, K., MASTERS, C. L. & YANAGISAWA, K. 2018. High performance plasma amyloid-beta biomarkers for Alzheimer's disease. *Nature,* 554**,** 249-254.

NAKAMURA, T., WATANABE, A., FUJINO, T., HOSONO, T. & MICHIKAWA, M. 2009. Apolipoprotein E4 (1-272) fragment is associated with mitochondrial proteins and affects mitochondrial function in neuronal cells. *Molecular neurodegeneration,* 4**,** 35.

NALIVAEVA, N. N. & TURNER, A. J. 2013. The amyloid precursor protein: A biochemical enigma in brain development, function and disease. *FEBS Letters,* 587**,** 2046-2054.

NASLUND, J., HAROUTUNIAN, V., MOHS, R., DAVIS, K. L., DAVIES, P., GREENGARD, P. & BUXBAUM, J. D. 2000. Correlation between elevated levels of amyloid beta-peptide in the brain and cognitive decline. *Jama,* 283**,** 1571-7.

NATHAN, B. P., BELLOSTA, S., SANAN, D. A., WEISGRABER, K. H., MAHLEY, R. W. & PITAS, R. E. 1994. Differential effects of apolipoproteins E3 and E4 on neuronal growth in vitro. *Science,* 264**,** 850-2.

NATHAN, B. P., CHANG, K. C., BELLOSTA, S., BRISCH, E., GE, N., MAHLEY, R. W. & PITAS, R. E. 1995. The inhibitory effect of apolipoprotein E4 on neurite outgrowth is associated with microtubule depolymerization. *J Biol Chem,* 270**,** 19791-9.

NEWELL, A. J., SUE, L. I., SCOTT, S., RAUSCHKOLB, P. K., WALKER, D. G., POTTER, P. E. & BEACH, T. G. 2003. Thiorphan-induced neprilysin inhibition raises amyloid beta levels in rabbit cortex and cerebrospinal fluid. *Neurosci Lett,* 350**,** 178-80.

NGUYEN, C. & BIBB, J. A. 2003. Cdk5 and the mystery of synaptic vesicle endocytosis. *J Cell Biol,* 163**,** 697-9.

NIEWEG, K., SCHALLER, H. & PFRIEGER, F. W. 2009. Marked differences in cholesterol synthesis between neurons and glial cells from postnatal rats. *J Neurochem,* 109**,** 125-34.

NILSSON, J., RUETSCHI, U., HALIM, A., HESSE, C., CARLSOHN, E., BRINKMALM, G. & LARSON, G. 2009. Enrichment of glycopeptides for glycan structure and attachment site identification. *Nat Methods,* 6**,** 809-11.

NOH, H. & SEO, H. 2014. Age-dependent effects of valproic acid in Alzheimer's disease (AD) mice are associated with nerve growth factor (NGF) regulation. *Neuroscience,* 266**,** 255-65.

NORDSTEDT, C., CAPORASO, G. L., THYBERG, J., GANDY, S. E. & GREENGARD, P. 1993. Identification of the Alzheimer beta/A4 amyloid precursor protein in clathrin-coated vesicles purified from PC12 cells. *J Biol Chem,* 268**,** 608-12.

ODDO, S., CACCAMO, A., SHEPHERD, J. D., MURPHY, M. P., GOLDE, T. E., KAYED, R., METHERATE, R., MATTSON, M. P., AKBARI, Y. & LAFERLA, F. M. 2003. Triple-transgenic model of Alzheimer's disease with plaques and tangles: intracellular Abeta and synaptic dysfunction. *Neuron,* 39**,** 409-21.

OVSEPIAN, S. V., O'LEARY, V. B., ZABORSZKY, L., NTZIACHRISTOS, V. & DOLLY, J. O. 2018. Synaptic vesicle cycle and amyloid beta: Biting the hand that feeds. *Alzheimers Dement,* 14**,** 502-513.

PADURARIU, M., CIOBICA, A., MAVROUDIS, I., FOTIOU, D. & BALOYANNIS, S. 2012. Hippocampal neuronal loss in the CA1 and CA3 areas of Alzheimer's disease patients. *Psychiatr Danub,* 24**,** 152-8.

PALMQVIST, S., ZETTERBERG, H., MATTSSON, N., JOHANSSON, P., MINTHON, L., BLENNOW, K., OLSSON, M. & HANSSON, O. 2015. Detailed comparison of amyloid PET and CSF biomarkers for identifying early Alzheimer disease. *Neurology,* 85**,** 1240-9.

PARK, D. & CHANG, S. 2018. Soluble Abeta1-42 increases the heterogeneity in synaptic vesicle pool size among synapses by suppressing intersynaptic vesicle sharing. *Mol Brain,* 11**,** 10.

PARK, D., NA, M., KIM, J. A., LEE, U., CHO, E., JANG, M. & CHANG, S. 2017. Activation of CaMKIV by soluble amyloid-beta1-42 impedes trafficking of axonal vesicles and impairs activity-dependent synaptogenesis. *Sci Signal,* 10.

PARK, J., JANG, M. & CHANG, S. 2013. Deleterious effects of soluble amyloid-beta oligomers on multiple steps of synaptic vesicle trafficking. *Neurobiol Dis,* 55**,** 129-39.

PARKS, K. M., SUGAR, J. E., HAROUTUNIAN, V., BIERER, L., PERL, D. & WALLACE, W. C. 1991. Reduced in vitro phosphorylation of synapsin I (site 1) in Alzheimer's disease postmortem tissues. *Brain Res Mol Brain Res,* 9**,** 125-34.

PARODI, J., SEPULVEDA, F. J., ROA, J., OPAZO, C., INESTROSA, N. C. & AGUAYO, L. G. 2010. Beta-amyloid causes depletion of synaptic vesicles leading to neurotransmission failure. *J Biol Chem,* 285**,** 2506-14.

PEDERSEN, W. A., CHAN, S. L. & MATTSON, M. P. 2000. A mechanism for the neuroprotective effect of apolipoprotein E: isoform-specific modification by the lipid peroxidation product 4-hydroxynonenal. *J Neurochem,* 74**,** 1426-33.

PERSSON, T., LATTANZIO, F., CALVO-GARRIDO, J., RIMONDINI, R., RUBIO-RODRIGO, M., SUNDSTROM, E., MAIOLI, S., SANDEBRING-MATTON, A. & CEDAZO-MINGUEZ, A. 2017. Apolipoprotein E4 Elicits Lysosomal Cathepsin D Release, Decreased Thioredoxin-1 Levels, and Apoptosis. *J Alzheimers Dis,* 56**,** 601-617.

PFRIEGER, F. W. 2003. Outsourcing in the brain: do neurons depend on cholesterol delivery by astrocytes? *Bioessays,* 25**,** 72-8.

PIKE, C. J., BURDICK, D., WALENCEWICZ, A. J., GLABE, C. G. & COTMAN, C. W. 1993. Neurodegeneration induced by beta-amyloid peptides in vitro: the role of peptide assembly state. *J Neurosci,* 13**,** 1676-87.

PIKE, C. J., WALENCEWICZ, A. J., GLABE, C. G. & COTMAN, C. W. 1991. In vitro aging of beta-amyloid protein causes peptide aggregation and neurotoxicity. *Brain Res,* 563**,** 311-4.

PITAS, R. E., BOYLES, J. K., LEE, S. H., FOSS, D. & MAHLEY, R. W. 1987. Astrocytes synthesize apolipoprotein E and metabolize apolipoprotein E-containing lipoproteins. *Biochim Biophys Acta,* 917**,** 148-61.

POSSE DE CHAVES, E. I., VANCE, D. E., CAMPENOT, R. B., KISS, R. S. & VANCE, J. E. 2000. Uptake of lipoproteins for axonal growth of sympathetic neurons. *J Biol Chem,* 275**,** 19883-90.

POTTER, H. & WISNIEWSKI, T. 2012. Apolipoprotein e: essential catalyst of the Alzheimer amyloid cascade. *Int J Alzheimers Dis,* 2012**,** 489428.

PREECE, P., VIRLEY, D. J., COSTANDI, M., COOMBES, R., MOSS, S. J., MUDGE, A. W., JAZIN, E. & CAIRNS, N. J. 2004. Amyloid precursor protein mRNA levels in Alzheimer's disease brain. *Brain Res Mol Brain Res,* 122**,** 1-9.

PUZZO, D., PRIVITERA, L., FA, M., STANISZEWSKI, A., HASHIMOTO, G., AZIZ, F., SAKURAI, M., RIBE, E. M., TROY, C. M., MERCKEN, M., JUNG, S. S., PALMERI, A. & ARANCIO, O. 2011. Endogenous amyloid-beta is necessary for hippocampal synaptic plasticity and memory. *Ann Neurol,* 69**,** 819-30.

PUZZO, D., PRIVITERA, L., LEZNIK, E., FA, M., STANISZEWSKI, A., PALMERI, A. & ARANCIO, O. 2008. Picomolar amyloid-beta positively modulates synaptic plasticity and memory in hippocampus. *J Neurosci,* 28**,** 14537-45.

QING, H., HE, G., LY, P. T., FOX, C. J., STAUFENBIEL, M., CAI, F., ZHANG, Z., WEI, S., SUN, X., CHEN, C. H., ZHOU, W., WANG, K. & SONG, W. 2008. Valproic acid inhibits Abeta production, neuritic plaque formation, and behavioral deficits in Alzheimer's disease mouse models. *J Exp Med,* 205**,** 2781-9.

RABER, J., WONG, D., BUTTINI, M., ORTH, M., BELLOSTA, S., PITAS, R. E., MAHLEY, R. W. & MUCKE, L. 1998. Isoform-specific effects of human apolipoprotein E on brain function revealed in ApoE knockout mice: increased susceptibility of females. *Proc Natl Acad Sci U S A,* 95**,** 10914-9.

RAFFAI, R., MAURICE, R., WEISGRABER, K., INNERARITY, T., WANG, X., MACKENZIE, R., HIRAMA, T., WATSON, D., RASSART, E. & MILNE, R. 1995. Molecular characterization of two monoclonal antibodies specific for the LDL receptor-binding site of human apolipoprotein E. *J Lipid Res,* 36**,** 1905-18.

RALL, S. C., JR., WEISGRABER, K. H. & MAHLEY, R. W. 1982. Human apolipoprotein E. The complete amino acid sequence. *J Biol Chem,* 257**,** 4171-8.

REARDON, C. A., HAY, R. V., GORDON, J. I. & GETZ, G. S. 1984. Processing of rat liver apoprotein E primary translation product. *J Lipid Res,* 25**,** 348-60.

REBECK, G. W. 2017. The role of APOE on lipid homeostasis and inflammation in normal brains. *J Lipid Res,* 58**,** 1493-1499.

RIEMENSCHNEIDER, M., WAGENPFEIL, S., VANDERSTICHELE, H., OTTO, M., WILTFANG, J., KRETZSCHMAR, H., VANMECHELEN, E., FORSTL, H. & KURZ, A. 2003. Phospho-tau/total tau ratio in cerebrospinal fluid discriminates Creutzfeldt-Jakob disease from other dementias. *Mol Psychiatry,* 8**,** 343-7.

RIPOLI, C., PIACENTINI, R., RICCARDI, E., LEONE, L., LI PUMA, D. D., BITAN, G. & GRASSI, C. 2013. Effects of different amyloid beta-protein analogues on synaptic function. *Neurobiol Aging,* 34**,** 1032-44.

RIZZOLI, S. O. 2014. Synaptic vesicle recycling: steps and principles. *Embo j,* 33**,** 788-822.

RIZZOLI, S. O. & BETZ, W. J. 2005. Synaptic vesicle pools. *Nat Rev Neurosci,* 6**,** 57-69.

RODRIGUEZ, G. A., BURNS, M. P., WEEBER, E. J. & REBECK, G. W. 2013. Young APOE4 targeted replacement mice exhibit poor spatial learning and memory, with

reduced dendritic spine density in the medial entorhinal cortex. *Learn Mem,* 20**,** 256-66.

ROHAN DE SILVA, H. A., JEN, A., WICKENDEN, C., JEN, L. S., WILKINSON, S. L. & PATEL, A. J. 1997. Cell-specific expression of beta-amyloid precursor protein isoform mRNAs and proteins in neurons and astrocytes. *Brain Res Mol Brain Res,* 47**,** 147-56.

ROHN, T. T. 2013. Proteolytic cleavage of apolipoprotein E4 as the keystone for the heightened risk associated with Alzheimer's disease. *International Journal of Molecular Sciences,* 14**,** 14908-14922.

ROHN, T. T., CATLIN, L. W., COONSE, K. G. & HABIG, J. W. 2012. Identification of an amino-terminal fragment of apolipoprotein E4 that localizes to neurofibrillary tangles of the Alzheimer's disease brain. *Brain research,* 1475**,** 106-15.

ROSS, R. A., SPENGLER, B. A. & BIEDLER, J. L. 1983. Coordinate morphological and biochemical interconversion of human neuroblastoma cells. *J Natl Cancer Inst,* 71**,** 741-7.

ROVELET-LECRUX, A., HANNEQUIN, D., RAUX, G., LE MEUR, N., LAQUERRIERE, A., VITAL, A., DUMANCHIN, C., FEUILLETTE, S., BRICE, A., VERCELLETTO, M., DUBAS, F., FREBOURG, T. & CAMPION, D. 2006. APP locus duplication causes autosomal dominant early-onset Alzheimer disease with cerebral amyloid angiopathy. *Nat Genet,* 38**,** 24-6.

ROWE, C. C., BOURGEAT, P., ELLIS, K. A., BROWN, B., LIM, Y. Y., MULLIGAN, R., JONES, G., MARUFF, P., WOODWARD, M., PRICE, R., ROBINS, P., TOCHON-DANGUY, H., O'KEEFE, G., PIKE, K. E., YATES, P., SZOEKE, C., SALVADO, O., MACAULAY, S. L., O'MEARA, T., HEAD, R., COBIAC, L., SAVAGE, G., MARTINS, R., MASTERS, C. L., AMES, D. & VILLEMAGNE, V. L. 2013. Predicting Alzheimer disease with beta-amyloid imaging: results from the Australian imaging, biomarkers, and lifestyle study of ageing. *Ann Neurol,* 74**,** 905-13.

ROYO, N. C., VANDENBERGHE, L. H., MA, J. Y., HAUSPURG, A., YU, L., MARONSKI, M., JOHNSTON, J., DICHTER, M. A., WILSON, J. M. & WATSON, D. J. 2008. Specific AAV serotypes stably transduce primary hippocampal and cortical cultures with high efficiency and low toxicity. *Brain Res,* 1190**,** 15-22.

RUSSELL, C. L., SEMERDJIEVA, S., EMPSON, R. M., AUSTEN, B. M., BEESLEY, P. W. & ALIFRAGIS, P. 2012. Amyloid-beta acts as a regulator of neurotransmitter release disrupting the interaction between synaptophysin and VAMP2. *PLoS One,* 7**,** e43201.

RUSSELL, D. W., HALFORD, R. W., RAMIREZ, D. M., SHAH, R. & KOTTI, T. 2009. Cholesterol 24-hydroxylase: an enzyme of cholesterol turnover in the brain. *Annu Rev Biochem,* 78**,** 1017-40.

SABARETNAM, T., HARRIS, M. J., KOCKX, M., WITTING, P. K., LE COUTEUR, D. G. & KRITHARIDES, L. 2009. Effects of hydrogen peroxide and apolipoprotein E isoforms on apolipoprotein E trafficking in HepG2 cells. *Clin Exp Pharmacol Physiol,* 36**,** e96-102.

SAITO, H., DHANASEKARAN, P., NGUYEN, D., BALDWIN, F., WEISGRABER, K. H., WEHRLI, S., PHILLIPS, M. C. & LUND-KATZ, S. 2003. Characterization of the heparin binding sites in human apolipoprotein E. *J Biol Chem,* 278**,** 14782-7.

SANDO, S. B., MELQUIST, S., CANNON, A., HUTTON, M., SLETVOLD, O., SALTVEDT, I., WHITE, L. R., LYDERSEN, S. & AASLY, J. 2008. Risk-reducing effect of education in Alzheimer's disease. *Int J Geriatr Psychiatry,* 23**,** 1156-62.

SAPOZNIK, S., IVENSHITZ, M. & SEGAL, M. 2006. Age-dependent glutamate induction of synaptic plasticity in cultured hippocampal neurons. *Learn Mem,* 13**,** 719-27.

SAUL, A. & WIRTHS, O. 2016. Endogenous Apolipoprotein E (ApoE) Fragmentation Is Linked to Amyloid Pathology in Transgenic Mouse Models of Alzheimer's Disease. *Molecular neurobiology*.

SAUNDERS, A. J., BERTRAM, L., MULLIN, K., SAMPSON, A. J., LATIFZAI, K., BASU, S., JONES, J., KINNEY, D., MACKENZIE-INGANO, L., YU, S., ALBERT, M. S., MOSCARILLO, T. J., GO, R. C., BASSETT, S. S., DALY, M. J., LAIRD, N. M., WANG, X., VELICELEBI, G., WAGNER, S. L., BECKER, D. K., TANZI, R. E. & BLACKER, D. 2003. Genetic association of Alzheimer's disease with multiple polymorphisms in alpha-2-macroglobulin. *Hum Mol Genet,* 12**,** 2765-76.

SCAHILL, R. I., SCHOTT, J. M., STEVENS, J. M., ROSSOR, M. N. & FOX, N. C. 2002. Mapping the evolution of regional atrophy in Alzheimer's disease: unbiased analysis of fluid-registered serial MRI. *Proc Natl Acad Sci U S A,* 99**,** 4703-7.

SCHEFF, S. W., PRICE, D. A., SCHMITT, F. A., DEKOSKY, S. T. & MUFSON, E. J. 2007. Synaptic alterations in CA1 in mild Alzheimer disease and mild cognitive impairment. *Neurology,* 68**,** 1501-8.

SCHEFF, S. W., PRICE, D. A., SCHMITT, F. A. & MUFSON, E. J. 2006. Hippocampal synaptic loss in early Alzheimer's disease and mild cognitive impairment. *Neurobiol Aging,* 27**,** 1372-84.

SCHNITZER, J., FRANKE, W. W. & SCHACHNER, M. 1981. Immunocytochemical demonstration of vimentin in astrocytes and ependymal cells of developing and adult mouse nervous system. *J Cell Biol,* 90**,** 435-47.

SCHOLL, M., LOCKHART, S. N., SCHONHAUT, D. R., O'NEIL, J. P., JANABI, M., OSSENKOPPELE, R., BAKER, S. L., VOGEL, J. W., FARIA, J., SCHWIMMER, H. D., RABINOVICI, G. D. & JAGUST, W. J. 2016. PET Imaging of Tau Deposition in the Aging Human Brain. *Neuron,* 89**,** 971-982.

SCHWARZ, A. J., YU, P., MILLER, B. B., SHCHERBININ, S., DICKSON, J., NAVITSKY, M., JOSHI, A. D., DEVOUS, M. D., SR. & MINTUN, M. S. 2016. Regional profiles of the candidate tau PET ligand 18F-AV-1451 recapitulate key features of Braak histopathological stages. *Brain,* 139**,** 1539-50.

SELBERT, M. A., ANDERSON, K. A., HUANG, Q. H., GOLDSTEIN, E. G., MEANS, A. R. & EDELMAN, A. M. 1995. Phosphorylation and activation of Ca(2+)-calmodulin-dependent protein kinase IV by Ca(2+)-calmodulin-dependent protein kinase Ia kinase. Phosphorylation of threonine 196 is essential for activation. *J Biol Chem,* 270**,** 17616-21.

SELKOE, D. J. 1991. The molecular pathology of Alzheimer's disease. *Neuron,* 6**,** 487-98.

SELKOE, D. J. & HARDY, J. 2016. The amyloid hypothesis of Alzheimer's disease at 25 years. *EMBO Mol Med,* 8**,** 595-608.

SEPULVEDA, F. J., PARODI, J., PEOPLES, R. W., OPAZO, C. & AGUAYO, L. G. 2010. Synaptotoxicity of Alzheimer beta amyloid can be explained by its membrane perforating property. *PLoS One,* 5**,** e11820.

SERRANO-POZO, A., FROSCH, M. P., MASLIAH, E. & HYMAN, B. T. 2011. Neuropathological alterations in Alzheimer disease. *Cold Spring Harb Perspect Med,* 1**,** a006189.

SHANKAR, G. M., BLOODGOOD, B. L., TOWNSEND, M., WALSH, D. M., SELKOE, D. J. & SABATINI, B. L. 2007. Natural oligomers of the Alzheimer amyloid-beta protein induce reversible synapse loss by modulating an NMDA-type glutamate receptor-dependent signaling pathway. *J Neurosci,* 27**,** 2866-75.

SHANKAR, G. M. & WALSH, D. M. 2009. Alzheimer's disease: synaptic dysfunction and Abeta. *Mol Neurodegener,* 4**,** 48.

SHEA, T. B. 1990. Transient increase in vimentin in axonal cytoskeletons during differentiation in NB2a/d1 cells. *Brain Res,* 521**,** 338-42.

SHEN, C. L. & MURPHY, R. M. 1995. Solvent effects on self-assembly of beta-amyloid peptide. *Biophys J,* 69**,** 640-51.

SHI, L., DU, X., ZHOU, H., TAO, C., LIU, Y., MENG, F., WU, G., XIONG, Y., XIA, C., WANG, Y., BI, G. & ZHOU, J. N. 2014. Cumulative effects of the ApoE genotype and gender on the synaptic proteome and oxidative stress in the mouse brain. *Int J Neuropsychopharmacol,* 17**,** 1863-1879.

SHIBATA, M., YAMADA, S., KUMAR, S. R., CALERO, M., BADING, J., FRANGIONE, B., HOLTZMAN, D. M., MILLER, C. A., STRICKLAND, D. K., GHISO, J. & ZLOKOVIC, B. V. 2000. Clearance of Alzheimer's amyloid-ss(1-40) peptide from brain by LDL receptor-related protein-1 at the blood-brain barrier. *J Clin Invest,* 106**,** 1489-99.

SHINODA, Y., TANAKA, T., TOMINAGA-YOSHINO, K. & OGURA, A. 2010. Persistent Synapse Loss Induced by Repetitive LTD in Developing Rat Hippocampal Neurons. *PLoS ONE,* 5**,** e10390.

SHUPLIAKOV, O., HAUCKE, V. & PECHSTEIN, A. 2011. How synapsin I may cluster synaptic vesicles. *Semin Cell Dev Biol,* 22**,** 393-9.

SJOGREN, M., DAVIDSSON, P., TULLBERG, M., MINTHON, L., WALLIN, A., WIKKELSO, C., GRANERUS, A. K., VANDERSTICHELE, H., VANMECHELEN, E. & BLENNOW, K. 2001. Both total and phosphorylated tau are increased in Alzheimer's disease. *J Neurol Neurosurg Psychiatry,* 70**,** 624-30.

SKILLBACK, T., ROSEN, C., ASZTELY, F., MATTSSON, N., BLENNOW, K. & ZETTERBERG, H. 2014. Diagnostic performance of cerebrospinal fluid total tau and phosphorylated tau in Creutzfeldt-Jakob disease: results from the Swedish Mortality Registry. *JAMA Neurol,* 71**,** 476-83.

SKOOG, I., DAVIDSSON, P., AEVARSSON, O., VANDERSTICHELE, H., VANMECHELEN, E. & BLENNOW, K. 2003. Cerebrospinal fluid beta-amyloid 42 is reduced before the onset of sporadic dementia: a population-based study in 85-year-olds. *Dement Geriatr Cogn Disord,* 15**,** 169-76.

SLEEGERS, K., BROUWERS, N., GIJSELINCK, I., THEUNS, J., GOOSSENS, D., WAUTERS, J., DEL-FAVERO, J., CRUTS, M., VAN DUIJN, C. M. & VAN BROECKHOVEN, C. 2006. APP duplication is sufficient to cause early onset Alzheimer's dementia with cerebral amyloid angiopathy. *Brain,* 129**,** 2977-83.

SNYDER, E. M., NONG, Y., ALMEIDA, C. G., PAUL, S., MORAN, T., CHOI, E. Y., NAIRN, A. C., SALTER, M. W., LOMBROSO, P. J., GOURAS, G. K. & GREENGARD, P. 2005. Regulation of NMDA receptor trafficking by amyloid-[beta]. *Nat Neurosci,* 8**,** 1051-1058.

SOULIÉ, C., MITCHELL, V., DUPONT-WALLOIS, L., CHARTIER-HARLIN, M. C., BEAUVILLAIN, J. C., DELACOURTE, A. & CAILLET-BOUDIN, M. L. 1999. Synthesis of apolipoprotein E (ApoE) mRNA by human neuronal-type SK N SH-SY 5Y cells and its regulation by nerve growth factor and ApoE. *Neuroscience Letters,* 265**,** 147-150.

SPERBER, B. R., LEIGHT, S., GOEDERT, M. & LEE, V. M. 1995. Glycogen synthase kinase-3 beta phosphorylates tau protein at multiple sites in intact cells. *Neurosci Lett,* 197**,** 149-53.

SPERLING, R. A., AISEN, P. S., BECKETT, L. A., BENNETT, D. A., CRAFT, S., FAGAN, A. M., IWATSUBO, T., JACK, C. R., JR., KAYE, J., MONTINE, T. J., PARK, D. C., REIMAN, E. M., ROWE, C. C., SIEMERS, E., STERN, Y., YAFFE, K., CARRILLO, M. C., THIES, B., MORRISON-BOGORAD, M., WAGSTER, M. V. & PHELPS, C. H. 2011. Toward defining the preclinical stages of Alzheimer's disease: recommendations from the National Institute on Aging-Alzheimer's Association workgroups on diagnostic guidelines for Alzheimer's disease. *Alzheimers Dement,* 7**,** 280-92.

SPUCH, C., ORTOLANO, S. & NAVARRO, C. 2012. LRP-1 and LRP-2 receptors function in the membrane neuron. Trafficking mechanisms and proteolytic processing in Alzheimer's disease. *Front Physiol,* 3**,** 269.

SPULBER, G., SIMMONS, A., MUEHLBOECK, J. S., MECOCCI, P., VELLAS, B., TSOLAKI, M., KLOSZEWSKA, I., SOININEN, H., SPENGER, C., LOVESTONE, S., WAHLUND, L. O. & WESTMAN, E. 2013. An MRI-based index to measure the severity of Alzheimer's disease-like structural pattern in subjects with mild cognitive impairment. *J Intern Med,* 273**,** 396-409.

STEINHILB, M. L., DIAS-SANTAGATA, D., FULGA, T. A., FELCH, D. L. & FEANY, M. B. 2007. Tau phosphorylation sites work in concert to promote neurotoxicity in vivo. *Mol Biol Cell,* 18**,** 5060-8.

STOMRUD, E., HANSSON, O., BLENNOW, K., MINTHON, L. & LONDOS, E. 2007. Cerebrospinal fluid biomarkers predict decline in subjective cognitive function over 3 years in healthy elderly. *Dement Geriatr Cogn Disord,* 24**,** 118-24.

STRITTMATTER, W. J., SAUNDERS, A. M., GOEDERT, M., WEISGRABER, K. H., DONG, L. M., JAKES, R., HUANG, D. Y., PERICAK-VANCE, M., SCHMECHEL, D. & ROSES, A. D. 1994a. Isoform-specific interactions of apolipoprotein E with microtubule-associated protein tau: implications for Alzheimer disease. *Proceedings of the National Academy of Sciences of the United States of America,* 91**,** 11183-11186.

STRITTMATTER, W. J., SAUNDERS, A. M., SCHMECHEL, D., PERICAK-VANCE, M., ENGHILD, J., SALVESEN, G. S. & ROSES, A. D. 1993. Apolipoprotein E: high-avidity binding to beta-amyloid and increased frequency of type 4 allele in late-onset familial Alzheimer disease. *Proc Natl Acad Sci U S A,* 90**,** 1977-81.

STRITTMATTER, W. J., WEISGRABER, K. H., GOEDERT, M., SAUNDERS, A. M., HUANG, D., CORDER, E. H., DONG, L. M., JAKES, R., ALBERTS, M. J., GILBERT, J. R. & ET AL. 1994b. Hypothesis: microtubule instability and paired helical filament formation in the Alzheimer disease brain are related to apolipoprotein E genotype. *Exp Neurol,* 125**,** 163-71; discussion 172-4.

SUGANO, M., YAMAUCHI, K., KAWASAKI, K., TOZUKA, M., FUJITA, K., OKUMURA, N. & OTA, H. 2008. Sialic acid moiety of apolipoprotein E3 at Thr(194) affects its interaction with beta-amyloid(1-42) peptides. *Clin Chim Acta,* 388**,** 123-9.

SUTHERLAND, C., LEIGHTON, I. A. & COHEN, P. 1993. Inactivation of glycogen synthase kinase-3 beta by phosphorylation: new kinase connections in insulin and growth-factor signalling. *Biochem J,* 296 (Pt 1)**,** 15-9.

SUTPHEN, C. L., JASIELEC, M. S., SHAH, A. R., MACY, E. M., XIONG, C., VLASSENKO, A. G., BENZINGER, T. L., STOOPS, E. E., VANDERSTICHELE, H. M., BRIX, B., DARBY, H. D., VANDIJCK, M. L., LADENSON, J. H., MORRIS, J. C., HOLTZMAN, D. M. & FAGAN, A. M. 2015. Longitudinal Cerebrospinal Fluid Biomarker Changes in Preclinical Alzheimer Disease During Middle Age. *JAMA Neurol,* 72**,** 1029-42.

SZE, C. I., BI, H., KLEINSCHMIDT-DEMASTERS, B. K., FILLEY, C. M. & MARTIN, L. J. 2000. Selective regional loss of exocytotic presynaptic vesicle proteins in Alzheimer's disease brains. *J Neurol Sci,* 175**,** 81-90.

TAI, L. M., BILOUSOVA, T., JUNGBAUER, L., ROESKE, S. K., YOUMANS, K. L., YU, C., POON, W. W., CORNWELL, L. B., MILLER, C. A., VINTERS, H. V., VAN ELDIK, L. J., FARDO, D. W., ESTUS, S., BU, G., GYLYS, K. H. & LADU, M. J. 2013. Levels of soluble apolipoprotein E/amyloid-beta (Abeta) complex are reduced and oligomeric Abeta increased with APOE4 and Alzheimer disease in a transgenic mouse model and human samples. *J Biol Chem,* 288**,** 5914-26.

TAI, L. M., MEHRA, S., SHETE, V., ESTUS, S., REBECK, G. W., BU, G. & LADU, M. J. 2014. Soluble apoE/Aβ complex: mechanism and therapeutic target for APOE4-induced AD risk. *Molecular neurodegeneration,* 9**,** 2.

TAI, L. M., YOUMANS, K. L., JUNGBAUER, L., YU, C. & LADU, M. J. 2011. Introducing Human APOE into Aβ Transgenic Mouse Models. *International journal of Alzheimer's disease,* 2011**,** 810981.

TAMAOKA, A. 1998. [Characterization of amyloid beta protein species in the plasma, cerebrospinal fluid and brains of patients with Alzheimer's disease]. *Nihon Ronen Igakkai Zasshi,* 35**,** 273-7.

TAMBOLI, I. Y., HEO, D. & REBECK, G. W. 2014. Extracellular proteolysis of apolipoprotein e (apoE) by secreted serine neuronal protease. *PLoS ONE,* 9**,** 1-12.

TAN, T. C., VALOVA, V. A., MALLADI, C. S., GRAHAM, M. E., BERVEN, L. A., JUPP, O. J., HANSRA, G., MCCLURE, S. J., SARCEVIC, B., BOADLE, R. A., LARSEN, M. R., COUSIN, M. A. & ROBINSON, P. J. 2003. Cdk5 is essential for synaptic vesicle endocytosis. *Nat Cell Biol,* 5**,** 701-10.

TANAKA, M., VEDHACHALAM, C., SAKAMOTO, T., DHANASEKARAN, P., PHILLIPS, M. C., LUND-KATZ, S. & SAITO, H. 2006. Effect of carboxyl-terminal truncation on structure and lipid interaction of human apolipoprotein E4. *Biochemistry,* 45**,** 4240-7.

TERRY, R. D., MASLIAH, E., SALMON, D. P., BUTTERS, N., DETERESA, R., HILL, R., HANSEN, L. A. & KATZMAN, R. 1991. Physical basis of cognitive alterations in Alzheimer's disease: synapse loss is the major correlate of cognitive impairment. *Ann Neurol,* 30**,** 572-80.

TESSEUR, I., VAN DORPE, J., BRUYNSEELS, K., BRONFMAN, F., SCIOT, R., VAN LOMMEL, A. & VAN LEUVEN, F. 2000a. Prominent axonopathy and disruption of axonal transport in transgenic mice expressing human apolipoprotein E4 in neurons of brain and spinal cord. *Am J Pathol,* 157**,** 1495-510.

TESSEUR, I., VAN DORPE, J., SPITTAELS, K., VAN DEN HAUTE, C., MOECHARS, D. & VAN LEUVEN, F. 2000b. Expression of human apolipoprotein E4 in neurons causes

hyperphosphorylation of protein tau in the brains of transgenic mice. *Am J Pathol,* 156**,** 951-64.

THEENDAKARA, V., BREDESEN, D. E. & RAO, R. V. 2017. Downregulation of protein phosphatase 2A by apolipoprotein E: Implications for Alzheimer's disease. *Mol Cell Neurosci,* 83**,** 83-91.

TOKUMITSU, H. & SODERLING, T. R. 1996. Requirements for calcium and calmodulin in the calmodulin kinase activation cascade. *J Biol Chem,* 271**,** 5617-22.

TOLAR, M., KELLER, J. N., CHAN, S., MATTSON, M. P., MARQUES, M. A. & CRUTCHER, K. A. 1999. Truncated apolipoprotein E (ApoE) causes increased intracellular calcium and may mediate ApoE neurotoxicity. *The Journal of neuroscience : the official journal of the Society for Neuroscience,* 19**,** 7100-10.

TOLAR, M., MARQUES, M. A., HARMONY, J. A. & CRUTCHER, K. A. 1997. Neurotoxicity of the 22 kDa thrombin-cleavage fragment of apolipoprotein E and related synthetic peptides is receptor-mediated. *The Journal of neuroscience : the official journal of the Society for Neuroscience,* 17**,** 5678-86.

TOMIYAMA, T., MATSUYAMA, S., ISO, H., UMEDA, T., TAKUMA, H., OHNISHI, K., ISHIBASHI, K., TERAOKA, R., SAKAMA, N., YAMASHITA, T., NISHITSUJI, K., ITO, K., SHIMADA, H., LAMBERT, M. P., KLEIN, W. L. & MORI, H. 2010. A mouse model of amyloid beta oligomers: their contribution to synaptic alteration, abnormal tau phosphorylation, glial activation, and neuronal loss in vivo. *J Neurosci,* 30**,** 4845-56.

TOMIZAWA, K., SUNADA, S., LU, Y. F., ODA, Y., KINUTA, M., OHSHIMA, T., SAITO, T., WEI, F. Y., MATSUSHITA, M., LI, S. T., TSUTSUI, K., HISANAGA, S., MIKOSHIBA, K., TAKEI, K. & MATSUI, H. 2003. Cophosphorylation of amphiphysin I and dynamin I by Cdk5 regulates clathrin-mediated endocytosis of synaptic vesicles. *J Cell Biol,* 163**,** 813-24.

TONI, N., BUCHS, P. A., NIKONENKO, I., BRON, C. R. & MULLER, D. 1999. LTP promotes formation of multiple spine synapses between a single axon terminal and a dendrite. *Nature,* 402**,** 421-5.

TOWNSEND, M., SHANKAR, G. M., MEHTA, T., WALSH, D. M. & SELKOE, D. J. 2006. Effects of secreted oligomers of amyloid beta-protein on hippocampal synaptic plasticity: a potent role for trimers. *J Physiol,* 572**,** 477-92.

UMEDA, T., MAEKAWA, S., KIMURA, T., TAKASHIMA, A., TOMIYAMA, T. & MORI, H. 2014. Neurofibrillary tangle formation by introducing wild-type human tau into APP transgenic mice. *Acta Neuropathol,* 127**,** 685-98.

VALLA, J., BERNDT, J. D. & GONZALEZ-LIMA, F. 2001. Energy hypometabolism in posterior cingulate cortex of Alzheimer's patients: superficial laminar cytochrome oxidase associated with disease duration. *J Neurosci,* 21**,** 4923-30.

VALLA, J., SCHNEIDER, L. E., SMALL, A. M. & GONZALEZ-LIMA, F. 2007. Quantitative Cytochrome Oxidase Histochemistry: Applications in Human Alzheimer's Disease and Animal Models. *Journal of Histotechnology,* 30**,** 235-247.

VALLA, J., YAARI, R., WOLF, A. B., KUSNE, Y., BEACH, T. G., ROHER, A. E., CORNEVEAUX, J. J., HUENTELMAN, M. J., CASELLI, R. J. & REIMAN, E. M. 2010. Reduced posterior cingulate mitochondrial activity in expired young adult carriers of the APOE epsilon4 allele, the major late-onset Alzheimer's susceptibility gene. *J Alzheimers Dis,* 22**,** 307-13.

VAN HARTEN, A. C., VISSER, P. J., PIJNENBURG, Y. A., TEUNISSEN, C. E., BLANKENSTEIN, M. A., SCHELTENS, P. & VAN DER FLIER, W. M. 2013. Cerebrospinal fluid Abeta42 is the best predictor of clinical progression in patients with subjective complaints. *Alzheimers Dement,* 9**,** 481-7.

VAN MEER, P., ACEVEDO, S. & RABER, J. 2007. Impairments in spatial memory retention of GFAP-apoE4 female mice. *Behav Brain Res,* 176**,** 372-5.

VANMECHELEN, E., VANDERSTICHELE, H., DAVIDSSON, P., VAN KERSCHAVER, E., VAN DER PERRE, B., SJOGREN, M., ANDREASEN, N. & BLENNOW, K. 2000. Quantification of tau phosphorylated at threonine 181 in human cerebrospinal fluid: a sandwich ELISA with a synthetic phosphopeptide for standardization. *Neurosci Lett,* 285**,** 49-52.

VEINBERGS, I., EVERSON, A., SAGARA, Y. & MASLIAH, E. 2002. Neurotoxic effects of apolipoprotein E4 are mediated via dysregulation of calcium homeostasis. *J Neurosci Res,* 67**,** 379-87.

VERSTEGEN, A. M., TAGLIATTI, E., LIGNANI, G., MARTE, A., STOLERO, T., ATIAS, M., CORRADI, A., VALTORTA, F., GITLER, D., ONOFRI, F., FASSIO, A. & BENFENATI, F. 2014. Phosphorylation of synapsin I by cyclin-dependent kinase-5 sets the ratio between the resting and recycling pools of synaptic vesicles at hippocampal synapses. *J Neurosci,* 34**,** 7266-80.

VILLEMAGNE, V. L., BURNHAM, S., BOURGEAT, P., BROWN, B., ELLIS, K. A., SALVADO, O., SZOEKE, C., MACAULAY, S. L., MARTINS, R., MARUFF, P., AMES, D., ROWE, C. C. & MASTERS, C. L. 2013. Amyloid beta deposition, neurodegeneration, and cognitive decline in sporadic Alzheimer's disease: a prospective cohort study. *Lancet Neurol,* 12**,** 357-67.

VISSER, P. J., SCHELTENS, P., VERHEY, F. R., SCHMAND, B., LAUNER, L. J., JOLLES, J. & JONKER, C. 1999. Medial temporal lobe atrophy and memory dysfunction as predictors for dementia in subjects with mild cognitive impairment. *J Neurol,* 246**,** 477-85.

VISSER, P. J., VERHEY, F., KNOL, D. L., SCHELTENS, P., WAHLUND, L. O., FREUND-LEVI, Y., TSOLAKI, M., MINTHON, L., WALLIN, A. K., HAMPEL, H., BURGER, K., PIRTTILA, T., SOININEN, H., RIKKERT, M. O., VERBEEK, M. M., SPIRU, L. & BLENNOW, K. 2009. Prevalence and prognostic value of CSF markers of Alzheimer's disease pathology in patients with subjective cognitive impairment or mild cognitive impairment in the DESCRIPA study: a prospective cohort study. *Lancet Neurol,* 8**,** 619-27.

WALKER, L. C., PAHNKE, J., MADAUSS, M., VOGELGESANG, S., PAHNKE, A., HERBST, E. W., STAUSSKE, D., WALTHER, R., KESSLER, C. & WARZOK, R. W. 2000. Apolipoprotein E4 promotes the early deposition of Abeta42 and then Abeta40 in the elderly. *Acta Neuropathol,* 100**,** 36-42.

WALSH, D. M., KLYUBIN, I., FADEEVA, J. V., CULLEN, W. K., ANWYL, R., WOLFE, M. S., ROWAN, M. J. & SELKOE, D. J. 2002. Naturally secreted oligomers of amyloid beta protein potently inhibit hippocampal long-term potentiation in vivo. *Nature,* 416**,** 535-9.

WALSH, D. M. & SELKOE, D. J. 2007. A beta oligomers - a decade of discovery. *J Neurochem,* 101**,** 1172-84.

WALSH, D. M., TOWNSEND, M., PODLISNY, M. B., SHANKAR, G. M., FADEEVA, J. V., EL AGNAF, O., HARTLEY, D. M. & SELKOE, D. J. 2005. Certain inhibitors of synthetic

amyloid beta-peptide (Abeta) fibrillogenesis block oligomerization of natural Abeta and thereby rescue long-term potentiation. *J Neurosci,* 25**,** 2455-62.

WANG, C., NAJM, R., XU, Q., JEONG, D. E., WALKER, D., BALESTRA, M. E., YOON, S. Y., YUAN, H., LI, G., MILLER, Z. A., MILLER, B. L., MALLOY, M. J. & HUANG, Y. 2018. Gain of toxic apolipoprotein E4 effects in human iPSC-derived neurons is ameliorated by a small-molecule structure corrector. *Nat Med,* 24**,** 647-657.

WANG, C., WILSON, W. A., MOORE, S. D., MACE, B. E., MAEDA, N., SCHMECHEL, D. E. & SULLIVAN, P. M. 2005. Human apoE4-targeted replacement mice display synaptic deficits in the absence of neuropathology. *Neurobiol Dis,* 18**,** 390-8.

WANG, H. W., PASTERNAK, J. F., KUO, H., RISTIC, H., LAMBERT, M. P., CHROMY, B., VIOLA, K. L., KLEIN, W. L., STINE, W. B., KRAFFT, G. A. & TROMMER, B. L. 2002. Soluble oligomers of beta amyloid (1-42) inhibit long-term potentiation but not long-term depression in rat dentate gyrus. *Brain Res,* 924**,** 133-40.

WANG, J., TUNG, Y. C., WANG, Y., LI, X. T., IQBAL, K. & GRUNDKE-IQBAL, I. 2001. Hyperphosphorylation and accumulation of neurofilament proteins in Alzheimer disease brain and in okadaic acid-treated SY5Y cells. *FEBS Lett,* 507**,** 81-7.

WANG, Q., WALSH, D. M., ROWAN, M. J., SELKOE, D. J. & ANWYL, R. 2004. Block of long-term potentiation by naturally secreted and synthetic amyloid beta-peptide in hippocampal slices is mediated via activation of the kinases c-Jun N-terminal kinase, cyclin-dependent kinase 5, and p38 mitogen-activated protein kinase as well as metabotropic glutamate receptor type 5. *J Neurosci,* 24**,** 3370-8.

WANISCH, K., KOVAC, S. & SCHORGE, S. 2013. Tackling obstacles for gene therapy targeting neurons: disrupting perineural nets with hyaluronidase improves transduction. *PLoS One,* 8**,** e53269.

WASHBOURNE, P. & MCALLISTER, A. K. 2002. Techniques for gene transfer into neurons. *Current Opinion in Neurobiology,* 12**,** 566-573.

WAVRANT-DEVRIEZE, F., LAMBERT, J. C., STAS, L., CROOK, R., COTTEL, D., PASQUIER, F., FRIGARD, B., LAMBRECHTS, M., THIRY, E., AMOUYEL, P., TUR, J. P., CHARTIER-HARLIN, M. C., HARDY, J. & VAN LEUVEN, F. 1999. Association between coding variability in the LRP gene and the risk of late-onset Alzheimer's disease. *Hum Genet,* 104**,** 432-4.

WEISGRABER, K. H., RALL, S. C., JR., MAHLEY, R. W., MILNE, R. W., MARCEL, Y. L. & SPARROW, J. T. 1986. Human apolipoprotein E. Determination of the heparin binding sites of apolipoprotein E3. *J Biol Chem,* 261**,** 2068-76.

WELLNITZ, S., FRIEDLEIN, A., BONANNI, C., ANQUEZ, V., GOEPFERT, F., LOETSCHER, H., ADESSI, C. & CZECH, C. 2005. A 13 kDa carboxy-terminal fragment of ApoE stabilizes Abeta hexamers. *Journal of Neurochemistry,* 94**,** 1351-1360.

WERNETTE-HAMMOND, M. E., LAUER, S. J., CORSINI, A., WALKER, D., TAYLOR, J. M. & RALL, S. C., JR. 1989. Glycosylation of human apolipoprotein E. The carbohydrate attachment site is threonine 194. *J Biol Chem,* 264**,** 9094-101.

WESTERLUND, J. A. & WEISGRABER, K. H. 1993. Discrete carboxyl-terminal segments of apolipoprotein E mediate lipoprotein association and protein oligomerization. *J Biol Chem,* 268**,** 15745-50.

WESTERMAN, M. A., COOPER-BLACKETER, D., MARIASH, A., KOTILINEK, L., KAWARABAYASHI, T., YOUNKIN, L. H., CARLSON, G. A., YOUNKIN, S. G. & ASHE, K. H. 2002. The relationship between Abeta and memory in the Tg2576 mouse model of Alzheimer's disease. *J Neurosci,* 22**,** 1858-67.

WETTERAU, J. R., AGGERBECK, L. P., RALL, S. C. & WEISGRABER, K. H. 1988. Human apolipoprotein E3 in aqueous solution. I. Evidence for two structural domains. *The Journal of biological chemistry,* 263**,** 6240-8.

WHITE, F., NICOLL, J. A. & HORSBURGH, K. 2001. Alterations in ApoE and ApoJ in relation to degeneration and regeneration in a mouse model of entorhinal cortex lesion. *Exp Neurol,* 169**,** 307-18.

WILDSMITH, K. R., HOLLEY, M., SAVAGE, J. C., SKERRETT, R. & LANDRETH, G. E. 2013. Evidence for impaired amyloid beta clearance in Alzheimer's disease. *Alzheimers Res Ther,* 5**,** 33.

WILLIAMS, B., CONVERTINO, M., DAS, J. & DOKHOLYAN, N. V. 2015. ApoE4-specific Misfolded Intermediate Identified by Molecular Dynamics Simulations. *PLoS Computational Biology,* 11**,** 1-20.

WILLIAMS, R. S. & BATE, C. 2016. An in vitro model for synaptic loss in neurodegenerative diseases suggests a neuroprotective role for valproic acid via inhibition of cPLA2 dependent signalling. *Neuropharmacology,* 101**,** 566-75.

WILSON, C., WARDELL, M. R., WEISGRABER, K. H., MAHLEY, R. W. & AGARD, D. A. 1991. Three-dimensional structure of the LDL receptor-binding domain of human apolipoprotein E. *Science,* 252**,** 1817-22.

WIMO, A., GUERCHET, M., ALI, G. C., WU, Y. T., PRINA, A. M., WINBLAD, B., JONSSON, L., LIU, Z. & PRINCE, M. 2017. The worldwide costs of dementia 2015 and comparisons with 2010. *Alzheimers Dement,* 13**,** 1-7.

WISNIEWSKI, T., LALOWSKI, M., GOLABEK, A., FRANGIONE, B. & VOGEL, T. 1995. Is Alzheimer's disease an apolipoprotein E amyloidosis? *The Lancet,* 345**,** 956-958.

WOLFE, M. S., XIA, W., OSTASZEWSKI, B. L., DIEHL, T. S., KIMBERLY, W. T. & SELKOE, D. J. 1999. Two transmembrane aspartates in presenilin-1 required for presenilin endoproteolysis and gamma-secretase activity. *Nature,* 398**,** 513-7.

XIA, W., ZHANG, J., KHOLODENKO, D., CITRON, M., PODLISNY, M. B., TEPLOW, D. B., HAASS, C., SEUBERT, P., KOO, E. H. & SELKOE, D. J. 1997. Enhanced production and oligomerization of the 42-residue amyloid beta-protein by Chinese hamster ovary cells stably expressing mutant presenilins. *J Biol Chem,* 272**,** 7977-82.

XIONG, H., CALLAGHAN, D., JONES, A., WALKER, D. G., LUE, L. F., BEACH, T. G., SUE, L. I., WOULFE, J., XU, H., STANIMIROVIC, D. B. & ZHANG, W. 2008. Cholesterol retention in Alzheimer's brain is responsible for high beta- and gamma-secretase activities and Abeta production. *Neurobiol Dis,* 29**,** 422-37.

XU, H., GUPTA, V. B., MARTINS, I. J., MARTINS, R. N., FOWLER, C. J., BUSH, A. I., FINKELSTEIN, D. I. & ADLARD, P. A. 2015a. Zinc affects the proteolytic stability of Apolipoprotein E in an isoform-dependent way. *Neurobiology of Disease,* 81**,** 38-48.

XU, P. T., GILBERT, J. R., QIU, H. L., ERVIN, J., ROTHROCK-CHRISTIAN, T. R., HULETTE, C. & SCHMECHEL, D. E. 1999. Specific regional transcription of apolipoprotein E in human brain neurons. *The American journal of pathology,* 154**,** 601-11.

XU, P. T., LI, Y. J., QIN, X. J., KRONER, C., GREEN-ODLUM, A., XU, H., WANG, T. Y., SCHMECHEL, D. E., HULETTE, C. M., ERVIN, J., HAUSER, M., HAINES, J., PERICAK-VANCE, M. A. & GILBERT, J. R. 2007a. A SAGE study of apolipoprotein E3/3, E3/4 and E4/4 allele-specific gene expression in hippocampus in Alzheimer disease. *Mol Cell Neurosci,* 36**,** 313-31.

XU, P. T., LI, Y. J., QIN, X. J., SCHERZER, C. R., XU, H., SCHMECHEL, D. E., HULETTE, C. M., ERVIN, J., GULLANS, S. R., HAINES, J., PERICAK-VANCE, M. A. & GILBERT, J. R. 2006a. Differences in apolipoprotein E3/3 and E4/4 allele-specific gene expression in hippocampus in Alzheimer disease. *Neurobiol Dis,* 21**,** 256-75.

XU, Q., BERNARDO, A., WALKER, D., KANEGAWA, T., MAHLEY, R. W. & HUANG, Y. 2006b. Profile and regulation of apolipoprotein E (ApoE) expression in the CNS in mice with targeting of green fluorescent protein gene to the ApoE locus. *J Neurosci,* 26**,** 4985-4994.

XU, Q., BRECHT, W. J., WEISGRABER, K. H., MAHLEY, R. W. & HUANG, Y. 2004. Apolipoprotein E4 domain interaction occurs in living neuronal cells as determined by fluorescence resonance energy transfer. *J Biol Chem,* 279**,** 25511-6.

XU, Q., WALKER, D., BERNARDO, A., BRODBECK, J., BALESTRA, M. E. & HUANG, Y. 2008. Intron-3 Retention / Splicing Controls Neuronal Expression of Apolipoprotein E in the CNS. *Journal of Neuroscience,* 28**,** 1452-1459.

XU, W., TAN, L., WANG, H. F., JIANG, T., TAN, M. S., TAN, L., ZHAO, Q. F., LI, J. Q., WANG, J. & YU, J. T. 2015b. Meta-analysis of modifiable risk factors for Alzheimer's disease. *J Neurol Neurosurg Psychiatry,* 86**,** 1299-306.

XU, X., MULLER-TAUBENBERGER, A., ADLEY, K. E., PAWOLLECK, N., LEE, V. W., WIEDEMANN, C., SIHRA, T. S., MANIAK, M., JIN, T. & WILLIAMS, R. S. 2007b. Attenuation of phospholipid signaling provides a novel mechanism for the action of valproic acid. *Eukaryot Cell,* 6**,** 899-906.

YANG, D. S., SMITH, J. D., ZHOU, Z., GANDY, S. E. & MARTINS, R. N. 1997. Characterization of the binding of amyloid-beta peptide to cell culture-derived native apolipoprotein E2, E3, and E4 isoforms and to isoforms from human plasma. *J Neurochem,* 68**,** 721-5.

YANG, Y., KIM, J., KIM, H. Y., RYOO, N., LEE, S., KIM, Y., RHIM, H. & SHIN, Y. K. 2015. Amyloid-beta Oligomers May Impair SNARE-Mediated Exocytosis by Direct Binding to Syntaxin 1a. *Cell Rep,* 12**,** 1244-51.

YAO, P. J., ZHU, M., PYUN, E. I., BROOKS, A. I., THERIANOS, S., MEYERS, V. E. & COLEMAN, P. D. 2003. Defects in expression of genes related to synaptic vesicle trafficking in frontal cortex of Alzheimer's disease. *Neurobiol Dis,* 12**,** 97-109.

YASSINE, H. N., FENG, Q., CHIANG, J., PETROSSPOUR, L. M., FONTEH, A. N., CHUI, H. C. & HARRINGTON, M. G. 2016. ABCA1-Mediated Cholesterol Efflux Capacity to Cerebrospinal Fluid Is Reduced in Patients With Mild Cognitive Impairment and Alzheimer's Disease. *J Am Heart Assoc,* 5.

YE, S., HUANG, Y., MULLENDORFF, K., DONG, L., GIEDT, G., MENG, E. C., COHEN, F. E., KUNTZ, I. D., WEISGRABER, K. H. & MAHLEY, R. W. 2005. Apolipoprotein (apo) E4 enhances amyloid beta peptide production in cultured neuronal cells: apoE structure as a potential therapeutic target. *Proc Natl Acad Sci U S A,* 102**,** 18700-5.

YOUMANS, K. L., TAI, L. M., NWABUISI-HEATH, E., JUNGBAUER, L., KANEKIYO, T., GAN, M., KIM, J., EIMER, W. A., ESTUS, S., REBECK, G. W., WEEBER, E. J., BU, G., YU, C. & LADU, M. J. 2012. APOE4-specific changes in Abeta accumulation in a new transgenic mouse model of Alzheimer disease. *J Biol Chem,* 287**,** 41774-86.

YU, J. T., TAN, L. & HARDY, J. 2014. Apolipoprotein E in Alzheimer's disease: an update. *Annu Rev Neurosci,* 37**,** 79-100.

ZANNIS, V. I. & BRESLOW, J. L. 1981. Human very low density lipoprotein apolipoprotein E isoprotein polymorphism is explained by genetic variation and posttranslational modification. *Biochemistry,* 20**,** 1033-41.

ZANNIS, V. I., MCPHERSON, J., GOLDBERGER, G., KARATHANASIS, S. K. & BRESLOW, J. L. 1984. Synthesis, intracellular processing, and signal peptide of human apolipoprotein E. *The Journal of biological chemistry,* 259**,** 5495-9.

ZEMPEL, H., THIES, E., MANDELKOW, E. & MANDELKOW, E. M. 2010. Abeta oligomers cause localized Ca(2+) elevation, missorting of endogenous Tau into dendrites, Tau phosphorylation, and destruction of microtubules and spines. *J Neurosci,* 30**,** 11938-50.

ZHANG, X.-M., MAO, X.-J., ZHANG, H.-L., ZHENG, X.-Y., PHAM, T., ADEM, A., WINBLAD, B., MIX, E. & ZHU, J. 2012. Overexpression of apolipoprotein E4 increases kainic-acid-induced hippocampal neurodegeneration. *Experimental neurology,* 233**,** 323-32.

ZHANG, X. Z., LI, X. J. & ZHANG, H. Y. 2010. Valproic acid as a promising agent to combat Alzheimer's disease. *Brain Res Bull,* 81**,** 3-6.

ZHANG, Y., MCLAUGHLIN, R., GOODYER, C. & LEBLANC, A. 2002. Selective cytotoxicity of intracellular amyloid beta peptide1-42 through p53 and Bax in cultured primary human neurons. *J Cell Biol,* 156**,** 519-29.

ZHAO, G., TAN, J., MAO, G., CUI, M. Z. & XU, X. 2007. The same gamma-secretase accounts for the multiple intramembrane cleavages of APP. *J Neurochem,* 100**,** 1234-46.

ZHENG, X., LIU, D., ROYCHAUDHURI, R., TEPLOW, D. B. & BOWERS, M. T. 2015. Amyloid beta-Protein Assembly: Differential Effects of the Protective A2T Mutation and Recessive A2V Familial Alzheimer's Disease Mutation. *ACS Chem Neurosci,* 6**,** 1732-40.

ZHOU, Q., HOMMA, K. J. & POO, M. M. 2004. Shrinkage of dendritic spines associated with long-term depression of hippocampal synapses. *Neuron,* 44**,** 749-57.

ZHOU, W., SCOTT, S. A., SHELTON, S. B. & CRUTCHER, K. A. 2006. Cathepsin D-mediated proteolysis of apolipoprotein E: possible role in Alzheimer's disease. *Neuroscience,* 143**,** 689-701.